LNGS - s.s. 17 bis km 18,910 67010 ASSERGI (AQ) ITALY
tel.+39 0862 4371 fax +39 0862 437559
email: document@lngs.infn.it
http://www.lngs.infn.it

ANNUAL REPORT 2016

LNGS/EXP-01/17
November 2017

INFN LNGS

Annual Report 2016

Laboratori Nazionali del Gran Sasso

Cover Image: LUNA Experiment

ISBN-978-88-940122-2-4

Codice ISBN
978-88-940122-2-4

Annual Report 2016

LNGS Director — Prof. Stefano Ragazzi

Editor — Dr. Roberta Antolini

Technical Assistants — Dr. Alessia Giampaoli
Mr. Marco Galeota

Contents

Borexino

M. Agostini[t], K. Altenmüller[r], S. Appel[r], V. Atroshchenko[h], Z. Bagdasarian[z,aa], D. Basilico[k], G. Bellini[k], J. Benziger[o], D. Bick[d], G. Bonfini[j], L. Borodikhina[h], D. Bravo[q,k], B. Caccianiga[k], F. Calaprice[n], A. Caminata[c], S. Caprioli[k], M. Carlini[j], P. Cavalcante[j,q], A. Chepurnov[s], K. Choi[y], D. D'Angelo[k], S. Davini[c], A. Derbin[m], X.F. Ding[t], L. Di Noto[c], I. Drachnev[t,m], S. Farinon[c], K. Fomenko[b], A. Formozov[k], D. Franco[a], F. Froborg[n], F. Gabriele[j], C. Galbiati[n], C. Ghiano[c], M. Giammarchi[k], M. Goeger-Neff[r], A. Goretti[n], M. Gromov[s], C. Hagner[d], T. Houdy[a], E. Hungerford[u], Aldo Ianni[j,1], Andrea Ianni[n], A. Jany[f], D. Jeschke[r], V. Kobychev[g], D. Korablev[b], G. Korga[u], D. Kryn[a], M. Laubenstein[j], E. Litvinovich[h,i], F. Lombardi[j,2], P. Lombardi[k], L. Ludhova[z,aa], G. Lukyanchenko[h], I. Machulin[h,i], G. Manuzio[c], S. Marcocci[t,c], J. Martyn[x], E. Meroni[k], M. Meyer[d], L. Miramonti[k], M. Misiaszek[f], V. Muratova[m], R. Musenich[c], B. Neumair[r], L. Oberauer[r], B. Opitz[d], F. Ortica[l], M. Pallavicini[c], L. Papp[r], A. Pocar[p], G. Ranucci[k], A. Razeto[j], A. Re[k], A. Romani[l], R. Roncin[j,a], N. Rossi[j], S. Schönert[r], D. Semenov[m], P. Shakina[m], M. Skorokhvatov[h,i], O. Smirnov[b], A. Sotnikov[b], L.F.F. Stokes[j], Y. Suvorov[w,h], R. Tartaglia[j], G. Testera[c], J. Thurn[v], M. Toropova[h], E. Unzhakov[m], A. Vishneva[b], R.B. Vogelaar[q], F. von Feilitzsch[r], H. Wang[w], S. Weinz[x], M. Wojcik[f], M. Wurm[x], Z. Yokley[q], O. Zaimidoroga[b], S. Zavatarelli[c], K. Zuber[v], G. Zuzel[f]

The Borexino Collaboration

[a] AstroParticule et Cosmologie, Université Paris Diderot, CNRS/IN2P3, CEA/IRFU, Observatoire de Paris, Sorbonne Paris Cité, 75205 Paris Cedex 13, France
[b] Joint Institute for Nuclear Research, 141980 Dubna, Russia
[c] Dipartimento di Fisica, Università degli Studi e INFN, 16146 Genova, Italy
[d] Institut für Experimentalphysik, Universität Hamburg, 22761 Hamburg, Germany
[e] Max-Planck-Institut für Kernphysik, 69117 Heidelberg, Germany
[f] M. Smoluchowski Institute of Physics, Jagiellonian University, 30059 Krakow, Poland
[g] Kiev Institute for Nuclear Research, 03680 Kiev, Ukraine
[h] National Research Centre Kurchatov Institute, 123182 Moscow, Russia
[i] National Research Nuclear University MEPhI (Moscow Engineering Physics Institute), 115409 Moscow, Russia
[j] INFN Laboratori Nazionali del Gran Sasso, 67010 Assergi (AQ), Italy
[k] Dipartimento di Fisica, Università degli Studi e INFN, 20133 Milano, Italy
[l] Dipartimento di Chimica, Biologia e Biotecnologie, Università degli Studi e INFN, 06123 Perugia, Italy
[m] St. Petersburg Nuclear Physics Institute NRC Kurchatov Institute, 188350 Gatchina, Russia
[n] Physics Department, Princeton University, Princeton, NJ 08544, USA
[o] Chemical Engineering Department, Princeton University, Princeton, NJ 08544, USA
[p] Amherst Center for Fundamental Interactions and Physics Department, University of Massachusetts, Amherst, MA 01003, USA
[q] Physics Department, Virginia Polytechnic Institute and State University, Blacksburg, VA 24061, USA
[r] Physik-Department and Excellence Cluster Universe, Technische Universität München, 85748 Garching, Germany
[s] Lomonosov Moscow State University Skobeltsyn Institute of Nuclear Physics, 119234 Moscow, Russia
[t] Gran Sasso Science Institute (INFN), 67100 L'Aquila, Italy
[u] Department of Physics, University of Houston, Houston, TX 77204, USA
[v] Department of Physics, Technische Universität Dresden, 01062 Dresden, Germany

[1] Also at: Laboratorio Subterráneo de Canfranc, Paseo de los Ayerbe S/N, 22880 Canfranc Estacion Huesca, Spain
[2] Present address: Physics Department, University of California, San Diego, CA 92093, USA

[w]*Physics and Astronomy Department, University of California Los Angeles (UCLA), Los Angeles, California 90095, USA*
[x]*Institute of Physics and Excellence Cluster PRISMA, Johannes Gutenberg-Universität Mainz, 55099 Mainz, Germany*
[y]*Department of Physics and Astronomy, University of Hawaii, Honolulu, HI 96822, USA*
[z]*IKP-2 Forschungzentrum Jülich, 52428 Jülich, Germany*
[aa]*RWTH Aachen University, 52062 Aachen, Germany*
[ab]*Institute for Theoretical and Experimental Physics, 117218 Moscow, Russia*

Abstract

The beginning of the Borexino experiment data taking dates back to 2007 May 15th. During almost 10 years of analysis we published results at the forefront of the measurements of the solar neutrino and geo-neutrino fluxes, and we set unprecedented limits on rare processes. In this report we will review the most important results focusing on the recent articles published during the last year, 2016.

In addition, we will briefly describe the current strategies for improving the detector sensitivity to CNO neutrino flux and the forthcoming updates that we are going to publish concerning the precision measurement of the solar neutrino fluxes.

Introduction

Solar neutrinos provide key pieces of information for either accurate solar physics modelling and neutrino oscillation understanding. The Borexino experiment is presently the only detector able to measure the solar neutrino interaction rate with a threshold of $\gtrsim 150$ keV and to reconstruct the energy spectrum of the events.

In this report, after a brief description of the detector, we will review the most important experimental results coming from the analysis of almost 10 years of data taking (Sec. 1), focusing on the last year (2016) results (Sec. 3). In Sec. 2 we will describe the updates of the status of the apparatus, describing the main ongoing and forthcoming operations on the experimental set-up. In Sec. 4 we will describe the main items of the present analysis concerning the results we are going to publish in the near future, within 2017.

1. The Borexino Detector

Borexino is located in the Hall C of Laboratori Nazionali Gran Sasso. The detector is made of concentric layers of increasing radiopurity (see for details e.g. [1]). According to the scheme sketched in Fig. 1, the innermost core consists of 300 tons of liquid scintillator (PC plus 1.5 g/l of PPO) contained in a 125 μm of ultrapure nylon vessel of radius 4.25 m. A stainless steel sphere (SSS) filled up with $\sim$ 1000 of buffer liquid (PC plus DMP quencher) is instrumented with more than 2000 PMTs for detecting the scintillation light. Finally, the SSS is immersed in a 2000 ton water Cherenkov detector, equipped with 200 PMTs. The position of events is reconstructed with an accuracy of $\sim$ 10 cm and the energy resolution scales approximately as $\sigma(E)/E = 5\%/\sqrt{(E/[MeV])}$. This sensitivity has been achieved after an accurate calibration

campaign [2] carried out in 2010. In addition the detector features a satisfactory pulse shape discrimination for α/β particles and even a challenging β^+/β^- separation, see as a review [1].

The intrinsic radiopurity of the scintillator reached unprecedented levels after an intense purification campaign carried out in between 2010 and 2011. The two stages, namely before and after the purification campaign, are referred as Phase-I and Phase-II. Tab. 1 shows the record background levels in the two Borexino phases.

Contaminant	Phase-I	Phase-II
$^{14}C/^{14}C$		2.7×10^{-18} [g/g]
^{238}U		$< 9.7 \times 10^{-19}$ [g/g] (95% CL)
^{232}Th		$< 1.2 \times 10^{-18}$ [g/g](95% CL)
^{210}Po	∼2000 [cpd/100t]	∼50 [cpd/100t] (2016)
^{210}Bi	∼45 [cpd/100t]	∼20 [cpd/100t] (2016)
^{85}Kr	∼30 [cpd/100t]	< 5 [cpd/100t] (95% CL)

Table 1: Borexino contaminant rates before and after the purification campaign.

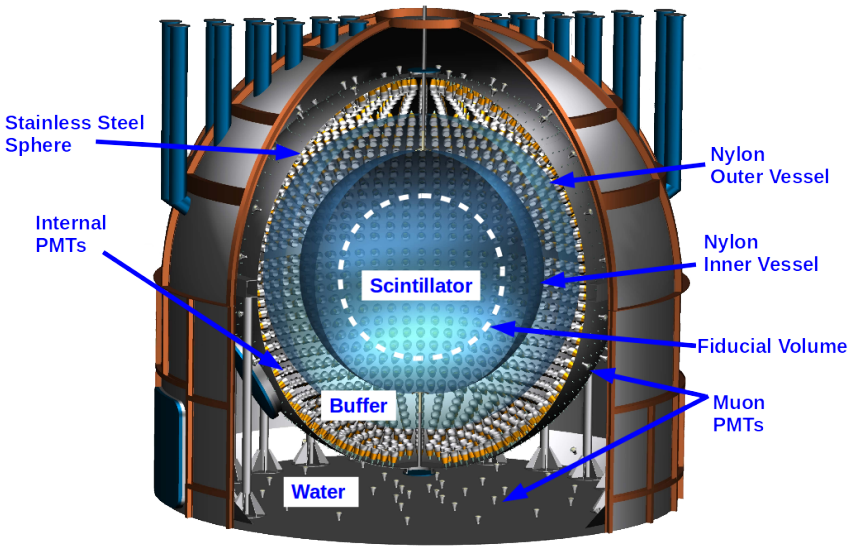

Figure 1: Schematic view of Borexino detector (Picture based on the original drawing, courtesy of A. Brigatti and P. Lombardi).

Thanks to its detection sensitivity, Borexino achieved the following goals: first measurement of the interaction rate of the ^{7}Be (862 keV) neutrinos with 5% accuracy [3], exclusion of any significant day-night asymmetry of the ^{7}Be solar neutrino flux [4], first direct observation of the mono-energetic 1440 keV *pep* solar neutrinos and strongest upper limit of the CNO solar neutrinos flux [6], measurement of the ^{8}B solar neutrinos with a low energy threshold at 3 MeV [5] and first spectroscopical observation of *pp* neutrinos [7]. All of these results are summarized in table Tab. 1

Species	Rate [cpd/100t]	Flux [cm^{-2} s^{-1}]
^{7}Be	$46.0 \pm 1.5^{+1.5}_{-1.6}$	$3.1 \pm 0.15 \times 10^{9}$
pep	$3.1 \pm 0.6 \pm 0.3$	$1.6 \pm 0.6 \times 10^{8}$
CNO	< 7.9 (95% CL)	7.7×10^{8}
^{8}B(> 3 MeV)	$0.22 \pm 0.04 \pm 0.01$	$2.4 \pm 0.4 \pm 0.1 \times 10^{6}$
pp	$144 \pm 13 \pm 10$	$6.6 \pm 0.7 \times 10^{10}$

Table 2: Solar neutrino interaction rates and fluxes measured by the Borexino experiment. Rates are normalized on a mass of 100 tons.

In addition Borexino detected a 5σ geo-netrino signal (see [8] and refs. in it) and set strong limits on rare processes as the last published on 2015 for the electron decay, resulting $> 6.6 \times 10^{28}$ y (90% CL).

2. Current Status of the Apparatus

2.1. Data Acquisition and Electronics

The data-taking is going on regularly with high duty-cycle. The PMT failure rate is under contronl and does not show any suspicious behaviour. A new trigger system was installed during the spring 2016. Detailed tests have shown the full compatibility with the old set-up. A re-arrangement of the electronics channels associated to the live PMTs (decreased of ∼800 units since the beginning of the DAQ) is planned in order to reduce the number of electronics boards in use and save electrical power.

2.1.1. Stabilization of the detector temperature

The Borexino water tank has been thermally insulated with a 20-cm thick layer of wool-rock to stabilize the detector temperature. This work has been completed since 2015. On November/December 2016 a final intervention was performed to further improve the insulation of the upper part of the water tank. The updated temperature profile just inside the stainless steel sphere is shown in Fig. 2 starting from November 2015 (end of insulation) until March 2017.

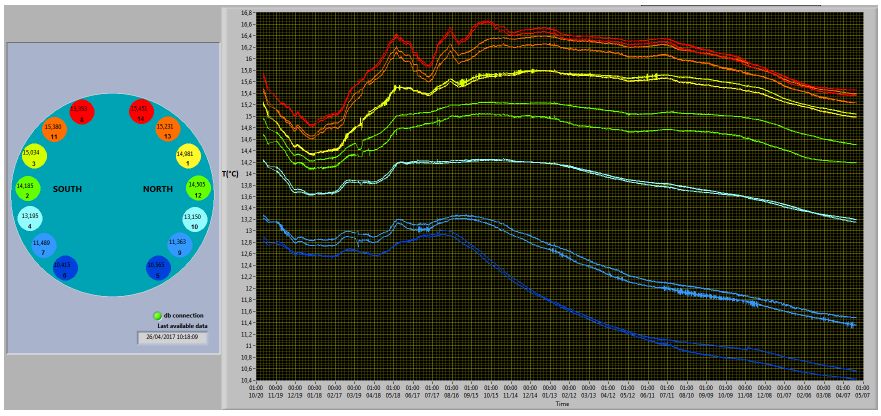

Figure 2: Evolution in time of the temperature profile of the BX detector (from November 2015 until March 2017)

Two main effects are currently affecting the temperature behavior of the detector: the heat sink of the cool rock from the bottom ($\sim 8°$C) and the seasonal variation of the Hall C temperature. As a result the gradient has been increasing due to the lowering of the bottom temperature, until $\sim$ July 2016. Since then it has started decreasing slowly.

In order to be able to control the top temperature and counter the gradient reduction, on January 10^{th} 2017 we have turned on the so-called Active Temperature Control System (TACS). This system is located on the top of the water tank underneath the insulation layer and consists of copper pipes where water can be circulated after being heated to the desired temperature. The TACS has been turned on gradually and we are still adjusting its settings while carefully monitoring the temperature profile at different heights of the detector. The final goal is to actively control the top temperature of the detector keeping it as stable as possible, thus countering the general cooling down of the detector and the seasonal variation of the Hall C temperature. Meanwhile a considerable effort is being devoted to implementing a full simulation of the thermal behavior of the detector based on an ANSYS Fluent Computational Fluid Dynamics simulation package. The wealth of data coming from the temperature probes located throughout the detector is providing an important input for the validation of the model which is in progress. Once this step is completed we expect that the numerical simulations will provide important insight into present and future thermal trends of the detector.

2.2. Polonium Evolution

The ^{210}Po activity measurement that highlights in particular the effects of the insulation has been updated until the end of February 2017.

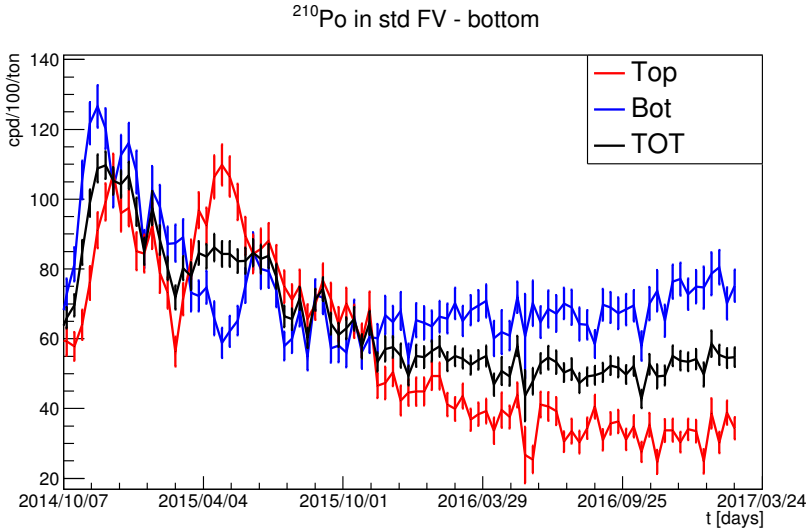

Figure 3: ^{210}Po activity inside the standard ^{7}Be fiducial volume.

Fig. 3 shows the ^{210}Po activity inside the standard ^{7}Be fiducial volume, i.e. $r < 3.021$ m and $|z| < 1.67$ m (*black* curve). The beginning of the detector insulation effects dates back to summer 2015, the period in which the installation of the insulating layers was not yet completed. *Red* and *blue* curves represent the rates for the top part ($z > 0$) and the bottom part ($z < 0$) respectively. The ^{210}Po rate on the bottom is slightly increasing, while the top rate is approaching a plateau.

Top/bottom standard fiducial volumes are big enough to average out all local fluctuations in ^{210}Po distribution.

The insulation stopped drastically the convective motion inside the scintillator since the summer 2015, when the insulation was already partially installed. At present, we have reached non-conclusive (but promising) clues regarding the cause for the top/bottom asymmetry in the rates described above, through the intense thermodynamical model development program currently in progress, aimed at extracting unambiguous conclusions on the influence of fluid dynamics on background concentrations.

2.3. Upgrade of the Scintillator Purification System

Preparations for another round of scintillator re-purification with an upgraded water extraction system has been progressing. The main upgrade is the installation of a more efficient distillation column to purify the water used for water extraction. The motivation for a more efficient distillation is based on measurements made after the 2010 purification campaign. These measurements gave poor efficiencies for removing ^{210}Pb and ^{210}Po in groundwater by reverse osmosis and ion exchange processes, the two processes used in our water purification plant. The new distillation column has structured packing and reflux capability, both of which will significantly increase the efficiency to remove non-volatile impurities in the water, especially the ^{210}Pb.

3. Recent Results

We detected the seasonal modulation of the ^{7}Be neutrino interaction rate. The period, amplitude, and phase of the observed time evolution of the signal are consistent with its solar origin, and the absence of an annual modulation is rejected at 99.99% C.L. The data are analyzed using three methods (in full agreement): the sinusoidal fit, the Lomb-Scargle and the Empirical Mode Decomposition techniques. Fig. 3 shows rate of β-like events passing selection cuts in 20-days bins starting from Dec 11, 2011. The red line is the resulting function from the sinusoidal fit.

A search for neutrino and antineutrino events correlated with 2350 gamma-ray bursts (GRBs) was performed with Borexino data collected between December 2007 and November 2015 [12]. No statistically significant excess over background was observed. We searched for electron antineutrinos ($\bar{\nu}_e$) through inverse beta decay on protons with energies from 1.8 MeV to 15 MeV and set the best limit on the neutrino fluence from GRBs below 8 MeV. The signals from neutrinos and antineutrinos from GRBs scattering on electrons were also investigated. We obtained the best limits on the neutrino fluence of all flavors and species below 7 MeV (Fig. 3). Finally, time correlations between GRBs and bursts of events was investigated.

4. Forthcoming Results

A paper describing the Monte Carlo simulation of the Borexino detector and its performances is submitted for publication [10]. The Borexino Monte Carlo is an *ab initio* simulation of the particle energy loss in all the detector materials, of the generation of the scintillation optical photons, of their propagation inside the large volume scintillator including absorption, reemission and scattering until they are lost or they reach a photomultiplier. The Monte Carlo includes the detailed simulation of the electronics chain. It was tuned using calibration data and it reproduces the energy response, its uniformity within the fiducial volume of the detector and the time distribution of the collected

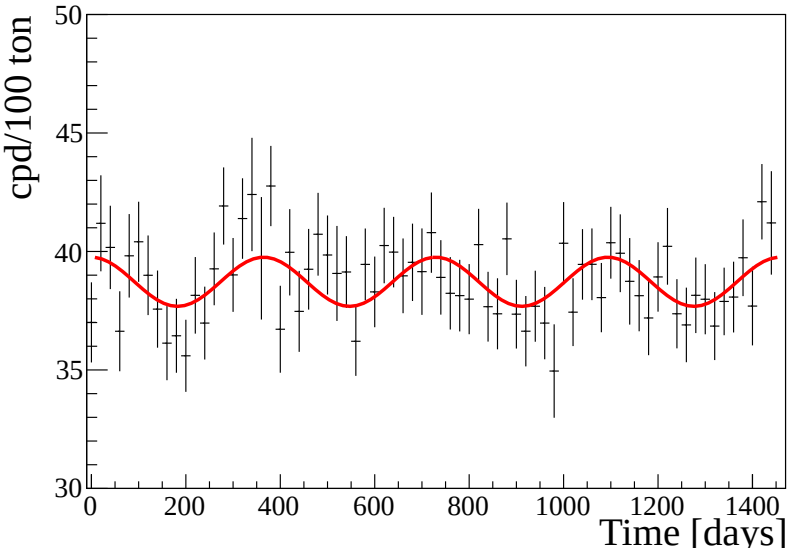

Figure 4: Measured rate of β-like events passing selection cuts in 20-days bins. The red line is the resulting function from the sinusoidal fit.

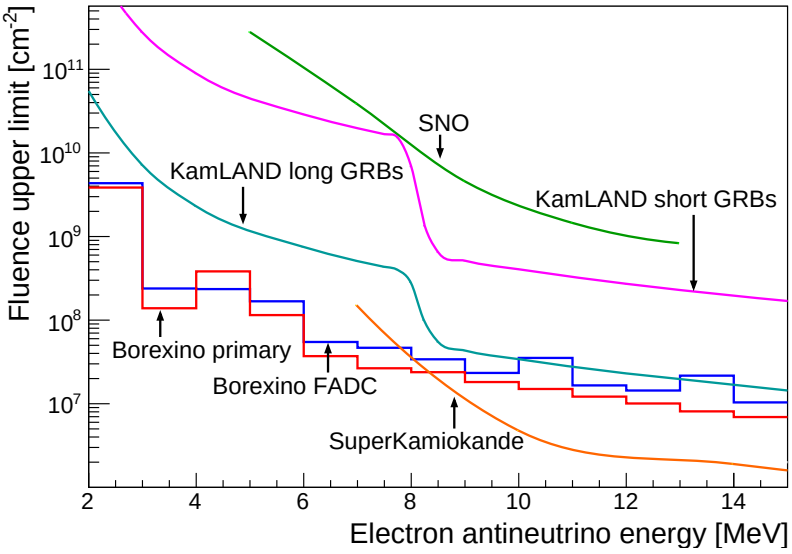

Figure 5: Fluence upper limits for electron antineutrinos from GRBs versus antineutrino energy. Borexino results are shown in comparison with results from SuperKamiokande, SNO, and KamLAND [12].

light to better than 1% from 100 keV up to few MeV. It is a fundamental tool for all the analysis and in particular for the measurement of the solar neutrino interaction rates.

Concering the Phase-II analysis, we are going to update the precision measurement of solar neutrino fluxes (^{7}Be, *pep* and *pp*) and a possible improvement on the CNO neutrino flux limit. The sensitivity to CNO could be further improved after the conclusion of the thermal insulation and

stabilization program in a subsequent analysis. The second stage of this analysis will include also an improvement of the ^{8}B at 3 MeV threshold.

References

[1] . G. Bellini *et al.* [Borexino Collaboration], Phys. Rev. D 89, 112007 (2014)

[2] H. Back *et al.* [Borexino Collaboration], JINST 7 P10018 (2012)

[3] G. Bellini *et al.* [Borexino Collaboration], Phys. Rev. Lett. 107, 141302 (2011)

[4] G. Bellini *et al.* [Borexino Collaboration], Phys. Lett. B 707, 22 (2012)

[5] G. Bellini *et al.* [Borexino Collaboration], Phys. Rev. D82:033006 (2010)

[6] G. Bellini *et al.* [Borexino Collaboration], Phys. Rev. Lett. 108, 051302 (2012)

[7] G. Bellini *et al.* [Borexino Collaboration], Nature, 512:383-386, (2014)

[8] M. Agostini *et al.* [Borexino Collaboration], Phys. Rev. D 92, 031101 (2015)

[9] M. Agostini *et al.* [Borexino Collaboration], Phys. Rev. Lett. **115** (2015) 231802 [arXiv:1509.01223 [hep-ex]].

[10] M. Agostini *et al.* [Borexino Collaboration], arXiv:1704.02291 [physics.ins-det].

[11] M. Agostini *et al.* [BOREXINO Collaboration], arXiv:1701.07970 [hep-ex].

[12] M. Agostini *et al.* [BOREXINO Collaboration], Astropart. Phys. **86** (2017) 11 doi:10.1016/j.astropartphys.2016.10.004 [arXiv:1607.05649 [astro-ph.HE]].

COBRA

The COBRA collaboration

Jan-Hendrik Arling[a], Joachim Ebert[b], Daniel Gehre[c], Marcel Gerhardt[a], Claus Gößling[a], Caren Hagner[b], Arne Heimbold[c], Reiner Klingenberg[a], Kevin Kröninger[a], Christian Nitsch[a], Thomas Quante[a], Katja Rohatsch[c], Jan Tebrügge[a], Robert Temminghoff[a], Robert Theinert[a], Björn Wonsak[b], Stefan Zatschler[c], Kai Zuber[c,*]

[a] *Technische Universität Dortmund* – Germany,
[b] *Universität Hamburg* – Germany,
[c] *Technische Universität Dresden* – Germany,
(* Spokesperson)

Abstract

The aim of the COBRA experiment (**C**admium Zinc Telluride **0**-Neutrino Double-**B**eta **R**esearch **A**pparatus) is to prove the existence of neutrinoless double beta-decay ($0\nu\beta\beta$-decay) and to measure its half-life. The COBRA demonstrator at LNGS is used to investigate the experimental issues of operating CZT detectors in low background mode while additional studies are proceeding in surface laboratories. The experiment consists of 64 monolithic, calorimetric detectors in a coplanar grid (CPG) design. These detectors are $1\times1\times1\,\mathrm{cm}^3$ in size and are operated in a $4\times4\times4$ detector array. CZT naturally contains several double beta-decay candidates. The most promising is ^{116}Cd with a Q-value of 2.8 MeV, which lies above the highest prominent γ-line occurring from natural radioactivity. In 2016, the focus of the collaboration was on the operation and analysis of the current demonstrator, and on preparations for the future detector installation.

1 Activities at the LNGS

1.1 The COBRA demonstrator at LNGS

The COBRA collaboration currently operates a demonstrator setup consisting of 4×4×4 detectors at the LNGS. A detailed description of the COBRA demonstrator operated at the LNGS can be found in a recent publication [**?**]. This paper reports on hardware aspects like the DAQ electronics as well as the experimental infrastructure to monitor and ensure a stable operation under low background conditions. The detectors are made of CdZnTe (CZT) – a commercially available room temperature semiconductor. Due to the poor mobility of holes inside CZT a special readout electrode has to be used to compensate for this effect. COBRA uses a so-called coplanar grid (CPG) consisting of two interlocking comb-shaped anodes held at slightly different potentials. The bias in between is referred to as grid bias (GB). This way, only one electrode collects the charge carriers created via a particle interaction in the end. A bias voltage (referred to as BV) at the order of -1 kV forces the electrons to drift towards the CPG anodes. The electrode at the lower potential collects these electrons and is called the collecting anode (CA) while the other one acts as a non-collecting anode (NCA). The complete signal reconstruction relies only on the induced electron signal, that is why CZT is referred to as single charge carrier device. Details on this reconstruction can be found in [**?**].

Each crystal is $1.0\times1.0\times1.0\,\mathrm{cm}^3$ in size and has a mass of about 6 g. Several isotopes which are candidates for double beta-decays are present in CZT according to their natural abundances. An overview can be found in Table 1. The most promising of which are ^{116}Cd due to the high Q-value of 2814 keV and ^{130}Te because of its high natural abundance of about 34% and considerably high Q-value of 2527 keV. In a first step a peak search for five $\beta^-\beta^-$ g.s. to g.s. transitions has been performed. The results of this analysis are summarized in section 3.2.

Table 1: List of $0\nu\beta\beta$-decay candidates contained in CZT with their corresponding decay modes, natural abundances [**?**] and Q-values [**?**].

Isotope	**Decay mode**	**Nat. ab.**	**Q-value [keV]**
^{64}Zn	$\beta^+/EC, EC/EC$	49.17%	1095.70
^{70}Zn	$\beta^-\beta^-$	0.61%	998.50
^{106}Cd	$\beta^+\beta^+, \beta^+/EC, EC/EC$	1.25%	2775.01
^{108}Cd	EC/EC	0.89%	272.04
^{114}Cd	$\beta^-\beta^-$	28.73%	542.30
^{116}Cd	$\beta^-\beta^-$	7.49%	2813.50
^{120}Te	$\beta^+/EC, EC/EC$	0.09%	1714.81
^{128}Te	$\beta^-\beta^-$	31.74%	865.87
^{130}Te	$\beta^-\beta^-$	34.08%	2526.97

Figure 1 shows an overview of the several shielding layers of the demonstrator. The outermost layer consists of 7 cm borated polyethylene acting as a shield against neutrons. Following, there is a frame of welded metal plates to prevent the first part of the readout chain to be affected by electromagnetic interferences (EMI). Inside this EMI box the custom made and actively cooled preamplifier devices are placed. The inner shielding consists of a multi-layered structure of standard lead, ultra low activity lead and copper surrounding the detectors themselves. This inner shielding is embedded into a polycarbonate box which is continuously flushed with evaporated dry nitrogen to prevent radon from diffusing into the setup.

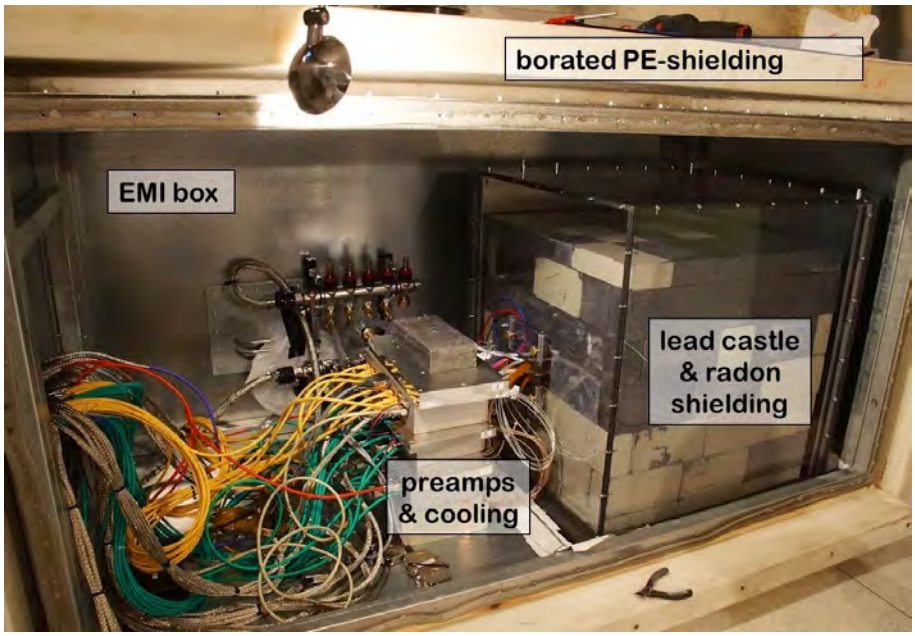

Figure 1: Overview of the experimental setup of the COBRA demonstrator. Highlighted are the different shielding layers and the first stage of the readout chain. The detectors themselves are housed within a so-called copper nest inside the lead castle which can be seen on the right side.

1.2 Maintenance at the LNGS

The COBRA demonstrator was completed to its full stage of 64 detectors in 2013. Hence, activities at LNGS in 2016 consisted mainly of maintenance works and upgrades for the planned low threshold runs discussed in section 2. Two shifts with a total working time of five man-weeks were done at LNGS.

At the end of 2015 it was noted that the flushing of the detectors with evaporated nitrogen did not work reliably anymore. The flushing is an important means of background reduction as it removes air and especially radon from the detectors. A new dewar vessel was installed in the beginning of 2016. The instrumentation of the dewar was exchanged partly. By this, the flushing of the detectors with nitrogen is ensured. A new contract with an external company was negotiated, the filling of the dewar is done biweekly now.

The COBRA collaboration decided to make a dedicated measurement campaign to measure the energy spectrum of ^{113}Cd. One key requirement for this is to reach low trigger thresholds to measure the energy spectrum to low values around 60 keV. Some hardware modifications at the demonstrator were done to reach this aim. Most important, the voltage supply for the preamplifiers was improved, so that detectors which cause electronic noise can be switched off remotely.

2 ^{113}Cd low-threshold run

Recently, the scientific discussion about the so-called quenching of the axial vector coupling constant g_A has triggered some new calculations in nuclear physics. The possibility of a quenched coupling strength has been introduced to reproduce experimental data of double beta-decay studies with theoretical models. Of special interest are highly forbidden single beta-decays since the spectral shape of the electron momentum distribution strongly depends on the effective value of g_A, but in a highly non-trivial way. One of the isotopes present in the CdZnTe detectors used by COBRA is ^{113}Cd with an abundance of about 12%. The ^{113}Cd nucleus undergoes a fourfold forbidden, non-unique single beta-decay with a half-life of about $8{\cdot}10^{15}$ years and a Q-value

of 322 keV. This decay causes by far the most prominent signal for the COBRA demonstrator without interfering with the double-beta decay ROI at higher energies.

2.1 Threshold study and experimental data

The COBRA demonstrator has excellent prospects to contribute to the experimental data that is available for the effective value of g_A in the nucleus. Hence, a dedicated run of at least three months is planned prior the installation of the new detector module XDEM (find details in section 4). A campaign to lower the detection thresholds as low as reasonably possible for all of the 128 signal channels of the COBRA demonstrator was started already last year. Since June 2016 the trigger thresholds of all channels are evaluated regularly by monitoring the total trigger rate and lowered as far as reasonable possible. An illustration of the trend and the current, averaged threshold levels are shown in Figure 2.

At the moment the cooling power is limited by the coolant itself, which is pure water only. The cooling unit is set to a target temperature of 4°C which leads to about 12°C next to the preamplifier boards and to about 15°C on top of the lead castle. To further improve the situation and to start investigating the detector behavior at even lower temperatures the coolant will be exchanged in spring 2017. Furthermore, the instrumentation of the dewar vessel as last piece of the completely reworked nitrogen flushing system will be replaced to further guarantee a stable operation. To study the impact of all this work new calibration sources have been ordered. The first data of the ongoing low-threshold run is currently used to evaluate the existing data cleaning cuts and to prepare the analysis of the final data set. This also requires to model the energy resolution at the optimal temperature as will be done in the next months using a recently purchased ^{152}Eu source.

2.2 Evaluation of event selection

During the processing of the raw pulses obtained from the single detectors, several quality criteria are used to discriminate between real physical events and events triggered by electronic noise or other disturbances, which are being flagged as such. These criteria have been developed to ensure a maximized signal efficiency at high energies around the Q-value of ^{116}Cd at 2.8 MeV. It has been observed that some criteria are too strict in the lower energy region, which leads to different rates of the ^{113}Cd decay compared between single detectors. Therefore, a careful review and evaluation process has been started at TU Dresden. First results can be found in [**?**]. The data used for this study was recorded between June and September 2016 after starting lowering

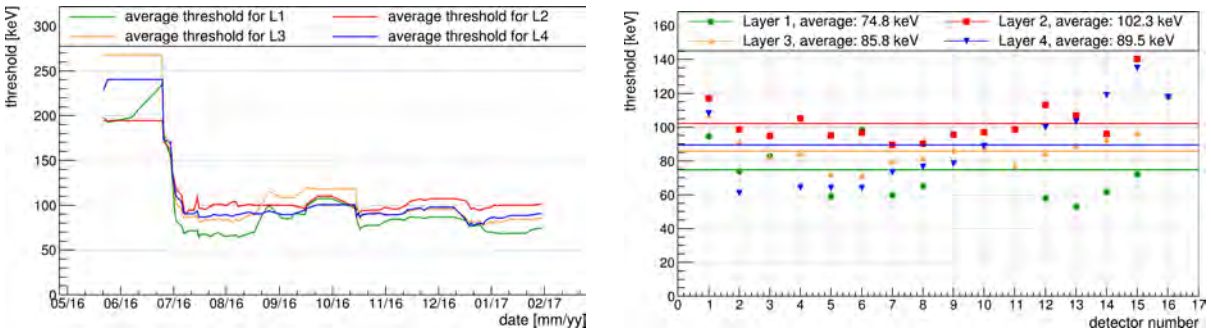

Figure 2: Left: threshold evolution of the COBRA demonstrator over time. Since June '16 all trigger thresholds have been lowered significantly due to the improved operation stability. Right: Overview of current detection thresholds per detector and average per layer.

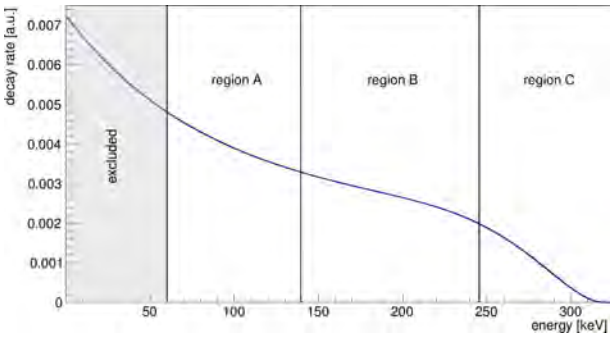

Figure 3: Example of ^{113}Cd spectrum segmentation for an assumed value of $g_A = 1.1$. The first region below 60 keV is excluded to mimic the experimental threshold limitations. For regions A, B and C the proportions are chosen to be (30%, 40%, 30%) of the remaining energy range up to the Q-value. For those regions the integrated count rate is calculated to obtain the ratios B/A and B/C.

the thresholds for the anticipated ^{113}Cd low-threshold run. In the current implementation, already one flag is enough to declare an event as unphysical, which is sufficient for pulses with a rather high amplitude, hence, a high energy deposition. Currently, the implementation of a new event selection and the improvement of the existing framework is work in progress. The main ideas here are to evaluate each flag with respect to the uncertainty on the pulse quantities used in the flag declaration (e.g. rise time, pulse height) and possibly to weight the single flags according to their impact.

2.3 Preparations of spectral shape analysis

The collaboration has access to recently published templates of the theoretical spectral shape of ^{113}Cd [**?**]. These templates have been calculated in a Nuclear Shell Model (NSM) for several assumed values of the axial vector coupling g_A, whereas the vector coupling g_V is set to unity. The spectral shape of ^{113}Cd for high ($g_A > 1.1$) and low values ($g_A \leq 0.8$) seems to be pretty similar along the whole energy range. As a starting point, the templates are used to search for a good discrimination variable to compare the theoretical predictions with the spectrum measured by COBRA. A first idea is to divide the templates into several regions and calculate the ratio of the integrated count rate in those regions. It has been found, that defining only two regions A and B covering both 50% of the total energy range leads to an ambiguous behavior if one compares the ratio A/B for the spectra of different values of g_A. In a plot of A/B versus g_A a parabola could be seen, so that the same ratio A/B hints to two different values of g_A. Hence, a more elaborated approach had to be found as illustrated in Figure 3. The result shown here is very preliminary but proves already good robustness meaning that the characteristic shape does not vary much for a different choice of the selected regions or their proportions.

3 Results of the low background operation

3.1 Data-taking at the LNGS

Figure 4 illustrates the total accumulated and selected exposure for the most recent neutrinoless double beta-decay search. Between Sept.'11 and Oct.'16 a total exposure of 400 kg d has been acquired with complete pulse shape sampling. Additionally indicated are upgrade works on-site like the installation of further detector layers and root causes for periods of lower data quality. At the end of 2016 about 430 kgd expose have been collected.

3.2 Results of neutrinoless double beta-decay search

The current analysis used a Bayesian signal estimation, published in [?]. To determine the efficiencies, also a pulse shape simulation was used. See table 2 for the latest reviewed results.

The next analysis iteration of the data of the demonstrator will use detector specific parameters like the energy resolution and calibration uncertainties, instead of parameters averaged over the whole detector array. Studies show that the A/E criterion developed by the GERDA experiment [?] can also be used by COBRA [?]. First tests indicate that the background suppression factor is as good as the LSE criteria [?] developed by COBRA, but with a 10 percent higher signal efficiency. Hence this criterion will be investigated further.

The largest systematic uncertainty in the current analysis was introduced by the efficiency calculation for the imposed pulse shape requirements. Therefore, a new efficiency fitter is under development, which estimates the signal efficiency at the double escape peak (DEP) of ^{208}Tl. One challenge is that on some detectors the ^{212}Bi line at 1620 keV overlaps with the DEP, which will be taken into account by the new fitter. The first iteration implies that the uncertainty can be reduced by a factor 1.5 to 2.

Table 2: Results of the Bayesian signal estimation after folding all systematic uncertainties. The second column shows the natural abundance of atoms per kg which is used for the signal estimation. In the third column the background index b for the different ROIs is presented. The fourth column reports the limit at 90 % credibility and the last column reports the calculated Bayes factor, taken from [?].

Isotope	$N/10^{23}$ $[\frac{\text{Atoms}}{\text{kg}}]$	b $[\frac{\text{counts}}{\text{keV kg yr}}]$	$T_{1/2}$ 90% C.L. $[10^{21}\text{yr}]$	K
^{114}Cd	6.59	$213.9^{+1.0}_{-1.7}$	1.6	0.07
^{128}Te	8.08	$65.5^{+0.5}_{-1.6}$	1.9	0.17
^{70}Zn	0.015	$45.1^{+0.6}_{-1.0}$	6.8×10^{-3}	0.06
^{130}Te	8.62	$3.6^{+0.1}_{-0.3}$	6.1	0.14
^{116}Cd	1.73	$2.7^{+0.1}_{-0.2}$	1.1	0.27

In the future the limits could be improved with newly evaluated methods of PSD to reject

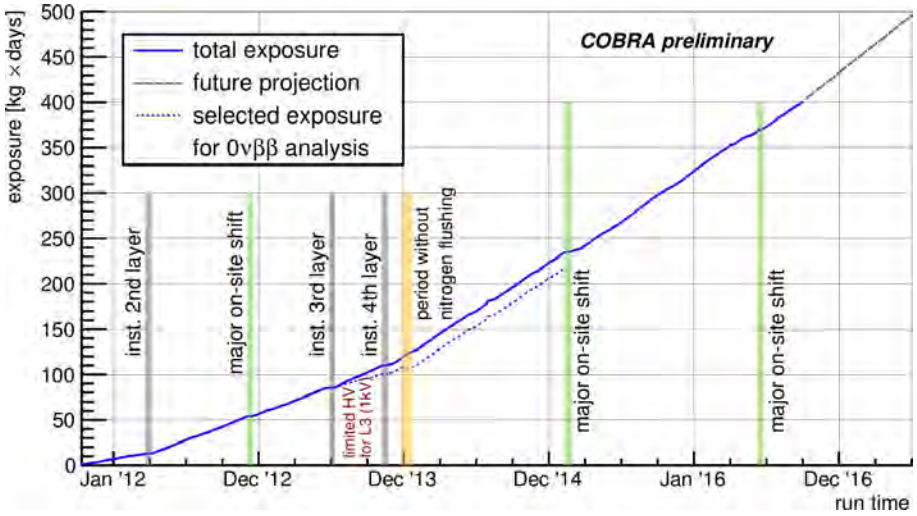

Figure 4: Accumulated low-background exposure of the COBRA demonstrator at LNGS versus run time of the experiment.

also multi-site events (MSEs). It is a known feature that the techniques used to identify lateral surface events are also sensitive to MSEs. Hence, the efficiency of the LSE cuts is expected to be significantly higher if multi-site events are rejected before the efficiency calculation. Due to the ongoing efficiency estimation for the developed MSE cut it is not included in the recent double beta analysis. Another way to improve the limits is to reject multi-detector events, which requires an accurate synchronization of all 16 ADC clocks at first. The evaluation of the software tool written for this purpose is still ongoing.

4 Preparations for the XDEM-installation

The COBRA collaboration was granted funding by the German research foundation (DFG) to install the XDEM (extended demonstrator) at LNGS. This is the smallest unit of a future large-scale experiment consisting of nine detectors with the size of $(20 \times 20 \times 15)\,\mathrm{mm}^3$ and volume of $6\,\mathrm{cm}^3$, operated in addition to the demonstrator with 64 detectors with the volume of $1\,\mathrm{cm}^3$. This installation will take place in the setup of the demonstrator, consequently no additional space is needed. The shielding of XDEM will be the same as for the demonstrator, changes arise mostly in the detector type. The understanding of the performance of the large quad-CPG detectors and the background reduction using an instrumented guard ring were extensively investigated.

4.1 Characterization of large quad-CPG CZT crystals

In the current demonstrator phase of COBRA 64 detectors with a volume of $(10 \times 10 \times 10)\,\mathrm{mm}^3$ are used and it has been shown that a long-term low-background experiment using CdZnTe is feasible [**?**]. In the next stage, $(20 \times 20 \times 15)\,\mathrm{mm}^3$ detectors with a coplanar quad-grid (CPqG) will be used [**?**,**?**]. The use of larger devices will not only lead to a higher detection efficiency, but can also help to suppress surface related backgrounds and allows for easier instrumentation. The novel quad-grid approach is used to maintain a good energy resolution for the larger detectors, because it achieves a lower leakage current and capacitance than a single large grid, while it also allows to compensate for inhomogeneous performance across the crystal. Several detectors of this design have been investigated in various laboratory set-ups at TU Dortmund and TU Dresden. Among these have been detailed measurements of the performance variations along several axes of the detector. This has been done with an automated apparatus designed for 'scanning' a detector with a collimated ^{137}Cs γ-source. The apparatus is shown in Figure 5. Some results of this scanning campaign can be seen in Figure 6 and 7. Figure 6 shows the variations in the rate and the measured energy of full energy events, when different spots on

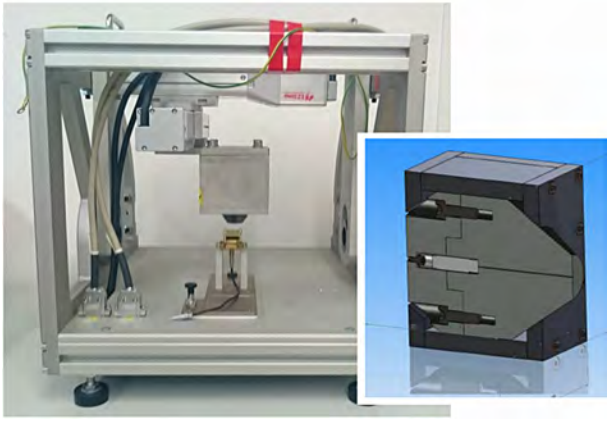

Figure 5: Experimental apparatus used for γ-scanning measurements. The detector can be seen in the middle of the picture, while the collimator is placed above the detector so that the source irradiates the detector perpendicular to the anode plane. The inset shows a construction schematic of the collimator.

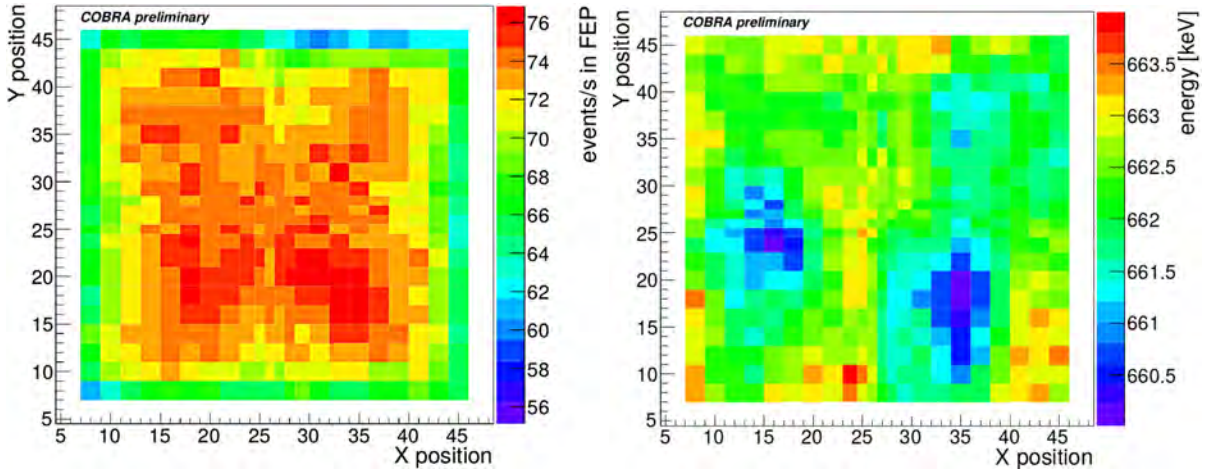

Figure 6: Spatially resolved irradiation of the top side of the detector. Left: The count rate in the full energy peak (FEP) of ^{137}Cs is shown for each source position. Right: The mean energy of the FEP is also quite homogeneous. The x- and y-positions are given in arbitrary units, but the complete anode-plane (20 mm × 20 mm) is shown and the step size of the scanning is 1 mm everywhere except in the middle of both dimension where it is 0.5 mm. Images modified from [**?**].

the top side (where the anode pattern is deposited) are irradiated. It can be seen that changes in the event rate are very small, except at the outer edges of the detector, where there is an enhanced probability of a photon leaving the detector after undergoing Compton scattering. The variations of the reconstructed energy across the detector ($\leq$2 keV) are much smaller than the average energy resolution of the complete detector ($\approx$20 keV FWHM at 662 keV). A similar picture can bee seen in Figure 7 where a scan of one of the lateral sides of the same detector is shown.

Further use of the scanning technique has been made by evaluating the performance of the interaction depth reconstruction with the CPqG detectors. The knowledge of the position of an interaction relative to the electrodes of a detector is a very powerful tool for background reduction in COBRA. With this technique – which has already been successfully employed with

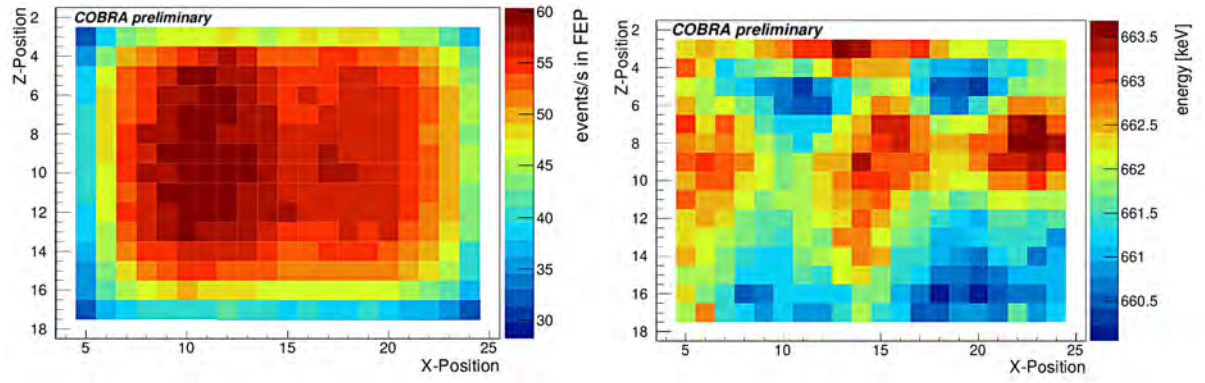

Figure 7: Spatially resolved irradiation of a lateral side wall of the detector. Left: The count rate in the full energy peak (FEP) of ^{137}Cs is shown for each source position. The x- and z-positions are given in arbitrary units, but the complete side-wall (20 mm × 15 mm) is shown and the step size of the scanning is 1 mm. Right: The mean energy of the FEP shows the distribution along the side that does not seem to be correlated with the grid-structure. Images modified from [**?**].

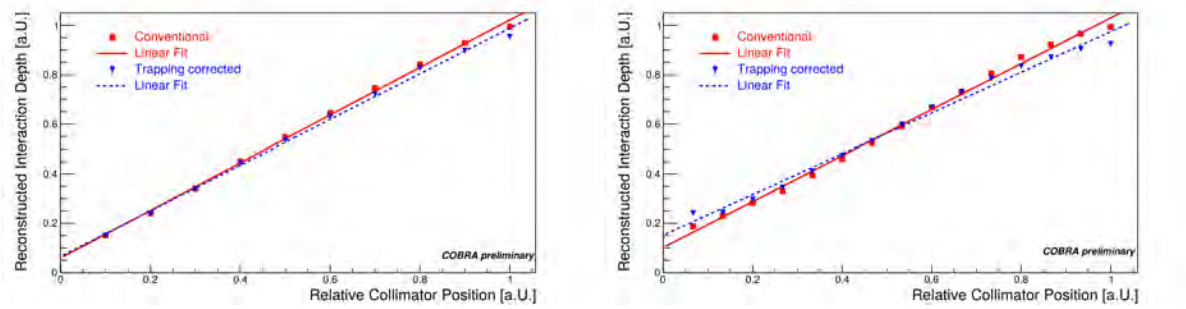

Figure 8: Reconstructed interaction depth (z-position) as a function of the position of the collimated γ-beam for a $1\,\mathrm{cm}^3$ CPG detector (left) and a $6\,\mathrm{cm}^3$ CPqG detector (right). The markers indicate the mean of the depth distribution. The results obtained with the conventional formula are shown in red and the results obtained with the trapping corrected formula are shown in blue. The uncertainties are not visible on this scale.

the singled-grid CPG detectors in the demonstrator phase – it is possible to veto background signals on the electrodes. These occur due to various effects, like the presence of a thin layer of platinum (containing radioactive ^{190}Pt) under the gold electrodes, electrostatic attraction of charged radon daughters to the cathode and surface contaminations in general.

While methods of interaction depth reconstruction is known for nearly as long as the CPG principle itself [**?**, **?**], so far it has not been tested for the coplanar quad-grid detector design, which will be used for the COBRA XDEM phase. The γ-scanning technique made it possible to map a distributions of true interaction depths, derived from the position of the γ-source, to another distribution of reconstructed interaction depths. Consequently the linearity of the relationship between true and reconstructed positions could be tested in this way. The results of this investigation can be seen in Figure 8, where the relationship for a single-grid and for a quad-grid detector is shown. For both detectors, the relationship is tested with the conventional reconstruction shown as red squares and a version which also includes a correction for charge trapping (as derived in [**?**]) as blue triangles. In each case a linear fit has been overlayed. These results show qualitatively that the behavior of the reconstruction is similar for both detector types and an approximate linear relationship is found, although with a slightly higher deviation from linearity in the case of the quad-grid detector. Nevertheless, background vetoing based on the interaction depth will also be possible in the XDEM phase of COBRA [**?**].

4.2 Instrumentation of the guard ring

The operation of the COBRA demonstrator indicates that alpha-induced lateral surface events are the dominant source of background events. All detectors are equipped with a guard ring, which is a boundary electrode surrounding the coplanar-grid anode structure. By instrumenting the guard-ring it is possible to suppress this type of background. Electric field calculations using "Comsol Multiphysics" were done to gain a deeper understanding of this process. The guard ring collects all charges that are generated in the proximity of the surfaces, so that they can be discriminated easily. Figure 9 shows a comparison of a floating guard ring and an instrumented guard ring.

In laboratory measurements the instrumentation of the guard ring achieved a suppression factor for alpha-induced lateral surface events of 5300^{+2660}_{-1380}, while retaining 85.3(1) % of gamma events occurring in the entire detector volume, see a spectrum in Figure 10. This suppression is superior to the pulse shape analysis methods used so far in COBRA by up to three orders of

magnitude. This method of the instrumented guard ring will be used in the coming installation of XDEM and should be as effective there, too. Possible gamma-lines that could be seen then would allow a deeper understanding of the remaining background. Furthermore, the efficiencies of the multi-site event and multi-detector event discrimination (coincidence analysis) could be investigated. The laboratory measurements and electric field simulations concerning this topic were done in 2016, the paper was submitted to arXiv [**?**] and JINST in January 2017.

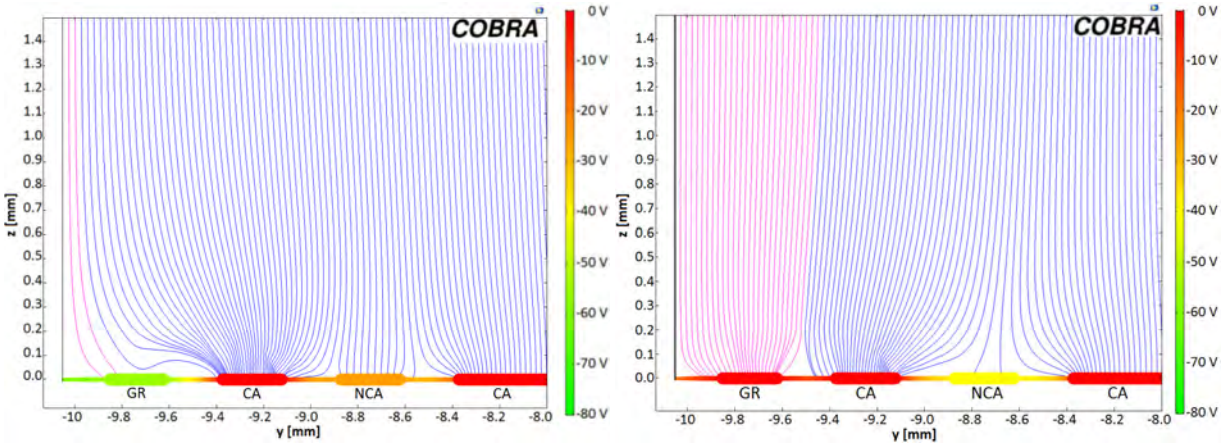

Figure 9: Simulation of electric field. Field lines ending on the guard ring are colored in magenta, those ending on the CPG anodes in blue. Left: floating guard ring. Right: instrumented guard ring.

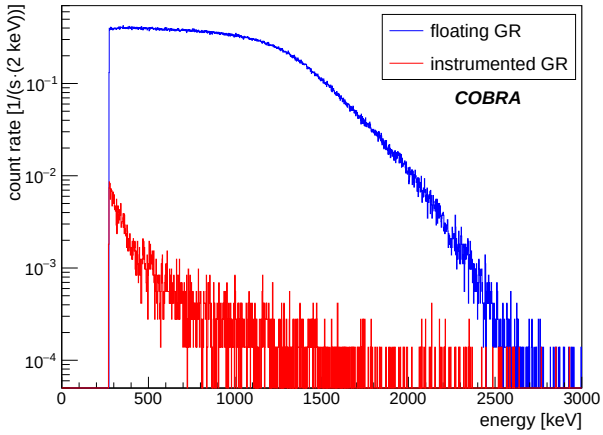

Figure 10: Energy spectra of a detector irradiated with a ^{241}Am alpha-source with the two guard ring configurations.

List of publications in 2016

- J. Ebert et al., *The COBRA demonstrator at the LNGS underground laboratory*, Nucl.Instrum.Meth. A807 (2016) 114-120, arXiv:1507.08177
- J. Ebert et al., *Characterization of a large CdZnTe coplanar quad-grid semiconductor detector*, Nucl.Instrum.Meth. A806 (2016) 159-168, arXiv:1509.02361
- J. Ebert et al., *Long-Term Stability of Underground Operated CZT Detectors Based on the Analysis of Intrinsic Cd-113 β-Decay*, Nucl.Instrum.Meth. A821 (2016) 109-115, arXiv:1508.03217
- J. Ebert et al., *Results of a search for neutrinoless double beta-decay using the COBRA demonstrator*, Phys.Rev. C94 (2016) no.2, 024603, arXiv:1509.04113
- H. Gastrich et al., *The Dortmund Low Background Facility - Low-Background Gamma Ray Spectrometry with an Artificial Overburden*, Appl. Radiat. Isot. 112 (2016) 165-176
- R. Theinert for the COBRA collaboration, *Characterization of a large CdZnTe detector with a coplanar quad-grid design*, Nucl. Instrum. Meth. A 845 (2017) 181
- J.-H. Arling et al., *Suppression of alpha-induced lateral surface events in the COBRA experiment using CdZnTe detectors with an instrumented guard-ring electrode*, submitted to JINST, arXiv:1701.07432

References

CRESST

G. Angloher [a], P. Bauer [a], A. Bento [a,b], C. Bucci [c], L. Canonica [c], X. Defay [d] A. Erb [d,e], F. von Feilitzsch [d], N. Ferreiro [a], P. Gorla [c], A. Gütlein [f,g], D. Hauff [a], J. Jochum [h], M. Kiefer [a], H. Kluck [f,g] H . Kraus [i], J.C. Lanfranchi [d], A. Langenkämper [d], J. Loebell [h], M. Mancuso [a], E. Mondragon [d], A. Münster [d], C. Pagliarone [c], F. Petricca [a,†], W. Potzel [d], F. Pröbst [a], R. Puig [f], F. Reind l[a], J. Rothe [a], K. Schäffner [c], J. Schieck [f,g] V. Schipperges [h], S. Schönert [d], W. Seidel [a,‡], M. Stahlberg [f,g] L. Stodolsky [a], C. Strandhagen [h], R. Strauss [a], A. Tanzke [a], H.H. Trinh Thi [d] C. Türkoğlu [f] M. Uffinger [h], A. Ulrich [d], I. Usherov [h], S. Wawoczny [d], M. Willers [d], M. Wüstrich [a], A. Zöller [d]

[a] *Max-Planck-Institut für Physik, 80805 Munich, Germany*
[b] *Departamento de Fisica, Universidade de Coimbra, 3004 516 Coimbra, Portugal*
[c] *Laboratori Nazionali del Gran Sasso, 67010 Assergi, Italy*
[d] *Technische Universität München, Physik Department, 85747 Garching, Germany*
[e] *Walther-Meißner-Institut für Tieftemperaturforschung, 85748 Garching, Germany*
[f] *Institut für Hochenergiephysik der Österreichischen Akademie der Wissenschaften 1050 Wien, Austria*
[g] *Atominstitut, Vienna University of Technology, 1020 Wien, Austria*
[h] *Eberhard-Karls-Universität Tübingen, 72076 Tübingen, Germany*
[i] *University of Oxford, Department of Physics, Oxford OX1 3RH, UK*
[†] *Spokesperson, e-mail address: petricca@mpp.mpg.de*
[‡] *Deceased*

Abstract

The CRESST experiment is searching for dark matter particles via their elastic scattering off nuclei in a target material. The CRESST target consists of scintillating $CaWO_4$ crystals which are operated as cryogenic calorimeters at millikelvin temperatures and read out by transition edge sensors. Each interaction in the $CaWO_4$ target crystal produces a phonon signal and also a light signal that is measured by a secondary cryogenic calorimeter. The low energy thresholds of these detectors, combined with the presence of light nuclei in the target material, allow to probe the low-mass region of the parameter space for spin-independent dark matter-nucleon scattering with high sensitivity.

1 Introduction

In this era of precision cosmology we know that ordinary matter constitutes less than 5% of the matter in the Universe [1] the remaining 95% is divided by Dark Matter ($\sim$ 27 %) and Dark Energy ($\sim$ 68 %). Despite its large abundance, the nature, the origin, and the composition of Dark Matter (DM) is still unknown. Unraveling this problem is one of the major challenges of modern physics. Direct DM searches exploit a great variety of different detector technologies, all aiming to observe dark matter particles via their scattering off nuclei in their detectors. In the last few years, many direct DM projects have probed with increasing sensitivity the mass-cross section parameter space for DM-nucleus elastic scattering in the so called "WIMP mass region"[2]. Most of these experiments are suitable for DM candidates with masses $\gtrsim$ 30 GeV/c^2, where the sensitivity gain is mainly driven by the exposure. Nevertheless, a number of theoretical models favouring lighter dark matter candidates (e.g. [3, 4, 5, 6, 7]) have recently moved the interest of the community to the mass region below 10 GeV/c^2. As such light dark matter particles produce only very low-energy nuclear recoils (below keV), the challenge for their detection is to achieve a sufficiently low threshold in terms of recoil energy, with enough background discrimination at these low energies. Cryogenic experiments currently provide the best sensitivity for light dark matter particles, with the CRESST-II [8, 10] experiment advancing to the sub-GeV/c^2 dark matter particle mass regime.

2 Detector principle

Cryogenic detectors are low-temperature ($\sim$ 10 - 20 mK) calorimeters that measure the energy deposited in an absorber material by an interacting particle as an increase of temperature in an appropriate temperature sensor. Experiments based on this type of detectors developed strategies to distinguish background from a possible dark matter signal on an event-by-event base.
The CRESST target consists of scintillating $CaWO_4$ crystals (*phonon detectors*). Each interaction in $CaWO_4$ produces a phonon signal in the target crystal, yielding a precise energy measurement (approximately independent of the type of interacting particle), and a light signal that is measured by a secondary independent cryogenic calorimeter (*light detector*) allowing for particle identification [11, 12]. A phonon detector and the corresponding light detector form a so-called *detector module*.
Both, phonon and light detectors are read out via tungsten transition edge sensors (TES) and are equipped with a heater to stabilize the temperature in their operating point in the transition between normal and superconducting state. The heater is also used to inject pulses which are needed for the energy calibration and for the determination of the energy threshold.

3 The CRESST Setup at LNGS

The main part of the facility at LNGS is a cryostat, whose design had to combine the requirements of low temperature with those of low background. As can be seen in Fig. 1, the dilution unit of the cryostat and the dewars containing cryogenic liquids do not extend into the experimental area.

The low temperatures are provided by a ^{3}He-^{4}He dilution refrigerator and transferred to the detectors via a 1.3 m long copper cold finger. The detectors are arranged in a common support structure, the so-called *carousel*, and mounted inside the *cold box* which consists of

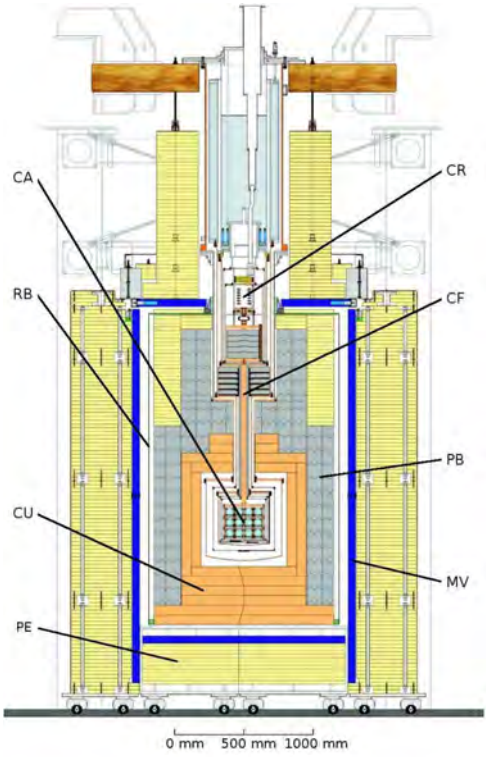

Figure 1: Schematic drawing of the CRESST setup. A cold finger (CF) links the cryostat (CR) to the experimental volume, where the detectors are arranged in a common support structure, the so called carousel (CA). This volume is surrounded by layers of shielding from copper (CU), lead (PB), and polyethylene (PE). The copper and lead shieldings are additionally enclosed in a radon box (RB). An active muon veto (MV) tags events which are induced by cosmic radiation.

five concentric radiation shields surrounding the experimental volume and the cold finger. Two internal cold shields consisting of low-level lead are attached to the mixing chamber ($\sim$ 10 mK) and to a thermal radiation shield at $\sim$ 77 K, respectively, in order to block any line-of-sight from the non-radio-pure parts of the dilution refrigerator to the detectors inside the cold box. The cold box is surrounded by several layers of shielding against the main types of background radiation: layers of highly pure copper and lead shield against γ-rays, while polyethylene serves as a moderator for neutrons. The inner layers of shielding are contained in a gas tight box to prevent radon from penetrating them. In addition, an active muon veto using plastic scintillator panels is installed to tag muons. The veto surrounds the lead and copper shielding and covers 98.7 % of the solid angle around the detectors, a small hole on top is necessary to leave space for the cryostat.

4 Results from CRESST-II Phase 2

CRESST-II Phase 2 operated form July 2013 to August 2015. The DM data acquired in the two years of measurement time was accompanied by calibrations with 122keV γ-rays (^{57}Co-source), high-energy γ-rays (^{232}Th-source) and neutrons (AmBe-source).

The results of this Run were published in two steps [8, 10], reporting the results obtained with two modules, TUM40 and Lise. These modules set leading limits on the spin-independent cross section for elastic DM-nucleon scattering, see Fig. 4. The results of TUM40, the detector

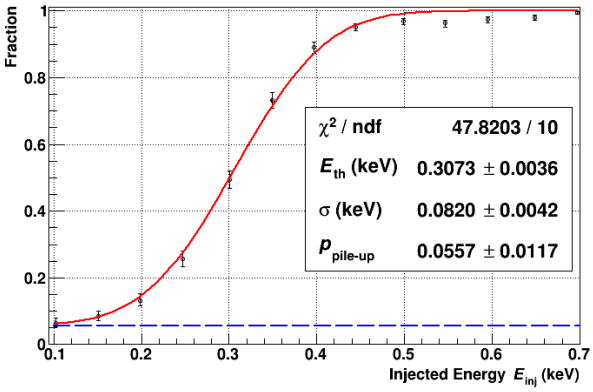

Figure 2: Fraction of heater pulses triggering, injected with discrete energies E_{inj}. The error bars indicate the statistical (binomial) uncertainty at the respective energy. The solid red curve is a fit with the sum of a scaled error function and a constant pile-up probability $p_{\text{pile-up}}$ (blue dashed line). The fit yields an energy threshold of $E_{\mathrm{th}} = (307.3 \pm 3.6)\,\mathrm{eV}$ and a width of $\sigma = (82.0 \pm 4.2)\,\mathrm{eV}$.

module with the best overall performance in terms of background level, trigger threshold and background rejection, were presented in 2014. This non-blind analysis proved that CRESST-II detectors provide reliable data for recoil energies down to the threshold of 0.6 keV [8]. As a consequence of this observation, the trigger thresholds of several detectors were optimized, achieving the lowest value of 0.3 keV with the module Lise. The results obtained from 52.2 kg·days of data taken with the module Lise with its threshold set at 0.3 keV are reported in [8]. It has to be stressed that the lower threshold of Lise (and TUM40) is neither connected to the holding concept, nor to the intrinsic background level of the crystal, but arises from a superior performance of the phonon sensor.

The threshold of the detector is determined directly by injecting low-energy heater pulses with a shape similar to pulses induced by particle interactions and measuring the fraction causing a trigger. The result of this dedicated measurement is illustrated in Fig. 2. The methods used for the analysis of the data are thoroughly described and discussed in [8, 10] and references therein. A blind analysis was carried out by first defining a statistically insignificant part of the data set as a training set, on which all methods of data preparation and selection are developed, that are then applied blindly without any change to the final data set. The validity of this approach is exhaustively discussed in [10]. The survival probability of the signal in the data selection is determined by performing the cuts on a set of artificial pulses with discrete energies. The fraction of signals with a certain simulated energy passing each cut yields the respective survival probability. All events surviving the selection criteria, corresponding to the 52.2 kg·days of exposure of the detector Lise, are presented in Fig. 3 in the light yield - energy plane. The light yield is defined for every event as the ratio of light to phonon signal. Electron recoils have a light yield set to one by calibration (at 122 keV). Nuclear recoils produce less light than electron recoils. The reduction is quantified by the quenching factors for the respective target nuclei, which are precisely known from dedicated independent measurements [9]. In Fig. 3 the solid blue lines mark the 90% upper and lower boundaries of the e^-/γ-band, with 80 % of electron recoil events expected in between. From this band, with the knowledge of the quenching factors for the different nuclei present in the target material, the nuclear recoil bands for scatterings off tungsten, calcium and oxygen (respectively solid green, not shown and solid red in Fig. 3) can be analytically calculated. The e^-/γ-band exhibits two prominent features, a double-peak

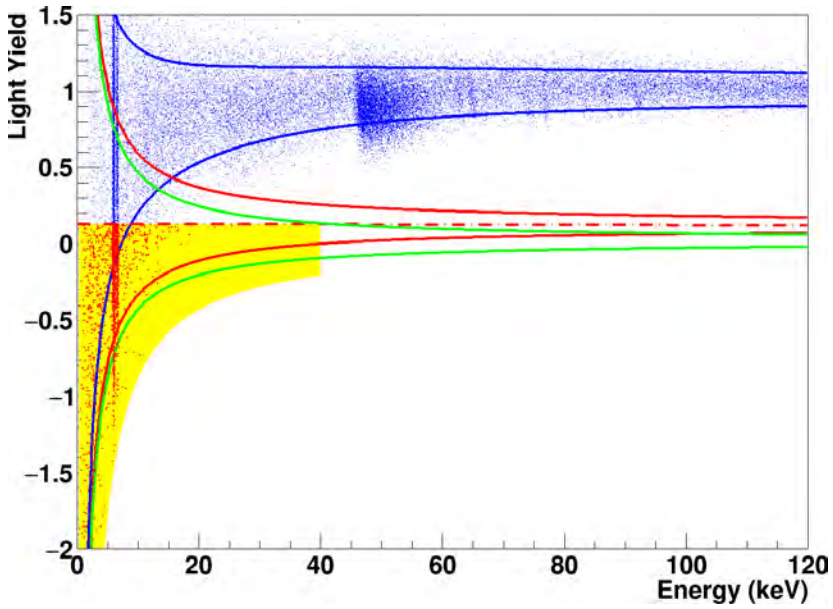

Figure 3: Data taken with the detector module Lise depicted in the light yield - energy plane. The solid lines mark the 90 % upper and lower boundaries of the e^-/γ-band (blue), the band for recoils off oxygen (red) and off tungsten (green). The upper boundary of the acceptance region (yellow area) is set to the middle of the oxygen band (dashed dotted red), the lower one to the 99.5 % lower boundary of the tungsten band. Events therein are additionally highlighted in red.

at $\sim$ 6 keV originating from an external ^{55}Fe-source and a β-decay spectrum from an intrinsic contamination of the crystal with ^{210}Pb starting at 46.5 keV. The acceptance region for the dark matter analysis (yellow region in Fig. 3) extends in energy from the threshold of 307 eV to 40 keV and in light yield the from the 99.5 % lower boundary of the tungsten band to the center of the oxygen band (dashed-dotted red line in Fig. 3).

For the calculation of the exclusion limit all events inside the acceptance region (highlighted in red) are considered as potential signal events. This assumption is extremely conservative due to the clear large leakage of e^-/γ-events into the acceptance region, which is caused by the limited resolution of the light detector in use in this detector module. Using the Yellin optimum interval method [13, 14] to calculate an upper limit with 90 % confidence level on the elastic spin-independent interaction cross-section of dark matter particles with nucleons, the exclusion limit resulting from the blind analysis reported in [10] is drawn in solid red in figure 4. For dark matter particle masses higher than 5 GeV/c^2 this module does not have a competitive sensitivity due to the large number of background events present in the acceptance region. However, for dark matter particles lighter than 2 GeV/c^2 we explore new regions of the parameter space. The improvement with respect to the 2014 result [8] (red dashed line) is due to the significantly lower threshold of the detector Lise and to the almost constant background level down to the threshold. The result for the first time extends the reach of direct dark matter searches to dark matter particle masses down to 0.5 GeV/c^2.

5 From CRESST-II to CRESST-III

The results of CRESST-II and the growing interest in the scientific community to explore DM regions different from the WIMP parameter space moved the focus of CRESST to explore the low DM mass part of the parameter space. The sensitivity in this region is dominated by the

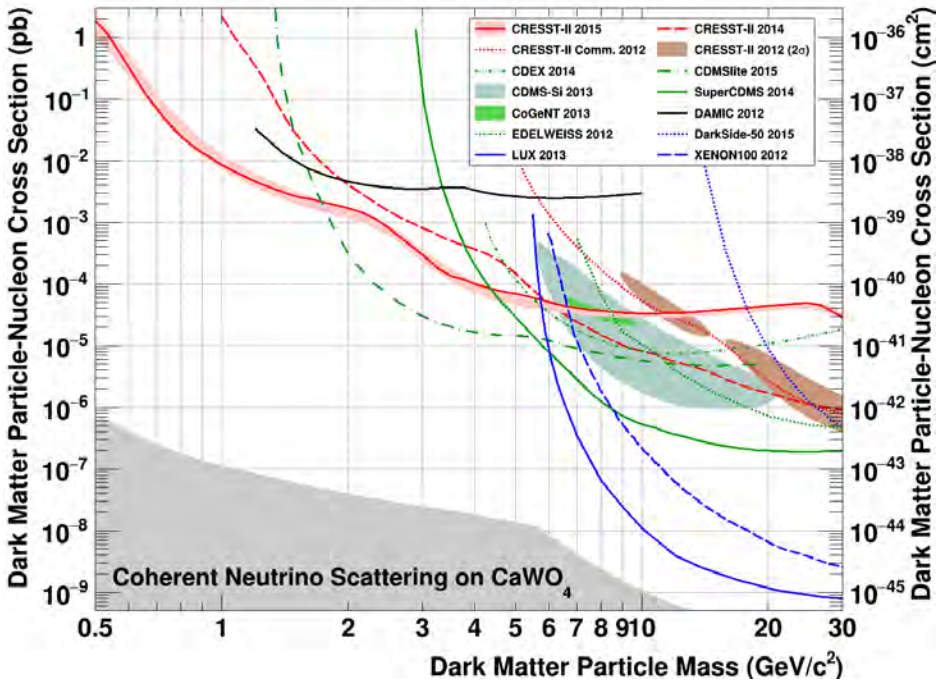

Figure 4: Parameter space for elastic spin-independent dark matter-nucleon scattering. The result from the analysis presented in [10] is drawn in solid red together with the expected sensitivity (1σ confidence level (C.L.)) from a data-driven background-only model (light red band). The remaining red lines correspond to previous CRESST-II limits [8, 15]. The favored parameter space reported by CRESST-II phase 1 [16], CDMS-Si [17] and CoGeNT [18] are drawn as shaded regions. For comparison, exclusion limits (90 % C.L.) of the liquid noble gas experiments [19, 20, 21] are depicted in blue, from germanium and silicon based experiments in green [22, 23, 24, 25, 26]. In the gray area coherent neutrino nucleus scattering, dominantly from solar neutrinos, will be an irreducible background for a $CaWO_4$-based dark matter search experiment [27].

performances (threshold) of the detectors. This is related to the fact that the spectrum of DM interaction for a given target material becomes steeper as the mass decreases. The amount of events that drops below a given threshold thus increases for lower DM masses. As a consequence lowering the threshold of the detectors open the access to parameters space regions that are strongly suppressed for higher threshold detectors. CRESST-II set a new state of the art for low threshold DM exploration opening the way to the exploration of sub GeV DM candidates.

The evolution of the CRESST performance during CRESST-II is related mainly to the evolution of the TES sensors. Further improvements can be obtained acting also on the design of the detector. One relevant parameter is the size of the absorber crystal, that is proportional to the density of athermal phonos generated by a given energy release. Reducing the volume of the crystal the density of phonons increases giving rise to a better phonon collection. If the noise is dominated by non thermal effects (electronic chain, DAQ, etc.) the S/N will increase consequently improving the achievable threshold.

Following these considerations, a new detector module with a ~ 24 g $CaWO_4$ absorber crystal was developed to replace the $\sim$ 200-250 g crystals used in CRESST-II. In fig 5 a schematic view of the new CRESST module and a picture of one of the CRESST-III detectors are shown. The goal for this setup is to increase the sensitivity of about an order of magnitude in cross section exploring the full region between ~ 7 and 0.5 GeV at the level of 10^{-41} cm^2 (10^{-5} pb). A more

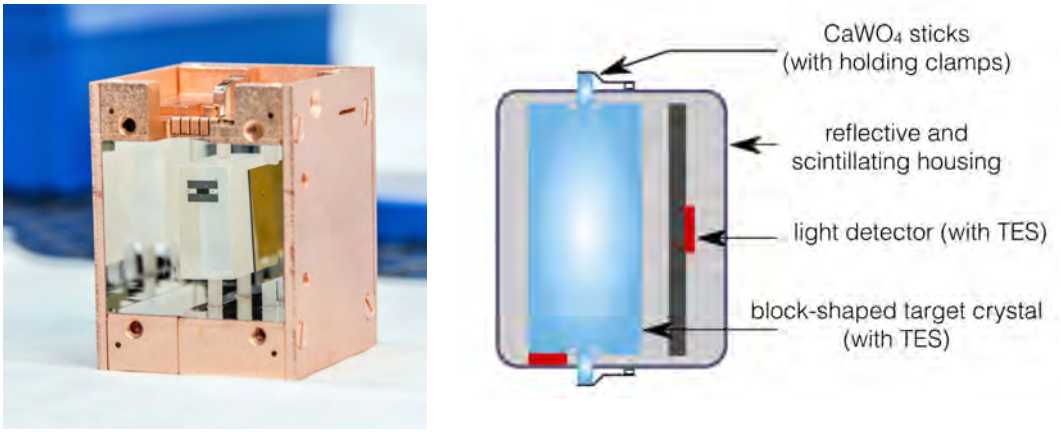

Figure 5: 24 g CRESST-III module. Left: picture of the module during preparation of Phase 1, with one of the side copper shields open. The $CaWO_4$ crystal (with the TES) and the light detector, both held by crystal sticks, are clearly visible inside the reflecting enclosure. Right : schematic sketch of the detector module.

detailed plan of the CRESST-III strategy can be found in [29] with a discussion of the needed performances to achieve the planned sensitivities. A conservative goal threshold of 100 eV has been set for the CRESST-III phase 1 detectors.

5.1 CRESST-III Phase 1

CRESST-III Phase 1 is an array of 10 modules, for a total mass of $\sim$ 240 g of $CaWO_4$. Seven of these crystals are of CRESST-II quality [28] , while three are $CaWO_4$ crystal of improved quality. The latter are grown in the crystal growth facility at TUM (Technische Universität München) from raw material which was purified by an extensive chemical treatment. Each of the modules requires three read-out channels. One is connected to the phonon detector ($CaWO_4$ absorber), one to the light detector and one to the instrumented holding sticks. Thelatter are implemented to veto possible events in the holding sticks themselves. The sticks of each holding system are purposely connected to a single SQUID to minimise the need of read out channels.

The CRESST cryostat was cooled down in May 2016. The cool down was followed by the commissioning of the detectors, a first brief gamma calibration needed for a first estimate of the detector sensitivity, a short period of data ($\sim$ 300 h) to gain a first understanding of detector performance and a second extensive gamma calibration. The latter was required to collect a large statistical samples of particle pulses needed for the subsequent analysis of the data and for a precise determination of the calibration factors for the different detectors in their final operating points. Since October the experiment is collecting dark matter data.

With a net exposure of 50 kg days we anticipate a significant progress in the exploration of the low-mass regime with an expected sensitivity shown in figure 6 assuming crystals of CRESST-II radiopurity. The reachable sensitivity is shown for for a threshold of 100 eV on 10 modules of TUM-40 quality.

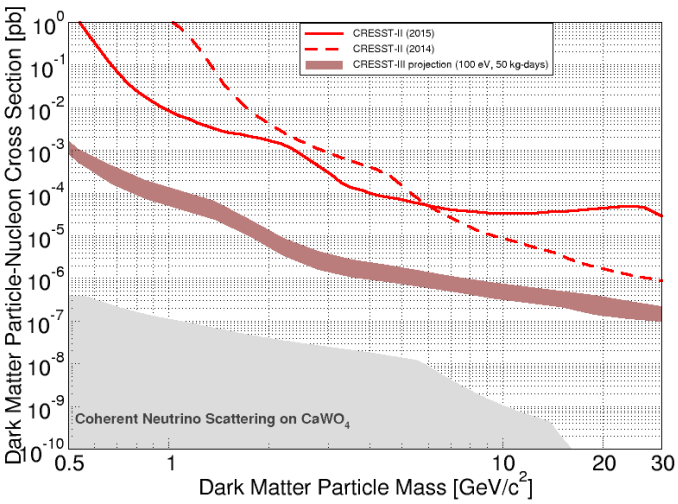

Figure 6: Sensitivity of CRESST-3 Phase 1. The reachable sensitivity is estimated for a threshold of 100 eV on 10 modules of TUM-40 quality.

6 Conclusions and Outlook

With an exposure of 52 kg live days and a threshold of 307 eV for nuclear recoils we obtain in [10] an unprecedented sensitivity for light dark matter, probing a new region of parameter space for dark matter particles of masses below 2 GeV/c^2, previously not covered in direct detection searches. With the results obtained we extend the reach of direct dark matter searches to the sub-GeV/c^2 region and we prove that a low energy threshold is the key requirement to achieve sensitivity to dark matter particles of 1 GeV/c^2 and below.
CRESST-III Phase 1, currently taking data at Laboratori Nazionali del Gran Sasso, with a goal threshold of 100 eV will improve the sensitivity of about an order of magnitude, shading light on a so far unexplored part of the DM parameter space.

7 List of Publications

1. G. Angloher et al., (CRESST Collaboration): Results on light dark matter particles with a low-threshold CRESST-II detector
Eur. Phys. J. C. 76 (2016) 25, arXiv:1509.01515[astro-ph.CO]

2. M. Kiefer et al., (CRESST Collaboration): In-situ study of light production and transport in phonon light detector modules for dark matter search NIM A 821 Pages: 116-121 (2016)

3. G. Angloher et al., (CRESST Collaboration): Limits on Momentum-Dependent Asymmetric Dark Matter with CRESST-II
Phys. Rev.. Lett. 117 Issue: 2 Article Number: 021303 (2016)

4. R. Strauss et al., (CRESST Collaboration):Exploring Low-Mass Dark Matter with CRESST
Jou. Low Temp. Phys. 184 Issue: 3-4 Pages: 866-872 (2016)

5. G. Angloher et al., (CRESST Collaboration): New limits on double electron capture of Ca-40 and W-180 Jou. of Phys. G 43 Issue: 9 (2016) arXiv:1604.08493

6. F. Petricca et al. , (CRESST Collaboration): New results on low-mass dark matter from the CRESST-II experiment
   Jou. of Phys. Conference Series 718 (2016) Conference: 14th International Conference on Topics in Astroparticle and Underground Physics (TAUP)

7. R. Strauss et al., (CRESST Collaboration): The CRESST-III low-mass WIMP detector
   Jou. of Phys. Conference Series 718 (2016) Conference: 14th International Conference on Topics in Astroparticle and Underground Physics (TAUP)

Acknowledgements

We are grateful to LNGS for the generous support of CRESST.

References

[1] P.A.R.Ade et al. (Planck Collaboration): 2014 A&A 571 A16, arXiv:1303.5076 [astro-ph.CO].
[2] P. Cushman et al.: arXiv:1310.8327 [hep-ex].
[3] T. Cohen et al.: Phys. Rev. D82 (2010) 056001, arXiv:1005.1655 [hep-ph].
[4] D. E. Kaplan et al.: Phys. Rev. D79 (2009) 115016, arXiv:0901.4117 [hep-ph].
[5] K. Sigurdson et al.: Phys. Rev. D70 (2004) 083501, arXiv:astro-ph/0406355.
[6] J. Fortin et al.: Phys. Rev. D85 (2012) 063506, arXiv:1103.3289 [hep-ph].
[7] J. Feng et al.: Phys. Lett. B 704 (2011) 534, arXiv:1102.4331 [hep-ph].
[8] G. Angloher et al., (CRESST Collaboration): Eur. Phys. J. C 74 (2014) 3184, arXiv:1407.3146[astro-ph.CO].
[9] R. Strauss et al., (CRESST Collaboration): Eur. Phys. J. C 74 (2014) 2957, arXiv:1401.3332[astro-ph.IM].
[10] G. Angloher et al., (CRESST Collaboration): Eur. Phys. J. C 76 (2016) 25, arXiv:1509.01515[astro-ph.CO].
[11] G. Angloher et al., (CRESST Collaboration): Astropart.Phys. 23 (2005) 325-339, arXiv:astro-ph/0408006.
[12] G. Angloher et al., (CRESST Collaboration): Astropart.Phys. 31 (2009) 270-276, arXiv:0809.1829[astro-ph].
[13] S. Yellin: Phys. Rev. D 66, 032005 (2002), arXiv:physics/0203002[physics.data-an].
[14] S. Yellin: Software for computing an upper limit given unknown background (02/2011) http://cdms.stanford.edu/Upperlimit/
[15] A. Brown et al.: Phys. Rev. D 85, 021301 (2012), arXiv:1109.2589[astro-ph.CO].
[16] G. Angloher et al., (CRESST Collaboration): 2012 Eur. Phys. J. C 72 (2012) 1971, arXiv:1109.0702[astro-ph.CO].
[17] R. Agnese et al., (CDMS Collaboration): Phys. Rev. Lett. 111, 251301 (2013), arXiv:1304.4279[hep-ex].
[18] C.E. Aalseth et al., (CoGeNT Collaboration): Phys. Rev. D 88, 012002 (2013), arXiv:1208.5737[astro-ph.CO].
[19] P. Agnes et al., (DarkSide Collaboration): Phys. Lett. B 743 (2015) 456-466, arXiv:1410.0653[astro-ph.CO].

[20] D.S. Akerib et al., (LUX Collaboration): 2014 Phys. Rev. Lett. 112, 091303 (2014), arXiv:1310.8214[astro-ph.CO].

[21] E. Aprile et al., (XENON100 Collaboration): Phys. Rev. Lett. 109, 181301 (2012), arXiv:1207.5988[astro-ph.CO].

[22] Q. Yue et al., (CDEX Collaboration): Phys. Rev. D 90 (2014) 091701, arXiv:1404.4946[hep-ex].

[23] R. Agnese et al., (SuperCDMS Collaboration): accepted for publication in Phys. Rev. Lett. (2015), arXiv: 1509.02448[astro-ph.CO].

[24] R. Agnese et al., (SuperCDMS Collaboration): Phys. Rev. Lett. 112, 241302 (2014), arXiv:1402.7137 [hep-ex].

[25] J. Barreto et al.: Physics Letters B 711 (2012) 264-269, arXiv:1105.5191 [astro-ph.IM].

[26] E. Armengaud et al., (EDELWEISS Collaboration): Phys. Rev. D 86 (2012) 051701, arXiv:1207.1815[astro-ph.CO].

[27] A. Gütlein et al., (CRESST Collaboration): Astropart. Phys. 69 (2015) 44-49, arXiv:1408.2357[hep-ph].

[28] A. Munster et al., (CRESST Collaboration) Jou. Cosm. and Astropar. Phys. 5 Article Number: 018 (2014)

[29] G. Angloher *et al.* [CRESST Collaboration], arXiv:1503.08065 [astro-ph.IM].

CUORE

C. Alduino,[1] K. Alfonso,[2] D. R. Artusa,[1,3] F. T. Avignone III,[1] O. Azzolini,[4] T. I. Banks,[5,6] G. Bari,[7] J.W. Beeman,[8] F. Bellini,[9,10] G. Benato,[5] A. Bersani,[11] M. Biassoni,[12,13] A. Branca,[14] C. Brofferio,[12,13] C. Bucci,[3] A. Camacho,[4] A. Caminata,[11] L. Canonica,[15,3] X. G. Cao,[16] S. Capelli,[12,13] L. Cappelli,[3] L. Carbone,[13] L. Cardani,[9,10] P. Carniti,[12,13] N. Casali,[9,10] L. Cassina,[12,13] D. Chiesa,[12,13] N. Chott,[1] M. Clemenza,[12,13] S. Copello,[17,11] C. Cosmelli,[9,10] O. Cremonesi[a],[13] R. J. Creswick,[1] J. S. Cushman,[18] A. D'Addabbo,[3] I. Dafinei,[10] C. J. Davis,[18] S. Dell'Oro,[3,19] M. M. Deninno,[7] S. Di Domizio,[17,11] M. L. Di Vacri,[3,20] A. Drobizhev,[5,6] D. Q. Fang,[16] M. Faverzani,[12,13] G. Fernandes,[17,11] E. Ferri,[13] F. Ferroni,[9,10] E. Fiorini,[13,12] M. A. Franceschi,[21] S. J. Freedman[b],[6,5] B. K. Fujikawa,[6] A. Giachero,[13] L. Gironi,[12,13] A. Giuliani,[22] L. Gladstone,[15] P. Gorla,[3] C. Gotti,[12,13] T. D. Gutierrez,[23] E. E. Haller,[8,24] K. Han,[25] E. Hansen,[15,2] K. M. Heeger,[18] R. Hennings-Yeomans,[5,6] K. P. Hickerson,[2] H. Z. Huang,[2] R. Kadel,[26] G. Keppel,[4] Yu. G. Kolomensky,[5,6] A. Leder,[15] C. Ligi,[21] K. E. Lim,[18] Y. G. Ma,[16] M. Maino,[12,13] L. Marini,[17,11] M. Martinez,[9,10,27] R. H. Maruyama,[18] Y. Mei,[6] N. Moggi,[28,7] S. Morganti,[10] P. J. Mosteiro,[10] T. Napolitano,[21] M. Nastasi,[12,13] C. Nones,[29] E. B. Norman,[30,31] V. Novati,[22] A. Nucciotti,[12,13] T. O'Donnell,[32] J. L. Ouellet,[15] C. E. Pagliarone,[3,33] M. Pallavicini,[17,11] V. Palmieri,[4] L. Pattavina,[3] M. Pavan,[12,13] G. Pessina,[13] V. Pettinacci,[10] G. Piperno,[9,10] C. Pira,[4] S. Pirro,[3] S. Pozzi,[12,13] E. Previtali,[13] C. Rosenfeld,[1] C. Rusconi,[1,3] M. Sakai,[2] S. Sangiorgio,[30] D. Santone,[3,20] B. Schmidt,[6] J. Schmidt,[2] N. D. Scielzo,[30] V. Singh,[5] M. Sisti,[12,13] A. R. Smith,[6] L. Taffarello,[14] M. Tenconi,[22] F. Terranova,[12,13] C. Tomei,[10] S. Trentalange,[2] M. Vignati,[10] S. L. Wagaarachchi,[5,6] B. S. Wang,[30,31] H. W. Wang,[16] B. Welliver,[6] J. Wilson,[1] L. A. Winslow,[15] T. Wise,[18,34] A. Woodcraft,[35] L. Zanotti,[12,13] G. Q. Zhang,[16] B. X. Zhu,[2] S. Zimmermann,[36] and S. Zucchelli[37,7]

[1] *Department of Physics and Astronomy, University of South Carolina, Columbia, SC 29208, USA*

[2] *Department of Physics and Astronomy, University of California, Los Angeles, CA 90095, USA*

[3] *INFN – Laboratori Nazionali del Gran Sasso, Assergi (L'Aquila) I-67100, Italy*

[4] *INFN – Laboratori Nazionali di Legnaro, Legnaro (Padova) I-35020, Italy*

[5] *Department of Physics, University of California, Berkeley, CA 94720, USA*

[6] *Nuclear Science Division, Lawrence Berkeley National Laboratory, Berkeley, CA 94720, USA*

[a] Spokesperson: O. Cremonesi, cuore-spokesperson@lngs.infn.it

[b] Deceased

[7] *INFN – Sezione di Bologna, Bologna I-40127, Italy*

[8] *Materials Science Division, Lawrence Berkeley National Laboratory, Berkeley, CA 94720, USA*

[9] *Dipartimento di Fisica, Sapienza Università di Roma, Roma I-00185, Italy*

[10] *INFN – Sezione di Roma, Roma I-00185, Italy*

[11] *INFN – Sezione di Genova, Genova I-16146, Italy*

[12] *Dipartimento di Fisica, Università di Milano-Bicocca, Milano I-20126, Italy*

[13] *INFN – Sezione di Milano Bicocca, Milano I-20126, Italy*

[14] *INFN – Sezione di Padova, Padova I-35131, Italy*

[15] *Massachusetts Institute of Technology, Cambridge, MA 02139, USA*

[16] *Shanghai Institute of Applied Physics, Chinese Academy of Sciences, Shanghai 201800, China*

[17] *Dipartimento di Fisica, Università di Genova, Genova I-16146, Italy*

[18] *Department of Physics, Yale University, New Haven, CT 06520, USA*

[19] *INFN – Gran Sasso Science Institute, L'Aquila I-67100, Italy*

[20] *Dipartimento di Scienze Fisiche e Chimiche,*
Università dell'Aquila, L'Aquila I-67100, Italy

[21] *INFN – Laboratori Nazionali di Frascati, Frascati (Roma) I-00044, Italy*

[22] *CSNSM, Univ. Paris-Sud, CNRS/IN2P3,*
Université Paris-Saclay, 91405 Orsay, France

[23] *Physics Department, California Polytechnic State University, San Luis Obispo, CA 93407, USA*

[24] *Department of Materials Science and Engineering,*
University of California, Berkeley, CA 94720, USA

[25] *Department of Physics and Astronomy,*
Shanghai Jiao Tong University, Shanghai 200240, China

[26] *Physics Division, Lawrence Berkeley National Laboratory, Berkeley, CA 94720, USA*

[27] *Laboratorio de Fisica Nuclear y Astroparticulas,*
Universidad de Zaragoza, Zaragoza 50009, Spain

[28] *Dipartimento di Scienze per la Qualità della Vita,*
Alma Mater Studiorum – Università di Bologna, Bologna I-47921, Italy

[29] *Service de Physique des Particules, CEA / Saclay, 91191 Gif-sur-Yvette, France*

[30] *Lawrence Livermore National Laboratory, Livermore, CA 94550, USA*

[31] *Department of Nuclear Engineering, University of California, Berkeley, CA 94720, USA*

[32] *Center for Neutrino Physics, Virginia Polytechnic Institute*
and State University, Blacksburg, Virginia 24061, USA

[33] *Dipartimento di Ingegneria Civile e Meccanica,*
Università degli Studi di Cassino e del Lazio Meridionale, Cassino I-03043, Italy

[34] *Department of Physics, University of Wisconsin, Madison, WI 53706, USA*

[35] *SUPA, Institute for Astronomy, University of Edinburgh, Blackford Hill, Edinburgh EH9 3HJ, UK*

[36] *Engineering Division, Lawrence Berkeley National Laboratory, Berkeley, CA 94720, USA*
[37] *Dipartimento di Fisica e Astronomia, Alma Mater Studiorum – Università di Bologna, Bologna I-40127, Italy*

CUORE (Cryogenic Underground Observatory for Rare Events) is an experiment which aims to achieve a half-life sensitivity of 10^{26} years for neutrinoless double beta decay ($0\nu\beta\beta$ decay) in ^{130}Te using cryogenic bolometry. $0\nu\beta\beta$ decay is one of the most sensitive probes for physics beyond the Standard Model, providing unique information on the nature of neutrinos. With this sensitivity we will begin to explore the inverted hierarchy region of neutrino masses. The detector consists of a close-packed array of TeO_2 crystals containing $\sim$206 kg of ^{130}Te in total which will be cooled to an operating temperature of $\sim$10 mK inside a large, dedicated cryostat.

In the enclosed report we summarize the activities of the collaboration in the past year at LNGS. It has been a productive period for CUORE in which we have successfully completed the critical installation and stable cool-down phases and are now at the cusp of starting the scientific mission of the experiment.

I. CUORE DETECTOR OVERVIEW

The CUORE detector consists of 988 ultra-radiopure TeO_2 crystals arranged into 19 identical towers. Each crystal is a state-of-the-art cryogenic bolometer that serves as both the source and detector of $0\nu\beta\beta$ decay in ^{130}Te. Each tower consists of 52 crystals held inside a copper structure by teflon (PDFE) brackets in an arrangement of 13 four-crystal floors as shown in Fig. (1).

A neutron transmutation doped (NTD) germanium thermistor and a joule heater are glued to one face of each crystal. The thermistors measure the μK-scale temperature fluctuations due to particle interactions with the crystal while the heaters provide a calibrated pulse of energy to the crystal for diagnostic an analysis purposes. These sensors are wire-bonded directly to readout ribbons held by copper trays fixed to the tower structure. All copper components directly facing the crystals were cleaned using an aggressive and intricate cleaning procedure developed and executed at Legnaro National Laboratory (LNL). To minimize recontamination of components during subsequent handling, all the towers were constructed in dedicated fluxed glove boxes for each assembly step.

In 2016, the installation phase was completed and the detector will now embark upon its scientific mission.

FIG. 1: Detailed view of the components of a single CUORE tower.

II. END OF CUORE CRYOSTAT COMMISSIONING

In early 2016, we successfully completed the commissioning of the Cryogenic Underground Observatory for Rare Events (CUORE) cryostat with the "Run 4" cooldown. During this run, we operated an 8 channel "Mini-Tower" at 10 mK. In terms of the cryogenic performance, the primary takeaway message of Run 4 was the need to minimize vibrations on the Main Support Plate (MSP), and we spent much of 2017 achieving this.

Prior to Run 4, the motor heads and the flex-lines were resting on the MSP and were transferring part of their vibrational energy to the cryostat. We re-routed the high-pressure helium lines such that they do not touch the MSP at any point. These lines now run along the inside of the Faraday Cage (FC) and drop down to their respective motor-heads without touching the MSP (see Figs. 2a and 2b). We switched to a combination of rigid and flexible lines inside the FC and all of them are

covered with neoprene sheets to reduce the ambient acoustic noise. We suspended the motor-heads from the ceiling so that they do not touch the MSP. We use ceramic isolators on the flex-lines to isolate their grounding from the FC. Outside the FC, the flex-lines pass through a custom made sandbox (Fig. 2c) to reduce the transmitted vibration from the pulse tube compressors on the ground floor of the CUORE hut.

We also modified the pumping system of the Dilution Unit (DU) to minimize vibrations to the cryostat. We installed a double gimbal movement joint on the Still pumping line to mitigate the vibrations originating from the Roots and the Turbo vacuum pumps. Further, we rigidly coupled the cryostat to the MSP to increasing its inertia to mechanical movements.

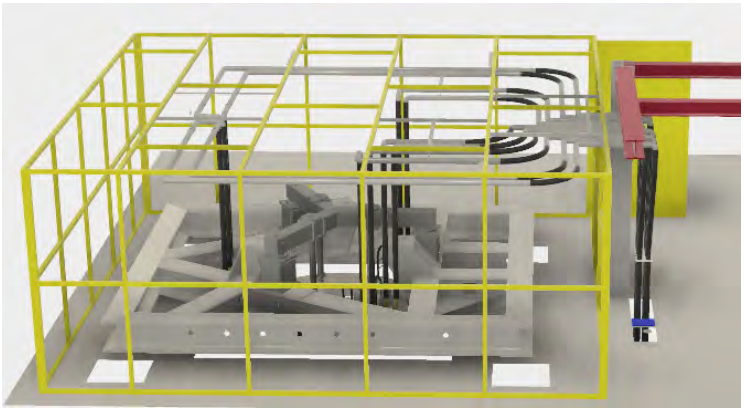

(a)

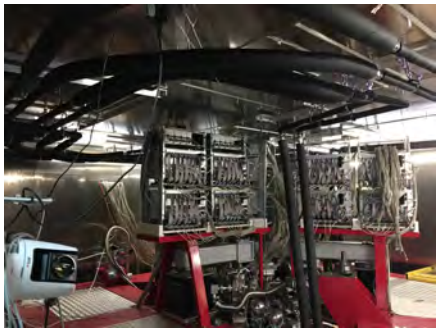

(b)

(c)

FIG. 2: (a) Layout of the flex-lines inside the FC. (b) High-pressure helium lines from the compressors running along the roof of the Faraday cage on the 2nd floor of CUORE hut. (c) All high-pressure lines pass through a sandbox at the ground floor to dampen vibrations from the compressors.

During Run 4, we also had to deal with the blockage of one of the two condensing lines in the DU circulation unit. We are not sure of the exact cause, but some burnt residue was found on

the exhaust side of the Roots pump, possibly indicating the presence of hydrocarbon/hydrogen.We have replaced the faulty pump and installed an inline gas filter for the helium circulation line. This should prevent a small amount of impurity in the gas circulation line from choking the circulation in the future.

In preparation for the detector cooldown, we re-cleaned the vacuum vessels (300 K and 4 K vessels) and the radiation shields (shields at 40 K, 600 mK and 50 mK stages). We rinsed the surfaces with ultra-clean water to remove dirt and oil and then chemically etched the copper surfaces with a combination of 5% citric acid and 5% hydrogen peroxide solution. This cleaning resulted in visibly shinier surfaces which have the added benefit of reflecting radiation and helping to reduce the heat load on the inner vessels. Figure 3 shows the 50 mK vessel before and after the cleaning procedure. We also replaced the super-insulation on the 40 K and 4 K stage thermal shields.

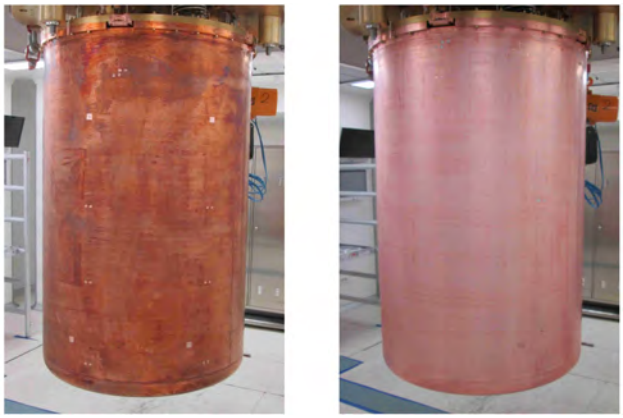

FIG. 3: Radiation shield at 50 mK stage, before (left) and after (right) the chemical etching.

III. DETECTOR CALIBRATION COMMISSIONING

The CUORE Detector Calibration System (DCS) deploys radioactive sources through the CUORE shielding and places them close to the detectors in order to calibrate each bolometer in the array. This requires moving the sources from room temperature into the 10 mK environment without disrupting the detector operation. Key features of this system include the active cooling through a mechanical squeezing contact at 4 K, motion of the lightweight source string under gravity to minimize friction and frictional heating, and the construction from pure and clean materials. The detector calibration group, lead by the Yale group, completed commissioning of this system

in early 2016 during Run 4 and published a detailed technical report in NIM (Nucl. Instrum. Methods A **844**, 32-44 (2017)).

During Run 4, we performed a full system test of the DCS. We successfully deployed all source strings and then extracted them, without raising the cryostat base temperature above 10 mK. We did see the base temperature increase during string deployment, but since the temperature never exceeded the expected operating temperature of the CUORE detector, this warming can be absorbed by a temperature stabilization system. Thus, we have verified that the calibration system has the ability to perform a full calibration sequence without affecting the temperature and operation of the detectors.

There are 12 source strings in total, split into 6 inner strings between the detector towers and and 6 outer strings surrounding the detector array. We began by testing individual inner strings to study the response of the cryostat to the warm calibration sources. We found that a "precooling" process of leaving the calibration sources overnight in tubes with a thermal gradient from 300 K to 4 K was very effective at removing heat from the sources. This, coupled with our active thermalization system at 4 K, allowed us to lower the source strings until they reached the mixing chamber level with only minimal effect on the cryostat base temperature. Once the strings passed this point, their effect on the cryostat increased significantly, and we found that we must lower one inner string at a time in this most sensitive region, a process that takes approximately 2 hours (see Fig. 4). Once this was established, we were able to develop more complete deployment plans, such that we are able to deploy all 12 calibration strings in under 24 hours, meeting our design goals for the experiment.

During source extraction, the heat load on the cryostat is almost entirely due to friction. This limits the speed with which we can extract a string to 10 mm/minute for the inner strings and 15 mm/minute for the outer strings. We extract the strings in pairs, one inner and one outer string at a time. We can begin to extract the next pair of strings when the previous pair is above the mixing chamber. In the warmer parts of the cryostat, extraction can continue at significantly greater speeds without impacting the base temperature. A 12-string, 16-hour extraction is represented in Fig. 5.

IV. RADON ABATEMENT AND CLEAN ROOM

To maintain radiopurity during detector construction, the CUORE towers were assembled and stored in a nitrogen atmosphere. Given that such an arrangement would not have been possible

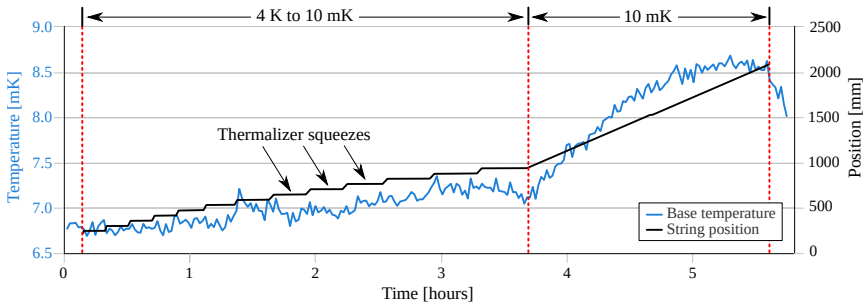

FIG. 4: Cryostat base temperature and string position during a full inner-string deployment. Downward motion is in the positive direction. Two regions are identified; the first consists of progressively longer thermalizer squeezes while the bottom of the string moves from the 4 K cryostat plate to the 10 mK plate, and the second is the movement of the string through the 10 mK plate to its final deployment position.

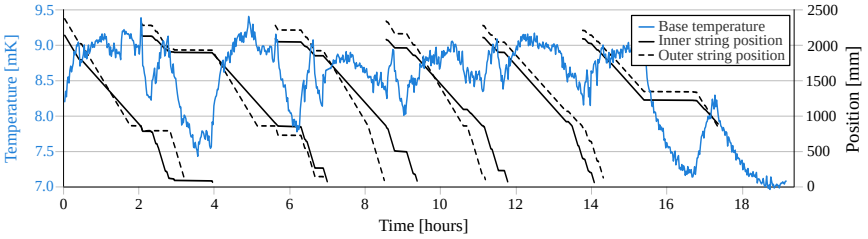

FIG. 5: Cryostat base temperature and string positions during a 12-string extraction. The 12 downward-going black lines represent the positions of the 12 strings (upward motion is in the negative direction). In this procedure, the strings were extracted from their deployment positions to their precooling positions near the 4 K plate. Horizontal segments in the lines representing the string positions correspond to periods of no motion to observe the temperature response and recovery time of the cryostat.

for installing the detector onto the CUORE cryostat, a temporary higher-specification cleanroom (CR6) with a radon-free air supply was erected within cleanroom 5 (CR5) around the CUORE cryostat. Installation was carried out over the course of a week in June 2016 by Joe Wallig, Tyler Sipla, and Alexey Drobizhev of LBNL/UC Berkeley.

Cleanroom 6 consists of a sealed tent-like structure of thick plastic sheeting on an aluminum frame. To improve cleanliness, a stainless steel floor backed with plastic sheeting was laid on top of the original tile floor. The plexiglass and aluminum door features a floor sweep and an interlocking hand-through port and a vestibule of the same sheet and frame construction is set up between the doors to CR5 and CR6, creating a space in which assembly workers wait for air to re-circulate

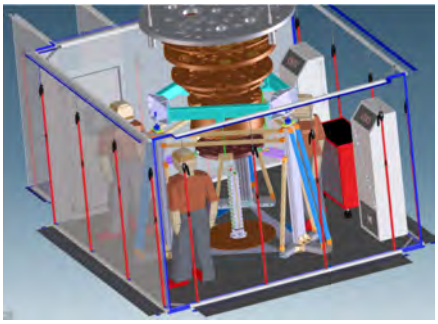

(a)

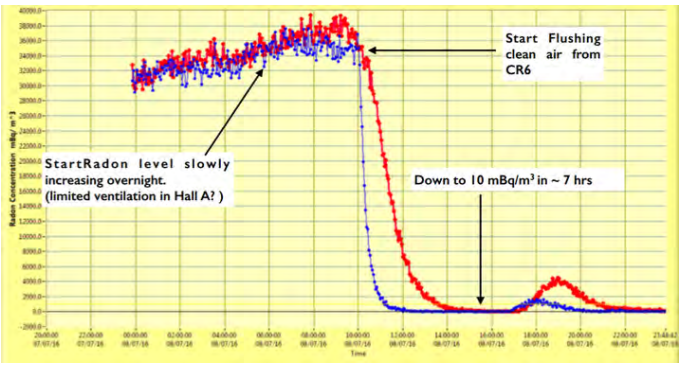

(b)

FIG. 6: (a) Drawing of the CR6 cleanroom within the CR5 cleanroom (b) Radon concentration in CR6 as a function of time as measured at the GERDA Radon cleanroom. Concentrations of ^{218}Po (blue) and ^{214}Po (red).

before entering the clean area. A second point of access is a zipper in the plastic sheeting on the side of CR6, aligned with a large double door leading to an adjacent cleanroom (CR4), in which detector towers and shield components were stored. All necessary cables, hoses, and nitrogen lines are brought in through sealed feedthroughs in the plastic walls.

The air to CR6 is provided by the Radon Abatement System (RAS), entering through a port near the ceiling. Measurement of the radon levels is performed with the GERDA experiment's radon monitor, which allowed for feedback on the order of minutes. Circulation and filtration of air within CR6 is carried out by two Envirco IsoClean HEPA filter cabinets retrofitted with cleaner Teflon-based ULPA filters. CR5's standard air handlers are disabled, with the HEPA filters sealed off to prevent the entry of radon-containing air. One of the two cabinets is fitted with a heat exchanger and connected to a chiller, helping to keep ambient temperatures lower during work. Enabling the RAS reduces the radon levels inside CR6 from the background value of 30000–40000 mBq/m^3 to a stable baseline of 10 mBq/m^3 in about 7 h.

CR6 was used throughout assembly operations. In early October 2016, it was dismounted to allow for opening of the CR5 floor hatch and closing the CUORE cryostat. Instead of returning to standard CR5 operations, a compromise arrangement was set up where gaps in CR5's walls and floor were sealed with plastic, the CR6 door and vestibule were kept in place (rotated 90 deg.), and air handling remained on the CR6 RAS and ULPA cabinets. This setup limited radon levels to around 50 mBq/m^3.

V. DETECTOR INSTALLATION

The CUORE detector was installed onto the tower support plate (TSP) in the cryostat between August and September 2016. The installation required the physical mounting of each of the 19 towers and the routing of the Cu-PEN cabling, to the Junction Boxes which then carry the electrical signals to the room temperature readout. In the months before the actual mounting, we tested the procedure with a full size mock-up tower.

The installation was performed inside the CR6 clean room. The towers were exposed to CR6 atmosphere for the smallest possible amount of time, typically about 1 hour per installation session, and then enclosed in a dedicated bag and flushed with nitrogen. During installation, three operators working inside CR6 wore clean room compliant garments and adopted a number of procedures to guarantee that the most critical operations were performed with fresh new tools. During installation, the operators used these tools and never themselves came into direct contact with any part of the detector assembly directly exposed to the sensitive TeO_2 crystals.

A number of pre-installation checks were performed on each tower to guarantee the structural integrity of the modules and of the copper threads and screws that mechanically connect each tower to the TSP. During installation of one tower, one of the mounting screws became stripped, but due to the precautions could be dismounted, repaired and re-installed without damage to the detectors.

Each tower was checked for electrical integrity before and during the installation, and was continuously monitored during installation of all the following towers using dedicated electronics boards. No thermistors were lost or damaged during installation.

The organization of the man-power was key to the success of the detector installation. We created an *installation team*, consisting of five physicists and technicians, three of which were working inside CR6 at any given time. A *support team* was responsible for the maintenance of CR6 and installation tools. They also handled moving the towers (still in their flushed storage boxes) between the storage area and the installation area. A *monitoring team* continuously monitored the status of all subsystems (anti-radon and monitoring, environmental control, nitrogen flushing, etc.) Finally, a *rescue team* was always ready to take over from the *installation team* in case of a problem on a tower or detector emergency.

Each installation session averaged around 3 hours for a single tower. During the session, operator could not enter or leave CR6 until the detector was closed safe inside the nitrogen flushed bag. (Of course, procedures for an emergency were in place and understood by everyone involved.)

After the detector was fully installed, several ancillary components were mounted, and the detector was closed into a nitrogen flushed bag to await cryostat closing.

VI. CUORE COOLDOWN TO BASE OPERATING TEMPERATURE

We closed the cryostat immediately after the successful installation of both the detectors and the 10 mK shield. We then started the cooldown process in the first week of December 2016. We confirmed that there were no leaks in the vacuum vessels nor the dilution unit and proceeded with the cooldown process with the Pulse tube coolers, assisted with the Fast Cooling System (FCS). The cooldown to the base temperature was uneventful except for two interruptions where we were obliged to stop the cooldown for few days. The first hiatus was when the system had already reached a temperature of 20 K. We observed a leak in our ^{3}He / ^{4}He gas handling unit. The repair took us about a week, after which we continued with the cool-down. Soon after we put a hold on the cooldown to debug our front-end electronics and the Data Acquisition System (DAQ) subsystem. The break was a prolonged one, but extremely fruitful. It allowed us to identify the sources of noise which were not related to the thermal effects of the detectors. Once we were satisfied with the level of the electronics noise, we continued with the cooldown to the base temperature. We reached a base temperature of ∼8 mK in January 2017. Figure 7 shows the temperature of the 10 mK stage, where the detectors are thermalized, during the cooldown.

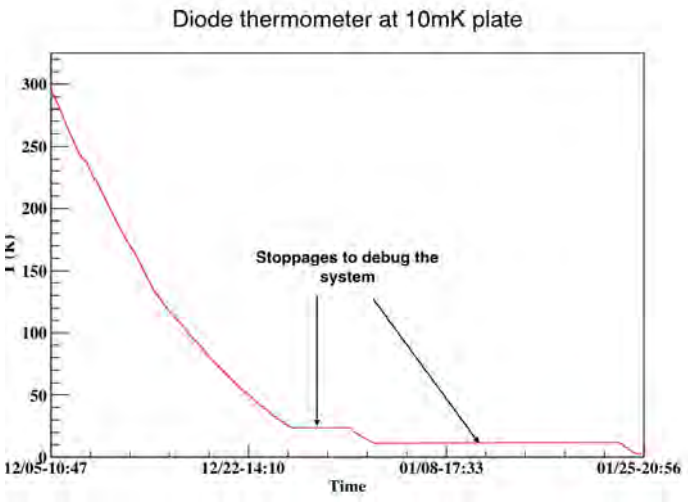

FIG. 7: Temperature of the 10 mK stage, where the detectors are thermalized, during the cooldown.

VII. ELECTRONICS FRONT-END COMMISSIONING

The goal of the electronics is to provide an effective low-noise system for reading and monitoring CUORE detectors. It interfaces to the CUORE DAQ which records the data and provides a link with the slow-control and data analysis tools. During early 2016 all the pre-installation tests were concluded and installation of the FC, we proceeded with on-site installation and commissioning of the electronics system.

We installed the electronic instrumentation on the second floor of the CUORE hut in Hall A. The front-end electronics (pre-amplifiers, main-boards and their linear-power supplies) and pulser boards were placed inside the FC, on top of the Y-beam supporting the cryostat, arranged in 7 fully autonomous racks. The electronics were arranged to maximize the ease of future intervention and to leave room for cryostat operations. The back-end electronics (Bessel filters and DAQ) were installed outside of the FC, next to the power supply racks which provide the power to all the electronics. The optical fiber drivers for CANbus communication to the electronics were also installed out of the FC, attached to the wall of the room, inside custom metal boxes.

The mapping of the complete detector cabling links were continuously tested during installation with automated scripts, allowing us to debug and promptly correct any possible hardware mapping error. A similar procedure was used to test all the cabling from the cryostat to the front-end. With a custom designed system, we measured inter-channel insulation and wire continuity and shorts. A database was compiled with all the measurement results. We benchmarked FC shielding effectiveness, and showed it provided adequate rejection of an artificial 50 Hz noise source applied outside the wall of the cage.

After installation we tested and debugged the communication between DAQ and the electronic front-end, and corrected any software-side and firmware-side communication errors. The commissioning of the electronics continued with on-site optimization of the setup, noise and other front-end parameters, using automatic tools developed for this purpose. The electronics installation and commissioning phase was completed on schedule.

VIII. DATA ACQUISITION COMMISSIONING

The CUORE DAQ was installed on the second floor of the CUORE hut in June 2016. It is composed of 64 NI-PXI-6284 digitizer boards, for a total of 1024 analog input channels. The digitizer boards are hosted in six PXI chassis that are contained in two rack cabinets (3 chassis

each). These two cabinets also contain passive interface boards used to match the cable connections between the Bessel and the digitizer boards. A third rack cabinet hosts the six computers dedicated to the data readout (one per chassis) and the event builder computer. The data acquisition and electronics control hardware and software were tested and debugged in the last months 2016, and they were ready to use since the beginning of the CUORE detector operation. The full debugging of the DAQ continued into 2017 once the detector channels reached base temperature.

IX. ONLINE MONITORING

CUORE Online/Offline Run Control (CORC), developed by the University of California, Berkeley (UCB) and Lawrence Berkeley National Labs (LBNL) groups, and Slow Monitoring (SM), developed by the Massachusetts Institute of Technology (MIT) group, are high-level interfaces for monitoring the detector parameters and cryostat operations data. The underlying backend is a Python-based web server utilizing MongoDB for database storage. This past year saw several upgrades to the backend software. MongoDB was upgraded from an older version which brought improved access times and a different storage engine that includes data compression, which allows for the use of less disk space when storing both data and index keys. The existing replica set was converted to this new format without any significant issue. The CORC/SM web page itself also underwent many significant upgrades to its underlying javascript libraries. Many of these libraries were initially still in the version they were from 2014, and two were customized in a way that made direct upgrades impossible. The APIs for several of these libraries underwent non-trivial changes that necessitated rewriting parts of the CORC webpage code. The result of this is a page that has improved responsiveness, is more secure, and handles timestamps in a more unified fashion.

Due to the software library upgrades portions of the SM code needed to be rewritten as well. It was discovered during the installation shifts that the pre-existing codebase contained several serious bugs related to handling timestamps. These affected time-zone dependent queries to the database for data spanning greater than a month. In order to avoid this, the SM time code was rewritten to use unix timestamps everywhere possible, only converting to dates for human-readable display purposes. After all the timestamp based upgrades were completed, together with the library updates, the entirety of the CORC/SM page was unified to use CET/CEST for its default time zone, and uses unix timestamps for internal queries from the database.

In order to aid in the use of quick overviews of the cryostat performance, the SM pages have an overview page which displays selected plots of various cryostat parameters. Great effort was

spent making these overview plots easier to read and the interface more user friendly. To prevent a plethora of plots from appearing on the SM front page, a new user permission was added which allows only certain users to create or edit the overview plots.

Another large item completed in 2016 was the alarms feature. Now alarms can be created by any user, and multiple users may subscribe to the same alarm. Users with a special permission are able to add alarms to alarm groups, which may be created for specific purposes and contain alarms common to that purpose. Any user may then subscribe to any alarm group. Membership to an alarm group will automatically subscribe a user to all the alarms belonging to that group. The alarm checks are performed with each update to the database (approximately once a minute). They are currently implemented as simple min/max alarms in which the current value for a component must be between the minimum and maximum value. If the component value is outside this range the alarm will be triggered. A triggered alarm will first email all users that are subscribed to it, and then if the alarm belongs to an alarm group it will use a dial-up phone modem installed underground to call users sequentially where it will then speak a simple alarm message meant to draw attention to the fact an alarm is currently active. On the webpage users have the ability to snooze an alarm for a specified amount of time in order to suspend further notifications while fixing the alarm condition, or they may acknowledge and dismiss the alarm if it is fixed. The alarms were successfully tested in early December of 2016 and further upgrades are planned to expand the capability.

The CUORE network and the Slow Monitor system are monitored using Nagios, a system implemented and supported by the INFN Bologna group. At the end of 2016 it monitored about 30 hosts and more than 200 services and processes. It promptly alerts in case of problems of the systems related to the detector control and in case of interruptions in the slow-control data flow.

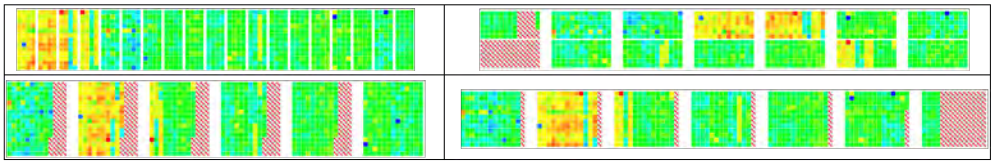

FIG. 8: Different CORC layouts. The tower view has 19 towers, with the standard 13 floors. All other views have rows as channel and columns as board or slot. *Top-left:* Standard tower view. *Top-right:* Front end board layout. *Bottom-left:* Digitizer board layout. *Bottom-right:* Bessel filter board layout

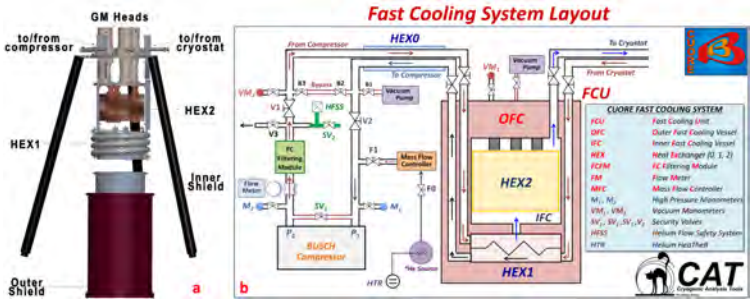

FIG. 9: (a) CUORE Fast Cooling Unit. (b) CUORE FCS complex layout.

X. FAST COOLING SYSTEM

A. The Fast Cooling System

Because of the large mass of CUORE experiment, the five Pulse Tubes (PT) alone are not able to cool down the whole cryostat and its contents from room temperature down to 4 K in an acceptable time (∼2 weeks). So, we designed a FCS to quickly pre-cool the CUORE IVC down to 20-30K. While CUORE uses a set of 5 PT to provide cooling to the detector mass through conduction, the FCS uses convection of ^{4}He to speed up this process. The CUORE FCS consists of an external FCU with two main Heat Exchangers (HEX1 and HEX2), a third one outside the FCU (see Fig. 9), three CRYOMECH AL600 Single Stage Gifford-McMahon cryocoolers, a ^{4}He blower, double-walled pipes, a gas handling system and finally an automated FC Monitor & Control System (FCMCS). The FCU is shown in Fig. 9.

In order to avoid any radioactive contaminants getting into the CUORE cryostat and onto the detector, we put substantial effort to clean all the relevant parts. These operations required several months of work during 2016. Since the Fast Cooling System injects ^{4}He into the Inner Vacuum Chamber (IVC), the gas needs to match restrictive purity requirements. Although all the FCS parts in contact with the ^{4}He gas have been cleaned, we add a He Filtering Module (FCFM) in order to prevent unexpected contaminants from entering the cryostat.

During 2016, the FCS was completely disassembled and cleaned. The cleaning process was performed in parallel at different facilities; the new tombaks, cryostat cold lines, the HEX0, the HEX1 and other components were cleaned in the BOREXINO cleaning facility. Several of these tombaks are very long pipes up to 15 m each, making the cleaning, rising and N_2 drying process difficult and long. The full cleaning procedure required several weeks. At the same time, the FCS valves, the Inner Fast Cooling Chamber (IFC), the Flow Meter, and other smaller or delicate

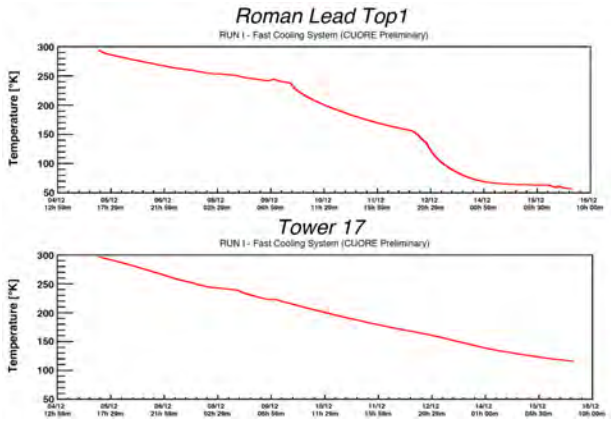

FIG. 10: Left: Run I FCS cooling down of CUORE Roman Lead and crystals.

pieces were cleaned in the Laboritori Nazionali del Gran Sasso (LNGS) Chemical Laboratory. We installed a new HEX2 has during the cool down of CUORE. Since it has the strictest cleanliness requirements, the IFC was been assembled inside the Xenon 1T Clean Room. Because of the large mass of the heat exchanger ($\sim$ 700 kg), the full assembling procedure took more than a month and required several weeks of planning and preparation before being able to use the facility. Afterward, the HEX2 was instrumented with several thermometers before being carefully sealed back inside the IFC vessel. We also made improvements to the FCS electronics and added a new rack to host them on the second floor of the CUORE hut. Finally, the Helium Flow Safety System (HFSS) was installed to prevent an overpressure inside the FCS and IVC.

On December 3, 2016, the FCS was switched on to prepare for the CUORE cooldown, which started two days later on December 5. The FCS operated without incident for 13 days, cooling the lead shielding down to $\sim$50 K, and the crystals to $\sim$100 K. See Fig. 10. The system was switched off on December 15, 2016 after successfully cooling the CUORE detetor down, and the next stages of the CUORE cooldown continued on.

B. Cryogeny Monitor and Control System

The CUORE Cryogeny Monitor & Control System (CMCS) is a LabVIEW-based software package developed by the UNICLAM-LNGS Group (the LNGS Group from University of Cassino and Southern Lazio). This software controls all the CUORE cryostat systems and interfaces to the CORC/SM monitoring software. CMCS monitors and controls all of elements of the CUORE Cryostat and associated systems by interfacing with each instrumentats own communication & control protocols. It also performs the online analysis of all the relevant variables and generates

time-ordered data files that are passed as an input to CORC/SM web interfaces. CMCS consists of several monitor/control packages and GUIs, each of them focused either on a particular physical variable (i.e. pressures, temperatures, fluxes, currents, status, etc.) or on a specific cooling system (PT, FCS, DU).

During 2016, the effort has been to move all the monitoring and controlling VIs to a customized National Instrument PXIe located inside the CUORE Cryogeny Rack. All the possible parameters, related to the cryogenic apparatus, are now acquired by the PXIe which writes log files in its own internal hard drive. The log files are continuously uploaded into the Slow Control Server as backup. We also added various other optimizations and features to the software.

XI. COMPUTING INFRASTRUCTURE

We make use of three computing clusters for data analysis and Monte Carlo simulations. The Unified LNGS IT Environment (U-LITE) at LNGS is the primary computing resource for CUORE. U-LITE has 32 CPUs (64 cores) and 90 terabytes (TB) of storage dedicated to CUORE. In addition, up to 400 cores are available when not in use by other experiments. CNAF and PDSF are secondary computing clusters available for user analyses, code development, and other tests. These secondary clusters are also used to backup the official CUORE data. CNAF, located in Bologna, Italy, has up to 1500 cores available to CUORE and 170 TB of dedicated storage. PSDF, which is part of the National Energy Research Scientific Computing Center (NERSC) located in Berkeley, California, has up to 1536 cores available to CUORE and 30 TB of dedicated storage. CUORE has more than 100 TB of dedicated tape backup storage on the High Performance Storage System (HPSS) also located at NERSC.

The CUORE DAQ collects about 50 GB of raw data per day. The data are automatically copied from storage in the underground labs to the U-LITE computing center in the above ground labs at LNGS. From there the collaboration begins the data analysis process. From the above ground labs the data are copied to 2 backup sites: one at the CNAF computing center in Italy and the second at NERSC HPSS in the USA.

We employ the open source relational database PostgreSQL to store and retrieve structured objects used by the data acquisition system and analysis, and the document-oriented database MongoDB to manage the diagnostics from the data analysis and the slow control. The master PostgreSQL database is located in the main surface building at LNGS and is copied, with native replication, to slave databases in the underground CUORE lab, to CNAF, and to the LBNL in

Berkeley, California. The rare event where communication to the master database is lost triggers a failover and the database located in the CUORE lab becomes the master to prevent interruptions to data taking. The master MongoDB is also located in the main surface building at LNGS and is natively replicated on slave databases located in the underground CUORE lab and at LBNL with a similar failover system.

We use the version control system `Git` to manage the source code for CUORE data acquisition and analysis, simulations, control systems, as well as drafts for journal articles and reports. We host the CUORE `Git` repository on an Enterprise `GitHub` server located at the MIT that includes issue tracking and online software documentation. We have also built a website that includes both public and collaborator specific information on CUORE. The collaborator specific information includes automatically generated Doxygen software documentation, author list generators, and shift management.

XII. PAPERS PUBLISHED IN 2016

CUORE physics results in 2016 are related to the analysis of the CUORE-0 data collected from March 2013 to March 2015 in Hall A, using the same cryostat that previously hosted CUORICINO.

A. Detector performance

In 2016, we published a technical paper on JINST, where we described the CUORE-0 detector and its performance in detail. We presented the design of the new TeO_2 bolometers and described the CUORE-0 detector components, the assembly technique, the electronic readout and data acquisition. We highlighted the CUORE-0 results concerning bolometer reproducibility and uniformity, energy resolution, and background rate.

The new CUORE-style assembly procedure exploited for CUORE-0 allowed us to improve the uniformity of the bolometric performance. Figure 11 shows the distribution of measured base temperatures for CUORE-0 and CUORICINO. The narrower spread seen in CUORE-0 is an indication of the improvement in assembly uniformity.

The energy resolution of CUORE-0 was similarly improved over the performance of CUORICINO. Figure 11 shows the distributions of the energy resolutions evaluated on the 2615 keV ^{208}Tl photopeak in CUORICINO and CUORE-0, for each bolometer in each dataset (one-month-long subset of data). The effective mean of the FWHM values in CUORE-0 is 4.9 keV compared to

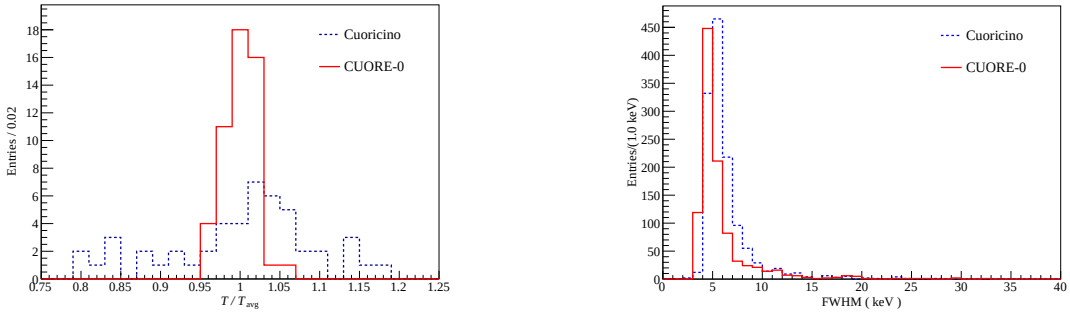

FIG. 11: Left: Comparison of the base temperatures of the bolometers normalized to their average temperature for CUORE-0 (red line) and CUORICINO (blue dashed line). Right: Comparison of the distribution of the energy resolutions (FWHM) measured in calibration for Cuoricino (blue dashed line) and CUORE-0 (red line).

5.8 keV in Cuoricino. This demonstrated the CUORE goal of 5 keV FWHM at 2.6 MeV.

We also demonstrated a decrease in the α background contributing to the region of interest (ROI) from 0.110 ± 0.001 cnts/(keV·kg·yr) to 0.016 ± 0.001 cnts/(keV·kg·yr). This factor of 7 improvement is due to the improved material selection and assembly procedures developed for CUORE. This result is consistent with the CUORE background goal of 0.01 cnts/(keV·kg·yr).

B. Analysis Techniques for the Evaluation of the $0\nu\beta\beta$ decay Lifetime in ^{130}Te with CUORE-0

The CUORE-0 results on the $0\nu\beta\beta$ decay lifetime of ^{130}Te were published in Physical Review Letters (PRL) in September 2015. In 2016, we published in Physical Review C (PRC) a more detailed paper describing the analysis techniques and methods used to obtain the lower bound on the lifetime and the associated limit on the effective Majorana mass of the neutrino, reported in PRL. In particular, we described the amplitude evaluation, thermal gain stabilization, energy calibration methods, and the analysis event selection used to create our final spectrum. We outlined the fitting methods near the hypothesized decay peak and catalogued the main sources of systematic uncertainty. We highlighted a few improvements in the analysis techniques that improve the energy resolution and allow to recover live time from channels without a working heater.

To improve energy resolution, we employed a new decorrelating optimum filter (DOF) that accounts for noise correlations between neighboring bolometers. The distribution of amplitudes of the noise pulses, see Fig. 12, are indicative of the amount of noise remaining after filtering.

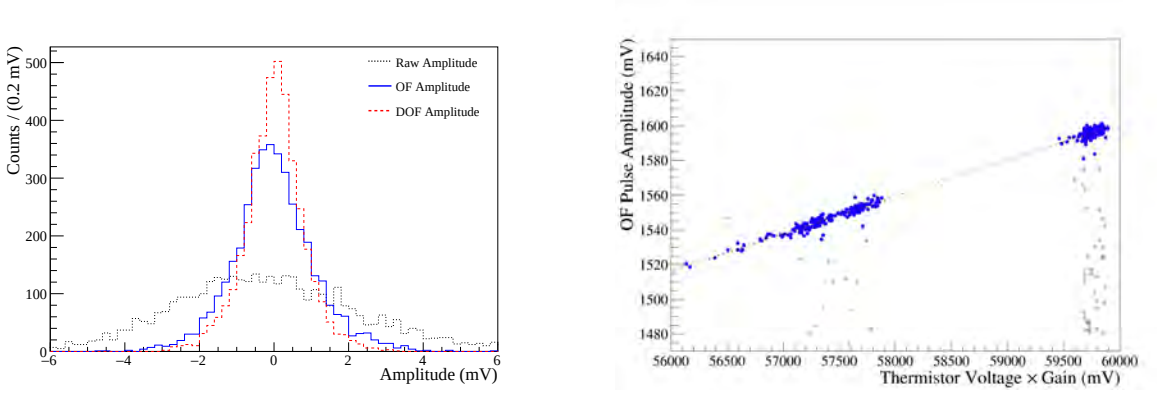

FIG. 12: Left: The distribution of amplitudes of the noise pulses collected from a single channel during the physics data of a dataset from Campaign I. The channel presented is one where the DOF performed well. The raw unfiltered RMS is 2.7 mV (*black dotted* histogram); the RMS after OF is 1.1 mV (*blue solid* histogram); the RMS after DOF is 0.8 mV (*red dashed* histogram). Right: Example of the calibration-TGS. The points are taken during the calibration runs for one of the CUORE-0 datasets. The solid blue points have energies around the 2615 keV ^{208}Tl peak and are used for calibration-TGS. By regressing the measured amplitudes of these points against the NTD voltage we can determine a stabilization curve (red dashed line) which is then applied to the physics runs taken between calibrations.

The thermal gain stabilization (TGS) compensates slow variation in the gain of the bolometers due to drifts of the operating temperature of the detector. We used a constant energy heater pulser to inject fixed-energy reference pulses into each bolometer every 300 s during each run. We developed a new algorithm, called Calibration-TGS, which uses the 2615 keV γ-line in the calibration runs in lieu of the monoenergetic pulser to map the temperature-dependent gain. We regress the gain dependence measured in the calibration runs (see Fig. 12) and use this to correct the amplitudes of events in both the calibration and physics runs. This calibration-TGS allowed us to recover about 80% of the lost exposure on the two bolometers with broken heaters. Additionally, in cases of large temperature drifts, the calibration-TGS routinely outperformed the heater-TGS.

C. Measurement of the Two-Neutrino Double Beta Decay Half-life of ^{130}Te with the CUORE-0 Experiment

We performed a Geant-4 based Monte Carlo study of the CUORE-0 background spectrum and were able to measure the two-neutrino double beta ($2\nu\beta\beta$) decay half-life of ^{130}Te. From an

exposure of 33.4 kg·y of TeO_2, the half-life was determined to be $T^{2\nu}_{1/2} = [8.2 \pm 0.2\ (\text{stat.}) \pm 0.6\ (\text{syst.})] \times 10^{20}$ y. This result was obtained after a detailed reconstruction of the 57 sources responsible for the CUORE-0 counting rate, with a specific study of those contributing to the ^{130}Te $0\nu\beta\beta$ decay region of interest. We published this in the European Physics Journal C (EPJC), and it was chosen as the cover article for January 2017.

Figure 13 shows the fit result compared with the CUORE-0 spectrum of single multiplicity. Compared to previous results obtained from MiDBD $[6.1 \pm 1.4(\text{stat.})^{+2.9}_{-3.5}(\text{syst.})] \times 10^{20}$ yr, from CUORICINO, and from NEMO $[7.0 \pm 0.9(\text{stat.}) \pm 1.1(\text{syst.})] \times 10^{20}$ yr, this is the most precise measurement to date.

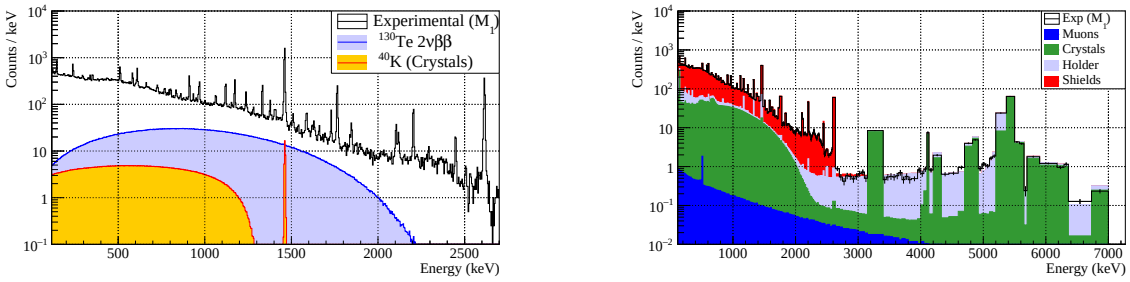

FIG. 13: Left: CUORE-0 single multiplicity spectrum compared to the ^{130}Te $2\nu\beta\beta$ contribution predicted by the reference fit and the radioactive source that has the strongest correlation with $2\nu\beta\beta$, ^{40}K in Crystal bulk. Right: Sources contributing to background reconstruction.

Finally, Fig. 14 shows the region centered around the $0\nu\beta\beta$ decay ROI and the reconstructed α vs non-α background components.

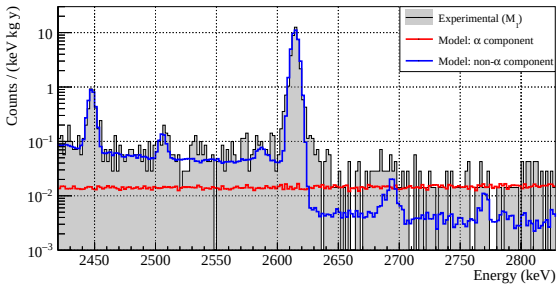

FIG. 14: Background reconstruction in the $0\nu\beta\beta$ decay ROI. Events due to alpha particles (about 24% of the ROI background) are shown in red. All the other events are shown in blue.

XIII. PUBLICATION LIST

[1] C. Alduino *et al.* (CUORE Collaboration), "CUORE-0 detector: design, construction and operation", Journal of Instrumentation, 11, P07009 (2016)

[2] C. Alduino *et al.* (CUORE Collaboration), "Analysis Techniques for the Evaluation of the Neutrinoless Double-β decay Lifetime in Te-130 with CUORE-0", Phys. Rev. C, 93-4, 045503 (2016)

[3] V. Singh *et al.*, "The CUORE cryostat: commissioning and performance", Journal of Physics: Conference Series 718, 062054 (2016)

[4] L. Canonica *et. al*, "Results from the CUORE-0 experiment", Journal of Physics: Conference Series 718, 062007 (2016).

[5] M. Sisti *et al.* (CUORE COllaboration), "Status of the CUORE and results from the CUORE-0 neutrinoless double beta decay experiments", Nuclear and Particle Physics Proceedings 273-275, 1719-1725 (2016).

[6] O. Cremonesi, "Neutrinoless Double Beta Decay", Journal of Physics: Conference Series 718, 022006 (2016)

[7] C. Arnaboldi *et al.*, "The supply voltage apparatus of the CUORE experiment", Nuclear Instruments and Methods A 824, 340-342 (2016)

[8] G. Piperno (for the CUORE COllaboration), "Low energy analysis in CUORE-0", Journal of Physics: Conference Series 718, 042045 (2016)

[9] L. Canonica (for the CUORE Collaboration), "Neutrinoless Double Beta Decay with CUORE-0: Physics Results and Detector Performance", Journal of Low Temperature Physics 184, 873-878 (2016)

[10] C. Ligi *et al.*, "The CUORE Cryostat: A 1-Ton Scale Setup for Bolometric Detectors", Journal of Low Temperature Physics 184, 590-596 (2016)

[11] S. Dell'Oro and S. Marcocci, "Recent results from cosmology and neutrinoless double beta decay", Journal of Physics: Conference Series 718, 062012 (2016)

[12] S. Dell'Oro *et al.*, " Neutrinoless Double Beta Decay: 2015 Review", Advances in High Energy Physics, Vol. 2016, 2162659 (2016)

CUPID-0

D. R. Artusa[a,b], O. Azzolini[h], M. T. Barrera[h], J. W. Beeman[e], F. Bellini[c,d], M. Beretta[f,g], M. Biassoni[g], C. Brofferio[f,g], C. Bucci[a], L. Canonica[a], S. Capelli[f,g], L. Cardani[e,d,i], P. Carniti[f,g], N. Casali[c,d], L. Cassina[f,g], M. Clemenza[f,g], O. Cremonesi[g], A. Cruciani[c,d], A. D'Addabbo[a], I. Dafinei[d], S. Di Domizio[j,k], M. L. di Vacri[a], F. Ferroni[c,d], L. Gironi[f,g], A. Giuliani[l,m], P. Gorla[a], C. Gotti[f,g], G. Keppel[h], M. Maino[f,g], M. Martinez[c,d], S. Morganti[d], S. Nagorny[o], M. Nastasi[f,g], S. Nisi[a], C. Nones[n], F. Orio[d], D. Orlandi[a], L. Pagnanini[o], M. Pallavicini[j,k], V. Palmieri[h], L. Pattavina[a], M. Pavan[f,g], G. Pessina[g], V. Pettinacci[d], S. Pirro[a], S. Pozzi[f,g], E. Previtali[g], A. Puiu[f,g], F. Reindl[d], C. Rusconi[g,m], K. Schäffner[o], L. Sinkunaite[f,g], C. Tomei[d], M. Vignati[d], A. Zolotarova[n]

INFN - Laboratori Nazionali del Gran Sasso, Assergi (L'Aquila) I-67010 - Italy [a]
Department of Physics and Astronomy, University of South Carolina, Columbia, SC 29208 - USA [b]
Dipartimento di Fisica, Sapienza Università di Roma, Roma I-00185 - Italy [c]
INFN - Sezione di Roma, Roma I-00185 - Italy [d]
Materials Science Division, Lawrence Berkeley National Laboratory, Berkeley, CA 94720 - USA [e]
Dipartimento di Fisica, Università di Milano-Bicocca, Milano I-20126 - Italy [f]
INFN - Sezione di Milano Bicocca, Milano I-20126 - Italy [g]
INFN - Laboratori Nazionali di Legnaro, Legnaro (Padova) I-35020 - Italy [h]
Physics Department - Princeton University, Washington Road, 08544, Princeton - NJ, USA [i]
Dipartimento di Fisica, Università di Genova, Genova I-16146 - Italy [j]
INFN - Sezione di Genova, Genova I-16146 - Italy [k]
CSNSM, Univ. Paris-Sud, CNRS/IN2P3, Université Paris-Saclay, 91405 Orsay, France [l]
DiSAT, Università dell'Insubria, 22100 Como, Italy [m]
IRFU, CEA, Universit Paris-Saclay, F-91191 Gif-sur-Yvette, France [n]
Gran Sasso Science Institute, 67100, L'Aquila - Italy [o]

Abstract

Isotopic enrichment and active background rejection are key features in the improvement of the sensitivity of next generation ton-scale $\beta\beta(0\nu)$ experiments. In the case of phonon detectors these two requirements can be simultaneously matched by the use of *scintillating bolometers*. This technique dates back to the '90es and is used since many years by the CRESST experiment to investigate Dark Matter interaction [1], its application to $\beta\beta(0\nu)$ research is recent [2] and the realization of the first kg-scale experiment discussed in this report (CUPID-0) is an important milestone made possible only after several years of R&D, pursued under the ERC LUCIFER grant that also funded the construction of the experiment [3]. While other scintillating crystals, suitable for $\beta\beta(0\nu)$ decay searches, have been considered and tested by our collaboration over the years, in year 2016 all the man-power and the efforts of the collaboration were dedicated to the CUPID-0 experiment. The main activities, their goals and achievements are discussed in this report.

CUPID-0 is a ZnSe based experiment commissioned between the end of year 2016 and the beginning of 2017 at Laboratori Nazionali del Gran Sasso (LNGS). The detector is an array of 26 ZnSe crystals, 24 made with ^{82}Se enriched material, operated as scintillating bolometers. It is the first $\beta\beta(0\nu)$ experiment based on scintillating bolometers. Each crystal is instrumented to read-out both the phonon and the scintillation-photon signals produced by particle traversing its volume. Shape and amplitude of these signals are used to identify the interacting particle and measure its energy deposition. The phonon signal drives the determination of the energy, the light signal allows to discriminate highly ionizing particles like β/γ (including $\beta\beta(0\nu)$ generated βs) from αs and nuclear recoils. The array is operated at about 10 mK in the Oxford Instrument dilution refrigerator formerly used by Cuoricino [4] and CUORE-0 [5].

The main physics goal of the experiment is the investigation of ^{82}Se $\beta\beta(0\nu)$ decay, signature of the decay is a monochromatic line in the phonon signal, equivalent to an energy deposition of 2998 keV in the crystal (the ^{82}Se Q-value [7]). Exploiting the particle discrimination capability of the detector, events with a similar energy deposition but produced by α particles can be rejected with high efficiency. The irreducible background will therefore derive from β/γ events, and is expected to be of the order (or below) 10^{-3} c/keV/kg/y. If successful, CUPID-0 would open the way for a CUORE Upgrade with Particle Identification (CUPID) [8, 9].

1 Technique

The phonon signal recorded by CUORE [6] TeO_2 or by LUCIFER ZnSe bolometers is a nearly thermal pulse (*heat*) almost completely blind to the particle species but extremely sensitive to the total energy released by the particle in the bolometer volume. These devices features a high density and good energy resolution, like semiconductor particle detectors, meanwhile offering a higher flexibility in material choice. One of their most remarkable property is that different crystals can use the same infrastructure, detector holder, read-out and cryogenic systems. In our case this implies that most of the know-how developed in the framework of TeO_2 bolometers is of direct usage also for bolometers based on other crystal compounds. In order to preserve its competitiveness in the field of $\beta\beta(0\nu)$ research, today bolometers need to be complemented with some active background suppression technique. Indeed, it is a generally accepted statement that future $\beta\beta(0\nu)$ experiments need to operate in a nearly zero background condition, since sensitivity improvements cannot be based solely on mass increase [10, 2]. Particle identification looks as the most promising technique: CUORE-0 data demonstrated that the major contribution to the event rate in the 3 MeV region (namely where the $\beta\beta(0\nu)$ line of several good candidates, including ^{82}Se, should appear) comes from α particles [11]. These are produced by radioactive contaminants (U, Th and their progenies) in the surfaces facing the bolometers.

For the time being, this contamination appears almost irreducible and it is expected to be the dominant source of event rate in the $\beta\beta(0\nu)$ region of any bolometric experiment.

The read-out of a ionization signal, like the scintillation one, can clearly be the way-out for the suppression of this α background. Indeed, for most scintillators, both amplitude and time development of the *light* signal depend not only on the energy but also on the charge and mass of the interacting particle. In scintillating bolometers, this characteristic can be exploited for particle discrimination. The energy released by the particle in the crystal is accurately measured by the *heat* signal, while the *light* signal (that subtracts a very small fraction of energy to the thermal channel) is used for particle identification. The scintillation pulse is usually large enough (a few keV or tens of keV depending on the crystal compound) to be easily detected with an auxiliary bolometer, a Si or Ge thin wafer, equipped with a suitable phonon sensor.

A number of crystal compounds, containing a $\beta\beta$ candidate in their molecule and having scintillating properties, have been tested so far. Examples are, ZnSe [12, 13], $ZnMoO_4$ [14, 15, 16, 17, 18, 19, 21], Li_2MoO_4 [22, 23], $CdWO_4$ [24]. Se and Mo based compounds appear the most promising ones. Both are characterized by a Q-value of the $\beta\beta$ emitter (^{82}Se and ^{100}Mo) that drops above the 2615 keV γ-line of ^{208}Tl namely the most energetic γ line from natural radioactivity with a relevant branching ratio. Both have today a technique that is mature for the realization of a pilot experiment with enriched and radiopure material. The ZnSe one being already running and discussed in this report, the $MoLiO_4$ that will come soon [25].

2 The first $Zn^{82}Se$ array

The performances of $Zn^{82}Se$ enriched crystals were investigated in early 2016. The first 3 enriched crystals from the LUCIFER production were assembled as a single column of CUPID-0 (see later for a detailed description of detector instrumentation and assembly). Each crystal (a ZnSe cylinder, 4.4 cm in diameter and 5.5 cm in height) was equipped with a thermistor to measure the heat signal and was faced on the top and bottom faces by a Ge light detector. A reflective foil surrounding the lateral face of each cylinder was used for light collection. The array was operated in the low temperature refrigerator of Hall C, LNGS. The results of this run are here summarized (details can be found in [26]). The energy resolution on the heat signal increases from a baseline FWHM of 7-20 keV to a FWHM of ∼30 keV at few MeV. This energy dependence cannot be accounted for by the statistic of phonons (neither considering the effect of the statistical fluctuation of the produced photons) but it seems to be an intrinsic property of the crystals (a worsening of the baseline resolution on γ peaks is observed also in TeO_2 crystals, but with a much smaller effect).

The light detectors performed quite well, with a baseline FWHM of 100 eV to be compared with light signals from a 3 MeV β/γ or α of the order of 10-50 keV. As always observed in this compound, the light collected from α particles is much higher than that produced by a β/γ event of the same energy. There are however outliers in the α light yield distribution, namely α for which the collected light is much lower than the average [12, 13, 27]. This still unexplained effect spoils the efficiency of particle identification obtained from light to-heat-ratio.

On the contrary the shape of light pulses proved to be extremely powerful in discriminating α from β/γ particles, and completely unaffected by the low light emission, as shown in Fig 1 where the data collected with one of the three enriched crystals in the ∼530 h physics run are shown. To compute the discrimination capability at the $\beta\beta(0\nu)$ energy, we divided the α and β/γ bands in intervals and made Gaussian fits to derive the mean value (μ) and the standard deviation (σ) of the Shape Parameter in each interval. We fitted the energy dependence of μ(E) and σ(E) with polynomial functions and defined the Discrimination Power (DP) as a function

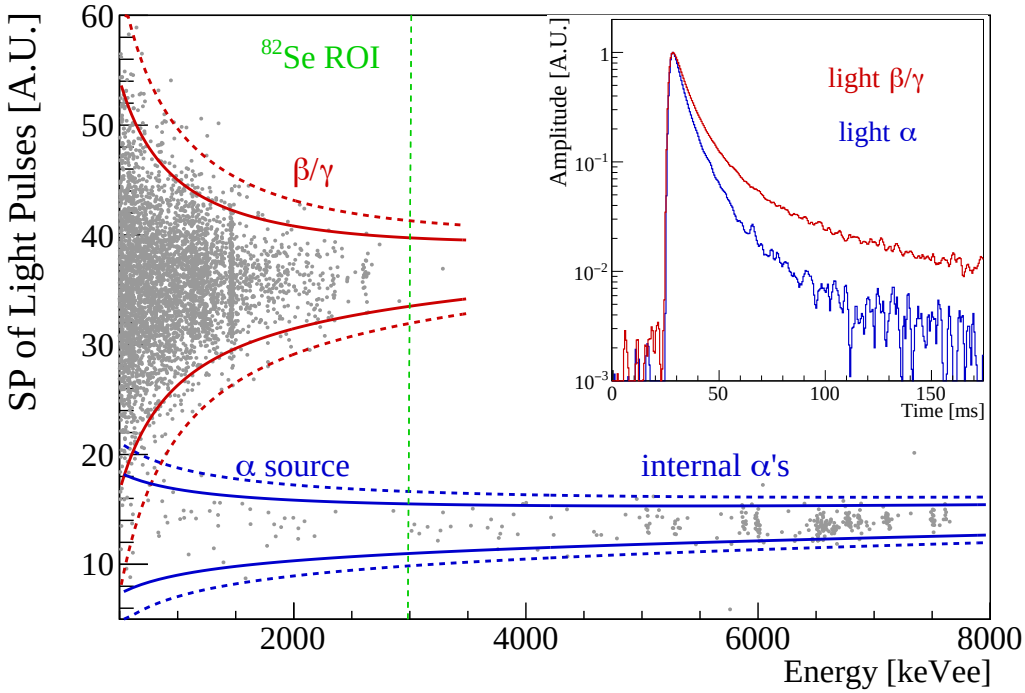

Figure 1: Shape parameter of a light detector as a function of the energy released in $Zn^{82}Se$-1 ($\sim$530 h). The red and blue lines indicate the 2σ (continous) and 3σ (dotted) β/γ and α bands respectively. α events produced by the smeared Sm source (below 3 MeV_{ee}) and by contaminations of the crystal bulk (peaks above 5 MeV_{ee}) can be easily rejected, in particular in the region of interest for the ^{82}Se $\beta\beta(0\nu)$ (green lines). The other crystals showed similar results. Inset: time development of light pulses produced by β/γ (blue) and α (red) interactions with energy of about 2.6 MeV.

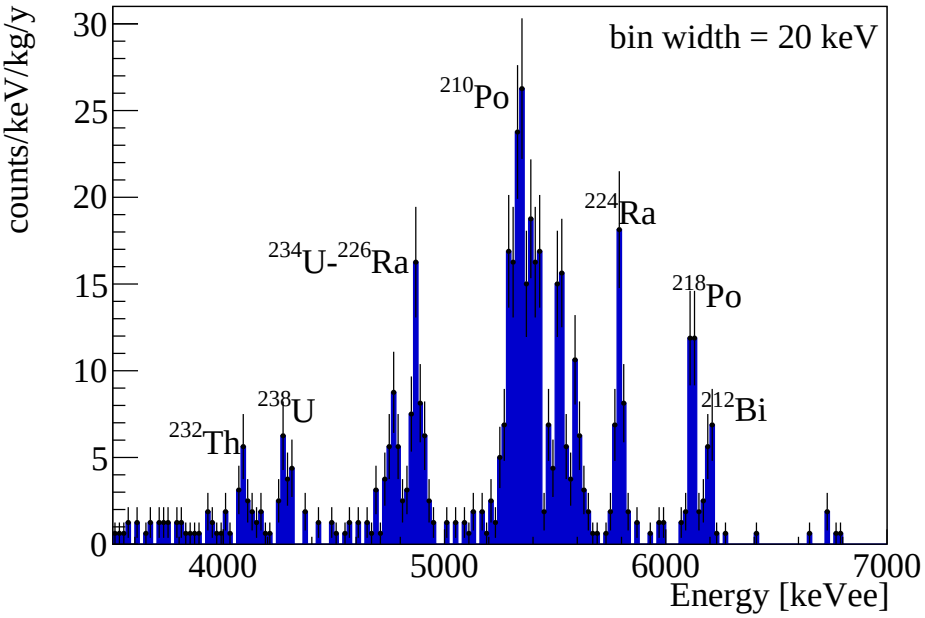

Figure 2: α region of the Zn^{82}Se array collected in 530 h. The spectrum was energy-calibrated using the nominal energy of the most prominent α peaks.

of the energy as:

$$DP(E) = \frac{|\mu_\alpha(E) - \mu_{\beta\gamma}(E)|}{\sqrt{\sigma^2_\alpha(E) + \sigma^2_{\beta\gamma}(E)}}$$

and found DP=12 at the ^{82}Se Q-value. The same analysis was made on the other two crystals, obtaining a DP of 11 and 10 for Zn^{82}Se-2 and Zn^{82}Se-3 respectively.

The 530 h long physics run was used to evaluate the internal contamination of the crystals, clearly identified from their α peaks (Fig. 2). These are reported in Table 1.

3 CUPID-0 Detector

CUPID-0 construction started in middle 2016. The detector (see Fig. 3) is an array of 26 ZnSe bolometers arranged in 5 columns that hung from a copper disk (detector support plate) mechanically secured to the cold finger of the dilution refrigerator through an anti-vibration suspension system. The array stands in the inner vacuum chamber of the cryostat.

A predominantly copper structure holds the detectors and provides the thermal link to the refrigerator. Four out of the five columns comprise 5 ZnSe crystals (cylindrical in shape, with a ∼44 mm diameter and a variable height). One column houses 6 ZnSe crystals, these were selected among those with shorter height in order to reduce to a minimum the difference among column lenghts. Two ring-shaped copper frames connected by three cylindrical copper bars make-up the single crystal holder and host the pins for the detector read-out (see Fig 4). Three S-shaped PTFE spacers secure the crystal to the frame and avoid a direct thermal link between the ZnSe bolometer and the copper structure. These modules are stacked one over the other, interleaved with a Ge wafer that is used as light detector. The disk-shaped Ge wafers result hence housed between two frames, each wafer simultaneously collecting light from the top and bottom ZnSe crystal (with the exclusion of the wafers at the top and bottom of a column). To

Table 1: Crystal contaminations in the isotopes of ^{238}U and ^{232}Th chains derived from the analysis of the α region (see Figure 2). We made the same analysis on the energy spectrum of each $Zn^{82}Se$ bolometer to highlight differences among crystals. Isotopes with long half-lives, that can break the secular equilibrium, are highlighted in bold type.

	$Zn^{82}Se$-1 [μBq/kg]	$Zn^{82}Se$-2 [μBq/kg]	$Zn^{82}Se$-3 [μBq/kg]	Array [μBq/kg]
^{232}Th	13 ± 4	13 ± 4	<5	7 ± 2
^{228}Th	32 ± 7	30 ± 6	22 ± 4	26 ± 2
^{224}Ra	29 ± 6	26 ± 5	23 ± 5	27 ± 3
^{212}Bi	31 ± 6	31 ± 6	23 ± 5	29 ± 3
^{238}U	17 ± 4	20 ± 5	<10	10 ± 2
^{234}U+^{226}Ra	42 ± 7	30 ± 6	23 ± 5	33 ± 4
^{230}Th	18 ± 5	19 ± 5	17 ± 4	18 ± 3
^{218}Po	20 ± 5	24 ± 5	21 ± 5	21 ± 2
^{210}Pb	100 ± 11	250 ± 17	100 ± 12	150 ± 8

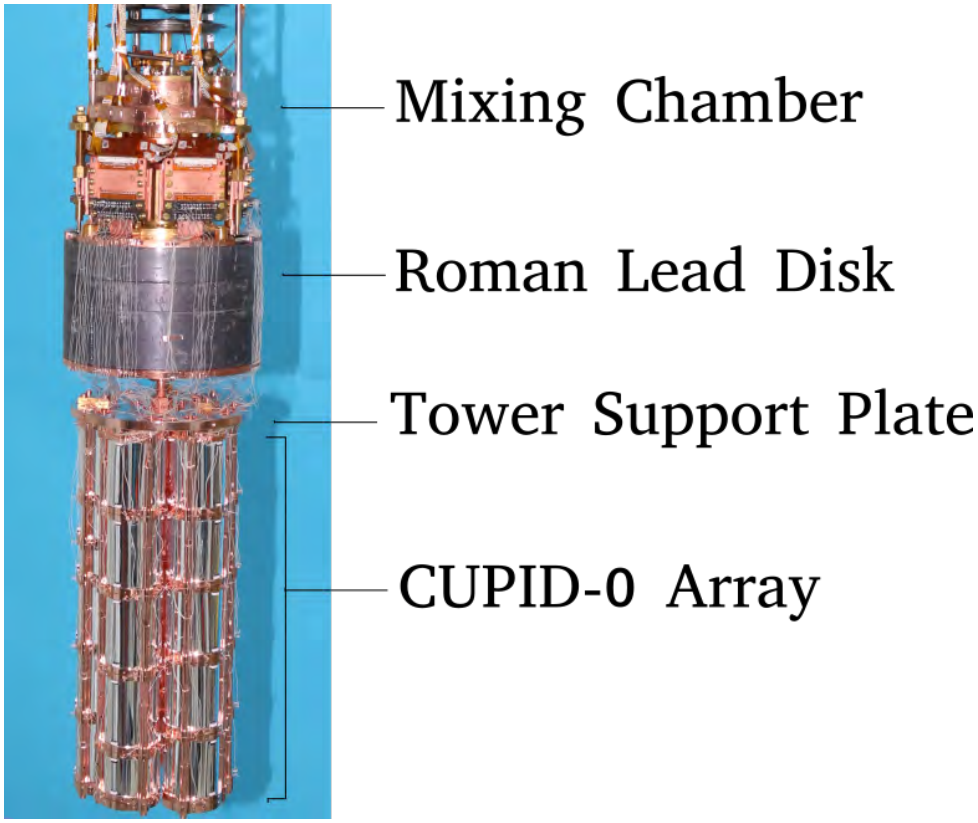

Figure 3: CUPID-0 tower once connected to the dilution refrigerator.

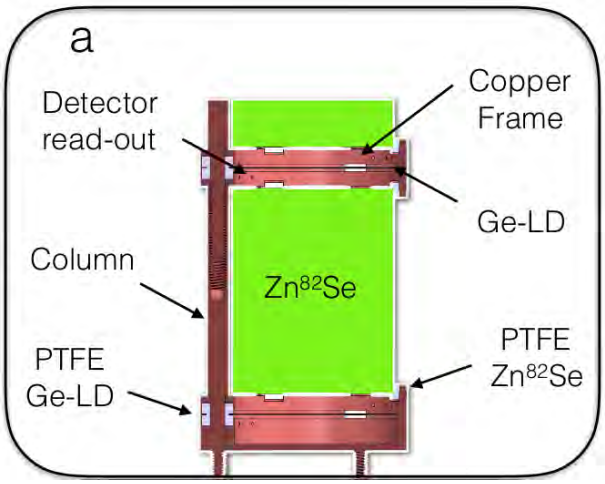

Figure 4: CUPID-0 single module.

avoid the loss of the scintillation photons from the side, a reflecting foil (3M Vikuiti) encloses each ZnSe crystal on the lateral surface.

3.1 ZnSe crystals

ZnSe crystals were grown at the ISMA institute in Karkhiv (Ukraine) using the enriched selenium produced by the URENCO Company and a specially selected high-purity zinc. Both the synthesis of the ZnSe powder and the process of crystal growth were optimized by ISMA under the supervision of the LUCIFER collaboration, focusing the efforts on the maximization of the production yield and the improvement of quality, size and radioactivity of the crystals (for more details see the LNGS Annual Report of year 2015). The ingots were found particularly brittle when heated by the friction of mechanical operation, implying that operations like cut and polishing are extremely delicate. This motivated the choice of delivering the ingots to LNGS where cut and polishing was done under controlled conditions. Starting from Spring 2016 a total of 26 crystals (24 enriched and 2 natural) were cut and lapped to dimensions and shape compatible with the tower structure of the experiment.

Since not all the crystals were grown in the same type of crucible and some of the ingots presented in-homogeneities and cracks, the final shape of the crystals is defined as the best compromise between maximal mass and defect removal. The result is that only few crystals have a really cylindrical shape. Cut (done with a precision diamond wire saw) and shaping (done with commercial waterproof abrasive papers of different roughness) was done in normal laboratory condition. Afterwards, all the crystals were treated in the underground clean room of the Princeton University (class 1000, radon activity <0.2 Bq/m^3). Crystals were at first washed with a water solution with 5% HF and later mechanically polished. The procedure was optimized to remove about a layer of about 10 μm, aiming at the removal of any possible surface contamination created by the previous mechanical treatments meanwhile bringing the crystal dimensions as close as possible to the required ones. The materials used in this phase were exclusively those selected for the CUORE ultraclean polishing procedure [20]: the abrasive powder (SiO_2 from Admatechs, product Admafine SO-E5, average particle diameter 1.5 μm), the polishing pad (Buehler pads Nylon 40-7068), and ultrapure water (with Rn stripped by N_2 fluxing), selected ultra clean gloves and polyethylene sheets.

The final sizes and masses are shown in Fig. 5. The total mass of the 24 enriched crystals is

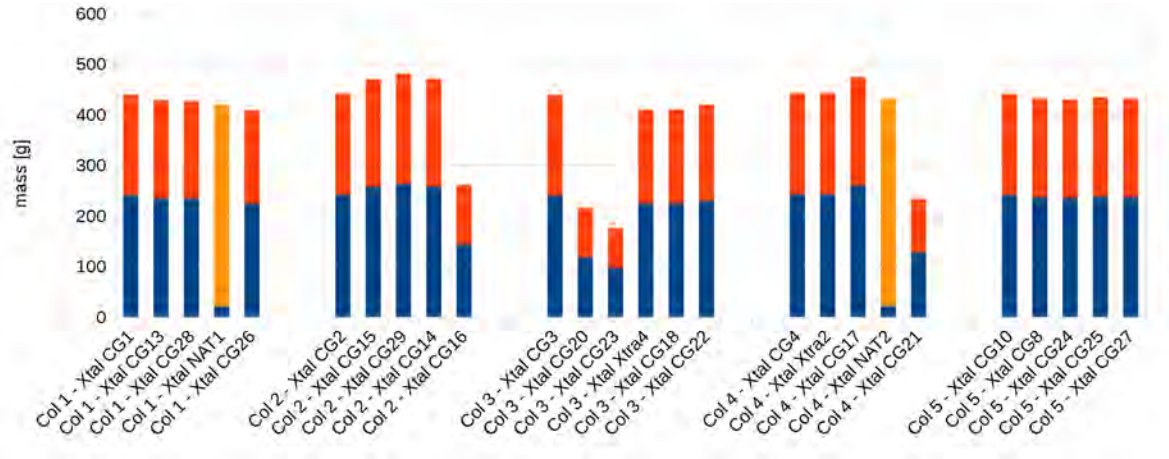

Figure 5: Crystal (Xtal) masses (bar height) and mass of ^{82}Se isotope for each crystal (blu bar height) for CUPID-0 array. Crystals are grouped by column.

9.65 kg corresponding to 5.28 kg of ^{82}Se. The two natural crystals have a total mass of 0.85 kg corresponding to 40 g of ^{82}Se.

3.2 ZnSe bolometers

In June 2016 each crystal was equipped with an NTD Ge thermistor (the temperature sensor) and a Si heater. NTD stands for Neutron Transmutation Doping, this procedure implies the exposure of a Ge wafer to a thermal neutron beam that creates, through neutron activation, a very uniform density of dopants. If the metal to insulator transition is achieved, the heavily doped germanium exhibits, at low temperature, a resistivity that is exponentially dependent on the lattice temperature. Once doping is optimized for the desired operating temperature, these devices become high sensitivity thermometers. Care have to be dedicated to the optimization of the contact geometry (that influences the device resistance and temperature sensitivity, but defines also the areas available for bonding and gluing) and the volume. The latter has to be kept small enough to avoid that the sensor heat capacity dominates over the crystal one, otherwise the signal is reduced in height spoiling the achievable energy resolution. In the case of the ZnSe crystals, the thermistor size is $2.8 \times 3 \times 1 mm^3$. Si heaters are heavily doped resistances that are used to produce a monochromatic heat signal in the bolometer volume. This provides a reference pulse used to check the bolometer gain (the ratio between pulse amplitude and injected energy) over time. The heating is obtained injecting into the resistor a voltage pulse with fixed amplitude. The consequent Joule dissipation injects a fixed amount of heat into the crystal and induces a temperature rise similar to those induced by particles traversing it. Both semiconductor devices were ball bonded with 50 μm diameter gold wires and glued with epoxy spots on the top face of each ZnSe crystal. To optimize the thermal conductance between the sensor and the crystal, as well as the reproducibility of the performances among the detectors, particular attention must be paid to the geometry of the glue interface (number of spots, spots size...). Therefore the gluing procedure was done through a semi-automated system (composed by a cartesian robot to dispense the glue spots and custom-designed posts to keep the sensor in the correct position with respect to the crystal) and performed inside the Princeton clean room to ensure low radioactive conditions.

3.3 Ge Light Detectors

The light detectors used for the CUPID-0 array are undoped Ge wafers, 44 mm in diameter and 0.17 mm in thickness, instrumented as bolometers. One side of the wafer is provided with an anti-reflecting SiO coating. On the opposite face are glued, as for ZnSe bolometers, an NTD Ge thermistor and a Si heater. Due to the small heat capacity of the Ge wafer, the NTD thermistors are smaller ($2.8 \times 2 \times 0.5 mm^3$) than those used for ZnSe bolometers. Bonding and gluing procedures were identical to those adopted for the ZnSe crystals.

3.4 Assembly

The detector assembly was done in compliance with the strategies adopted for the construction of the CUORE detector [5].

The copper used for the detector holding system is a special alloy from Aurubis company suitable for cryogenic use, its Th and U contaminations are below 2×10^{-6} Bq/kg (C.L. 90%). The holder parts were produced during 2015 and stored underground. Only the small bars that connect the frames had to be modified in 2016 to match the different crystals lengths. Following, all the copper elements were cleaned with the same TECM procedure developed for CUORE by the Legnaro INFN Laboratories. TECMS stands for abrasive tumbling, electro-polishing, chemical etching, and magnetron plasma etching. This procedure proved to efficiently reduce the surface contamination of copper parts [28] in long lived alpha emitters from the U and Th chains. PTFE spacers were produced with a specially selected material with Th and U contaminations respectively lower than 6.1×10^{-6} Bq/kg (C.L. 90%) and 2.2×10^{-5} Bq/kg. After the shaping they were cleaned in a ultra-sonic bath with soap and ultra-pure nitric acid solution.

After cleaning all the pieces were vacuum sealed and stored underground, ready to be used in the tower assembly.

The CUPID-0 assembly line consists of a garage, equipped with a motorized linear actuator (for the vertical motion) with a rotation stage and an assembly plate on top (see Fig.6). Each column is built from the bottom floor, stacking Ge light detectors and ZnSe crystals one over the other, once embedded in their copper frames. While growing in height the column descends into the garage so that operator work always in the same position. Once the tower is completed, the detector is removed from the garage and inserted into a sealed acrylic (PMMA) canister. This storage box is equipped with inlet-outlet plugs to flux continuously nitrogen through its volume, creating a small overpressure that ensures against radon inlet from external air.

3.5 Cryogenics

The CUPID-0 array was installed in October 2016 in the Oxford Instruments dilution refrigerator already used by Cuoricino and CUORE-0. The refrigerator provides the cooling power necessary to keep the bolometers at their working temperature, it comprises a ^{3}He/^{4}He dilution unit and a system of nested cylindrical copper vessels (the cryostat) that act as decoupling thermal stages. The array is suspended to the cold finger of the dilution unit, in the very core of the cryostat. A cylindrical low-background Roman lead shield protect the tower from the radioactivity of the dilution unit and of the outermost thermal stages. The suspension system was re-designed after CUORE-0 decomissioning, to improve the mechanical decoupling of the CUPID-0 tower from the cryostat. Indeed, vibrations are a dominant source of noise that spoils bolometer energy resolution and long-time stability. In the new suspension system three stainless steel wires are

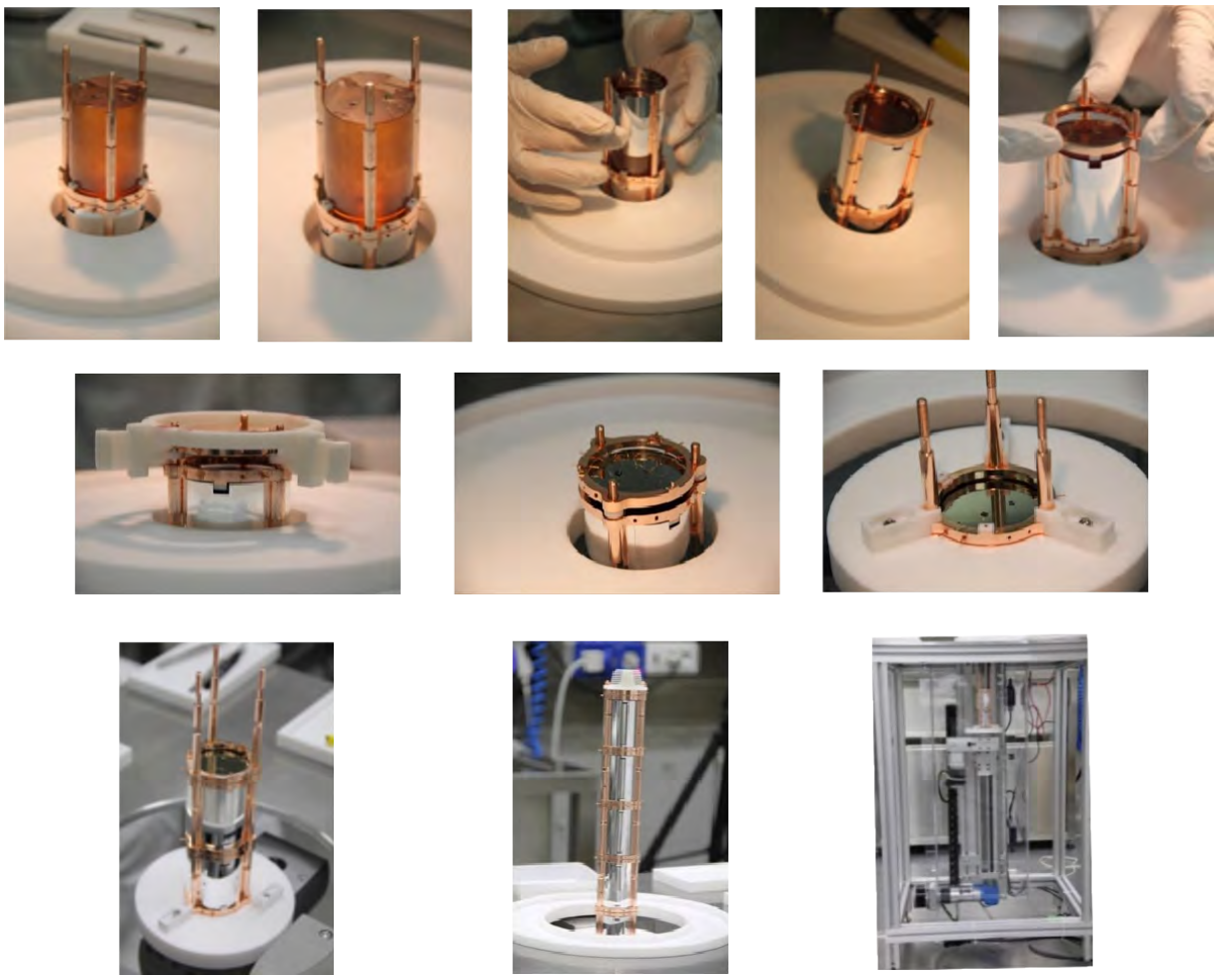

Figure 6: Assembly of one of the CUPID-0 columns. From top: a ZnSe crystal is mounted in the copper frame+bars structure, the reflecting foil is added, the Ge detector is stacked over crystal. In the bottom row the right picture shows the garage used for the assembly.

used to suspend the top lead disk of the internal lead shield to the mixing chamber. A spring connects the lead disk to the detector copper support plate.

Vacuum and wiring systems were completely refurbished after CUORE-0 decommissioning. The reconfiguration of the vacuum system included the realization of a completely new pumping-line for the ^{3}He/^{4}He mixture (condenser line). A leak on that line was probably responsible, during CUORE-0 operations, of the inlet of impurities in the mixture circulation system. The consequent need of periodic maintenance of the cryogenic system increased the dead time of the experiment. The wiring system of the cryostat below the mixing chamber was completely renewed in order to increase the number of readable channels.

The innermost copper vessels were mechanically and chemically treated to remove contaminants that may have deposited on their surface over the years.

3.6 Electronics

The electronic bias and read-out systems are identical for both ZnSe bolometers and Ge light detectors, both were designed to ensure low noise and high stability and are located close to the refrigerator, but at room temperature. The NTD Ge thermistors feature a very large impedance (10-100 of MΩ), they are DC biased through two GΩ ultra-stable low-noise film resistors with a dedicated bias channel for each sensor. Temperature variations in ZnSe/Ge bolometers induce a temporarily change in the NTD Ge thermistor resistance that is converted into a voltage pulse. The resistance recovers to its original value upon restoring of the thermal equilibrium. The signal (ranging typically from tens of μm to hundreds of μm for a MeV deposit in the crystal) is slow, with rise time (90-10%) of the order of 10/4 ms and decay times (70-30%) of the order of 40/8 ms respectively for ZnSe/Ge bolometers. The read-out system is consequently optimized to reduce low frequency noise: a set of twisted connecting wires routes the signal out of the cryostat toward the front-end. To suppress interference and cross-talk the input stage of the front-end is differential, with a pair of JFET custom-designed to have the gate current very small, making negligible the parallel noise. The signal is amplified, filtered and finally fed to the DAQ. Both the amplification gain and the cut-off of the antialiasing filter are programmable and channel dependent in order to better match the detector characteristics. Electronic channels exhibit a very small thermal drift, of the order of a few ppm/C, thanks to a very stable power supply system designed for this purpose.

The system is instrumented with a voltage pulser (ppm stable in both time and temperature) that allows to feed a reference pulse to Si heater. The Joule dissipation in the small Si heater mimic a particle signal, producing a monochromatic reference line that is used in the off-line analysis for gain equalization. This technique allows to reduce the effects of bolometer temperature drifts that otherwise would spoil the energy resolution of the detectors.

CUPID-0 front-end was entirely designed and constructed in the INFN Electronic Laboratory of Milano-Bicocca in the years 2015 and 2016. The installation at LNGS was completed at the end of 2016.

3.7 DAQ

The data acquisition (DAQ) system is based on commercial digitiser boards from National Instruments, NI-PXI628x. These boards feature 18-bit ADCs, configurable sampling frequency up to 500 kHz, configurable input range up to +/-10 V, digitization of up to 16 analog signals in differential input configuration. The DAQ boards are contained in a PXI chassis remotely controlled via computer. The data link between the DAQ chassis and computers is made through

optical fiber connection providing a proper data transmission bandwidth and a complete electrical decoupling between the computers and the detectors.

The bolometer waveforms are digitized with sampling frequencies of 1 kHz for both heat and light detectors. The complete data stream is transferred from the PXI chassis to the computers; triggers are implemented via software. This approach allows to implement arbitrarily complex signal detection algorithms, the only constraint being the computing resources.

The CUPID-0 raw data consist in Root files containing the continuous data stream of all channels recorded by the DAQ at sampling frequencies of 1 kHz. Triggers are implemented via software and saved in a custom format based on the ROOT data analysis framework. Each event contains the waveform of the triggering bolometer and of those geometrically close to it, plus some ancillary information. The non event-based information is stored in a PostgreSQL database that is also accessed by the offline data analysis software. The data taking is arranged in runs, each run lasting about one day. Raw data are transferred from the DAQ computers to the permanent storage area (located at CNAF) at the end of each run. A full copy of data is preserved also on tape.

The data analysis flow consists in two steps; in the first level analysis the event-based quantities are evaluated, while in the second level analysis the energy spectra are produced. The analysis software is organized in sequences. Each sequence consists in a collection of modules that scan the events in the Root files sequentially, evaluate some relevant quantities and store them back in the events. The analysis flow consists in several fundamental steps that can be summarized in pulse amplitude estimation, detector gain correction, energy calibration and search for events in coincidence among multiple bolometers.

4 Perspectives

CUPID-0 started the physics run in early 2017, it is expected to run at least for 1 y of live-time to prove the potential of the scintillating bolometers technology, and the high number of emitters will allow to reach a remarkable sensitivity on the ^{82}Se $\beta\beta(0\nu)$. Thanks to the low crystal contaminations, the expected background should be lower than 1.5×10^{-3} counts/keV/kg/y, mainly produced by the cryogenic setup [11, 26]. The sensitivity can be computed in the "zero background" approximation and results $\sim10^{25}$ y at 90% C.L. in 1 year of data taking.

5 Acknowledgements

The CUPID-0 collaboration would like to thank the University of Princeton by permission of using their Clean Room installed underground at LNGS. This work was partially supported by the LUCIFER experiment, funded by ERC under the European Union's Seventh Framework Programme (FP7/2007-2013)/ERC grant agreement n. 247115, funded within the ASPERA 2nd Common Call for R&D Activities. We are particularly grateful to M. Iannone for its help in all the stages of the detector construction, to M. Guetti for the assistance in the cryogenic operations and to the mechanical workshop of LNGS (in particular E. Tatananni, A. Rotilio, A. Corsi, and B. Romualdi) for continuous and constructive help in the overall set-up design.

6 Publications in 2016

1. D. R. Artusa *et al.*, Eur. Phys. J. C **76** 364 (2016)

2. J. W. Beeman *et al.*, J LOW TEMP PHYS, **184** 852 (2016)
3. L. Pattavina *et al.*, J LOW TEMP PHYS, **184** 286 (2016)
4. N. Casali *et al.*, J LOW TEMP PHYS, **184** 952 (2016)
5. N. Casali *et al.*, J PHYS CONF SER, **718** 062048 (2016)
6. L. Gironi *et al.*, Phys. Rev C, **94-5** 054608 (2016)

References

[1] R. Strauss, R., Angloher, G., Bento, A. *et al.*, Eur. Phys. J. C **74** 2957 (2014)

[2] D. R. Artusa *et al.* (CUORE Collaboration), Eur. Phys. J. C (2014) 74:3096

[3] J.W. Beeman *et al.*, Adv. High Energy Phys. **2013**, 237973 (2013)

[4] C. Arnaboldi *et al.* (Cuoricino Collaboration), Phys. Rev. Lett. **95** (2005) 14501
E. Andreotti, *et al.* (Cuoricino Collaboration), Astropart. Phys. **34** 822 (2011)

[5] C. Alduino *et al.* (CUORE Collaboration), J. Instrum. (2016)

[6] C. Arnaboldi *et al.* (CUORE Collaboration), Astropart. Phys. **20** (2003) 91.
C. Arnaboldi *et al.* (CUORE Collaboration), Nucl. Instr. Meth. A **518**(2004) 775

[7] D.L. Lincoln *et al.*, Phys.Rev.Lett. **110**, 012501 (2013)

[8] G. Wang *et al.*, arXiv:1504.03612 (2015)

[9] G. Wang *et al.*, arXiv:1504.03599 (2015)

[10] O. Cremonesi M. Pavan, Adv. High En. Phys. 2014, Article ID 951432

[11] C. Alduino *et al.* (CUORE Collaboration), Eur. Phys. J. C **77**, 13 (2016)

[12] C. Arnaboldi *et al.*, Astropart. Phys. **34**, 344 (2011)

[13] J.W. Beeman *et al.*, JINST **8**, P05021 (2013)

[14] L. Gironi *et al.*, JINST **5**, P11007 (2010)

[15] J.W. Beeman *et al.*, Eur. Phys. J. **C72**, 2142 (2012)

[16] J.W. Beeman *et al.*, Astropart. Phys. **35**, 813 (2012)

[17] J.W. Beeman, et al., Phys. Lett. B **710**, 318 (2012)

[18] L. Cardani *et al.*, J. Phys. **G41**, 075204 (2014)

[19] E. Armengaud *et al.*, JINST **10**(05), P05007 (2015)

[20] C. Arnaboldi *et al.* (CUORE Collaboration), J. Cryst. Growth **312**(20), 2999 (2010)

[21] L. Berge *et al.*, JINST **9**, P06004 (2014)

[22] L. Cardani *et al.*, JINST **8**, P10002 (2013)

[23] T.B. Bekker *et al.*, Astropart. Phys. **72**, 38 (2016)

[24] C. Arnaboldi *et al.*, Astropart. Phys. **34**, 143 (2010)

[25] E. Armengaud *et al.*, Submitted to EPJC, arXiv:1704.01758

[26] D. R. Artusa *et al.*, Eur. Phys. J. C **76**, 364 (2016)

[27] LNGS Annual Report year 2015

[28] F. Alessandria *et al.* (CUORE Collaboration), Astropart. Phys.**45**, 13 (2013)

[29] N. Casali *et al.*, Eur. Phys. J. **C75**(1), 12 (2015)

DAMA

Collaboration:

P. Belli[a], R. Bernabei[a,@], A. Bussolotti[a,*], A. Di Marco[a], V. Merlo[a], F. Montecchia[a], S. Ghorui[a,m], A. d'Angelo[b], A. Incicchitti[b], A. Mattei[b,*], V.M. Mokina[b,c], O.G. Polischuk[b,c], F. Cappella[d], V. Caracciolo[d], R. Cerulli[d], C.J. Dai[e], H.L. He[e], H.H. Kuang[e], X.H. Ma[e], X.D. Sheng[e], R.G. Wang[e], Z.P. Ye[e,f]

in some detector developments, by-product results and small scale experiments:

A. Addazi[g,d], A.S. Barabash[h], Z. Berezhiani[g,d], R.S. Boiko[c], V.B. Brudanin[i], D.M. Chernyak[c], F.A. Danevich[c], V.Yu. Denisov[c], O.V. Hladkovska[c], D.V. Kasperovych[c], V.V. Kobychev[c], S.I. Konovalov[h], G.P. Kovtun[j], N.G. Kovtun[j], B.N. Kropivyansky[c], M. Laubenstein[d], S. Nisi[d], D.V. Poda[c], A.P. Shcherban[j], V.N. Shlegel[k], V.I. Tretyak[c], I.A. Tupitsyna[l], V.I. Umatov[h], Ya.V. Vasiliev[k], I.M. Vyshnevskyi[c],

[a]Dep. Phys., Univ. Roma "Tor Vergata" and INFN Tor Vergata, 00133 Roma, Italy.
[b]Dep. Phys., Univ. Roma "La Sapienza" and INFN-Roma, 00185 Roma, Italy.
[c]Institute for Nuclear Research, MSP 03680, Kiev, Ukraine.
[d]Laboratorio Nazionale del Gran Sasso, INFN, 67010 Assergi (Aq), Italy.
[e]IHEP, Chinese Academy of Sciences, P.O. Box 918/3, Beijing 100049, China.
[f]Dep. Phys., Jinggangshan University 343009, Jiangxi, China.
[g]Dep. Phys., Univ. L'Aquila, 67100 Coppito, AQ, Italy
[h]Institute of Theoretical and Experimental Physics, 117259 Moscow, Russia
[i]Joint Institute for Nuclear Research, 141980 Dubna, Russia.
[j]Nat. Science Center Kharkiv Institute of Physics and Technology, Kharkiv, Ukraine.
[k]Nikolaev Institute of Inorganic Chemistry, 630090 Novosibirsk, Russia.
[l]Institute for Scintillation Materials, 61001 Kharkiv, Ukraine.
[m]Indian Institute of Technology Ropar, Ropar, India.
[@] Spokesperson; [*] technical staff

Abstract

DAMA is as an observatory for rare processes developing and exploiting highly radiopure scintillators. It is located deep underground at the Gran Sasso National Laboratory of the I.N.F.N. (LNGS). In 2016 the main experimental activities have been performed with: i) the phase 2 of the second generation DAMA/LIBRA set-up (DAMA/LIBRA–phase2 sensitive mass: $\simeq$ 250 kg highly radiopure NaI(Tl)), upgraded so far in 2008, 2010 and at the end of 2012; ii) the DAMA/LXe set-up (sensitive mass: $\simeq$ 6.5 kg liquid Kr-free Xenon enriched either in ^{129}Xe or in ^{136}Xe); iii) the DAMA/R&D set-up (a facility dedicated to perform relatively small scale experiments, mainly investigating double beta decay modes

in various isotopes); iv) the DAMA/Ge set-up (mainly dedicated to sample measurements and to specific measurements on rare processes); some activities are also performed with the detectors Ge-Multi, GeCris and the recently-installed Broad Energy Germanium detector of the STELLA facility; v) a small set-up (named DAMA/CRYS) for prototype tests, detectors' qualification and small scale experiments. The main DAMA activities during 2016 are shortly summarized in the following.

1 DAMA/LIBRA

DAMA/LIBRA (Large sodium Iodide Bulk for Rare processes) is a unique apparatus for its sensitive mass, target material, intrinsic radio-purity, methodological approach and all the controls performed on the experimental parameters (see Ref. [1, 2, 3, 4, 5, 6, 7, 8, 9, 10, 11, 12, 13, 14, 15] an the 2016 publication list). It is the successor of DAMA/NaI [16, 17, 18, 19, 20, 21, 22, 23, 24, 25, 26, 27, 28], with a larger exposed mass, higher duty cycle and increased sensitivity. The main goal of DAMA/LIBRA is the investigation of the Dark Matter (DM) particles in the galactic halo by exploiting the DM model independent annual modulation signature [29, 30].

The granularity of the apparatus (25 detectors in a matrix 5×5) is an important feature to study DM and for background identification since DM particles can just contribute to events where only one of the 25 detectors fires (*single-hit* events) and not to whose where more than one detector fire in coincidence (*multiple-hit* events). The apparatus has also the unique feature (as well as DAMA/NaI) that gamma calibrations are regularly performed down to the software energy threshold in the same conditions as the production runs, without any contact with the environment and without switching-off the electronics. The high light yield and other response features have allowed working in a safe and reliable way down to 2 keV (DAMA/LIBRA–phase1). At the end of 2010 the installation of DAMA/LIBRA–phase2 started with new photomultipliers (PMTs) of higher quantum efficiency [6] and some improvements on the electronics and DAQ; new preamplifiers were installed in 2012.

Among the scientific goals of this running set-up we mention here: i) investigation with high sensitivity of the DM particle component in the galactic halo by the model independent approach known as DM annual modulation signature, with highly precise determination of the modulation parameters (which carry crucial information); ii) corollary investigations on the nature of the candidate and on the many possible astrophysical, nuclear and particle physics scenarios; iii) investigations on other possible model dependent and/or model independent approaches to study DM particles, second order effects and some exotic scenarios; iv) improvement on the sensitivity to explore rare processes other than DM as performed by the former DAMA/NaI apparatus in the past [28] and by itself so far [9, 10, 11].

This requires dedicated work for reliable collection and analysis of very large exposures to reach more competitive sensitivities. As regards the DM features, see e.g. the Sect 6 of Ref. [21] and the Appendix of Ref. [2]. In particular, the latter shows how the decreasing of the software energy threshold as in the present DAMA/LIBRA–phase2 offers the unique possibility to investigate the modulation amplitude at the lowest energy, where a discrimination power can disentangle among many of the possible DM scenarios.

1.1 Final model-independent result of DAMA/LIBRA–phase1 on DM annual modulation

The total exposure of DAMA/LIBRA–phase1 is 1.04 ton × yr in seven annual cycles; when including also that of the first generation DAMA/NaI experiment it is 1.33 ton × yr, corresponding

to 14 independent annual cycles [4].

Fig. 1 shows the time behaviour of the experimental residual rates of the *single-hit* scintillation events in the (2–6) keV energy interval for the complete DAMA/LIBRA–phase1. The residuals of the DAMA/NaI data (0.29 ton × yr) are given in Refs. [2, 20, 21].

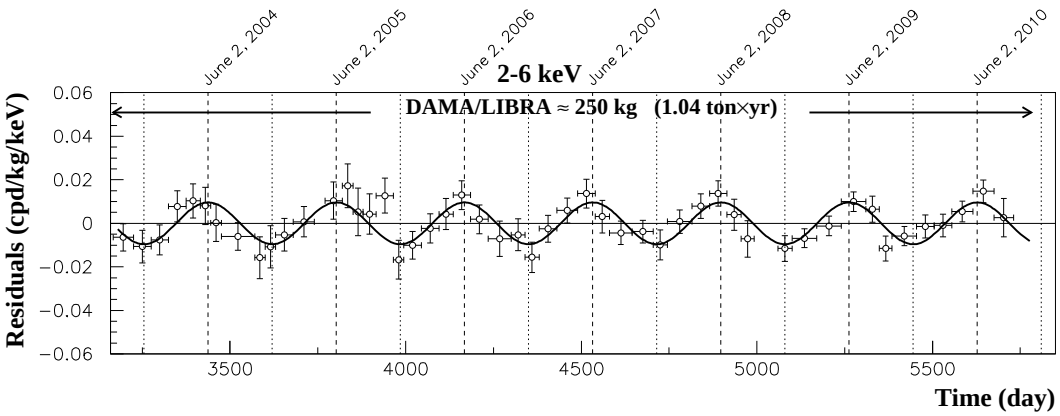

Figure 1: Experimental residual rate of the *single-hit* scintillation events measured by DAMA/LIBRA–phase1 in the (2–6) keV energy interval as a function of the time. The time scale is maintained the same of the previous DAMA papers for coherence. The data points present the experimental errors as vertical bars and the associated time bin width as horizontal bars. The superimposed curve is the cosinusoidal function behaviour $A\cos\omega(t-t_0)$ with a period $T=\frac{2\pi}{\omega}=1$ yr, a phase $t_0=152.5$ day (June 2^{nd}) and modulation amplitude, A, equal to the central value obtained by best fit on the data points of the entire DAMA/LIBRA–phase1. The dashed vertical lines correspond to the maximum expected for the DM signal (June 2^{nd}), while the dotted vertical lines correspond to the minimum.

The DAMA/LIBRA–phase1 data give evidence for the presence of DM particles in the galactic halo, on the basis of the exploited model independent DM annual modulation signature by using highly radio-pure NaI(Tl) target, at 7.5 σ C.L.. Including also the first generation DAMA/NaI experiment (cumulative exposure 1.33 ton × yr, corresponding to 14 annual cycles), the C.L. is 9.3 σ. At present status of technology the DM annual modulation is the only model independent signature available in direct DM investigation that can be effectively exploited. All the many specific requirements of the signature are fulfilled by the data and no systematic or side reaction able to mimic the exploited DM signature is available (see e.g. Refs.[2, 3, 4, 19, 20, 21, 31, 32, 33, 34, 35, 36, 7, 8, 13] and the 2016 publication list). In particular, only systematic effects or side reactions simultaneously able to fulfil all the specific requirements of the DM annual modulation signature and to account for the whole observed modulation amplitude could mimic this signature; thus, no other effect investigated so far in the field of rare processes offers a so stringent and unambiguous signature.

The DAMA obtained model independent evidence is compatible with a wide set of scenarios regarding the nature of the DM candidate and related astrophysical, nuclear and particle Physics. For example, some of the scenarios available in literature and the different parameters are discussed in Refs. [20, 21, 17, 22, 23, 24, 25, 26, 27, 5, 37, 38, 14, 15], in Appendix A of Ref. [2], and in the 2016 publication list. A further large literature is available on the topics; many possibilities are open.

No other experiment exists, whose result – at least in principle – can directly be compared in a model independent way with those by DAMA/NaI and DAMA/LIBRA. In particular, all the results presented so far in the field are not in conflict with the model independent DM

annual modulation result by DAMA in many scenarios, also considering the large uncertainties in theoretical and experimental aspects, the same holds for indirect approaches; see e.g. some arguments in 2016 publication list and quoted references.

Studies for measurements with data taking dedicated to other rare processes are continuing. Studies on other DM features, second order effects, and several other rare processes are in progress with the aim to reach very high sensitivity thanks to the progressive increasing of the exposure. In particular a new analysis of the DM model-independent annual modulation result obtained by DAMA/NaI and DAMA/LIBRA–phase1 in terms of mirror DM, an exact duplicate of ordinary matter from parallel hidden sector, has been performed. Dark mirror atoms are considered to interact with the target nuclei in the detector via Rutherford-like scattering induced by kinetic mixing between mirror and ordinary photons, both being massless. Various possible scenarios for the mirror matter chemical composition has been considered. The paper has been published in 2017 and it is not included in this report.

1.2 DAMA/LIBRA–phase2 during 2016 and prospects

- The upgrades performed on DAMA/LIBRA (DAMA/LIBRA–phase2) have allowed us to lower the software energy threshold of the experiment to 1 keV and to improve also other features as e.g. the energy resolution [6].

- During 2016 DAMA/LIBRA–phase2 has continued to take data in the new phase2 configuration with the PMTs of higher quantum efficiency [6] and new preamplifiers.

- In 2016 the data taking of the 5th full annual cycle of DAMA/LIBRA–phase2 was concluded, and the data taking of the 6th cycle started (we recall that the first year of measurements started in 2011 was mainly commissioning run). It will be completed at fall 2017. After, many data analyses on the whole available exposure will be performed and at their ends the first DAMA/LIBRA–phase2 data release will occur.

- A new study of the DM annual modulation signal, by using the DAMA/LIBRA–phase1 data, in the framework of various new scenarios of mirror dark matter with different chemical composition has been published in 2017. Many configurations and halo models favoured by the annual modulation effect observed by DAMA correspond to kinetic mixing parameter values well in agreement with cosmological bounds. Various existing uncertainties in nuclear and particle physics quantities have also been taken into account.

- On invitation an entire issue of Int. J. of Mod. Phys. A has been dedicated to DAMA; 11 papers on various aspects of related topics have been published.

- In order to disentangle in the corollary investigation on the candidate particle(s) at least some of the many possible astrophysical, nuclear and particle Physics scenarios and related experimental and theoretical uncertainties, the decreasing of the software energy threshold and larger exposures are necessary. Finally the ultimate challenge and the only effective method for such studies is the investigation of a model independent signature and of second order effects. Many topics can be investigated: the peculiarities of the annual modulation phase; the peculiarities of the DM interaction mechanisms; the velocity and spatial distribution of the DM particles in the galactic halo; the effects induced on the DM particles distribution in the galactic halo by contributions from satellite galaxies tidal streams; the detection of possible solar wakes or gravitational focusing effect of the Sun on the DM particle; the investigation of diurnal modulation of the rate on the sidereal

time, expected when taking into account the contribution of the Earth rotation velocity, and so on. Some of these studies have been preliminarily performed with DAMA/LIBRA–phase1 and will be continued with DAMA/LIBRA–phase2 with increased sensitivity as the exposure increases.

- Studies on other DM features, second order effects, and several other rare processes are in progress with the aim to reach very high sensitivity thanks to the progressive increasing of the exposure.

- Studies for feasibility towards the DAMA/LIBRA–phase3 with the aim to further enhance the sensitivity of the experiment by improving the light collection of the detectors are going on. In particular an R&D on new further highly radio-pure PMTs with high quantum efficiency is in progress.

- A multi-purpose 1 ton (full sensitive mass) set-up made of highly radio-pure NaI(Tl) was proposed in 1996 to INFN-CSN2, and the funded R&D-II, DAMA/LIBRA and R&D-III were considered as intermediate steps. It is worth noting that the whole 1 ton will be fully sensitive to the processes of interest. As previously reported, the final design is based on the fulfillment of three additional replica of the present DAMA/LIBRA set-up, solution that offers many technical and scientific advantages; thus, the technical design is completely known, since DAMA/LIBRA is operative. As already mentioned, some activities were/are/will-be carried out in the light of overcoming the present problems regarding the supplying and purifications of high quality NaI and, mainly, TlI powders and the creation of suitable protocols.

2 DAMA/LXe

We pointed out since 1990 [39] the possible interest in using the liquid Xenon as target-detector material for particle DM investigations. Since the end of 80's (former Xelidon experiment of the INFN) we have built several liquid Xenon (LXe) prototype detectors. Since 1996 we pointed out to the INFN-CSN2 the intrinsic problems of this detector medium for large scale experiments dedicated to DM investigation (poor collection of the far UV light, response non-uniformity on large detectors, self-absorption, rebuilding of the sensitive part for each liquefaction with no proof of the same condition, no possibility of routine calibration in keV region, degassing of materials, operating parameters stability, etc.) and agreed to pursue the activity by exploiting Kr-free enriched Xenon gases in limited volume.

The presently running set-up (with a Cu inner vessel filled by $\simeq$ 6.5 kg, that is $\simeq$2 l, of liquid Xenon) can work either with Kr-free Xenon enriched in ^{129}Xe at 99.5% or Kr-free Xenon enriched in ^{136}Xe at 68.8% [40, 41, 42]. Many competing results were achieved on several rare processes [40, 41, 42, 43, 44, 45].

In the period of interest, the set-up has been in data taking filled with Xenon enriched in ^{136}Xe, still mainly focusing the high energy region. Data analyses are continuing.

3 DAMA/R&D

The DAMA/R&D installation is a general-purpose low background set-up used for measurements on low background prototypes and for relatively small-scale experiments [46, 47, 48, 49, 50, 51, 52, 53, 54].

The measurements mainly investigate 2β decay modes in various isotopes; both the active and the passive source techniques have been exploited as well as the coincidence technique. Particular attention is dedicated to the isotopes allowing the investigation of the $2\beta^+$ processes and, in particular, to resonant 2ϵ or $\epsilon\beta^+$ decay channels. The investigation of neutrino-less $2\beta^+$, 2ϵ and $\epsilon\beta^+$ processes can refine the understanding of the contribution of right-handed currents to neutrino-less 2β decay; therefore developments of experimental technique to search for 2ϵ, $\epsilon\beta^+$, and $2\beta^+$ processes are strongly required considering also that in the $2\beta^+$ investigations a gap of several orders of magnitude between theoretical expectations and experimental results is the usual situation and the better achieved sensitivities do not exceed the level of $T_{1/2} \simeq 10^{21}$ yr. Even more important motivation to search for double electron capture appears from possibility of a resonant process thanks to energy degeneracy between initial and final state of the parent and daughter nuclei. Such a resonant process could occur if the energy of transition ($Q_{2\beta}$) minus the energies of two bounded electrons on K or/and L atomic shells of daughter nucleus is near to the energy of an excited level (E_{exc}) of the daughter isotope.

Therefore, investigations on various kinds of new scintillators and preliminary works for the future measurements are also in progress within the DAMA activities.

Some of the main results during 2016 are listed in the following.

- The Aurora measurements to investigate double beta decay of ^{116}Cd with the help of 1.162 kg cadmium tungstate crystal scintillators enriched in ^{116}Cd to 82% is continuously in data taking. The half-life of ^{116}Cd relatively to the two neutrino double beta decay was measured with the highest up-to-date accuracy $T_{1/2} = [2.69 \pm 0.14\ (\text{syst.}) \pm 0.02\ (\text{stat.})] \times 10^{19}$ yr. The sensitivity of the experiment to the neutrinoless double beta decay of ^{116}Cd to the ground state of ^{116}Sn is estimated as $T_{1/2} \geq 2.0 \times 10^{23}$ yr at 90% CL, which corresponds to the effective Majorana neutrino mass limit $\langle m_\nu \rangle \leq (1.2 - 1.8)$ eV. New limits were obtained for the double beta decay of ^{116}Cd to the excited levels of ^{116}Sn, and for the neutrinoless double beta decay with emission of majorons. Partial exposures have been already released in several Conferences (see Sect. 3.1).

- Previous measurements on ^{116}Cd, when considering a suitable energy threshold, allow the investigation on the highly forbidden ^{113}Cd and of the first forbidden ^{113m}Cd beta decays. A paper is in preparation.

- Investigation of radioactive elements segregation in crystals to develop ultra-radio-pure scintillators for rare events searches is continuing.

- Works about the future (several years from now) installation of $^{116}CdWO_4$ detectors in the low background GeMulti set-up for studying the $2\nu2\beta$ transitions of ^{116}Cd to the excited states of ^{116}Sn are continuing. The reachable sensitivity is planned to be at level of the theoretical expectations.

- At the end of the $^{116}CdWO_4$ measurements, new measurements are foreseen in DAMA/R&D. Among them: developments on new SrI_2(Eu) crystals, on new enriched $CdWO_4$ depleted in ^{113}Cd, on highly radio-pure $ZnWO_4$...

3.1 Aurora experiment for 2β decay of ^{116}Cd with $^{116}CdWO_4$ crystal scintillators

The Aurora measurement in DAMA/R&D is in progress to investigate 2β processes in ^{116}Cd by using enriched $^{116}CdWO_4$ scintillation detectors. In details, two $^{116}CdWO_4$ crystal scintillators

with a total mass 1.162 kg (1.584×10^{24} of ^{116}Cd nuclei) are installed in the DAMA/R&D set-up. The low background set-up with the $^{116}CdWO_4$ detectors has been modified several times to improve the energy resolution and to decrease background. In the last configuration of the set-up the $^{116}CdWO_4$ crystal scintillators are fixed in polytetrafluoroethylene containers filled with ultra-pure liquid scintillator. The liquid scintillator improves the light collection from the $^{116}CdWO_4$ crystal scintillators and serves as an anti-coincidence veto counter. The scintillators are viewed through high purity quartz light-guides ($\oslash 7 \times 40$ cm) by low background high quantum efficiency PMTs (See 2016 publication list).

The following half-life of ^{116}Cd relatively to the $2\nu2\beta$ decay to the ground state of ^{116}Sn has been measured: $T_{1/2}^{2\nu2\beta} = [2.69 \pm 0.02(stat.) \pm 0.14(syst.)] \times 10^{19}$ yr.

The signal to background ratio is 2.6:1 in the energy interval $(1.1 - 2.8)$ MeV. The result is in agreement with the previous experiments [55, 56, 57, 58, 59, 60], however the half-life of ^{116}Cd is determined in the present study with the highest accuracy.

To estimate limit on $0\nu2\beta$ decay of ^{116}Cd to the ground state of ^{116}Sn we have used data of two runs with the lowest background in the region of interest: the current one and that accumulated over 8696 h in the set-up described in [61]. The sum energy spectrum is presented in Fig.2.

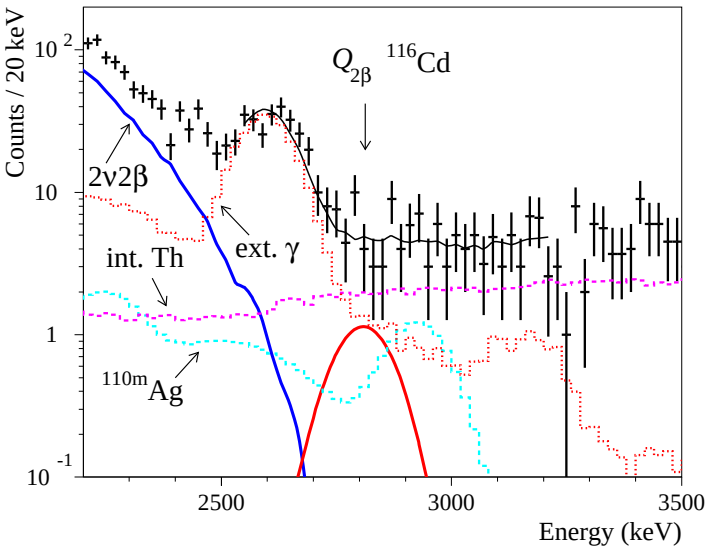

Figure 2: The energy spectrum of β and γ events accumulated over 20711 h with the $^{116}CdWO_4$ detectors in the region of interest together with the background model: the $2\nu2\beta$ decay of ^{116}Cd ("$2\nu2\beta$"), the internal contamination of the $^{116}CdWO_4$ crystals by cosmogenic ^{110m}Ag ("^{110m}Ag") and ^{228}Th ("int. Th"), and the contribution from external γ quanta ("ext. γ").

The background counting rate of the detector in the energy interval $(2.7 - 2.9)$ MeV (which contains 80% of the $0\nu2\beta$ distribution) is ≈ 0.1 counts/(yr×kg×keV). A fit of the spectrum in the energy interval $(2560-3200)$ keV by the background model constructed from the distributions of the $0\nu2\beta$ decay of ^{116}Cd (effect searched for), the $2\nu2\beta$ decay of ^{116}Cd with the half-life 2.69×10^{19} yr, the internal contamination of the crystals by ^{110m}Ag and ^{228}Th, and the contribution from external γ quanta gives an area of the expected peak $S = -3.7 \pm 10.2$, which gives no evidence of the effect, obtaining the following limit for the $0\nu2\beta$ decay of ^{116}Cd to the ground state of ^{116}Sn (see the 2016 publication list): $T_{1/2}^{0\nu2\beta} \geq 2.0 \times 10^{23}$ yr at 90% CL.

The half-life limit corresponds to the effective neutrino mass limit $\langle m_\nu \rangle \leq (1.2 - 1.8)$ eV, obtained by using the recent nuclear matrix elements reported in [62, 63, 64, 65], the phase space factor from [66] and the value of the axial vector coupling constant $g_A = 1.27$.

New limits on the 2β decay to excited levels of ^{116}Sn and the $0\nu2\beta$ decay with emission of one, two and bulk majorons are shown in Table 1 they are at the level of $T_{1/2} \geq (10^{20} - 10^{22})$ yr. Using the limit $T_{1/2} \geq 1.1 \times 10^{22}$ yr on the $0\nu2\beta$ decay with one majoron emission we

Table 1: The half-life limits and half-life value on the 2β decay processes in ^{116}Cd. The most stringent limits obtained in the previous experiments are given for comparison. The limits are given at the 90% CL except the results [67], which are given at the 68% CL.

Decay mode	Transition, level of ^{116}Cd (keV)	$T_{1/2}$ (yr)	Previous result
0ν	g.s.	$\geq 2.0 \times 10^{23}$	$\geq 1.7 \times 10^{23}$ [60]
0ν	$2^+(1294)$	$\geq 6.2 \times 10^{22}$	$\geq 2.9 \times 10^{22}$ [60]
0ν	$0^+(1757)$	$\geq 6.3 \times 10^{22}$	$\geq 1.4 \times 10^{22}$ [60]
0ν	$0^+(2027)$	$\geq 4.5 \times 10^{22}$	$\geq 6.0 \times 10^{21}$ [60]
0ν	$2^+(2112)$	$\geq 3.6 \times 10^{22}$	$\geq 1.7 \times 10^{20}$ [67]
0ν	$2^+(2225)$	$\geq 4.1 \times 10^{22}$	$\geq 1.0 \times 10^{20}$ [67]
$0\nu\chi$	g.s.	$\geq 1.1 \times 10^{22}$	$\geq 8.0 \times 10^{21}$ [60]
$0\nu 2\chi$	g.s.	$\geq 9.0 \times 10^{20}$	$\geq 8.0 \times 10^{20}$ [60]
$0\nu\chi^{bulk}$	g.s.	$\geq 2.1 \times 10^{21}$	$\geq 1.7 \times 10^{21}$ [60]
2ν	g.s.	$= (2.69 \pm 0.14) \times 10^{19}$	
2ν	$2^+(1294)$	$\geq 9.0 \times 10^{20}$	$\geq 2.3 \times 10^{21}$ [68]
2ν	$2^+(1757)$	$\geq 1.0 \times 10^{21}$	$\geq 2.0 \times 10^{21}$ [68]
2ν	$2^+(2027)$	$\geq 1.1 \times 10^{21}$	$\geq 2.0 \times 10^{21}$ [68]
2ν	$2^+(2112)$	$\geq 2.3 \times 10^{21}$	$\geq 1.7 \times 10^{20}$ [67]
2ν	$2^+(2225)$	$\geq 2.5 \times 10^{21}$	$\geq 1.0 \times 10^{20}$ [67]

have obtained one of the strongest limits on the effective majoron neutrino coupling constant $g_{\nu\chi} \leq (5.3 - 8.5) \times 10^{-5}$.

It is worth noting that we have observed a segregation of thorium, radium and potassium in the crystal growing process, which provides a possibility to substantially improve the radiopurity of the $^{116}CdWO_4$ crystal scintillators by re-crystallization, as demonstrated in a paper published in 2016 (see the 2016 publication list). The experiment is running and further efforts are in preparation.

4 DAMA/CRYS

DAMA/CRYS is a small test set-up mainly dedicated to tests on new scintillation detectors' performances and small scale experiments. The activities in the period of interest are briefly summarized in the following.

- The $^{106}CdWO_4$ crystal scintillator – used in the experiment reported in Sect. 5.1 – was installed in the DAMA/CRYS set-up to search for double beta processes in ^{106}Cd by using the $^{106}CdWO_4$ crystal scintillator in coincidence with two large volume $CdWO_4$ scintillation detectors in close geometry. The sensitivity is at level of the most sensitive double β^+ experiments ($T_{1/2} \simeq (10^{20} - 10^{22})$ yr). An enhancement of the sensitivity is expected thanks to increase of detection efficiency to some 2β processes in ^{106}Cd and improvement of background conditions, in particular to $2\nu\epsilon\beta^+$ decay of ^{106}Cd, near to the theoretical predictions, $T_{1/2} \simeq (10^{20} - 10^{22})$ yr. Several improved limits on different channels of double beta processes in ^{106}Cd could be established.

- The shape of ^{113m}Cd beta spectrum was measured (for the first time) with the help of the $^{106}CdWO_4$ scintillation detector (contaminated by ^{113m}Cd at the level of $\approx$ 100 Bq/kg) in the DAMA/CRYS low background set-up over 391 h. The experimental spectral shape can be fitted by convolution of the detector response function with the theoretical shape; the latter is the allowed β shape with a correction function $C(w) = \alpha_1 + \alpha_2/w + \alpha_3 w + \alpha_4 w^2$. Values of the α_i parameters and the Q_β value are found by fitting. A paper describing the results is in preparation.

- The cryogenic system to be installed in DAMA/CRYS (to allow also measurements of the responses of various scintillators as a function of the temperature) has been tested at LNGS (see Fig. 3); a second one, which can be coupled to the previous one to enlarge the cryogenic volume to allocate the detectors, has been realized.

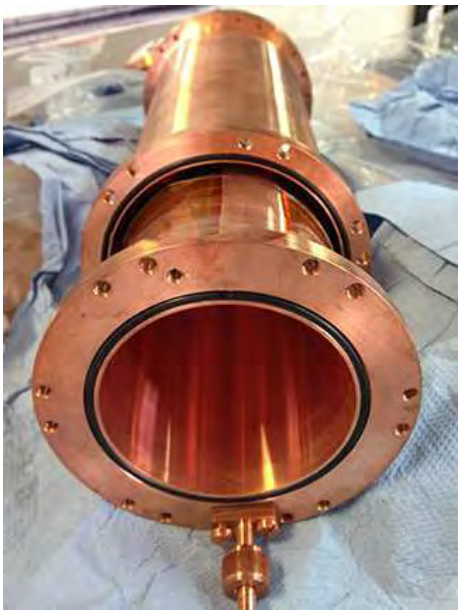

Figure 3: The cryostat to be installed in DAMA/CRYS (to allow also measurements of the responses of various scintillators as a function of the temperature) under test.

- Preparations of other future measurements are in progress

5 DAMA/Ge and LNGS STELLA facility

The measurements on samples and on various R&D developments are performed by means of the DAMA low background Ge detector, specially built with a low Z window; it is operative deep underground in the STELLA facility of the LNGS. In addition other Ge detectors (in particular, GeMulti, GeCris and the recently-installed Broad Energy Germanium detector) are also used for some peculiar measurements. Published results can be found in Ref. [69, 70, 71] and in the 2016 publication list.

The main data takings/results during year 2016 with DAMA/Ge and LNGS STELLA facility are summarized in the following.

- The results of the experiment to search for double beta processes in ^{106}Cd by using cadmium tungstate crystal scintillator enriched in ^{106}Cd ($^{106}CdWO_4$, mass of 216 g [47]) in coincidence with the four crystals HPGe detector GeMulti (the volume of each germanium crystal is 225 cm^3) at the STELLA facility were published in 2016 (see Sect. 5.1).

- There are two positive experiments where the 2β decay of ^{150}Nd to to the first 0^+ excited state of ^{150}Sm was detected with the half-life at the level of $T_{1/2} \simeq 10^{20}$ yr with rather modest accuracy at the level of $\approx 30\%$ [72, 73] and precise measurements of the two neutrino mode of double beta decay is important to develop the theoretical calculations of the process. An advanced experiment is in progress with deeply purified 2381 g (and pressed to improve the detection efficiency) neodymium sample installed in the GeMulti set-up with four HPGe detectors in one cryostat to detect two gamma quanta (333.9 keV and 406.5 keV) also in coincidence. The samples contents 4.8×10^{23} nuclei of ^{150}Nd. The sensitivity to the double beta processes in ^{148}Nd can be improved too. The measurements will be continued at least one year more to detect the effect (or disprove the previous experimental positive evidences).

- Cerium contains three potentially 2β active isotopes: ^{136}Ce, ^{138}Ce and ^{142}Ce. The ^{136}Ce isotope is of particular interest because it has one of the highest Q-value among the six nuclides which decay $2\beta^+$. An experiment to search for double beta decay of cerium was completed after 2299 h of data taking; Monte Carlo simulations of the detector response to the 2β decay of ^{136,138}Ce and to radioactive contamination of the cerium sample was completed too. The data analysis is in progress. The cerium oxide sample was successfully purified in thorium with the help of liquid-liquid extraction method by a factor of 50. This allows the improvement – of one order of magnitude – of the experimental sensitivity to the different channels and modes of double beta decay in ^{136}Ce and ^{138}Ce in comparison to our preliminary results [71]. A paper describing the results of the experiment is in preparation.

- An experiment to search for α decay of ^{184}Os and ^{186}Os to the first excited levels of daughter nuclei, and for 2β decay of ^{184}Os and ^{192}Os, is in progress by using a sample of thin plates of ultra-pure osmium. The investigation of the neutrinoless double electron capture in ^{184}Os to the 1322.2 keV, 1386.3 keV and 1431.0 keV excited states of ^{184}W is of special interest thanks to a possibility of resonant process [74]. The samples are installed in a BEGe ultra-low background HPGe gamma-detector of the STELLA facility. There is an indication of α decay of ^{186}Om to the first excited level of ^{182}W with half-life $T_{1/2} = (2.9^{+3.2}_{-1.2}) \times 10^{17}$ yr, which is near to theoretical estimations. The data taking in this configuration is in progress for at least one year more. We plan also to improve the sensitivity to the double beta decay processes in comparison to the earlier stage of the experiment (with the osmium sample in form of roads installed on HPGe detector) [70], thanks to the higher (approximately by a factor 5) detection efficiency in the present experiment. Also measurements of the isotopic composition of the osmium sample are in progress.

- The R&D of low background GSO(Ce) crystal scintillators to investigate double beta processes in ^{152}Gd and ^{160}Gd is in progress.

- The R&D of low background barium containing crystal scintillators to investigate double beta processes in ^{130}Ba and ^{132}Ba is in progress.

- The R&D of methods to purify samarium, ytterbium and erbium is going on to search for neutrinoless resonant double electron capture processes in ^{144}Sm, ^{162}Er, ^{164}Er and ^{168}Yb. Deep purification of the samples is under investigation in order to improve the sensitivity reachable in the measurements in preparation.

- Preparations of other future measurements are in progress.

5.1 Search for 2β decay of ^{106}Cd with enriched ^{106}CdWO$_4$ crystal scintillator in coincidence with four HPGe detectors

A second stage experiment to search for double beta decay processes in ^{106}Cd with the help of enriched in ^{106}Cd (to 66%) low background ^{106}CdWO$_4$ scintillation detector at the STELLA facility was completed. The ^{106}CdWO$_4$ scintillator, viewed by a low background PMT through the lead tungstate crystal light-guide produced from deeply purified archaeological lead, was operated in coincidence with the four ultra-low background high purity germanium detectors in a single cryostat GeMulti. New improved limits on the double beta processes in ^{106}Cd have been set at the level of $10^{20} - 10^{21}$ yr after 13085 h of data taking. In particular, the limit on the two neutrino electron capture with positron emission, $T^{\varepsilon\beta^+ 2\nu}_{1/2} \geq 1.1 \times 10^{21}$ yr, has reached the region of theoretical predictions. The resonant neutrinoless double electron captures to the 2718, 2741 and 2748 keV excited states of ^{106}Pd are restricted at the level of $T^{2\varepsilon 0\nu}_{1/2} \geq (8.5 \times 10^{20} - 1.4 \times 10^{21})$ yr.

Fig.4(left) shows the energy spectra accumulated over 13085 h by the ^{106}CdWO$_4$ detector in anticoincidence with the HPGe detectors, in coincidence with event(s) in at least one of the HPGe detectors with energy $E > 200$ keV, $E = 511$ keV and $E = 1160$ keV. The fit of the ^{106}CdWO$_4$ anticoincidence spectrum by the background model, and its main components are shown in Fig.4(right).

Results have been presented at Conferences and the paper describing the final results of the 2nd stage experiment was published (see the 2016 publication list).

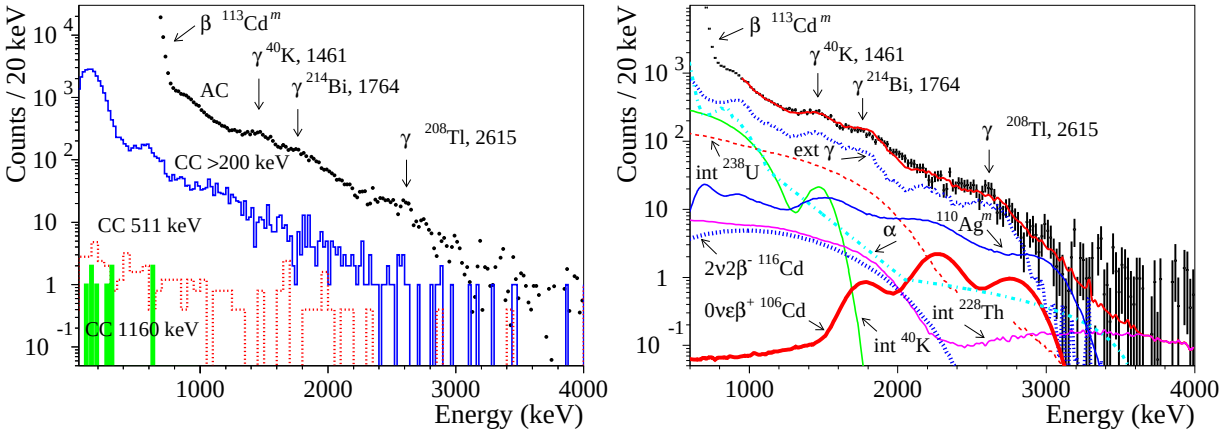

Figure 4: Left: ^{106}CdWO$_4$ energy spectra collected during 13085 h in anticoincidence with the HPGe detectors ("AC"), in coincidence with event(s) in at least one of the HPGe detectors with the energy $E > 200$ keV ("CC >200 keV"), $E = 511 \pm 3\sigma_{511}$ keV ("CC 511 keV"), and $E = 1160 \pm 2.3\sigma_{1160}$ keV ("CC 1160 keV"). Right: Fit of the anticoincidence spectrum by background model, and its main components. The excluded distribution of the $\varepsilon\beta^+ 0\nu$ decay of ^{106}Cd to the ground state of ^{106}Pd with $T_{1/2} = 1.5 \times 10^{21}$ yr is shown too.

Some of the obtained half-life limits on different 2β processes in ^{106}Cd are given in Table 2, where results of the most sensitive previous experiments are also given for comparison.

Table 2: $T_{1/2}$ limits on 2β processes in ^{106}Cd (AC – anticoincidence with HPGe; CC – coincidence with the given energy in HPGe; HPGe – using data of only HPGe detectors).

Decay and	$T_{1/2}$ limit (yr) at 90% C.L.	
^{106}Pd level (keV)	Present work (data)	Best previous limit
$2\beta^+0\nu$, g.s.	$\geq 3.0 \times 10^{21}$ (CC 511 keV)	$\geq 1.2 \times 10^{21}$ [50]
$2\beta^+2\nu$, g.s.	$\geq 2.3 \times 10^{21}$ (CC 511 keV)	$\geq 4.3 \times 10^{20}$ [50]
$\varepsilon\beta^+0\nu$, g.s.	$\geq 1.5 \times 10^{21}$ (AC)	$\geq 2.2 \times 10^{21}$ [50]
$\varepsilon\beta^+2\nu$, g.s.	$\geq 1.1 \times 10^{21}$ (CC 511 keV)	$\geq 4.1 \times 10^{20}$ [75]
$\varepsilon\beta^+2\nu$, 0^+ 1134	$\geq 1.1 \times 10^{21}$ (CC 622 keV)	$\geq 3.7 \times 10^{20}$ [50]
$2K0\nu$, g.s.	$\geq 4.2 \times 10^{20}$ (HPGe)	$\geq 1.0 \times 10^{21}$ [50]
$2\varepsilon2\nu$, 0^+ 1134	$\geq 1.0 \times 10^{21}$ (CC 622 keV)	$\geq 1.7 \times 10^{20}$ [50]
Res. $2K0\nu$, 2718	$\geq 1.1 \times 10^{21}$ (CC 1160 keV)	$\geq 4.3 \times 10^{20}$ [50]
Res. $KL_10\nu$, 4^+ 2741	$\geq 8.5 \times 10^{20}$ (HPGe)	$\geq 9.5 \times 10^{20}$ [50]
Res. $KL_30\nu$, $2, 3^-$ 2748	$\geq 1.4 \times 10^{21}$ (CC 2236 keV)	$\geq 4.3 \times 10^{20}$ [50]

An advanced stage of the experiment is at present running in DAMA/CRYS using the $^{106}CdWO_4$ detector in coincidence with two large volume $CdWO_4$ scintillation detectors in close geometry to improve the detection efficiency to gamma quanta emitted in the double beta processes in ^{106}Cd.

6 Other activities

In 2016 the feasibility of a directionality experiment for DM was explored, to investigate on DM candidates inducing nuclear recoils by exploiting the correlation of the nuclear recoils with the Earth galactic motion.

In recent years we have made extensive efforts and measurements with $ZnWO_4$ crystal scintillators, already interesting to investigate double beta decay of Zn and W isotopes [48, 49]. These scintillators [76] have the particular feature to be anisotropic in the light output and in the pulse shape for heavy particles (p, α, nuclear recoils) depending on the direction with respect to the crystal axes. The response to γ/β radiation is isotropic instead. Among the anisotropic scintillators, the $ZnWO_4$ has unique features, which make it an excellent candidate for this type of research, and there is still plenty of room for the improvement of its performances. The possibility of a low background pioneer experiment (named ADAMO, Anisotropic detectors for DArk Matter Observation) to exploit deep underground the directionality approach by using anisotropic $ZnWO_4$ scintillators has been explored [76] (see also 2016 publication list). Finally, we have also discussed as first in written project and Conferences the potentiality to build detectors with anisotropic features by using Carbon Nanotubes (CNT) [77].

A possible significant improvement of $ZnWO_4$ radio-purity by recrystallization, which could be an important methodological step to advance sensitivity for the double beta decay and DM applications (and the same procedure can be applied to $CdWO_4$ crystal scintillators too), is in progress (see Sect. 6.1). In the 2016 we published a paper describing measurements on $CdWO_4$ and on $ZnWO_4$ crystal scintillators produced after recrystallization by the low-thermal-gradient Czochralski technique.

6.1 Improvement of radio-purity level of enriched $^{116}CdWO_4$ and $ZnWO_4$ crystal scintillators by recrystallization

As low as possible radioactive contamination of a detector plays a crucial role to improve sensitivity of a double beta decay experiment. The radioactive contamination of a sample of $^{116}CdWO_4$ crystal scintillator by thorium was reduced by a factor ≈ 10, down to the level 0.01 mBq/kg (^{228}Th), by exploiting the recrystallization procedure. The total alpha activity of uranium and thorium daughters was reduced by a factor ≈ 3, down to 1.6 mBq/kg. No change in the specific activity (the total α activity and ^{228}Th) was observed in a sample of $ZnWO_4$ crystal produced by recrystallization after removing ≈ 0.4 mm surface layer of the crystal.

The radioactive contamination of the samples was measured in the DAMA/CRYS set-up at the Gran Sasso underground laboratory (see for the details 2016 publication list).

The energy spectra of α particles selected by the optimal filter method from the data accumulated with the $^{116}CdWO_4$ crystal scintillators before and after the recrystallization are presented in Fig. 5. The spectra were fitted by the model, which includes α peaks of ^{232}Th, ^{238}U and their daughters. Equilibrium in the ^{232}Th and ^{238}U chains was assumed to be broken.

The activity of ^{228}Th in the crystals was estimated with the help of the time-amplitude analysis. The arrival time, the energy and the pulse shape of each event were used to select the fast decay chain in the ^{228}Th sub-chain of the ^{232}Th family: $^{224}Ra \rightarrow {}^{220}Rn \rightarrow {}^{216}Po \rightarrow {}^{212}Pb$.

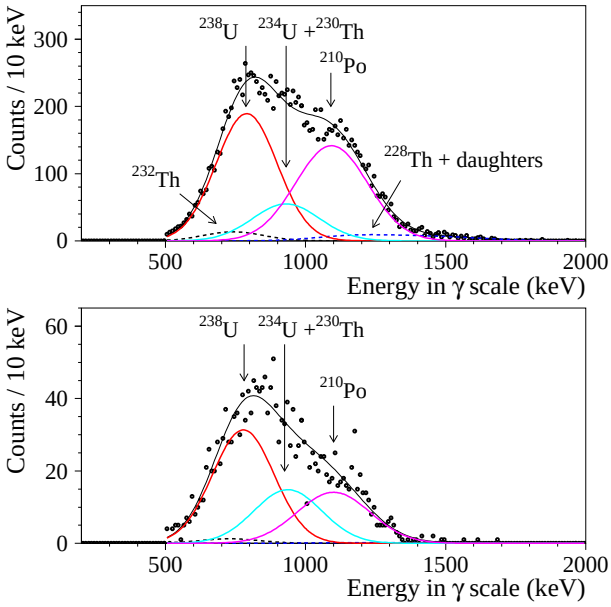

Figure 5: (Color online) The energy spectrum of α events selected by the pulse-shape discrimination from the data accumulated in the low-background set-up with the $^{116}CdWO_4$ crystal scintillator before (upper figure, time of measurement 2394 h) and after the recrystallization (lower figure, 1623 h).

The results of the fits are presented in Fig. 5 and in Table 3. One can see a clear decrease of the total alpha activity in the $^{116}CdWO_4$ crystal scintillator after the recrystallization by a factor ≈ 3. Segregation of uranium and lead in the $^{116}CdWO_4$ crystal growth process was also observed in ref. [78], where a sample produced from the growth cone was tested as low temperature scintillating bolometer.

Table 3: Radioactive contamination of the $^{116}CdWO_4$ crystal before and after recrystallization.

Chain	Nuclide (sub-chain)	Activity (mBq/kg)	
		before recrystallization	after recrystallization
^{232}Th	^{232}Th	0.13(7)	0.03(2)
	^{228}Th	0.10(1)	0.010(3)
^{238}U	^{238}U	1.8(2)	0.8(2)
	^{226}Ra	≤ 0.1	≤ 0.015
	^{234}U+^{230}Th	0.6(2)	0.4(1)
	^{210}Po	1.6(2)	0.4(1)
Total α		4.44(4)	1.62(4)

The effictiveness of recristallization, as well as the much higher contamination of the rest of the melt remaining in the platinum crucible after the crystal growing process by potassium, radium and thorium, indicates strong segregation of the radioactive elements in the $CdWO_4$ crystals growing process. This feature can be used in order to produce highly radiopure $CdWO_4$ crystal scintillators for high sensitivity double beta decay experiments. Similar studies are also in progress on $ZnWO_4$ crystal scintillators.

7 Conclusions

During 2016 DAMA/LIBRA has continued to take data in the phase2 configuration.
Studies on other DM features, second order effects, and several other rare processes are in progress with the aim to reach very high sensitivity also thanks to the progressive increasing of the exposure.
Studies are under way towards possible DAMA/LIBRA–phase3 (whose R&D has been funded) and/or DAMA/1ton (proposed since 1996).
Moreover, results on several 2β decay processes of ^{116}Cd and ^{106}Cd, and developments on new highly radio-pure scintillators for the search of rare processes have been published and are under further developments.
Finally, in 2016 all the DAMA set-ups have regularly been in data taking and various kinds of measurements are in progress and planned for the future.
During 2016, more than sixteen presentations at Conferences and Workshops (many of them by invitation) have been performed.

8 List of Publications during 2016

1. P. Belli, "Results and strategies in dark matter detection", Int. J. Mod. Phys. D 25 (2016) 1630013

2. R. Bernabei, P. Belli, F. Cappella, V. Caracciolo, R. Cerulli, C.J. Dai, A. d'Angelo, S. d'Angelo, A. Di Marco, H.L. He, A. Incicchitti, H.H. Kuang, X.H. Ma, F. Montecchia, X.D. Sheng, R.G. Wang, Z.P. Ye, "DAMA/LIBRA–phase1 results and perspectives of the phase2", to appear in the Proceed. of MG14

3. V.I. Tretyak, P. Belli, R. Bernabei, V.B. Brudanin, F. Cappella, V. Caracciolo, R. Cerulli, D.M. Chernyak, F.A. Danevich, S. d'Angelo, A. Di Marco, A. Incicchitti, M. Laubenstein, V.M. Mokina, D.V. Poda, O.G. Polischuk, I.A. Tupitsyna, "New limits on 2β processes in ^{106}Cd", J. of Phys.: Conf. Series 718 (2016) 062062 [arXiv:1601.05698]

4. F. A. Danevich, A. S. Barabash, P. Belli, R. Bernabei, F. Cappella, V. Caracciolo, R. Cerulli, D. M. Chernyak, S. d'Angelo, A. Incicchitti, V. V. Kobychev, S. I. Konovalov, M. Laubenstein, V. M. Mokina, D. V. Poda, O. G. Polischuk, V. N. Shlegel, V. I. Tretyak, V. I. Umatov, "Search for double beta decay of ^{116}Cd with enriched $^{116}CdWO_4$ crystal scintillators (Aurora experiment)", J. of Phys.: Conf. Series 718 (2016) 062009 [arXiv:1601.05578]

5. P. Belli, "Dark Matter direct detection: crystals", J. of Phys.: Conf. Series 718 (2016) 022003

6. R. Bernabei, P. Belli, A. Di Marco, F. Montecchia, A. d'Angelo, A. Incicchitti, F. Cappella, V. Caracciolo, R. Cerulli, C.J. Dai, H.L. He, H.H. Kuang, X.H. Ma, X.D. Sheng, R.G. Wang, Z.P. Ye, "Recent analyses on the DAMA/LIBRA–phase1 data", J. of Phys.: Conf. Series 718 (2016) 042013

7. V. Caracciolo, R. Bernabei, P. Belli, F. Cappella, R. Cerulli, F.A. Danevich, A. d'Angelo, A. Di Marco, A. Incicchitti, D.V. Poda, V.I. Tretyak, "The ADAMO project and developments", J. of Phys.: Conf. Series 718 (2016) 042011

8. R. Bernabei, P. Belli, S. d'Angelo, A. Di Marco, F. Montecchia, A. d'Angelo, A. Incicchitti, D. Prosperi, F. Cappella, V. Caracciolo, R. Cerulli, C.J. Dai, H.L. He, H.H. Kuang, X.H. Ma, X.D. Sheng, R.G. Wang, Z.P. Ye, "Recent results from DAMA/LIBRA and perspectives", to appear in the Proceed. of Lomonosov Conf., Moscow August 2015

9. R. Bernabei, P. Belli, S. d'Angelo, A. Di Marco, F. Montecchia, A. d'Angelo, A. Incicchitti, F. Cappella, V. Caracciolo, R. Cerulli, C.J. Dai, H.L. He, H.H. Kuang, X.H. Ma, X.D. Sheng, R.G. Wang, Z.P. Ye, "Recent results from DAMA/LIBRA–phase1 and perspectives", to appear in the Proceed. of 5th Gamow Inter. Conf., Odessa August 2015

10. P. Belli, R. Bernabei, V.B. Brudanin, F. Cappella, V. Caracciolo, R. Cerulli, D.M. Chernyak, F.A. Danevich, S. d'Angelo, A. Di Marco, A. Incicchitti, M. Laubenstein, V.M. Mokina, D.V. Poda, O.G. Polischuk, V.I. Tretyak, I.A. Tupitsyna, "Search for 2β decay of ^{106}Cd with enriched $^{106}CdWO_4$ crystal scintillator in coincidence with four HPGe detectors", Phys. Rev. C 93 (2016) 045502 [arXiv:1603.06363]

11. R. Bernabei, P. Belli, F. Cappella, V. Caracciolo, R. Cerulli, C.J. Dai, A. d'Angelo, S. d'Angelo, A. Di Marco, H.L. He, A. Incicchitti, H.H. Kuang, X.H. Ma, F. Montecchia, X.D. Sheng, R.G. Wang, Z.P. Ye, "Recent results from DAMA/LIBRA–phase1 and perspectives", Nucl. and Part. Phys. Proc. 273-275 (2016) 321-327

12. R. Bernabei, "Particle dark matter direct detection", Int. J. of Mod. Phys. D 25 (2016) 1630018

13. A.S. Barabash, P. Belli, R. Bernabei, Yu.A. Borovle, V. Caracciolo, R. Cerulli, F.A. Danevich, A. Incicchitti, V.V. Kobychev, S.I. Konovalov, M. Laubenstein, V.M. Mokina, O.G. Polischuk, O.E. Safonova, V.N. Shlegel, V.I. Tretyak, I.A. Tupitsyna, V.I. Umatov, V.N. Zhdankov, "Improvement of radiopurity level of enriched $^{116}CdWO_4$ and $ZnWO_4$ crystal scintillators by recrystallization", Nucl. Instr. and Meth. A 833 (2016) 77

14. R. Bernabei, P. Belli, S. d'Angelo, A. Di Marco, F. Montecchia, F. Cappella, A. d'Angelo, A. Incicchitti, V. Caracciolo, R. Cerulli, C.J. Dai, H.L. He, X.H. Ma, X.D. Sheng, R.G. Wang, Z.P. Ye, "DAMA/LIBRA Results and Perspectives", Bled Workshops in Physics vol. 17, no. 2 (2016) 1

15. P. Belli, "Direct detection of Dark Matter", EPJ Web of Conf. 121 (2016) 06001

16. R. Bernabei, P. Belli, F. Cappella, V. Caracciolo, R. Cerulli, C.J. Dai, A. d'Angelo, S. d'Angelo, A. Di Marco, H.L. He, A. Incicchitti, H.H. Kuang, X.H. Ma, F. Montecchia, X.D. Sheng, R.G. Wang, Z.P. Ye, "DAMA/LIBRA–phase1 results and perspectives of the phase2", EPJ Web of Conf. 121 (2016) 06005

17. R. Bernabei, P. Belli, A. d'Angelo, S. d'Angelo, A. Di Marco, F. Montecchia, A. Incicchitti, F. Cappella, V. Caracciolo, R. Cerulli, C.J. Dai, H.L. He, H.H. Kuang, X.H. Ma, X.D. Sheng, R.G. Wang and Z.P. Ye, "Highlights of DAMA/LIBRA", EPJ Web of Conf. 126 (2016) 02014

Int. J. of Mod. Phys. A invited issue dedicated to DAMA:

18. R. Bernabei, "The DAMA project", Int. J. of Mod. Phys. A 31 (2016) 1642001

19. R. Bernabei, P. Belli, A. Incicchitti, A. Mattei, F. Cappella, R. Cerulli, C.J. Dai, X.H. Ma, Z. P. Ye, "The highly radiopure NaI(Tl) DAMA/LIBRA setup", Int. J. of Mod. Phys. A 31 (2016) 1642002

20. R. Bernabei, P. Belli, A. Incicchitti, C.J. Dai, "Adopted low background techniques and analysis of radioactive trace impurities", Int. J. of Mod. Phys. A 31 (2016) 1642003

21. F. Cappella, V. Caracciolo, R. Cerulli, A. Bussolotti, A. Mattei, "The calibration and the monitoring/alarm system", Int. J. of Mod. Phys. A 31 (2016) 1642004

22. P. Belli, A. Bussolotti, V. Caracciolo, R. Cerulli, C. J. Dai, X. H. Ma, "The electronics and DAQ system in DAMA/LIBRA", Int. J. of Mod. Phys. A 31 (2016) 1642005

23. R. Bernabei, P. Belli, S. d'Angelo, A. Di Marco, F. Montecchia, A. d'Angelo, A. Incicchitti, D. Prosperi, F. Cappella, V. Caracciolo, R. Cerulli, C.J. Dai, H.L. He, H.H. Kuang, X.H. Ma, X.D. Sheng, R.G. Wang, Z.P. Ye, "DAMA/LIBRA–phase1 model independent results", Int. J. of Mod. Phys. A 31 (2016) 1642006

24. A. Di Marco, F. Cappella, R. Cerulli, "Other rare processes with DAMA/LIBRA", Int. J. of Mod. Phys. A 31 (2016) 1642007

25. R. Bernabei, P. Belli, A. Di Marco, A. d'Angelo, A. Incicchitti, F. Cappella, R. Cerulli, C.J. Dai, X.H. Ma, Z.P. Ye, "Investigation on possible systematics and side processes", Int. J. of Mod. Phys. A 31 (2016) 1642008

26. R. Bernabei, P. Belli, A. Incicchitti, R. Cerulli, C.J. Dai, X.H. Ma, Z.P. Ye, "On corollary model-dependent analyses and comparisons", Int. J. of Mod. Phys. A 31 (2016) 1642009

27. R. Bernabei, P. Belli, A. Incicchitti, F. Cappella, R. Cerulli, C.J. Dai, H.L. He, H.H. Kuang, X.H. Ma, X.D. Sheng, R.G. Wang, Z.P. Ye, R.S. Boiko, F.A. Danevich, V.V. Kobychev, D.V. Poda, O.G. Polischuk, V.I. Tretyak, "Main results and perspectives on other rare processes with DAMA experiments", Int. J. of Mod. Phys. A 31 (2016) 1642010

28. R. Bernabei, P. Belli, A. Incicchitti, R. Cerulli, C.J. Dai, X.H. Ma, "Towards the next and far future", Int. J. of Mod. Phys. A 31 (2016) 1642011

References

[1] R. Bernabei et al., Nucl. Instr. and Meth. A 592 (2008) 297.

[2] R. Bernabei et al., Eur. Phys. J. C 56 (2008) 333.

[3] R. Bernabei et al., Eur. Phys. J. C 67 (2010) 39.

[4] R. Bernabei et al., Eur. Phys. J. C 73 (2013) 2648.

[5] P. Belli et al., Phys. Rev. D 84 (2011) 055014.

[6] R. Bernabei et al., J. of Instr. 7 (2012) P03009.

[7] R. Bernabei et al., Eur. Phys. J. C 72 (2012) 2064.

[8] R. Bernabei et al., Int. J. of Mod. Phys. A 28 (2013) 1330022 (73 pages).

[9] R. Bernabei et al., Eur. Phys. J. C 62 (2009) 327.

[10] R. Bernabei et al., Eur. Phys. J. C 72 (2012) 1920.

[11] R. Bernabei et al., Eur. Phys. J. A 49 (2013) 64.

[12] R. Bernabei et al., Eur. Phys. J. C 74 (2014) 2827.

[13] R. Bernabei et al., Eur. Phys. J. C 74 (2014) 3196.

[14] R. Bernabei, et al., Eur. Phys. J. C 75 (2015) 239.

[15] A. Addazi, et al., Eur. Phys. J. C 75 (2015) 400.

[16] P. Belli, R. Bernabei, C. Bacci, A. Incicchitti, R. Marcovaldi, D. Prosperi, DAMA proposal to INFN Scientific Committee II, April 24^{th} 1990.

[17] R. Bernabei et al., Phys. Lett. B 389 (1996) 757; R. Bernabei et al., Phys. Lett. B 424 (1998) 195; R. Bernabei et al., Phys. Lett. B 450 (1999) 448; P. Belli et al., Phys. Rev. D 61 (2000) 023512; R. Bernabei et al., Phys. Lett. B 480 (2000) 23; R. Bernabei et al., Phys. Lett. B 509 (2001) 197; R. Bernabei et al., Eur. Phys. J. C 23 (2002) 61; P. Belli et al., Phys. Rev. D 66 (2002) 043503.

[18] R. Bernabei et al., Il Nuovo Cim. A 112 (1999) 545.

[19] R. Bernabei et al., Eur. Phys. J. C18 (2000) 283.

[20] R. Bernabei el al., La Rivista del Nuovo Cimento 26 n.1 (2003) 1-73.

[21] R. Bernabei et al., Int. J. Mod. Phys. D 13 (2004) 2127.

[22] R. Bernabei et al., Int. J. Mod. Phys. A 21 (2006) 1445.

[23] R. Bernabei et al., Eur. Phys. J. C 47 (2006) 263.

[24] R. Bernabei et al., Int. J. Mod. Phys. A 22 (2007) 3155.

[25] R. Bernabei et al., Eur. Phys. J. C 53 (2008) 205.

[26] R. Bernabei et al., Phys. Rev. D 77 (2008) 023506.

[27] R. Bernabei et al., Mod. Phys. Lett. A 23 (2008) 2125.

[28] R. Bernabei et al., Phys. Lett. B408 (1997) 439; P. Belli et al., Phys. Lett. B460 (1999) 236; R. Bernabei et al., Phys. Rev. Lett. 83 (1999) 4918; P. Belli et al., Phys. Rev. C60 (1999) 065501; R. Bernabei et al., Il Nuovo Cimento A112 (1999) 1541; R. Bernabei et al., Phys. Lett. B 515 (2001) 6; F. Cappella et al., Eur. Phys. J.-direct C14 (2002) 1; R. Bernabei et al., Eur. Phys. J. A 23 (2005) 7; R. Bernabei et al., Eur. Phys. J. A 24 (2005) 51; R. Bernabei et al., Astrop. Phys. 4 (1995) 45.

[29] K.A. Drukier et al., Phys. Rev. D 33 (1986) 3495.

[30] K. Freese et al., Phys. Rev. D 37 (1988) 3388.

[31] R. Bernabei et al., AIP Conf. Proceed. 1223 (2010) 50 (arXiv:0912.0660).

[32] R. Bernabei et al., J. Phys.: Conf. Ser. 203 (2010) 012040 (arXiv:0912.4200); http://taup2009.lngs.infn.it/slides/jul3/nozzoli.pdf, talk given by F. Nozzoli.

[33] R. Bernabei et al., in the volume Frontier Objects in Astrophysics and Particle Physics (Vulcano 2010), S.I.F. Ed. (2011) 157 (arXiv:1007.0595).

[34] R. Bernabei et al., Can. J. Phys. 89 (2011) 11.

[35] R. Bernabei et al., Physics Procedia 37 (2012) 1095.

[36] R. Bernabei et al., arXiv:1210.6199; arXiv:1211.6346.

[37] A. Bottino et al., Phys. Rev. D 85 (2012) 095013.

[38] A. Bottino et al., arXiv:1112.5666.

[39] P. Belli et al., Il Nuovo Cim. 103A (1990) 767.

[40] P. Belli et al., Phys. Lett. B 387 (1996) 222 and Phys. Lett. B 389 (1996) 783 (erratum); R. Bernabei et al., New J. Phys. 2 (2000) 15.1; Eur. Phys. J.-direct C11 (2001) 1; Phys. Lett. B 436 (1998) 379; R. Bernabei et al., in the volume "Beyond the Desert 2003", Springer (2003) 365.

[41] R. Bernabei et al., Nucl. Instrum. and Meth. A 482 (2002) 728.

[42] R. Bernabei et al., Phys. Lett. B 546 (2002) 23; F. Cappella, PhD Thesis, Università di Roma "Tor Vergata", 2005.

[43] P. Belli et al., Il Nuovo Cim. C 19 (1996) 537; Astrop. Phys. 5 (1996) 217.

[44] R. Bernabei et al., Phys. Lett. B 527 (2002) 182.

[45] P. Belli et al., Phys. Rev. D 61 (2000) 117301; Phys. Lett. B 465 (1999) 315; R. Bernabei et al., Phys. Lett. B 493 (2000) 12; Eur. Phys. J. A 27 s01 (2006) 35.

[46] R. Bernabei et al., Astropart. Phys. 7 (1997) 73; R. Bernabei et al., Il Nuovo Cim. A 110 (1997) 189; P. Belli et al., Astropart. Phys. 10 (1999) 115; P. Belli et al., Nucl. Phys. B 563 (1999) 97; R. Bernabei et al., Nucl. Phys. A 705 (2002) 29; P. Belli et al., Nucl. Instrum. and Meth. A 498 (2003) 352; R. Cerulli et al., Nucl. Instrum. and Meth. A 525 (2004) 535; R. Bernabei et al., Nucl. Instrum. and Meth. A 555 (2005) 270; R. Bernabei et al., Ukr. J. Phys. 51 (2006) 1037; P. Belli et al., Nucl. Phys. A 789 (2007) 15; P. Belli et al., Phys. Rev. C 76 (2007) 064603; P. Belli et al., Eur. Phys. J. A 36 (2008) 167; P. Belli et al., J. Phys. G 38 (2011) 015103; D. Poda et al., Radiation Measurements 56 (2013) 66.

[47] P. Belli et al., Nucl. Instrum. and Meth. A 615 (2010) 301.

[48] P. Belli et al., Nucl. Phys. A 826 (2009) 256; P. Belli et al., Phys. Lett. B 658 (2008) 193.

[49] P. Belli et al., Nucl. Instrum. and Meth. A 626-627 (2011) 31.

[50] P. Belli et al., Phys. Rev. C 85 (2012) 044610.

[51] P. Belli et al., J. Phys. G: Nucl. Part. Phys. 38 (2011) 115107.

[52] A.S. Barabash et al., JINST. 6 (2011) P08011.

[53] P. Belli et al., Eur. Phys. J. A 50 (2014) 134.

[54] P. Belli et al., Phys. Scripta 90 (2015) 085301.

[55] H. Ejiri et al., J. Phys. Soc. Japan 64 (1995) 339.

[56] R. Arnold et al., Z. Phys. C 72 (1996) 239.

[57] V.I. Tretyak et al., AIP Conf. Proc. 1572 (2013) 110.

[58] F.A. Danevich et al., Phys. Lett. B 344 (1995) 72.

[59] F.A. Danevich et al., Phys. Rev. C 62 (2000) 045501.

[60] F.A. Danevich et al., Phys. Rev. C 68 (2003) 035501.

[61] D.V. Poda et al., EPJ Web of Conferences 65 (2014) 01005.

[62] T.R. Rodriguez, G. Martinez-Pinedo, Phys. Rev. Lett. 105 (2010) 252503.

[63] F. Šimkovic et al., Phys. Rev. C 87 (2013) 045501.

[64] J. Hyvärinen, J. Suhonen, Phys. Rev. C 91 (2015) 024613.

[65] J. Barea et al., Phys. Rev. C 91 (2015) 034304.

[66] J. Kotila, F. Iachello, Phys. Rev. C 85 (2012) 034316.

[67] Barabash A S, Kopylov A V, Cherehovsky V I, Phys. Lett. B249, (1990) 186.

[68] Piepke A et al., Nucl. Phys. A577, (1994) 493.

[69] P. Belli et al., Nucl. Instr. and Meth. A 572 (2007) 734; P. Belli et al., Nucl. Phys. A 806 (2008) 388; P. Belli et al., Nucl. Phys. A 824 (2009) 101; O. P. Barinova et al., Nucl. Instrum. and Meth. A 607 (2009) 573; P. Belli et al., Eur. Phys. J. A 42 (2009) 171; P. Belli et al., Nucl. Phys. A 846 (2010) 143; P. Belli et al., Nucl. Phys. At. Energy 11 (2010) 362; P. Belli et al., Nucl. Phys. A 859 (2011) 126; P. Belli et al., Phys. Rev. C 83 (2011) 034603; P. Belli et al., Eur. Phys. J. A 47 (2011) 91; P. Belli et al., Nucl. Instrum. and Meth. A 670 (2012) 10; P. Belli et al., Phys. Lett. B 711 (2012) 41; P. Belli et al., Nucl. Instrum. and Meth. A 704 (2013) 40; P. Belli et al., Phys. Rev. C 87 (2013) 034607; S. Das et al., Nucl. Instrum. and Meth. A 797 (2015) 130.

[70] P. Belli et al., Eur. Phys. J. A 49 (2013) 24.

[71] P. Belli et al., Nucl. Phys. A 930 (2014) 195.

[72] A.S. Barabash et al., Phys. Rev. C 79 (2009) 045501.

[73] M.F. Kidd et al., Phys. Rev. C 90 (2014) 055501.

[74] M.I. Krivoruchenko et al., Nucl. Phys. A 859 (2011) 140.

[75] Belli P et al., Astropart. Phys.10 (1999) 115.

[76] F. Cappella et al., Eur. Phys. J. C 73 (2013) 2276.

[77] FIRB 2013: "Sviluppo di rivelatori a risposta anisotropa", PI: Cappella Fabio, Reference number: RBFR13THVM; Talk by R. Cerulli at Int. Conf. Dark matter, Dark Energy and their detection, Novosibirsk, Russia, July 2013, http://people.roma2.infn.it/∼dama/pdf/cerulli_novosibirsk2013.pdf; Talk by P. Belli at What Next workshop, Tor Vergata University, Rome, Italy, March 2014, http://people.roma2.infn.it/∼belli/belli_TorVergata_mar14.pdf.

[78] A.S. Barabash et al., arXiv:1606.07806v1 [physics.ins-det], submitted to Eur. Phys. J. C.

DarkSide

C. E. Aalseth,[1] S. Abdelhakim,[2] F. Acerbi,[3,4] P. Agnes,[5] I. F. M. Albuquerque,[6] T. Alexander,[1] A. Alici,[7,8] A. K. Alton,[9] P. Antonioli,[8] S. Arcelli,[7,8] R. Ardito,[10,11] I. J. Arnquist,[1] D. M. Asner,[1] M. P. Ave,[6] H. O. Back,[1] A. Barrado Olmedo,[12] G. Batignani,[13,14] E. Bertoldo,[15] S. Bettarini,[13,14] M. G. Bisogni,[13,14] V. Bocci,[16] A. Bondar,[17,18] G. Bonfini,[19] W. Bonivento,[20] M. Bossa,[21,19] B. Bottino,[22,23] M. Boulay,[24] R. Bunker,[1] S. Bussino,[25,26] A. Buzulutskov,[17,18] M. Cadeddu,[27,20] M. Cadoni,[27,20] A. Caminata,[23] L. Campajola,[28,29] N. Canci,[5,19] A. Candela,[19] C. Cantini,[30] M. Caravati,[27,20] J. Carey,[31] M. Cariello,[23] M. Carlini,[19] M. Carpinelli,[32,33] A. Castellani,[10,11] S. Catalanotti,[28,29] V. Cataudella,[28,29] P. Cavalcante,[34,19] S. Cavouti,[28,29] R. Cereseto,[23] A. Chepurnov,[35] C. Cicalò,[20] L. Cifarelli,[7,8] M. Citterio,[11] A. G. Cocco,[29] M. Colocci,[7,8] S. Corgiolu,[36,20] G. Covone,[28,29] P. Crivelli,[30] I. D'Antone,[8] M. D'Incecco,[19] D. D'Urso,[32] M. D. Da Rocha Rolo,[37] M. Daniel,[12] S. Davini,[23,21] A. De Candia,[28,29] S. De Cecco,[38] M. De Deo,[19] G. De Filippis,[28,29] D. De Gruttola,[39] G. De Guido,[40,11] G. De Rosa,[28,29] G. Dellacasa,[37] P. Demontis,[32,33,41] S. DePaquale,[39] A. V. Derbin,[42] A. Devoto,[27,20] F. Di Eusanio,[43] G. Di Pietro,[19,11] C. Dionisi,[16,38] A. Dolgov,[18] I. Dormia,[40,11] S. Dussoni,[14,13] A. Empl,[5] M. Fernandez Diaz,[12] A. Ferri,[3,4] C. Filip,[44] G. Fiorillo,[28,29] K. Fomenko,[45] A. Franceschi,[46] D. Franco,[47] G. E. Froudakis,[48] F. Gabriele,[19] A. Gabrieli,[32,33] C. Galbiati,[43,11] P. Garcia Abia,[12] A. Gendotti,[30] A. Ghisi,[10,11] S. Giagu,[16,38] P. Giampa,[49] G. Gibertoni,[40,11] C. Giganti,[50] M. A. Giorgi,[14,13] G. K. Giovanetti,[43] M. L. Gligan,[44] A. Gola,[3,4] O. Gorchakov,[45] A. M. Goretti,[19] F. Granato,[51] M. Grassi,[13] J. W. Grate,[1] G. Y. Grigoriev,[52] M. Gromov,[35] M. Guan,[53] M. B. B. Guerra,[54] M. Guerzoni,[8] M. Gulino,[55,33] R. K. Haaland,[56] A. Hallin,[57] B. Harrop,[43] E. W. Hoppe,[1] S. Horikawa,[30] B. Hosseini,[20] D. Hughes,[43] P. Humble,[1] E. V. Hungerford,[5] An. Ianni,[43,19] E. V. Jauregui,[58] C. Jillings,[59,60] S. Jimenez Cabre,[12] T. N. Johnson,[61] K. Keeter,[54] C. L. Kendziora,[62] S. Kim,[51] G. Koh,[43] D. Korablev,[45] G. Korga,[5,19] A. Kubankin,[63] R. Kugathasan,[37,64] M. Kuss,[13] M. Kuzniak,[24] M. Lebois,[2] B. Lehnert,[24] X. Li,[43] Q. Liqiang,[2] M. Lissia,[20] G. U. Lodi,[40,11] B. Loer,[1] G. Longo,[28,29] P. Loverre,[16,38] R. Lussana,[65,11] L. Luzzi,[66,11] Y. Ma,[53] A. A. Machado,[67] I. N. Machulin,[52,68] A. Mandarano,[21,19] L. Mapelli,[43] M. Marcante,[69,4,3] A. Margotti,[8] S. M. Mari,[25,26] M. Mariani,[66,11] J. Maricic,[70] M. Marinelli,[22,23] D. Marras,[20] C. J. Martoff,[51] M. Mascia,[36,20] A. McDonald,[71] A. Messina,[16,38] P. D. Meyers,[43] R. Milincic,[70] A. Moggi,[13] S. Moioli,[40,11] J. Monroe,[72] A. Monte,[31] M. Morrocchi,[14,13] W. Mu,[30] V. N. Muratova,[42] S. Murphy,[30] P. Musico,[23] R. Nania,[8] T. Napolitano,[46] A. Navrer Agasson,[50] I. Nikulin,[63] V. Nosov,[17,18] A. O. Nozdrina,[52,68] N. N. Nurakhov,[52] A. Oleinik,[63] V. Oleynikov,[17,18] M. Orsini,[19] F. Ortica,[73,74] L. Pagani,[61] M. Pallavicini,[22,23] S. Palmas,[36,20] L. Pandola,[33] E. Pantic,[61] E. Paoloni,[13,14] G. Paternoster,[3,4] V. Pavletcov,[35] F. Pazzona,[32,33] S. Peeters,[75] K. Pelczar,[76] L. A. Pellegrini,[40,11] N. Pelliccia,[73,74] F. Perotti,[10,11] R. Perruzza,[19] V. Pesudo Fortes,[12] C. Piemonte,[3,4] F. Pilo,[13] A. Pocar,[31] T. Pollman,[77] D. Portaluppi,[65,11] S. S. Poudel,[5] D. A. Pugachev,[52] H. Qian,[43] B. Radics,[30] F. Raffaelli,[13] F. Ragusa,[78,11] M. Razeti,[20] A. Razeto,[19,43] V. Regazzoni,[69,4,3] C. Regenfus,[30] B. Reinhold,[70] A. L. Renshaw,[5] M. Rescigno,[16] F. Retiere,[49] Q. Riffard,[47] A. Rivetti,[37] S. Rizzardini,[43,20] A. Romani,[73,74] L. Romero,[12] B. Rossi,[29] N. Rossi,[19] A. Rubbia,[30] D. Sablone,[43,19] P. Salatino,[79,29] O. Samoylov,[45] E. Sànchez Garcìa,[12] W. Sands,[43] M. Sant,[32,33] R. Santorelli,[12] C. Savarese,[21,19] E. Scapparone,[8] B. Schlitzer,[61] G. Scioli,[7,8] E. Segreto,[67] A. Seifert,[1] D. A. Semenov,[42] A. Shchagin,[63] L. Shekhtman,[17,18] E. Shemyakina,[17,18] A. Sheshukov,[45] M. Simeone,[79,29] P. N. Singh,[5] P. Skensved,[71] M. D. Skorokhvatov,[52,68] O. Smirnov,[45] G. Sobrero,[23] A. Sokolov,[17,18] A. Sotnikov,[45] F. Speziale,[33] R. Stainforth,[24] C. Stanford,[43] G. B. Suffritti,[32,33,41] Y. Suvorov,[80,19,52] R. Tartaglia,[19] G. Testera,[23] A. Tonazzo,[47] A. Tosi,[65,11] P. Trinchese,[28,29] E. V. Unzhakov,[42] A. Vacca,[36,20] M. Verducci,[16,38] T. Viant,[30] F. Villa,[65,11] A. Vishneva,[45] B. Vogelaar,[34] M. Wada,[43] J. Wahl,[1] J. J. Walding,[72] S. Walker,[28,29] H. Wang,[80] Y. Wang,[80] A. W. Watson,[51] S. Westerdale,[24] R. J. Wheadon,[37] R. Williams,[1] J. Wilson,[2] M. M. Wojcik,[76] S. Wu,[30] X. Xiang,[43] X. Xiao,[80] C. Yang,[53] Z. Ye,[5] F. Zappa,[65,11] G. Zappalà,[69,4,3] C. Zhu,[43] A. Zichichi,[7,8] M. Zullo,[16] A. Zullo,[16] and G. Zuzel[76]

[1] *Pacific Northwest National Laboratory, Richland, WA 99352, USA*

[2] *Institut de Physique Nuclèaire dOrsay, 91406, Orsay, France*

[3] *Fondazione Bruno Kessler, Povo 38123, Italy*

[4] *Trento Institute for Fundamental Physics and Applications, Povo 38123, Italy*

[5] *Department of Physics, University of Houston, Houston, TX 77204, USA*
[6] *Instituto de Física, Universidade de São Paulo, São Paulo 05508-090, Brazil*
[7] *Physics Department, Università degli Studi di Bologna, Bologna 40126, Italy*
[8] *INFN Bologna, Bologna 40126, Italy*
[9] *Physics Department, Augustana University, Sioux Falls, SD 57197, USA*
[10] *Civil and Environmental Engineering Department, Politecnico di Milano, Milano 20133, Italy*
[11] *INFN Milano, Milano 20133, Italy*
[12] *CIEMAT, Centro de Investigaciones Energéticas, Medioambientales y Tecnológicas, Madrid 28040, Spain*
[13] *INFN Pisa, Pisa 56127, Italy*
[14] *Physics Department, Università degli Studi di Pisa, Pisa 56127, Italy*
[15] *INFN Milano Bicocca, Milano 20126, Italy*
[16] *INFN Sezione di Roma, Roma 00185, Italy*
[17] *Budker Institute of Nuclear Physics, Novosibirsk 630090, Russia*
[18] *Novosibirsk State University, Novosibirsk 630090, Russia*
[19] *INFN Laboratori Nazionali del Gran Sasso, Assergi (AQ) 67100, Italy*
[20] *INFN Cagliari, Cagliari 09042, Italy*
[21] *Gran Sasso Science Institute, L'Aquila 67100, Italy*
[22] *Physics Department, Università degli Studi di Genova, Genova 16146, Italy*
[23] *INFN Genova, Genova 16146, Italy*
[24] *Department of Physics, Carleton University, Ottawa, ON K1S 5B6, Canada*
[25] *INFN Roma Tre, Roma 00146, Italy*
[26] *Mathematics and Physics Department, Università degli Studi Roma Tre, Roma 00146, Italy*
[27] *Physics Department, Università degli Studi di Cagliari, Cagliari 09042, Italy*
[28] *Physics Department, Università degli Studi "Federico II" di Napoli, Napoli 80126, Italy*
[29] *INFN Napoli, Napoli 80126, Italy*
[30] *Institute for Particle Physics, ETH Zürich, Zürich 8093, Switzerland*
[31] *Amherst Center for Fundamental Interactions and Physics Department, University of Massachusetts, Amherst, MA 01003, USA*
[32] *Chemistry and Pharmacy Department, Università degli Studi di Sassari, Sassari 07100, Italy*
[33] *INFN Laboratori Nazionali del Sud, Catania 95123, Italy*
[34] *Virginia Tech, Blacksburg, VA 24061, USA*
[35] *Skobeltsyn Institute of Nuclear Physics, Lomonosov Moscow State University, Moscow 119991, Russia*
[36] *Department of Mechanical, Chemical, and Materials Engineering, Università degli Studi, Cagliari 09042, Italy*
[37] *INFN Torino, Torino 10125, Italy*
[38] *Physics Department, Sapienza Università di Roma, Roma 00185, Italy*
[39] *INFN Salerno, Salerno 84084, Italy*
[40] *Chemistry, Materials and Chemical Engineering Department "G. Natta", Politecnico di Milano, Milano 20133, Italy*
[41] *Interuniversity Consortium for Science and Technology of Materials, Firenze 50121, Italy*
[42] *Saint Petersburg Nuclear Physics Institute, Gatchina 188350, Russia*
[43] *Physics Department, Princeton University, Princeton, NJ 08544, USA*
[44] *National Institute for R&D of Isotopic and Molecular Technologies, Cluj-Napoca, 400293, Romania*
[45] *Joint Institute for Nuclear Research, Dubna 141980, Russia*
[46] *INFN Laboratori Nazionali di Frascati, Frascati 00044, Italy*
[47] *APC, Université Paris Diderot, CNRS/IN2P3, CEA/Irfu, Obs de Paris, USPC, Paris 75205, France*
[48] *Department of Chemistry, University of Crete, P.O. Box 2208, 71003 Heraklion, Crete, Greece*
[49] *TRIUMF, 4004 Wesbrook Mall, Vancouver, British Columbia V6T2A3, Canada*
[50] *LPNHE, Université Pierre et Marie Curie, CNRS/IN2P3, Sorbonne Universités, Paris 75252, France*
[51] *Physics Department, Temple University, Philadelphia, PA 19122, USA*
[52] *National Research Centre Kurchatov Institute, Moscow 123182, Russia*
[53] *Institute of High Energy Physics, Beijing 100049, China*
[54] *School of Natural Sciences, Black Hills State University, Spearfish, SD 57799, USA*
[55] *Civil and Environmental Engineering Department, Università degli Studi di Enna "Kore", Enna 94100, Italy*
[56] *Department of Physics and Engineering, Fort Lewis College, Durango, CO 81301, USA*
[57] *Department of Physics, University of Alberta, Edmonton, AB T6G 2R3, Canada*
[58] *InstitutodeF´sica,Universidad Nacional Autońomade México(UNAM), México 01000, Mexico*
[59] *Department of Physics and Astronomy, Laurentian University, Sudbury, ON P3E 2C6, Canada*
[60] *SNOLAB, Lively, ON P3Y 1N2, Canada*
[61] *Department of Physics, University of California, Davis, CA 95616, USA*
[62] *Fermi National Accelerator Laboratory, Batavia, IL 60510, USA*
[63] *Radiation Physics Laboratory, Belgorod National Research University, Belgorod 308007, Russia*
[64] *Department of Electronics and Communications, Politecnico di Torino, Torino 10129, Italy*

[65] *Electronics, Information, and Bioengineering Department, Politecnico di Milano, Milano 20133, Italy*
[66] *Energy Department, Politecnico di Milano, Milano 20133, Italy*
[67] *Physics Institute, Universidade Estadual de Campinas, Campinas 13083, Brazil*
[68] *National Research Nuclear University MEPhI, Moscow 115409, Russia*
[69] *Physics Department, Università degli Studi di Trento, Povo 38123, Italy*
[70] *Department of Physics and Astronomy, University of Hawai'i, Honolulu, HI 96822, USA*
[71] *Department of Physics, Engineering Physics and Astronomy, Queens University, Kingston, ON K7L 3N6, Canada*
[72] *Department of Physics, Royal Holloway University of London, Egham TW20 0EX, UK*
[73] *Chemistry, Biology and Biotechnology Department, Università degli Studi di Perugia, Perugia 06123, Italy*
[74] *INFN Perugia, Perugia 06123, Italy*
[75] *Physics and Astronomy, University of Sussex, Brighton BN1 9QH, UK*
[76] *M. Smoluchowski Institute of Physics, Jagiellonian University, 30-348 Krakow , Poland*
[77] *Physik Department, Technische Universität München, Munich 80333, Germany*
[78] *Physics Department, Università degli Studi di Milano, Milano 20133, Italy*
[79] *Chemical, Materials, and Industrial Production Engineering Department, Università degli Studi "Federico II" di Napoli, Napoli 80126, Italy*
[80] *Physics and Astronomy Department, University of California, Los Angeles, CA 90095, USA*

I. EXECUTIVE SUMMARY

In April 2017, LNGS and the INFN Commissione Nazionale Seconda approved DarkSide-20k.

The key progress areas compared to the status presented in the last year progress report are listed here and detailed in the following sections:

- Infrastructural issues related to the location of the DarkSide-20k experiment in Hall C were addressed in collaboration with the LNGS Directorate.
- Following strong indications by the LNGS management, new candidates for the organic liquid scintillator of choice for the liquid scintillator veto (LSV), characterized by reduced safety and environmental hazard, are under active consideration by the DarkSide-20k Collaboration, also with detailed simulations; a potential alternative scintillator cocktail has been identified
- A plan for the specific implementation of all safety reviews necessary for the successful construction and commissioning of the DarkSide-20k experiment is in preparation;
- Full size SiPM tiles with related cryogenic electronics were successfully tested with results that satisfy the DarkSide-20k specifications.
- The first module of the full scale condenser for the cryogenic system of DarkSide-20k, planned for use in DarkSide-Proto, was fabricated and tested. The DarkSide-20k specifications were met;
- A pilot plant of the PSA unit for Urania was built and is currently under test at Università degli Studi "Federico II" of Naples;
- All Seruci-0 modules and the first set of Seruci-I modules were successfully tested both at the factory and at CERN. The Seruci-0 modules are ready for shipping to Sardinia. Seruci-I module production and testing is going ahead at full steam.
- the Collaboration is growing with new collaborators also coming from institution and countries that were not mentioned in the YB.
- A new management structure with names identified has been set up.

This report also includes a detailed status report and future plans of the PhotoElectronics, DarkSide-Proto, Urania, and Seruci-I. It also includes, for completeness, an update on the status of the organisation of the DarkSide collaboration as well as an update of the ongoing reviews of DarkSide-20k by INFN and by the US NSF.

II. INFRASTRUCTURAL AND SAFETY ISSUES

During the last months, detailed discussions were led between the LNGS Technical Coordination, S. Gazzana, and the DarkSide-20k Technical Coordinator, An. Ianni. The outcome of these discussions was the identification of the specific configuration for the layout of the installation of DarkSide-20k in Hall C: see

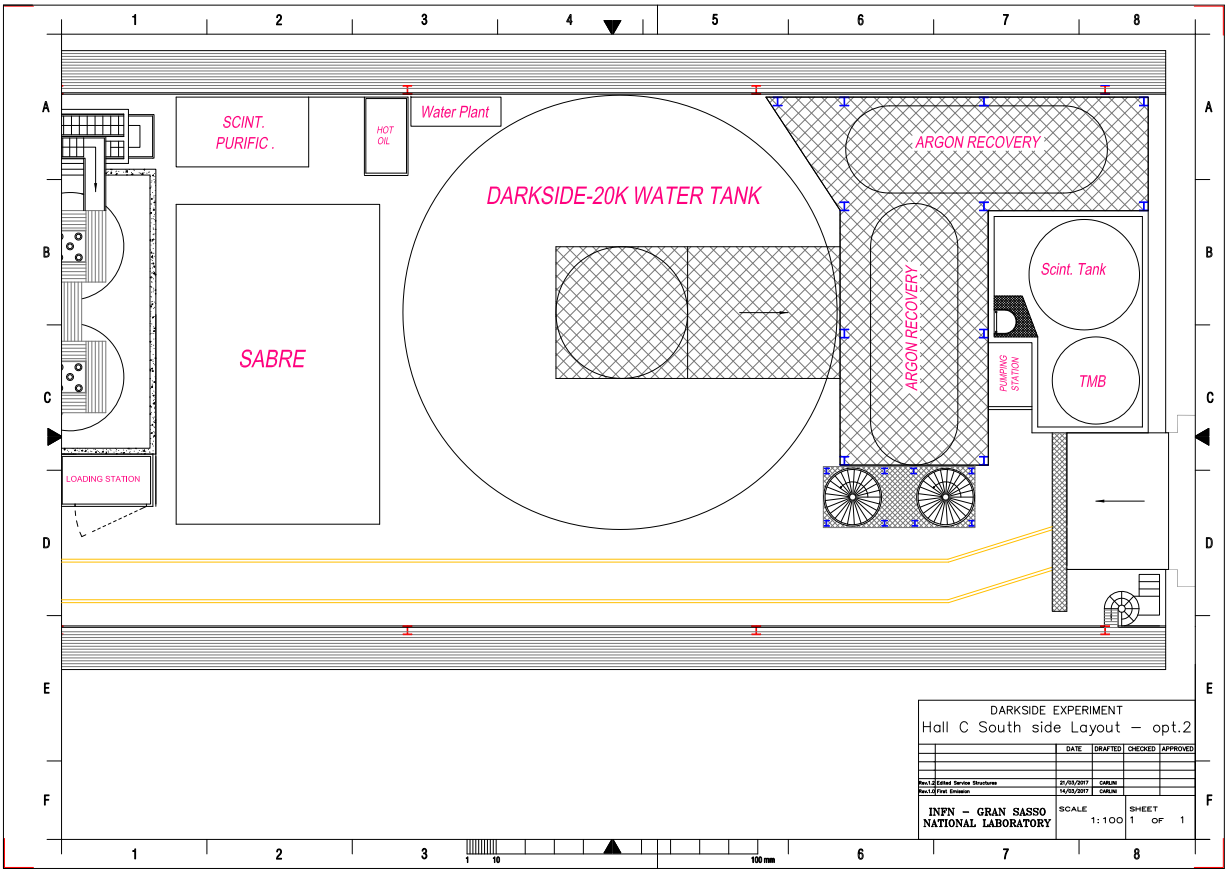

FIG. 1. DarkSide-20k : hall C Configuration #2: DarkSide-20k close to the Hall C main entrance, SABRE R&D near Borexino storage area.

Sec. II A. The chosen configuration satisfies the constraint of installation within the perimeter vacated by the OPERA experiment. It also satisfies the constraint of allocating independent facilities for the veto as well as for the processing and storage of scintillator components and for the production of ultra-pure water. In addition, it satisfies the constraint of compliance with the LNGS requirement to leave sufficient space for transit and movement of large apparati as well as not to hinder the movement of existing cranes.

A. Organization of Hall C

DarkSide-20k will be located in the underground Hall C of LNGS. The estimated available surface will cover approximately 30 m of length of the available width of Hall C. The configuration agreed upon by the LNGS Technical Coordinator and by the DarkSide Technical Coordinator take into account that part of the Hall C surface previously covered by the OPERA experiment will be reserved, through the year 2019, for the SABRE R&D Project.

The chosen configuration is with DarkSide-20k close to the Hall C main entrance, SABRE R&D near Borexino storage area as shown in Fig. 1.

The layout allocation includes not only the space required for the water tank, but also that required for the ultrapure water purification plant, for the scintillator purification, for the scintillator storage, for the hot oil system, for the electronics room, and for the control room.

We confirm that all the major plants and systems will fit within the area preliminarily allotted to the installation of DarkSide-20k experiment. There is no interference with other experiments installed in Hall C. The DarkSide Collaboration also plans to install in Hall C an independent, very compact, exhaust system to abate any organic vapor in the nitrogen blanketing lines. We plan to request the shared use of the regular

TABLE I. DarkSide-20k : chemical properties of solvents under consideration. PC is pseudocumene; DIN is Di-isopropylnaphthalene; LAB is Linear alkyl benzene; and PXE is phenylxylylethane. TMB is trimethylborate and is included in this table for the sake of comparison of the chemical properties.

	PC	DIN	LAB	PXE	TMB
Formula	C_9H_{12}	$C_{16}H_{20}$	$C_6H_5C_nH_{2n+1}$ [10<n<16]	$C_{16}H_{18}$	$B(OCH_3)_3$
Flash point [°C]	48	>140	130	145	−8
Vapor pressure at room temperature [mbar]	1.6	0.77	<0.07	8×10^{-4}	4×10^3
Density [g/mL]	0.89	0.96	0.86	0.99	0.93
Hydrogen atoms density [10^{22}/cm^3]	5.35	5.45	6.31	4.34	4.90
Absorption maximum [nm]	267	279	260	269	270

nitrogen storage tank installed in the truck tunnel connecting Hall C and Hall B, which is being equipped with a nitrogen recovery system.

B. Choice of Scintillator for the VETO

The baseline choice discussed in the YB for DarkSide-20k was to use the same scintillator cocktail as in DarkSide-50. Simulation showed that the neutron background could be kept to <0.1 events level in the full exposure with PC mixed with 20 % of TMB .

We are aware of the safety concerns related to the handling of large amount of TMB and PC due to their very low flash point and rather large vapor pressure at room temperature. In reaction to the hypothesis that the LNGS safety regulations could disfavour the use of TMB and PC, as recently conveyed to us, we investigated the possibility of using a scintillator with a safer choice for both solvent and dopant.

The primary goal of the liquid scintillator veto (LSV) of DarkSide-20k is the vetoing of neutrons yielding signals in the LAr TPC by anti-coincidence.

The criteria driving the choice of the liquid scintillator cocktail are: high photon yield, high transparency (attenuation lengths of several m), ultra-low impurity content mainly of natural radioactive contaminants, such as uranium, thorium, radium, and radon, long term stability, chemical compatibility with the materials in contact and, most important, capability of detecting neutrons with extremely high efficiency.

Organic liquid scintillators are all good neutron moderators thanks to their relatively high density of hydrogen atoms. Typically neutrons with kinetic energies of a few MeV thermalise within a time scale of few tens of ns yielding a prompt scintillation signal, mostly from recoiling protons. The thermal neutrons diffuse until captured on hydrogen atoms, with a characteristic time constant that, driven by the density of hydrogen atoms, is or the order of 200 µs.

This process yields two signals: the thermalisation signal, that is barely detectable due to the high quenching of low energy recoiling protons and the capture signal, that yields a 2.2 MeV γ-ray. The latter can, in a fraction of the events, be absorbed by the nearby cryostat, resulting in inefficiencies in the vetoing of neutrons.

The addition of dopants with large neutron capture cross section can enhance the capture signal, thus increasing the vetoing efficiency, as well as reduce the capture time, which also helps by permitting a tighter correlation between the thermalisation and capture signals. One common dopant is ^{nat}Gd, with its very large (48 890 barn) capture cross section for thermal neutrons. The capture of thermal neutrons on ^{nat}Gd results in the emission of several γ-rays, with cumulative energies of up to 8 MeV, which do result in a very large signal when the γ-rays are fully contained in the scintillator, but also result in limitations in the ultimate possible vetoing efficiency due to the finite possibility of γ-rays escape from the scintillator. The addition of ^{6}Li or ^{10}B as dopants is, in this respect, particularly intriguing since the both nuclides have relatively very large cross section for capture of thermal neutrons (941 barn and 3840 barn respectively) and the capture process produces always results in the emission of charged particles with a very short range, with a null probability of escaping the scintillator volume. On the positive side, the technology for the preparation of ^{nat}Gd-loaded LAB-based scintillator has recently significantly improved [2–4].

The DarkSide-50 LAr TPC is operated within a LSV filled with a boron-loaded scintillator, made of a PC solvent with the addition of the organoboron TMB at 5 % concentration in weight and of the scintillation fluor PPO (2,5-diphenyloxazole) at the concentration of 1.4 g/L. Preparation of the scintillator solution is particularly easy because TMB is liquid and can be easily mixed with PC with concentrations of up to 30 % in weight. Capture of thermal neutrons on ^{10}B (natural abundance 20 %) occurs with a 22 µs lifetime

through two channels [5–7] and always results in the emission of one α particle:

$$^{10}\mathrm{B} + n \rightarrow \alpha\,(1775\,\mathrm{keV}) + {}^{7}\mathrm{Li} \qquad (\mathrm{BR}: 6.4\,\%)$$
$$^{10}\mathrm{B} + n \rightarrow \alpha\,(1471\,\mathrm{keV}) + {}^{7}\mathrm{Li}^{*} \qquad (\mathrm{BR}: 93.6\,\%)$$
$$^{7}\mathrm{Li}^{*} \rightarrow {}^{7}\mathrm{Li} + \gamma\,(478\,\mathrm{keV})$$

The electron-equivalent energy of the lowest energy α particle is 30 to 35 keV_{ee}.

Table I shows the solvents under consideration and a few selected physical properties of interest for the selection. We included PC and TMB for the purpose of comparison. The higher flash point and lower room temperature vapor pressure of DIN, LAB, and PXE makes them particularly attractive as a choice for solvent; an additional benefit is that they are less chemical aggressive than PC. LAB is particularly interesting as it is gaining rapidly acceptance for use in many large volume detectors.

The loss of scintillation light yield when switching from a PC-based scintillator to a LAB-based scintillator is limited: the yield reported for LAB+PPO+bisMSB is 70 % of that of PC+PPO [8] and it can be compensated, where needed, by a modest increase in the number of PMTs.

Another nucleus with large neutron capture cross section is ^{6}Li. Indeed, the reaction with neutron produces charged particles with a very short range:

$$^{6}\mathrm{Li} + n \rightarrow t\,(2.73\,\mathrm{MeV}) + \alpha\,(2.05\,\mathrm{MeV}) \tag{1}$$

In this case, though, the higher energy of the α particle and the lower quenching of the triton result in an electron equivalent energy from 400 to 500 keV_{ee} [9], nearly ten times as large as that for the lowest energy α particle from capture on ^{10}B cited above. A number of authors [4, 9, 10], and among them the PROSPECT Collaboration [11], studied in detail the possibility of loading organic liquid solvents with aqueous solutions of ^{6}LiCl, and their collective work has established a sound and safe avenue for the development of ^{6}Li-loaded organic liquid scintillators. The abundance of ^{6}Li in natural Lithium is about 7%. Isotopic enrichment has been accomplished by the PROSPECT Collaboration and they have reached a ^{6}Li concentration of 0.7% in weight. The Lithium salt ^{6}LiCl can be dissolved in several solvents or mixture of solvents [10] with addition of proper surfactants.

A recent development [12] identified the possibility of loading organic liquid solvents with an organoboron compound of fairly limited safety and environmental impact: ortho-carborane, (1,2-Dicarbadodecaborane(12), $C_2B_{10}H_{12}$), a solid at room temperature with a melting point of 260 °C. It has be shown that it can be dissolved in several solvents (PC,DIN,LAB and other solvents [13]) up to concentration of 8.5% in weight. The scintillation yield of such mixtures was measured under γ-ray irradiation and also with neutrons.

The addition of ortho-carburane quenches the scintillation yield. The size of the quenching effect (not more than 50% in the worst case) depends on the choice of the solvent and of the fluor and can be tolerated and compensated if neceessary by increasing the optical coverage of the detectors with more PMTs. Exposure of a LAB+ortho-carborane scintillator to neutrons showed that the α-particle quenching is the same as the one measured in DarkSide-50 [12].

As reported in the DarkSide-20k YB, TDR neutrons originated by (α,n) reactions induced by the radioactive contaminants of the TPC are generated and tracked using the Monte Carlo. The fraction of these neutron events producing a signal in the LAr TPC and surviving a set of standard TPC cuts cannot be distinguished by a true WIMP energy deposit without using the information of the veto detectors. The energy deposit in the LSV is analysed within a time window of about 7 τ's around the TPC signal (τ is the thermal neutron capture time relative to the specific dopant of choice for the scintillator). The fraction of events that are not tagged as neutrons as a function of the minimum threshold energy in the LSV represents the residual background.

The comparison between the four scintillator options has to consider what threshold can be applied vs deadtime. The short capture times of the two boron-based scintillators allow to lower the threshold down to a few photoelectrons (7p.e. in DarkSide-50): even in presence of 2.5 kBq of ^{14}C, the deadtime introduced by the veto will be <8%. For the other two scintillator options, the long capture times obliges to set the threshold above the ^{14}C Q-value (80 p.e.), where the neutron rejection efficiency is 3-4 times lower than in the boron case. For the Gd option, the background from PMTs would anyway induce a deadtime of the order 30 to 50%.

Fig. 2 shows the upper limit on the residual background in a 100 t yr exposure. We remind the reader that in the YB only an upper limit to the residual neutron background was obtained, ultimately originating from

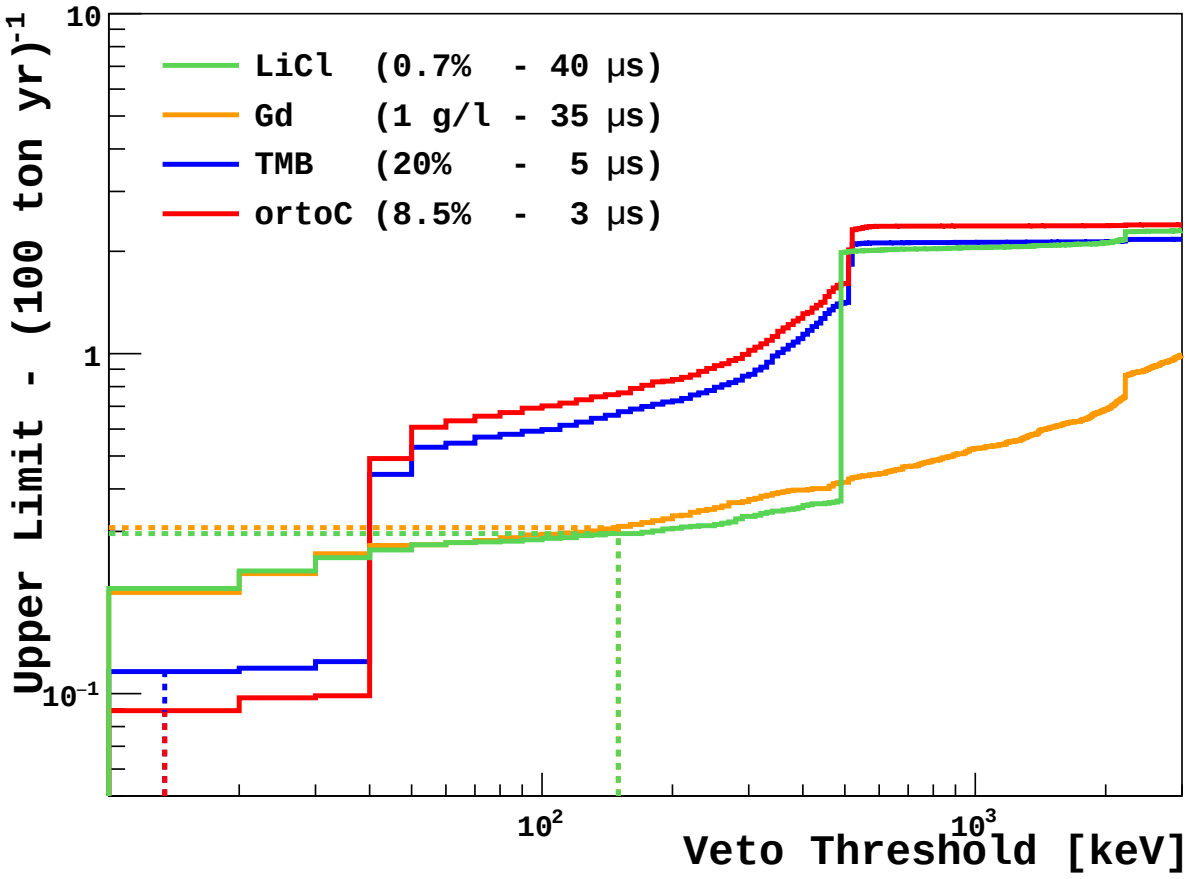

FIG. 2. DarkSide-20k : upper limit to residual neutron background after LSV cuts for four different possible loading of the LSV solvent with scintillator dopants, as indicated in the legenda, with the relative concentration and thermal neutron capture time. The dotted lines indicate realistic thresholds values that can be applied to limit the dead time, as explained in the text.

an upper limit to the radioactivity of the PTFE of the TPC. The plot is independent of the solvent type given the horizontal axis is expressed in deposited energy.

The curves were obtained with a fraction of dopant that has already been tested by other experiments.

Indeed, the option of loading the scintillator with orto-carburane turns out to be particularly appealing. Further studies on the long term chemical and optical stability, chemical compatibility etc. are needed to fully validate the choice, but we believe that both costwise and also with respect to the foreseen infrastructure the choice should not be considered a risk factor for the project.

During the LNGS meeting of March 28th between the DarkSide-20k management and the LNGS management we got a strong encouragement towards deeply investigating, while keeping as baseline the PC loaded wth TMB, the option of LAB loaded with ortho-carborane.

C. Planning of Safety and Authorization Documents

The DarkSide Collaboration has already carried out a preliminary risk assessment (PRA) of the DarkSide-20k cryogenic systems. Concerning operations in Colorado, we are beginning a preliminary hazard analysis (PHA) through Kinder Morgan for the Urania plant and it operations at Doe Canyon. Kinder Morgan is going to guide us in this process, providing us the help of one of their safety management experts.

The DarkSide Collaboration is now selecting through a tender a company with expertise in the field of safety to carry out the studies necessary for all other future steps. The list of documents currently planned for the LNGS installation and operations includes:

- A new PRA, with extension of the scope such as to cover the complete set of DarkSide-20k sub-plants;
- Quantitative risk analysis (QRA) of the entire set of DarkSide-20k sub-plants;
- "Relazione di Non Aggravio di Rischio", as mandated by "Seveso-Ter EC Directive", received by the Italian D. Lgs. 105/15;
- Explosion risk assessment (ERA);
- Reliability system assessment (RSA).

All these steps, as well as any other future steps that may become necessary for completion of all safety reviews, authorisations, and associated preparation of documents, will be tightly coordinated with the LNGS Directorate.

The DarkSide Collaboration, in agreement with the LNGS Directorate, has appointed F. Gabriele as group leader in matter of safety and environmental experiment responsible (GLIMOS/RAE). In order to best cope with all safety, health, and environment requirements, the Collaboration intends to create a safety and environmental office, introducing the figure of shift leaders in matters of safety (SLIMOS). SLIMOS will be trained by the GLIMOS to take special care of the experiment and of collaborators working on the experiment during shift periods, including all phases of the experiment, from installation, through commissioning, to operation. Specific responsibilities for the SLIMOS will include the continuous monitoring of access in the area allocated to the experiment, raising awareness concerning ongoing operations, including installation of heavy equipment, as well liaising with the LNGS emergency services in the event of a problem.

III. PHOTOELECTRONICS

A. Introduction

The SiPMs production of choice, the so called NUV-HD-LF, have an individual size $10 \times 10\,\mathrm{mm}^2$, thus requiring 25 SiPMs to cover the $50 \times 50\,\mathrm{mm}^2$ required for the DarkSide-20k PDMs.

However, as discussed in Sec. III B, we identified a new and more optimised and optimal readout configuration with 24 SiPMs, with four transimpedance amplifiers (TIAs), each one connected to three parallel combinations of two SiPMs in series, a configuration that we identify as 4×3p2s. We therefore report results of tests performed with tiles of 24 SiPMs, covering an area of $24\,\mathrm{cm}^2$.

Indeed, the baseline for the DarkSide-20k PDMs becomes a tile of 24 SiPMs with $7.9 \times 11.7\,\mathrm{mm}^2$ area, ensuring a fill factor of about 90 %, that could be increased later on when switching, as planned for the production of the PDMs for DarkSide-20k, to SiPMs equipped with Through Silicon Vias (TSVs). SiPMs of $7.9 \times 11.7\,\mathrm{mm}^2$ area will be produced with the next FBK run in the fall 2017.

At the beginning of 2017, the DarkSide-20k Collaboration had a very limited stock of NUV-HD-LF SiPMs: 119 in total. Production of the SiPMs of choice was restricted in 2016 due to the ongoing INFN bidding procedure and to the modification of the contract with FBK. The number of SiPMs available was enough to only mount four full tiles. We decided to devote nearly half of the available SiPMs to mount two new 24-SiPM tiles in anticipation of the XLVII LNGS SC meeting. The remainder of the stock of NUV-HD-LF was set aside, for the purpose of feeding the plan for PDMs testing in the next few months, before the delivery of the next production of SiPMs anticipated for the fall 2017. Indeed we believe that the test of two tiles, with the corresponding cryogenic electronics, is a significant validation test of the whole chain: the very positive results give us strong confidence in the project.

Sec. III B describe the production and results of tests on the two 24-SiPM tiles produced with NUV-HD-LF of individual area $10 \times 10\,\mathrm{mm}^2$. Sec. III C describes the tests of uniformity performed on a large sample of NUV-HD-LF SiPMs with individual area of $5 \times 5\,\mathrm{mm}^2$.

B. Tiles assembling and performance tests

Two 24-SiPM tiles, that are called tile #1 and tile #2 in the following, assembled with NUV-HD-LF of individual area $10 \times 10\,\mathrm{mm}^2$, for a total area of $24\,\mathrm{cm}^2$, were mounted at Princeton University Laboratory, see Fig. 3. The SiPMs were connected by wire-bonding procedure to a standard PCB substrate.

Each SiPM connection was linked to a common connector placed on the back-side of the tile. An electronic front end board (FEB), containing the transimpedence amplifiers (TIA), was plugged on the tile.

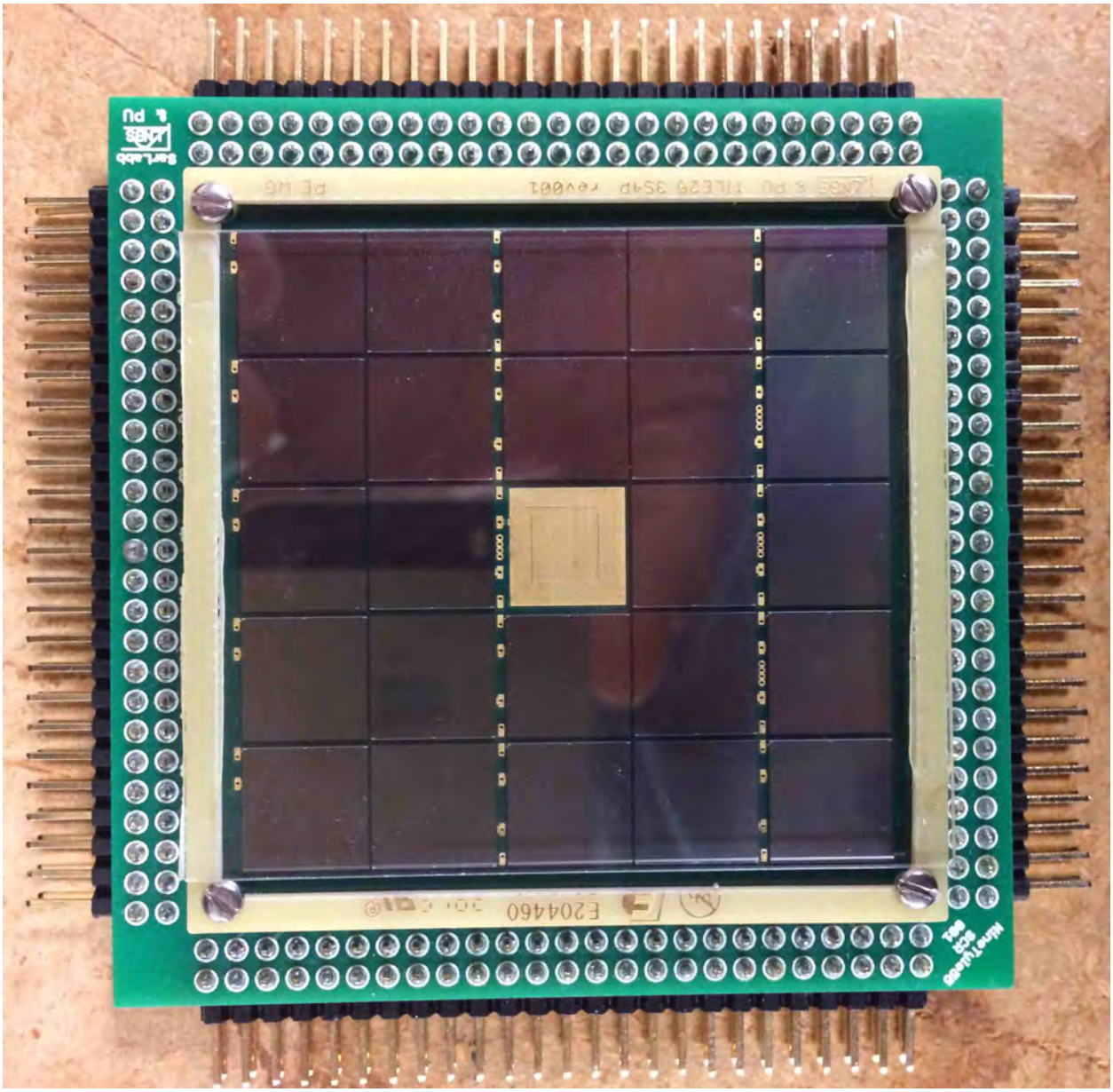

FIG. 3. DarkSide-20k : a 24-SiPM tile assembled with NUV-HD-LF of individual area $10 \times 10\,\mathrm{mm}^2$

With respect to the results presented at the XLVI LNGS SC meeting, we identified a new and more optimised readout scheme, with the SiPMs arranged in a 4×3p2s configuration (see Fig. 4), *i.e.*, three pairs of SiPMs in a series combination are connected in parallel. Four chains, each one equipped with a TIA, whose output signals are analog summed, are required to read 24 SiPMs.

The tiles underwent a preliminary test at Princeton and a full test at LNGS in liquid nitrogen. The TIA offset differences due to input bias currents are minimized at cryogenic temperature, relying on an good low voltage filtering. The tiles were pulsed by a laser light, at the frequency of 500 Hz. The signals were acquired using a fast digitiser followed by a software cross correlation filter with τ of 400 ns.

The signal-to-noise ratio (SNR) was obtained as the difference between the mean values of the single and the two-PE peaks, divided by the standard deviation of the noise, obtained by extrapolating to zero PEs the widths of the different PE peaks.

While during the tests at Princeton Tile #1 had all the 24 SiPMs fully working, after shipping to LNGS only 22 out of 24 SiPMs were found to be working. The tile was anyway measured yielding a SNR (scaled

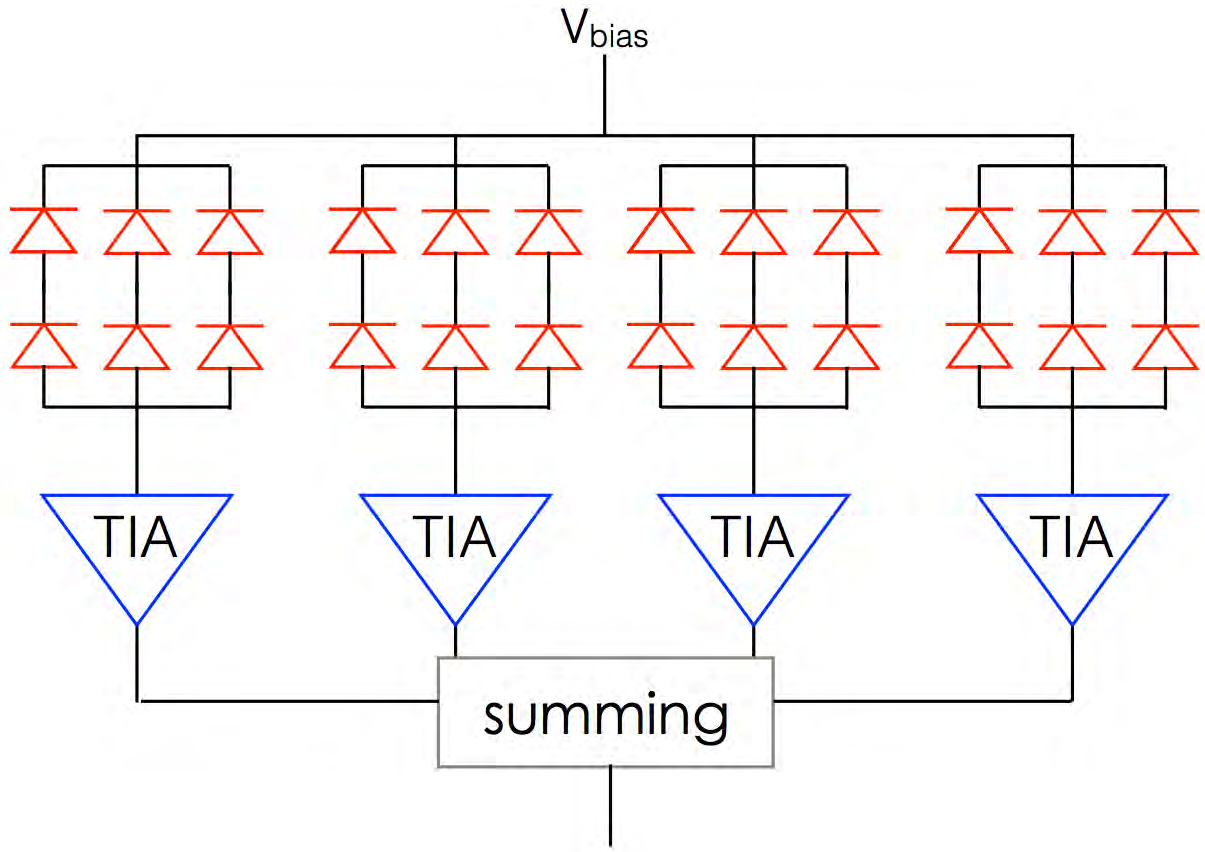

FIG. 4. DarkSide-20k : schematics of the 4×3p2s readout configuration of a tile.

to that of the 24 SiPMs tile) of 14.3 (13.6).

Tile #2 was also tested, with all the 24 SiPM properly working and yielded an SNR of 13.8, as shown in the Lower Fig. 5.

We made an attempt to repair tile #1 by replacing the two non working SiPMs, although the procedure is quite risky requiring the reheating of the whole tile. Then we repeated the test on the repaired tile, obtaining an SNR of 10.5, as shown in the Upper Fig. 5.. As expected, the result is not as good as that of tile #2, but is nevertheless within the experiment specifications described in the YB of a SNR of 8.

With these results, all specifications detailed in the DarkSide-20k YB for SiPMs and tiles are now fulfilled.

C. SiPMs Uniformity Tests

We assembled two large tiles with 70 NUV-HD-LF SiPMs each of dimensions $5 \times 5\,\mathrm{mm}^2$, for the purpose of larger scale tests of uniformity of the performance of FBK SiPMs. Tests were performed at INFN Naples at 94 K and 296 K. We measured the I-V curves for 129 of the SiPMs available, of which 61 with a $25 \times 25\,\mu\mathrm{m}^2$ cell size and 68 with a $35 \times 35\,\mu\mathrm{m}^2$ cell size.

Table II shows the variation of breakdown voltage V_{bd} and quenching resistor R_q for the two batches of NUV-HD-LF SiPMs subjected to large-scale uniformity tests at the temperatures of 94 K and 296 K: the results reported above show a remarkable uniformity of the measured SiPMs.

As an example the measured breakdown voltage uniformity can be compared to that obtained by commercial SensL SiPMs [14], showing an average breakdown voltage V_{bd} of 24.69 V with a $\sigma_{V_{bd}}$ of 73 mV, resulting in $\sigma_{V_{bd}}/V_{bd}$ of 0.3 %, slightly larger than that of SiPMs produced by FBK.

As a consistency test with the larger area SiPMs, tile #2 was also tested in liquid argon at University of Napoli. Breakdown voltage was measured for individual TIAs obtaining results between 55.8 and 56.2 with an uncertainty of 0.2%, that is consistent with results shown in Table II, taking into that each TIA reads

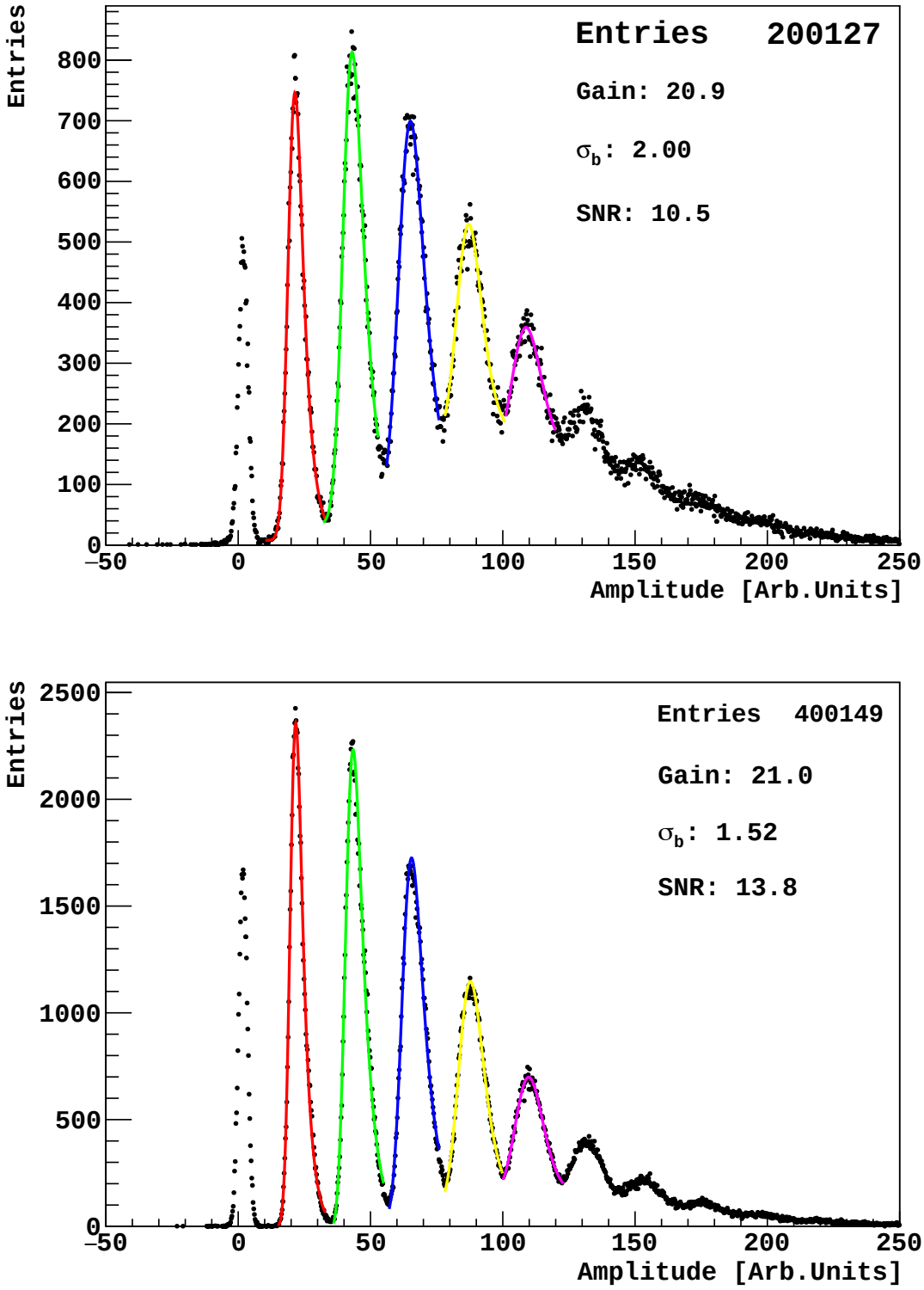

FIG. 5. DarkSide-20k : amplitude spectrum of signals for two 24-SiPM tiles. Upper: tile #1 on which two SiPMs were repaired Lower: tile #2;

two SiPMs in series.

TABLE II. DarkSide-20k : variation of breakdown voltage V_{bd} and quenching resistor R_q for the two batches of NUV-HD-LF SiPMs subjected to large-scale uniformity tests at the temperatures of 94 K and 296 K.

Cell Size	$25 \times 25\,\mu m^2$		$35 \times 35\,\mu m^2$	
Temperature	94 K	296 K	94 K	296 K
V_{bd}	(28.05 ± 0.01) V	(33.86 ± 0.01) V	(28.110 ± 0.005) V	(34.04 ± 0.01) V
$\sigma_{V_{bd}}/V_{bd}$	0.18 %	0.23 %	0.11 %	0.32 %
R_q	(12.94 ± 0.09) MΩ	(1.99 ± 0.04) MΩ	(11.30 ± 0.09) MΩ	(1.56 ± 0.01) MΩ
σ_{R_q}/R_q	4.4 %	14 %	5.7 %	6.3 %

IV. DARKSIDE-PROTO

DarkSide-Proto project aims at constructing and operating a prototype detector of intermediate size, incorporating the new DarkSide-20k technologies for their integration and full validation. The choice of the 1t mass scale allows for a full validation of the technological choices for DarkSide-20k.

The DarkSide-Proto will be equipped with the full-scale cryogenics system of DarkSide-20k designed by scaling that of DarkSide-50 which achieved excellent performance for long-term thermal stability and purity of the argon target.

The program for DarkSide-Proto is expected to span over three different phases, with a total timeline of three years:

Proto 0: Test of cryogenic system concept at the test site; identification and preparation of full readout and DAQ of 50 pre-production PDMs;

Proto I: Design, construction and assembly at test site of cryostat and LAr TPC equipped with 50 pre-production PDMs; assembly, commissioning, and operation of full read-out and DAQ for 50 PDMs;

Proto II: Assembly and commissioning of full system, including 400 first production PDMs; full readout and DAQ operational; evolution towards final configuration.

The plan for DarkSide-Proto was reviewed, approved, and funded by the CNS2 of INFN. Requests for funding from other participating groups are being evaluated or will be submitted in the near future.

Based on the recommendations of INFN CSN2, the DarkSide-20k collaboration submitted at the end of 2016 a proposal to carry out the above plan at CERN, to take advantage of their cryogenic infrastructures. An application was made for the status of CERN Recognised Experiment. The application was discussed on January 19, 2017 and a recommendation prepared by the REC Committee for the Research Board. We received in March a negative response.

Since DarkSide-20k will be hosted at LNGS, it is natural to consider that LNGS be the experimental site for the DarkSide-Proto. As suggested by the LNGS SC, this choice would enable the establishment of the infrastructure required for DarkSide-20k. This decision would of course require the approval of LNGS director and the LNGS SC and a certain amount of support from LNGS. The DarkSide collaboration has started an extended evaluation of possible options and relative requirements. A final decision on the location of the on-surface test is expected by the next June collaboration meeting.

A. Technical specifications

The cryogenics system is going to be built using the full scale condenser, heat exchanger, and piping, in order to test the full scale capability of the cooling system. We report here that the first full scale condenser has been fabricated and tested at UCLA, as shown in Fig. 6 and 7, achieving cooling power at 200% of the required maximum operational needed.

The TPC mechanics, including the structural elements, the field cage, the reflector cage, the transparent cathode, the transparent anode (also serving as a diving bell for the containment of the gaseous phase), the SiPM assemblies, the high-voltage feed system, will all be built utilising, on a scaled down overall dimension, the same design and construction techniques foreseen for the baseline of DarkSide-20k.

The photodetector modules will be arranged to cover the top and bottom of the TPC. For that, the total number of photodetector modules required is 370, equivalent to 8% of DarkSide-20k. The read-out chain will evolve from commercial components used in the first phase allowing full digitisation of pulse shape, towards the planned final components as they become available at each stage of the development. Also optical signal transmission, once and if available, can be tested on a significant number of channel.

FIG. 6. DarkSide-Proto : the condenser heat exchanger.

As shown in Fig. 8, both top and bottom planes consist of 185 photodetector modules assembled into 5 SQBs and 4 triangular motherboards (TRBs).

The DarkSide-Proto LAr TPC detector parameters and characteristics are shown in Table III.

The construction of the elements detailed above and their basic functionality tests do not require, in the first phase, low background underground facilities. At the same time, they are on the critical path for

FIG. 7. DarkSide-Proto : laboratory test of the full scale condenser.

the timely completion of the DarkSide-Proto program, which in turn is on the critical path in the overall schedule of DarkSide-20k. We need therefore to guarantee that the on-surface construction and operations are performed at the most convenient location and with expert support.

V. ARGON PROCUREMENT AND PURIFICATION

For the sake of clarity, we will use the following naming convention: Urania is the argon extraction and chemical purification plant of underground argon, UAr, that has a specific content of ^{39}Ar of less than one thousandth of the atmospheric level, to be located at the Doe Canyon CO_2 wells of Kinder Morgan in Cortez,

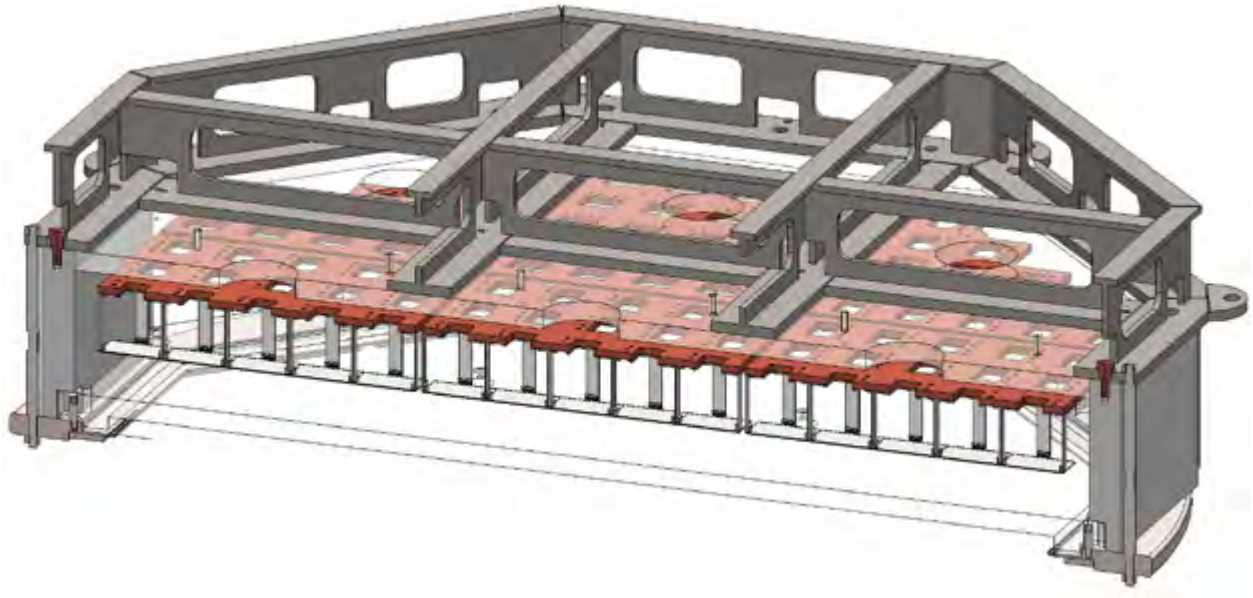

FIG. 8. DarkSide-Proto : the top photon readout plane.

TABLE III. DarkSide-Proto : LAr TPC detector characteristics.

LAr TPC Dimensions	
Height	58 cm
Effective Diameter	72 cm
Total LAr Mass	800 kg
Nominal TPC Fields and Grid	
Drift Field	200 V/cm
Extraction Field	2.8 kV/cm
Luminescence Field	4.2 kV/cm
Operating Cathode Voltage	−15 kV
Operating Extraction Grid Voltage	−3.8 kV
Operating Anode Voltage	ground
Luminescence Distance	7 mm
Grid Wire Spacing	3 mm
Grid Optical Transparency	98 %
SiPM Tiles	
Number of Tiles	370
Size of Tiles	$50 \times 50\,\mathrm{mm}^2$

CO, USA; Seruci-0 stands for the chemical purification test column of height 24 m, to be installed in the "Laveria" building in the Nuraxi Figus site of the "Monte Sinni" mine of Carbosulcis S.p.A. in Sardinia, Italy; Seruci-I stands for the chemical purification and isotopic purification column of 350 m height to be installed in the Seruci mine shaft of the same mine. Seruci-0 and Seruci-I are part of a bigger and wider scope project, Aria, that covers the needs of DarkSide-20k but also extends beyond its scope. The ultimate aim of Aria is isotopic distillation of the argon to further reduce the ^{39}Ar content, with respect to that of the UAr coming from Urania, for the use in future projects like Argo, as well as for the production of other stables isotopes for medical applications, with scaled up productions expected with the construction of a larger column (Seruci-II) that has yet to be funded.

Isotopic separation by cryogenic distillation of the entire UAr batch of DarkSide-20k is not part of the baseline for DarkSide-20k.

TABLE IV. Urania/Aria: Inlet purity required by the getter of DarkSide-20k.

Element	Inlet Purity Requirements (ppm)
CH_4	<0.25
CO	<0.1
CO_2	<0.1
H_2	<1
H_2O	<1
N_2	<1
O_2	<1

A. Introduction

The underground argon extracted in Colorado and purified in Sardinia will be delivered to DarkSide-20k passing through a getter. The inlet purity required by the getter, reported in Table IV, defines the argon purity requirements of the UAr after production by Urania and chemical purification by Seruci-I.

The strategy for the argon procurement for DarkSide-20k consists of two major operations:

- Extraction: the Urania plant will extract 50 t of UAr from the CO_2 wells in Cortez, CO and purify it to the 99.9 % level;
- Chemical purification: two passes of cryogenic distillation in the Seruci-I column will reduce heavy and light contaminants below the requirements dictated by the getters and reported in Table IV. The combined UAr recovery of the two distillation operations in Seruci-I is expected to be higher than 85 %, thus providing more than the required 32 t to 35 t of ultrapure UAr required for the fill of DarkSide-20k.

B. Underground Argon Extraction and Purification: Urania

This Section will detail the progress and plans towards the construction of Urania.

1. *Description of the Extraction Process*

The Urania feed gas stream is ∼95 % CO_2, plus a few percent of N_2, one percent CH_4, and 440 ppm of underground argon (UAr). The plant that is being specially designed and built to extract the small fraction of UAr from this gas stream, and then return the remaining gas (99.9 % of the original content) to the supply gas stream, will be installed at the Kinder Morgan CO_2 extraction facility located in Cortez, Colorado (USA). The Urania UAr extraction plant will consist of two main sections: a first section for removing CO_2, followed by the cryogenic distillation section.

a. CO_2 Separation Section CO_2 separation is done by two separated strippers, run in series. The feed gas which is at high pressure (50 bar) is first cooled through a chiller to approximately 5 °C. At these conditions the CO_2 partially condenses and the stream is separated into 2-phases (gas/liquid) as it goes to the first stripper. In the column a controlled quantity of heat is given by a hot fluid working between the chiller condenser and the column reboilers. The light products are vaporised and recovered from the top of the column in gas phase. The heavy products (mainly CO_2) are collected from the bottom, pumped, and sent to a CO_2 recovery unit, to be recycled towards the main gas feed stream of Kinder Morgan. The light products coming from the column head are cooled down in the second step to approximately −50 °C and sent to the second stripper. Here, the CO_2 is again removed from the bottom and collected and pumped together with the CO_2 coming from the first separation column. The gas coming from the top of the second stripper is re-heated in a heat exchanger and delivered to the PSA unit. The purpose of the PSA system is to improve the purification of the gas stream by removal of the residual CO_2. The PSA is composed of four adsorption beds to allow continuous operation with short time adsorption cycles. The desorption of CO_2 is made decreasing the pressure on the bed. To optimize the performances, the operation of the adsorbers are combined by coupling purge and pressure swing phases. At the outlet of the PSA adsorption tanks, one buffer tank is provided in order to dampen the fluctuations and allow a continuous operation in the distillation section. The PSA off-gas is delivered to a recycle compressor and sent back at the second CO_2 stripper inlet.

b. Cryogenic distillation section The CO_2-free stream from the PSA is pre-cooled and sent to the cryogenic distillation section that works at a lower pressure level (approx. 9 barg). In the first cryogenic distillation column CH_4 is separated from the bottom while the UAr and other light gases are taken from the top. In the second cryogenic distillation column, the UAr is taken from the bottom while N_2 and He are separated as light off-gas from the top and recycled back into the loop for reprocessing. Both the CH_4 stream and the N_2/He stream are collected together and merged with the CO_2 flow coming from the previous CO_2 separation section. To get the desired UAr recovery and purity a third batch column is provided to separate the UAr from the residual CH_4 and N_2. The 99.9 % pure liquid UAr product is taken from the top of this final column and sent to both a collection tank, and partially to a collection tank used to check the quality of the UAr product. The gas generated as the UAr boils in these thanks will be continually re-condensed using a LN_2 fed vent condenser. These tanks will also serve at the transportation vessels, for shipping the UAr from Cortez to Sardinia, and then to LNGS. The intermediate distillate fractions are recycled back to off-gas tank of the PSA unit. When no more argon is present in the boiler, the residual methane is sent back to the methane collection tank for recovery. The distillation columns are made with internal structured packing to have a large mass and heat transfer between liquid and vapor phase and are enclosed in a vacuum insulated cold box.

2. R&D activity in support of PSA design

The PSA is the most critical unit of the entire process, since the dynamic adsorption conditions are the most difficult to simulate and predict. An R&D activity is ongoing at the University of Naples to identify the most appropriate sorbent and to define the PSA operational parameters. Sorbent screening relies on breakthrough tests, performed on a lab scale rig. Promising sorbents have already been identified. Definition of the operational parameters of the PSA unit relies on experiments to be performed on a 4-vessel PSA unit pilot plant. The pilot plant was installed in the laboratories of the Università degli Studi "Federico II", Naples, see Fig. 9.

The full R&D process should be completed by the end of June 2017, according to the foreseen timeline:

- Sorbent Screening - completed by end of April 2017
- PSA Pilot Plant Commissioning - completed by end of April 2017
- PSA Pilot Plant Operations - May-June 2017
- Results expected - end of June 2017

3. UAr Shipping and Storage

The shipping of the UAr will be done using the same tanks that will serve as the collection tanks for the UAr extraction plant. The customised cryogenic vessels fit within a Wessington Cryogenics Standard Cryopack 3000 frame, and will contain two vacuum isolated inner vessels, sealed within the main tank. The main inner vessel will be capable of storing and shipping up to 8.8 t of UAr, while the second will hold a reserve of liquid nitrogen, used to continually condense the UAr inside the tank so that a zero-loss condition can be held for the duration of the shipping time from Cortez, CO to Sardinia, Italy. To do this, the two inner vessels will be linked via the custom made LN_2 fed UAr condenser, modeled after the condenser designed for the DarkSide-20k cryogenics system. To stay away from the need of electronics control of the condenser, a custom designed cryogenic valve will be used to regulate the condenser N_2 vent flow (and hence cooling power for condensing UAr) based on the pressure inside the inner UAr vessel. The design of this vessel is now at a stage of optimisation with Wessington Cryogenics, as the baseline features have now been decided and the basics requirements frozen. Because the tanks are custom vessels that will need to be operated at both US and Italian facilities, as well as act as transportation vessels, they will need to have all the required engineering certifications. Wessington Cryogenics is aware of our needs and will be working with us all along the way to ensure that all certifications and requirements are met. It is expected that the cryogenic tanks can be delivered to Cortez, CO about 9 months from the date of order. As stated, the cryogenic vessels will serve as the collection tanks for the the UAr extraction plant, and so will each have a similar bayonet access to the inner UAr storage vessel. There will also be a matching bayonet giving access to the LN_2 inner vessel, for source of LN_2 to keep the UAr in liquid phase during storage, and then provide the final fill of LN_2 before shipment. Once a single cryogenic vessel is full (8.8 t of liquid UAr), it can easily be disconnected

FIG. 9. Urania: PSA pilot plant in the laboratories of the Università degli Studi "Federico II", Naples.

from the bayonet side of the cryogenic liquid transfer line coming from the extraction plant, then loaded onto a truck for transportation to the ship yard, where it will then be loaded onto a boat and shipped to Sardinia, Italy. A single shipping vessel can be filled in about 3 months, at the expected 100 kg/day UAr production rate, with shipment to Sardinia then taking around 45 days more. It is expected that one vessel will start out in Sardinia at the site of Seruci-I, to act as the collection tank for the product coming from the Seruci-I chemical purification process. With this in mind, 5-cryogenic vessels will be required, with four of them beginning their journey at Cortez, CO, and one at the location of Seruci-I, in Sardinia, Italy. Two of the vessels will then need to be shipped back to Cortez, CO to make the final two shipments of UAr to Sardinia, and completing the procurement of the 50 t agreed by Kinder Morgan. The entire extraction, and then shipping of the 50 t of UAr to Sardinia is expected to take a little less of 18 months, from the start of full time operations of the plant.

4. UAr Extraction Timeline

The timeline for the extraction of the UAr is strictly dependent on the release of funding, since preparation of the extraction site needs to proceed ahead of the plant installation. The original schedule of DarkSide-20k foresaw installation of the Urania plant beginning during the second quarter of 2017, and installation of the plant finalised and the plant commissioned by the end of second quarter in 2018. Since we are at that point now, we have basically started the delay process now. The delivery and approval of the final design of the plant will happen just after the release of funding, and site preparations can begin not long after that. With this in mind, the timeline for the extraction and delivery of the UAr to Sardinia is currently delayed 2-3 months, plus the additional time between now and that when funding becomes available. This is starting to get close to the contingency time that was in place for the extraction of the UAr, which originally called for 2 years, but should in reality only take 18 months, and so if funding is not available within the next few months, DarkSide-20k will be at risk of delay.

C. Final Argon Purification: Seruci-I

The Seruci-I column consists of 30 modules covering the 350 m height of the Seruci shaft: the bottom module (reboiler), 28 central modules and the top module (condenser). Activities are ongoing and split in three different sites: production and initial leak check on single pipes at Polaris, final leak check on complete modules at CERN, and site preparation for installation at Carbosulcis.

1. Activities at Polaris

At Polaris, all modules are through the phase of pre-construction, with a number of them still awaiting for the final assembly and certification. Two complementary helium leak tests of the Seruci-I modules are performed. The first step takes place directly at Polaris, where the process column and all the pipes (argon feed, liquid nitrogen, nitrogen gas and degassing line) are individually leak checked at room temperature. All the leak tests done so far showed no leak with a background of about 1×10^{-9} std cm^3/s. Following this first leak check step, the column and the pipes are wrapped with superinsulation and finally assembled within the cold box, prior to shipping to CERN.

Status and plan of the construction and first step of leak check:

- The bottom reboiler, top condenser, and first 5 central modules are built, certified on site for leak tightness, and shipped to CERN for the final leak check;
- 4 additional central modules are in assembly and will be ready to be shipped to CERN by the end of March;
- Pre-construction of the remaining 19 modules is complete, and their final assembly and first step of leak checking will proceed at an expected pace of 4 modules per month.

FIG. 10. Aria: top and first 4 central Seruci-I modules at CERN.

2. *Activities at CERN*

Upon reception of modules at CERN, an integral leak test of the modules is performed. This activity is done in the framework of a Service Agreement with CERN, established in June 2016, by which experts of the CERN Technology Department supervise the performance of such leak tests. The leak check also includes the cold box. Leak test of all process pipes is repeated. So far, we did not observe any leak above a background in the range from 1×10^{-8} std cm^3/s to 1×10^{-9} std cm^3/s. For the sole bottom reboiler, the leak check procedure will be repeated a second time after cooling the internals of the module to 77 K.

Status and plan of the leak tests:

- The bottom reboiler, top condenser, and first central modules have been successfully tested (see Fig. 10);
- The bottom reboiler is currently undergoing cooling to 77 K;
- The first set of 4 central modules of the series production is being prepared for test.

3. *Carbosulcis*

Status and plan of the authorisations and of the preparation of sites:

- Carbosulcis obtained from the municipality of Gonnesa all authorisations required for Seruci-0;
- The "Laveria" building, which will host the Seruci-0 column has been already prepared and almost equipped with all the utilities.
- A plan to obtain the authorization for Seruci-I is being finalised;
- Refurbishment of the roof covering the building for the winze serving the Seruci shaft is complete, see

FIG. 11. Aria: refurbishment of the roof covering the Seruci winze building, Summer 2016.

Fig. 11;
- Refurbishment of the winze serving the Seruci shaft is complete, see Fig. 12;
- Carbosulcis personnel has entered the Seruci shaft and has started the refurbishment of the shaft walls, see Fig. 13;
- The refurbishment of the surface buildings near the Seruci has started.

Upon clearing of shipping of the units to Carbosulcis, as soon as administrative procedures are complete, we plan to start the following actions:
- Installation, commissioning, and operation of the Seruci-0 column.
- Installation into the shaft of the column support structure.
- Installation of the Seruci-I column into the shaft.
- Commissioning and operation of the Seruci-I column.

VI. STATUS OF DARKSIDE-50

DarkSide-50 is an experiment currently operating in Hall C at LNGS. It consists of a LAr TPC with (46.4 ± 0.7) kg of active LAr, a surrounding liquid-scintillator neutron veto (LSV), all in a instrumented water shield, and is supported by an array of radon-suppressed cleanrooms for assembly and installation. It thus serves as an excellent test of many concepts to be exploited in DarkSide-20k.

After a trial assembly and brief run in the spring and summer of 2013, DarkSide-50 was reassembled in final form in September of 2013 and commissioned with an atmospheric argon (AAr) fill and operating vetoes. The AAr run lasted until March 2014, and produced a wealth of useful data, most notably a very large sample of ^{39}Ar decays for high-statistics tests of LAr pulse shape discrimination (PSD) and a WIMP search using 47.1 live-days ((1422 ± 67) kg day) of exposure [6].

In April 2014, the cryostat was emptied and refilled with 150 kg of underground argon (UAr) for the main science run. An immediate result was the first measurement of the UAr ^{39}Ar depletion factor relative to AAr of 1400 ± 200. This was followed by a WIMP search with 70.9 live-days ((2616 ± 43) kg day) of exposure, resulting in an upper limit on the spin-independent WIMP-nucleon cross section of 2.0×10^{-44} cm^2 for a 100 GeV/c^2 WIMP mass [7].

Other published results based on early running are:

FIG. 12. Aria: first coupling of the motor to the Seruci winze wheel, Summer 2016.

- "CALIS – a CALibration Insertion System for the DarkSide-50 dark matter search experiment" [15],
- "Effect of Low Electric Fields on Alpha Scintillation Light Yield in Liquid Argon" [16],
- "The Electronics and Data Acquisition System for the DarkSide-50 Veto Detectors" [17], and
- "The veto system of the DarkSide-50 experiment", [18]

Papers currently in preparation are:

- "Measurement of longitudinal diffusion in electron drift in liquid argon",
- "The DarkSide-50 WIMP search limits in models with various scattering operators",
- "The DarkSide-50 TPC electronics and data acquisition system",
- "The DarkSide GEANT-based Monte Carlo simulation",
- "Models for the pulse shape discrimination parameter f_{90}", and
- "The DarkSide-50 TPC event, S1, S2, energy, and position reconstruction".

Since the end of the data taking for the first paper with the UAr target, we have continued to take data with DarkSide-50. We have now acquired 520 day of UAr data. Fig. 14 shows our WIMP-search data history with UAr.The flat regions are primarily calibration campaigns, including runs with Am–Be and Am–^{13}C neutron sources deployed in the liquid scintillator veto (LSV) just outside the cryostat and ^{83}Kr dispersed into the recirculating argon flow. For the past 300 day, the live-time fraction was 88 %. The deadtime includes **all** losses, monthly PMT shutdowns (3.3 %), laser calibration runs (0.7 %) and DAQ deadtime. The running has been very stable (for example, it is typically not interrupted at all by lab-wide power outages) and this speaks well for the cryogenic, recirculation, and high voltage systems. The designs for these systems for DarkSide-20k are based on those in DarkSide-50.

With over a live-year of data already acquired, the DarkSide-50 group is preparing another WIMP search. This will be DarkSide's first blind analysis. All WIMP-search data since the 70-day sample has been blinded, with events in a region of the f_{90}-S1 plane that includes any reasonable WIMP-search window (and is

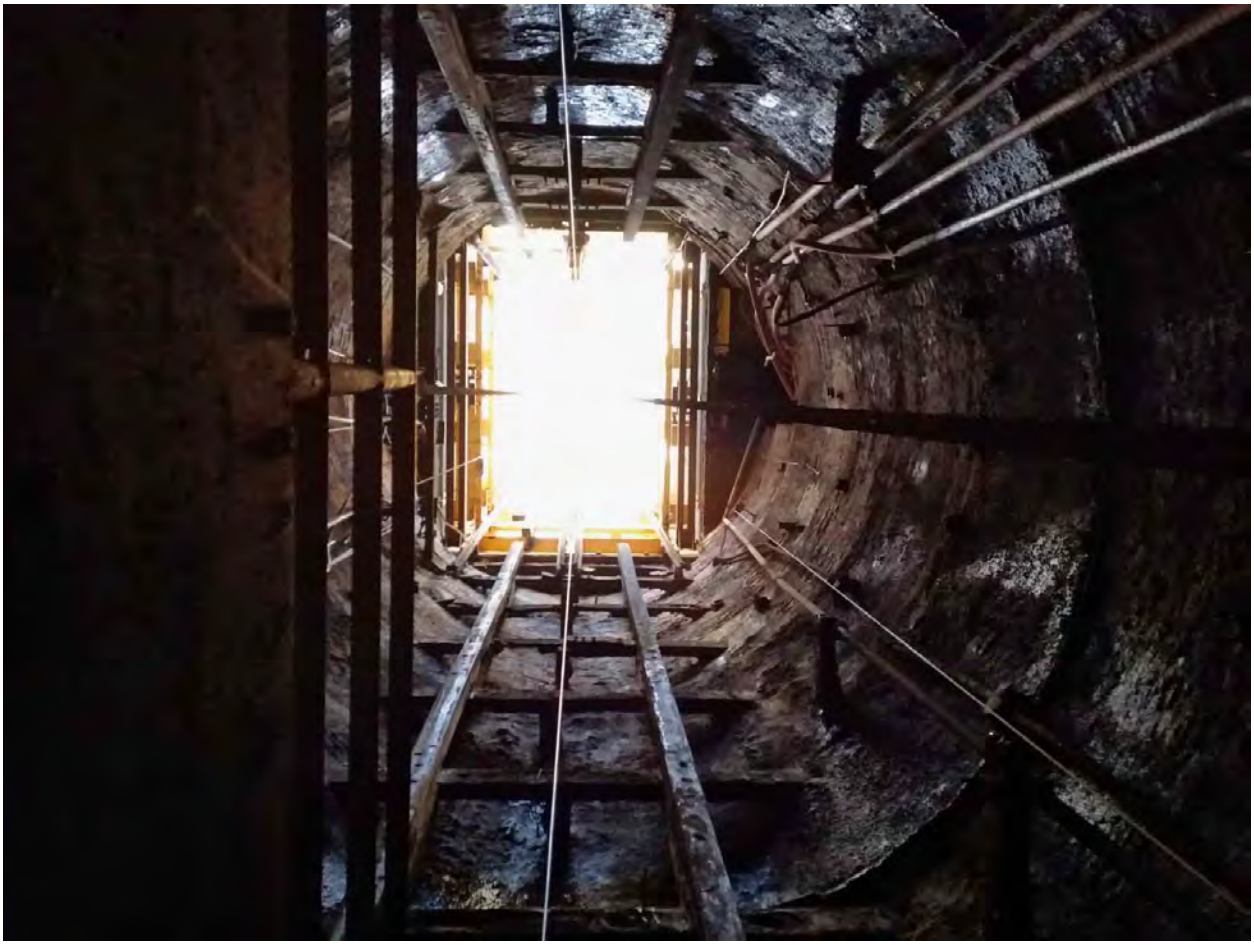

FIG. 13. Aria: sky-view from within the Seruci shaft.

considerably larger) hidden from analysers.

[1] M. Boulay, presentation at New Ideas in Dark Matter 2017 (2017).
[2] C. Aberle et al., JINST **6**, P11006 (2011).
[3] W. Beriguete et al., Nucl. Inst. Meth. A **763**, 82 (2014).
[4] B. R. Kim et al., Journal of the Korean Physical Society **66**, 768 (2015).
[5] A. Wright, P. Mosteiro, B. Loer, and F. P. Calaprice, Nucl. Inst. Meth. A **644**, 18 (2011).
[6] P. Agnes et al., Phys. Lett. B **743**, 456 (2015).
[7] P. Agnes et al., Phys. Rev. D **93**, 081101 (2016).
[8] C. Buck and M. Yeh, J. Phys. G: Nucl. Part. Phys. **43**, 093001 (2016).
[9] C. D. Bass et al., App. Radiat. Isot. **77**, 130 (2013).
[10] B. R. Kim et al., Phys. Scr. **90**, 055302 (2015).
[11] J. Ashenfelter et al., JINST **10**, P11004 (2015).
[12] G. Bentoumi et al., AECL Nuclear Review **1**, 57 (2012).
[13] Z. Chang et al., Nucl. Inst. Meth. A **769**, 112 (2015).
[14] C. Jackson, K. O'Neill, L. Wall, and B. McGarvey, Optical Engineering **53**, 081909 (2014).
[15] P. Agnes et al., arXiv:1611.02750v1 (2016).
[16] P. Agnes et al., JINST **12**, P01021 (2017).
[17] P. Agnes et al., arXiv:1606.03316v1 (2016).
[18] P. Agnes et al., JINST **11**, P03016 (2016).

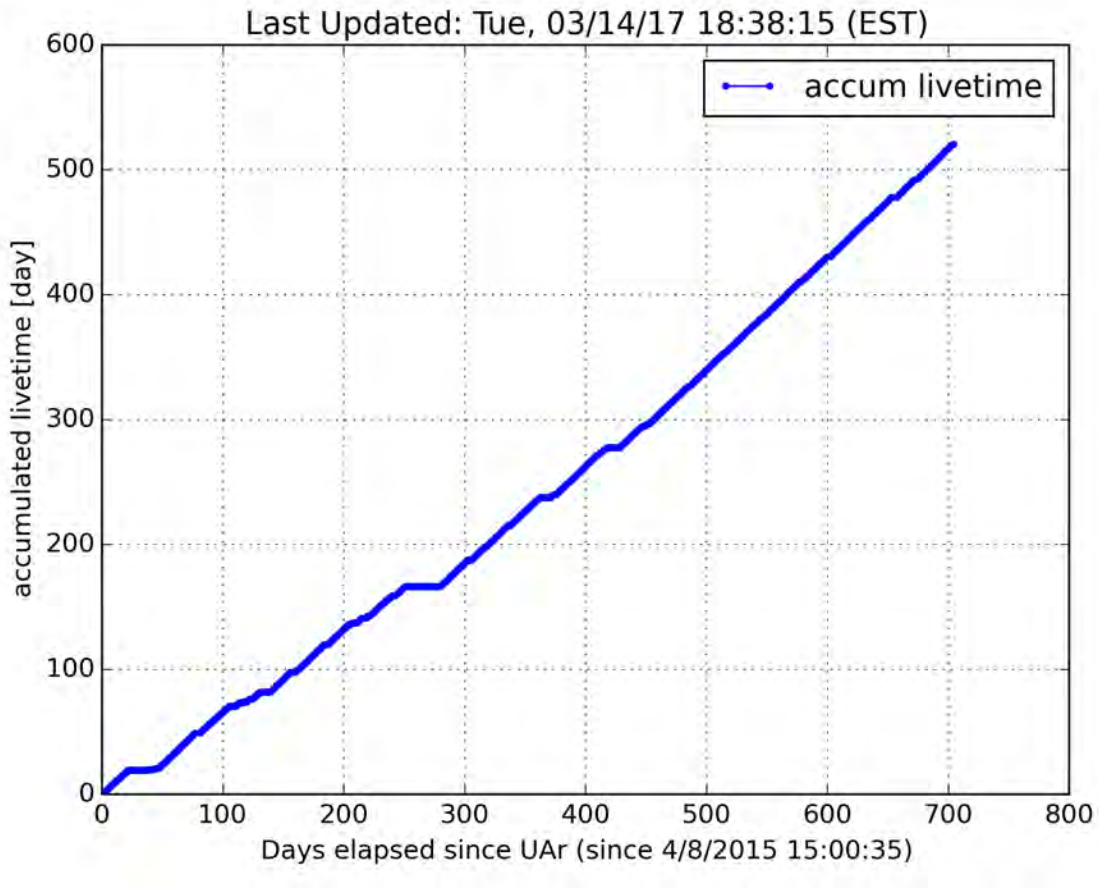

FIG. 14. DarkSide-50 : livetime history of the UAr run.

GERDA

M. Agostini [a], A.M. Bakalyarov [l], M. Balata [a], I. Barabanov [j], L. Baudis [r], C. Bauer [f], E. Bellotti [g,h], S. Belogurov [k,j], A. Bettini [o,p], L. Bezrukov [j], T. Bode [n], D. Borowicz [c,e], V. Brudanin [d], R. Brugnera [o,p], A. Caldwell [m], C. Cattadori [h], A. Chernogorov [k], V. D'Andrea [a], E.V. Demidova [k], N. Di Marco [a], A. Domula [c], E. Doroshkevich [j], V. Egorov [d], R. Falkenstein [q], N. Frodyma [b], A. Gangapshev [j,f], A. Garfagnini [o,p], C. Gooch [m], P. Grabmayr [q], V. Gurentsov [j], K. Gusev [e,m,o], C. Hahne [c], J. Hakenmüller [f], A. Hegai [q], M. Heisel [f], S. Hemmer [p], R. Hiller [r], W. Hofmann [f], P. Holl [m], M. Hult [e], L.V. Inzhechik [j], L. Ioannucci [a], J. Janicskó Csáthy [n], J. Jochum [q], M. Junker [a], V. Kazalov [j], Y. Kermaidic [f], T. Kihm [f], I.V. Kirpichnikov [k], A. Kirsch [f], A. Kish [r], A. Klimenko [f,d], R. Kneißl [m], K.T. Knöpfle [f], O. Kochetov [d], V.N. Kornoukhov [k,j], V.V. Kuzminov [j], M. Laubenstein [a], A. Lazzaro [n], V.I. Lebedev [l], H.Y. Liao [m], M. Lindner [f], I. Lippi [p], A. Lubashevskiy [f,d], B. Lubsandorzhiev [j], G. Lutter [e], C. Macolino [a], B. Majorovits [m], W. Maneschg [f], G. Marissens [e], M. Miloradovic [r], R. Mingazheva [r], M. Misiaszek [b], P. Moseev [j], I. Nemchenok [d], S. Nisi [a], K. Panas [b], L. Pandola [b], K. Pelczar [b], A. Pullia [i], C. Ransom [r], M. Reissfelder [f], S. Riboldi [i], N. Rumyantseva [d], C. Sada [o,p], F. Salamida [h], C. Schmitt [q], B. Schneider [c], S. Schönert [n], J. Schreiner [f], O. Schulz [m], A-K. Schütz [q], B. Schwingenheuer [f], H. Seitz [m], O. Selivanenko [j], E. Shevchik [d], M. Shirchenko [d], H. Simgen [f], A. Smolnikov [f,d], L. Stanco [p], L. Vanhoefer [m], A.A. Vasenko [k], A. Veresnikova [j], K. von Sturm [o,p], V. Wagner [f], A. Wegmann [f], T. Wester [c], C. Wiesinger [n], M. Wojcik [b], E. Yanovich [j], I. Zhitnikov [d], S.V. Zhukov [l], D. Zinatulina [d], A.J. Zsigmond [m], K. Zuber [c], and G. Zuzel [b].

[a] INFN Laboratori Nazionali del Gran Sasso and Gran Sasso Science Institute, Assergi, Italy
[s] INFN Laboratori Nazionali del Sud, Catania, Italy
[b] Institute of Physics, Jagiellonian University, Cracow, Poland
[c] Institut für Kern- und Teilchenphysik, Technische Universität Dresden, Dresden, Germany
[d] Joint Institute for Nuclear Research, Dubna, Russia
[e] Joint Institute for Nuclear Research, Dubna, Russia
[f] Max-Planck-Institut für Kernphysik, Heidelberg, Germany
[g] Dipartimento di Fisica, Università Milano Bicocca, Milano, Italy
[h] INFN Milano Bicocca, Milano, Italy
[i] Dipartimento di Fisica, Università degli Studi di Milano e INFN Milano, Milano, Italy
[j] Institute for Nuclear Research of the Russian Academy of Sciences, Moscow, Russia
[k] Institute for Theoretical and Experimental Physics, NRC "Kurchatov Institute", Moscow, Russia
[l] National Research Centre "Kurchatov Institute", Moscow, Russia
[m] Max-Planck-Institut für Physik, München, Germany
[n] Physik Department and Excellence Cluster Universe, Technische Universität München, Germany
[o] Dipartimento di Fisica e Astronomia dell'Università di Padova, Padova, Italy
[p] INFN Padova, Padova, Italy
[q] Physikalisches Institut, Eberhard Karls Universität Tübingen, Tübingen, Germany
[r] Physik Institut der Universität Zürich, Zürich, Switzerland

Spokesperson: B. Schwingenheuer (*B.Schwingenheuer@mpi-hd.mpg.de*)
Co-Spokesperson: S. Schönert (*Stefan.Schoenert@ph.tum.de*)

Physics coordinator:	L. Pandola	chair of collaboration board:	R. Brugnera
technical coordinator:	B. Majorovits	chairs of speakers bureau:	J. Jochum, K. Zuber
GLIMOS/RAE:	M. Balata	chair of editorial board:	P. Grabmayr

URL: `http://www.mpi-hd.mpg.de/gerda/`

Abstract

The GERmanium Detector Array (GERDA) at the Laboratori Nazionali del Gran Sasso of INFN, Italy, searches for neutrinoless double beta ($0\nu\beta\beta$) decay of ^{76}Ge. In December 2015, the second data taking phase started. The exposure of 10.8 kg·yr collected in the first five months was used to set a new limit on the half-life of $T^{0\nu}_{1/2} > 5.3 \cdot 10^{25}$ yr (90% C.L.) (sensitivity $4.0 \cdot 10^{25}$ yr). The background at $Q_{\beta\beta}$ is currently $0.6^{+0.6}_{-0.4} \cdot 10^{-3}$ cts/(keV·kg·yr) for BEGe detectors and $2.2^{+1.1}_{-0.8} \cdot 10^{-3}$ cts/(keV·kg·yr) for coaxial detectors (weighted average is $1.3 \cdot 10^{-3}$ cts/(keV·kg·yr)). Hence, the GERDA background goal for Phase II of 10^{-3} cts/(keV·kg·yr) has been achieved. This level is the lowest one in the field if weighted by the superior energy resolution. Up to the design exposure of GERDA (100 kg·yr) the expected background at the Q value of the decay is less than one in an energy window defined by the resolution. GERDA is hence background-free.

1 Introduction

Neutrinoless double beta decay is a process predicted by extensions of the Standard Model where a nucleus with A nucleons and Z protons decays like $(A, Z) \rightarrow (A, Z + 2) + 2e^-$. Here, lepton number is violated by 2 units. If observed it would be the rarest decay ever seen and would motivate that neutrinos are their own antiparticles (Majorana particle). Since the half-life will be beyond 10^{26} yr background reduction is most important for a discovery.

This process may be observable for nuclei like ^{76}Ge for which single beta decay is energetically forbidden but double beta decay with neutrino emission ($2\nu\beta\beta$) is allowed: $(A, Z) \rightarrow (A, Z+2)+2e^{-}+2\bar{\nu}$. In this case the neutrinos will carry a fraction of the available energy $Q_{\beta\beta}$ while for $0\nu\beta\beta$ decay the sum of the electron energies is exactly $Q_{\beta\beta}$. The latter is the prime experimental signature for a $0\nu\beta\beta$ signal which explains why a good energy resolution is needed for a discovery.

GERDA uses germanium detectors made out of material with a ^{76}Ge isotope fraction enriched from 7.8 % to about 87 %. The detectors are mounted in low mass holders and operated in 64 m^3 of liquid argon. Argon cools the detectors to their operating temperature and shields against external radioactivity. The cryostat is inside a tank filled with 590 m^3 pure water which also shields against external radiation and is instrumented with PMTs to detector Cherenkov light from muons traversing the experiment. A clean room on top is used for detector handling and mounting of the argon veto system and the detector array (see Fig. 1,a). Plastic panels on top of the clean room complete the muon veto.

In Phase II, seven coaxial detectors from the former Heidelberg-Moscow and IGEX experiments (15 kg total mass) and 30 newly produced BEGe detectors (20 kg) are mounted in six strings. A seventh string of three coaxial detectors from natural germanium completes the array. BEGe detectors exhibit a small p+ electrode which is beneficial for the energy resolution due to a smaller capacitance (see Fig. 1,b,c). This geometry also helps for the background reduction using the analysis of the time structure of the recorded signal (see below).

A cylindrical volume of 0.5 m diameter and 2.2 m height around the detector array is instrumented in Phase II to detect scintillation light from energy deposition of background events in the argon. The instrumentation consists of 16 PMTs at the end surfaces and a curtain of 810 wavelength shifting fibers readout out by 90 SiPM in the central 1 m cylindrical part (see Fig. 1,b).

GERDA Phase II started in December 2015. This report discusses the performance of the experiment and the first result on neutrinoless double beta decay.

2 Detector stability

All detector channels are digitized by Flash ADCs with 100 MHz sampling rate. An energy deposition of at least 100 keV in one germanium detector triggers the readout of the germanium and argon veto channels and all traces are stored on disk. Offline digital filters are used to find an optimal energy resolution. Peaks in ^{228}Th calibration data from γs with known energy are used to measure the resolution and to define the absolute energy scale.

The gain of the entire readout chain for the germanium detectors should be stable at the level better than 0.1 %. We monitor the stability by the injection of test charges at the input of the amplifier every 20 s and by ^{228}Th calibrations every 1-2 weeks. The latter gives the absolute energy calibration of the entire chain while the former allows to track changes of the electronics on a short time scale.

Fig. 2 shows the shifts of the 2615 keV peak in the calibration spectrum between consecutive calibrations. Typically the shift is less than 1 keV, i.e. smaller than 0.05%.

Fig. 3 shows for the combined BEGe and the combined coaxial detectors the energy resolutions (full width at half maximum, FWHM) of γ peaks at different energies E from the summed calibration spectrum. The points are fitted with the function $\sqrt{a + b \cdot E}$. Also shown are the measured resolutions in physics data from a fit to the ^{40}K peak at 1461 keV and the ^{42}K peak at 1525 keV (common FWHM for both peaks). For coaxial detectors the resolution is somewhat worse than expected from the calibration data.

All argon veto channels are working and the detection of single photo electrons is possible with simple algorithms. All channels are quite stable in gain. An event is vetoed if at least one hit is reconstructed with at least ≈0.5 p.e. amplitude and within a time window of 5 μs after the germanium detector energy deposition. With this definition about 2.3 % of the events are rejected due to a random coincidence between a germanium detector signal and the veto.

The muon veto has currently 60 of 66 PMTs operational. The loss rate is small considering the 8 years of operation and the efficiency of the veto to reject background events from muons remains well above 99 %.

Fig. 4 shows the leakage current of the germanium detectors during Phase II. During the first months, the current increased for some detectors during calibration runs and decreased afterwards, visible as spikes

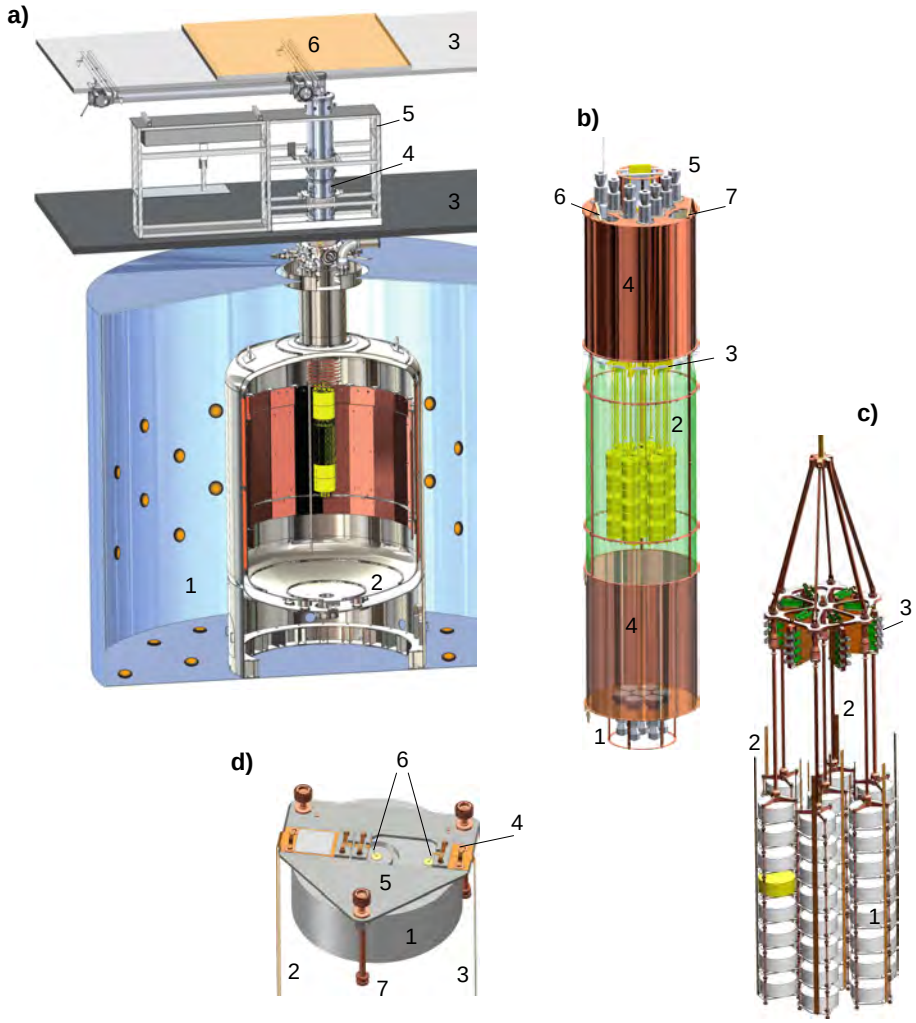

Figure 1: GERDA Phase II experimental setup.
a) overview: (1) water tank with muon veto system PMTs (590 m^3, diameter 10 m), (2) LAr cryostat (64 m^3, diameter 4 m), (3) floor & roof of clean room, (4) lock, (5) glove box, (6) plastic muon veto system;
b) LAr veto system: (1/5) bottom/top plate (diameter 49 cm) with 7/9 3" PMTs (R11065-10/20 MOD) with low radioactivity of U and Th (<2 mBq/PMT), (2) fiber curtain (height 90 cm) coated with wavelength shifter, (3) optical couplers and SiPMs, (4) thin-walled (0.1 mm) Cu cylinders (height 60 cm) covered with a Tyvek reflector on the inside, (6) calibration source entering slot in top plate, (7) slot for second of three calibration sources;
c) detector array: (1) Ge detectors arranged in 7 strings, (2) flexible bias and readout cables, (3) amplifiers;
d) detector module, view from bottom: (1) BEGe diode, (2/3) signal/high voltage cables attached by (4) bronze clamps to (5) silicon support plate, (6) bond wire connections from diode to signal and high voltage cable, (7) Cu support rods. Plot from Ref. [1].

in the plot. This problem is now no longer present. No detector shows a long term current increase.

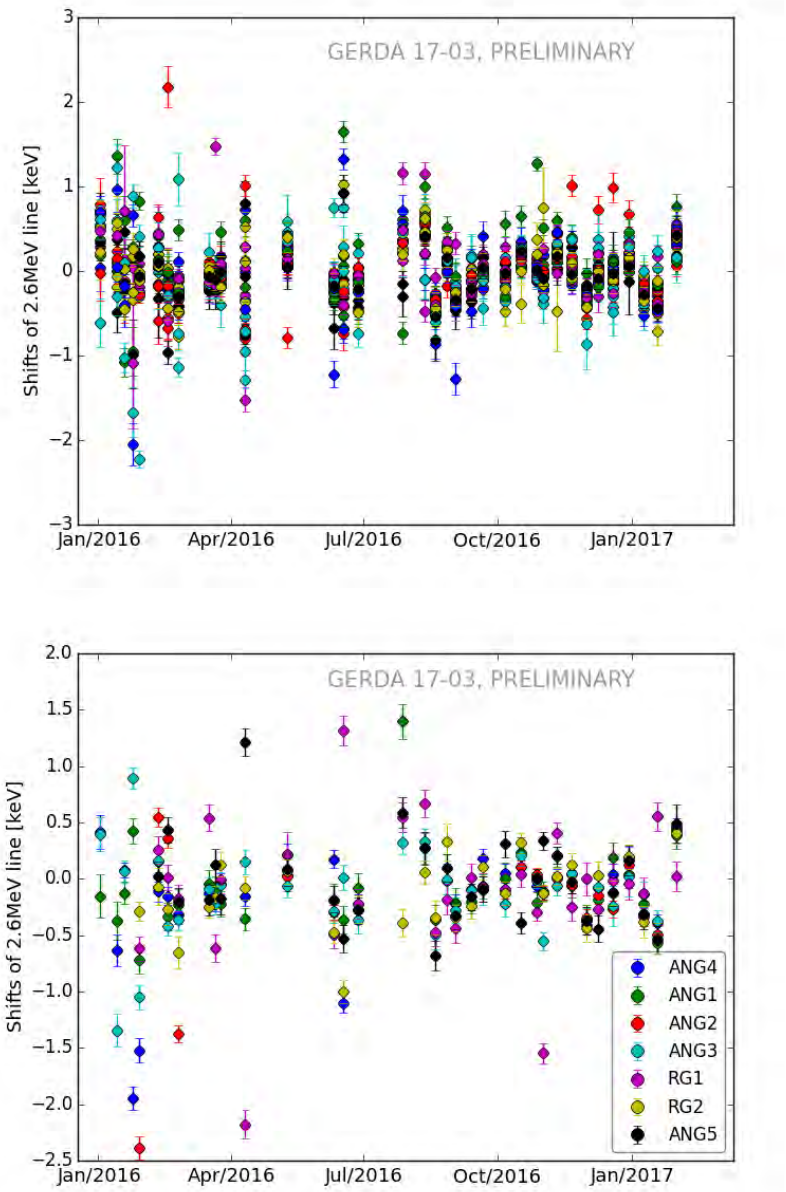

Figure 2: Shift of the 2615 keV peak of ^{208}Tl between consecutive calibrations for BEGe detectors (top) and coaxial detectors (bottom).

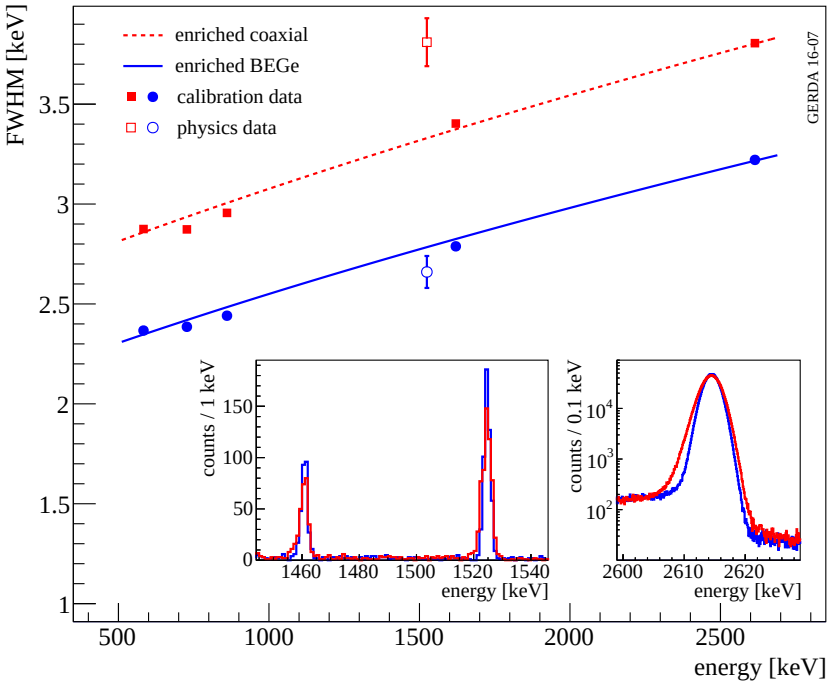

Figure 3: Energy resolution (FWHM) for γ lines of the calibration spectrum (filled symbols) and for the ^{40}K and ^{42}K lines from physics data (open symbols) for BEGe (symbols and solid line in blue) and coaxial (symbols and dashed line in red) detectors. The insets show the potassium lines and the 2615 keV calibration peak. Plot from Ref. [1].

3 Physics spectrum

In a first analysis step, an approximate energy is calculated for the germanium detectors. Events within 25 keV of $Q_{\beta\beta} = 2039$ keV are only stored in a restricted area. After the entire analysis chain is finalized and frozen, the box is opened, i.e. the blinded events are processed.

The two electrons leaving the germanium nucleus in neutrinoless double beta decay deposit their energy very localized in a detector (unless bremsstrahlung leads to a larger spread) and are therefore called single-site events. On the other hand, multiple Compton scatterings of MeV γs are separated by typically 1 cm (multi-site events). The time structures of the detector current signals are in general different for these two classes as well as for events on the detector surface. This fact can be used to discriminate background events. The analysis method can be developed and tested using double escape peak events of 2615 keV γs from the ^{228}Th calibration data and $2\nu\beta\beta$ events in physics data.

Fig. 5 shows for BEGe detectors for the physics data a simple one parameter pulse shape variable versus the energy. Events marked in red around $\zeta = 0$ are signal-like and accepted. Remarkable is that all events above 3 MeV coming from α decays on the detector surface are readily identified. Events around $Q_{\beta\beta}$ are blinded as marked by the grey band.

Fig. 6 shows the physics spectra for coaxial and BEGe detectors before argon veto and pulse shape discrimination (PSD) as well as with these selection cuts. The lower panel includes some labels for the different background contributions. Note: the ^{40}K line at 1461 keV is from an electron capture process. Hence no energy is deposited in the argon and and only random coincidences with the veto are removed (see inset in lower panel). On the other hand ^{42}K is a beta decay which deposits up to 2 MeV in the argon. Therefore this line is reduced by a factor of 5 by the argon veto. Pulse shape discrimination (applied to events above 1 MeV) removes surface events (above 3 MeV) and multi-site events like the two γ lines.

The background in the energy window 1930 - 2190 keV is evaluated next. For the coaxial detec-

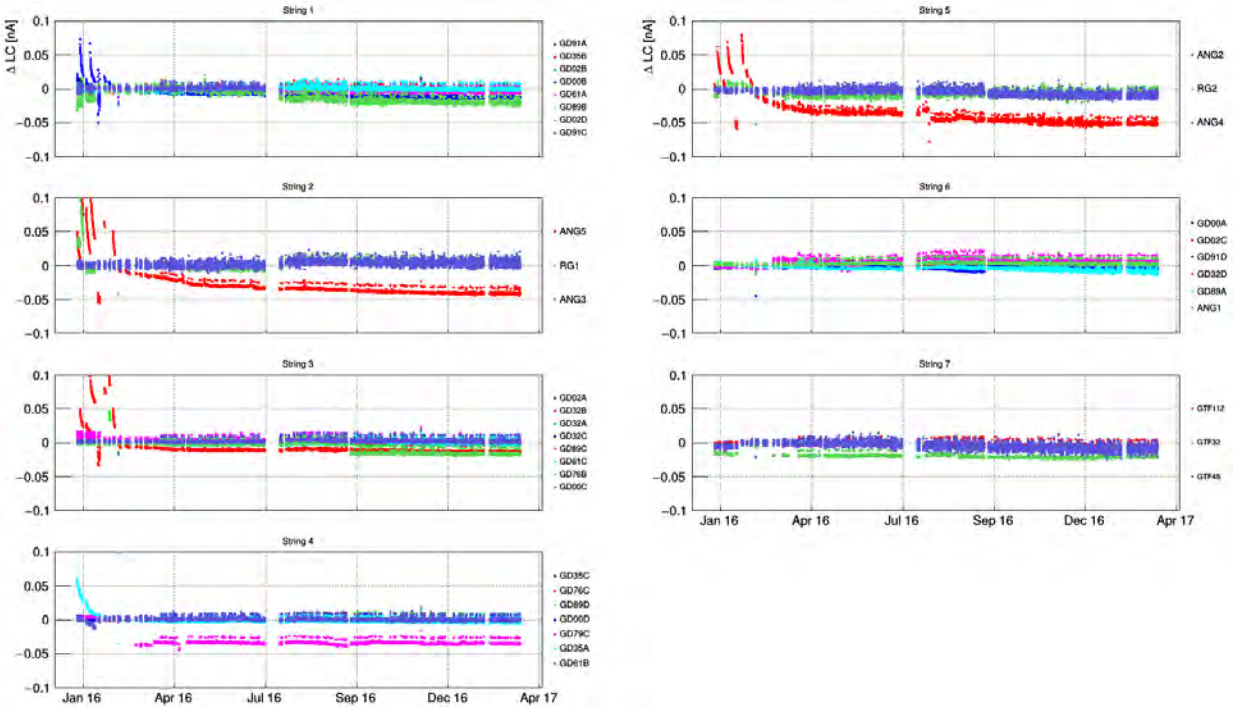

Figure 4: Change of leakage current during Phase II for all detectors used in the physics analysis.

tors presently the background index (BI) is $2.2^{+1.1}_{-0.8} \cdot 10^{-3}$ cts/(keV·kg·yr) and for BEGes it is $0.6^{+0.6}_{-0.4} \cdot 10^{-3}$ cts/(keV·kg·yr). The exposure weighted average is $1.3 \cdot 10^{-3}$ cts/(keV·kg·yr). Consequently, GERDA has reached its ambitious background goal of 10^{-3} cts/(keV·kg·yr). This level is an order of magnitude lower than for competing experiments if the energy resolution and efficiency is taken into account (BI·FWHM/ϵ).

A first data set of 10.8 kg·yr has been unblinded in June 2016. Combined with Phase I data no $0\nu\beta\beta$ decay signal is found and a limit of

$$T^{0\nu}_{1/2} > 5.3 \cdot 10^{25}\,\text{yr}\,(90\%\text{C.L.}) \tag{1}$$

is extracted for ^{76}Ge using a frequentist analysis. The median sensitivity is $4.0 \cdot 10^{25}$ yr which is only moderately worse than the latest Kamland-Zen sensitivity for ^{136}Xe of $5.6 \cdot 10^{25}$ yr despite their tenfold exposure.

GERDA will continue data taking until the design exposure of about 100 kg·yr is reached. Until then the average background is less than 1 in an energy window of 1·FWHM around $Q_{\beta\beta}$. GERDA is therefore the first background-free experiment in this field of research.

4 Further analyses

Muon flux modulation

The muon veto data taken between November 2010 and July 2013 were analyzed for coincidences of muon events with the CNGS beam and for annual modulations of the flux.

The GPS time stamp of our events allow us to correlate to the 10.5 μs wide beam structure of the CNGS beam. The random coincidences with cosmic muons is about 0.025 %, i.e. all muons detected in the time window of the beam are originating from muon neutrinos of the CERN beam. The flux is (4.41 ± 0.16) muons per 10^{16} protons on target which corresponds to about 2 % of the muons observed in GERDA.

Density fluctuations in the atmosphere due to temperature changes between summer and winter result in different energy distributions of pions and kaon when they decay to muons. Thus the muon

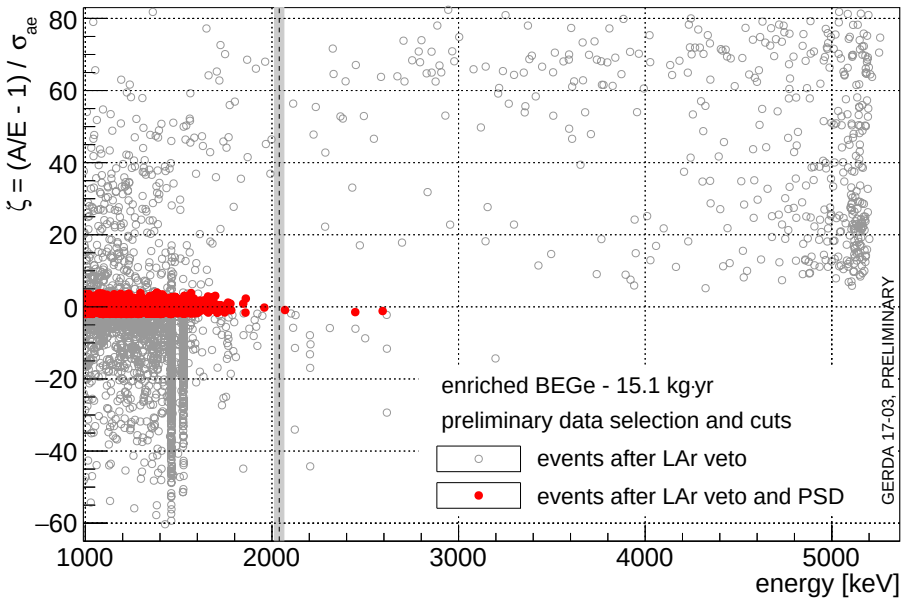

Figure 5: For BEGe detectors: Pulse shape parameter ζ versus energy for physics data. Red circles indicate events passing the pulse shape discrimination. Events above 3 MeV are almost exclusively α decays on the detector p+ electrode.

spectrum and therefore the rate measured underground shows seasonal variations of $(1.4 \pm 0.1)\%$ with an average value of $(3.477 \pm 0.0067) \cdot 10^{-4}/(\mathrm{s \cdot m^2})$. These numbers agree well with previous measurements at LNGS. We confirm a strong dependence of the modulation with the variation of the effective atmospheric temperature. Combining experimental data from other laboratories with different shielding depth an atmospheric kaon to pion fraction of 0.10 ± 0.03 is extracted [4].

Uranium and Thorium in HPGe detectors

The decay chains of ^{235}U, ^{238}U and ^{232}Th each contain a characteristic sequence of α and β decays. We searched for event sequences consistent with sub-chains of 3-4 decays for each of the isotopes and found no candidate in our Phase I data. As a consequence we can place stringent upper limits in order of few nBq/kg. These limits are low enough to ensure that internal U/Th contamination of HPGe crystal will not be a relevant source of background even for ton scale $0\nu\beta\beta$ decay experiments [2].

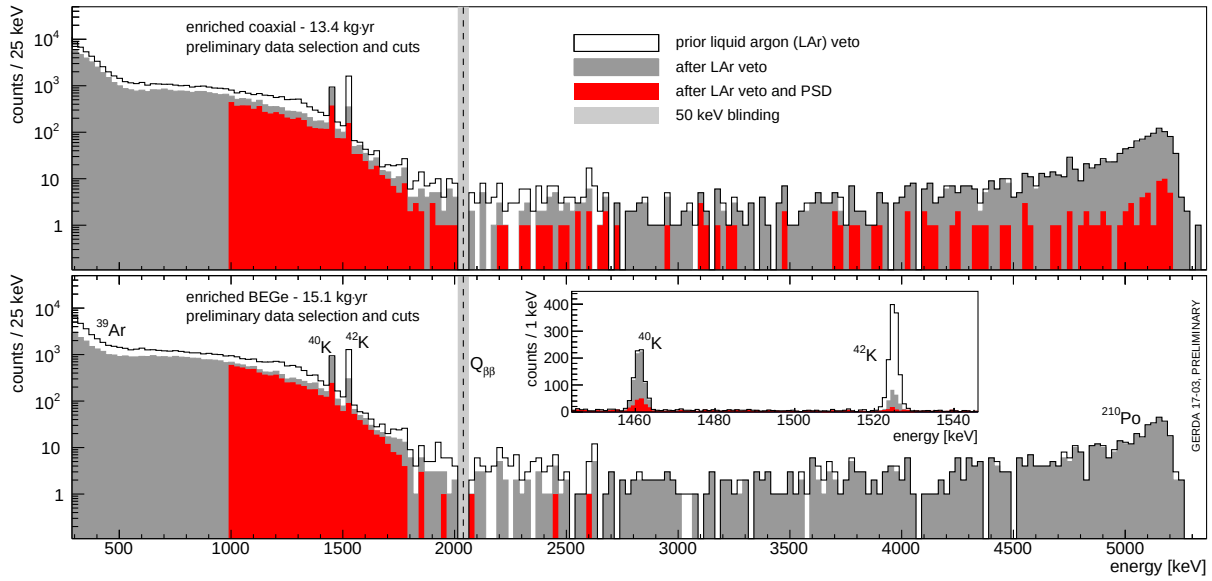

Figure 6: Phase II spectra for coaxial detectors (top) and BEGe detectors (bottom) without liquid argon veto and pulse shape discrimination (open histogram), after veto (grey histogram) and after all cuts (red histogram). The insert shows the BEGe spectrum around the two potassium lines.

List of Publications

[1] *Background-free search for neutrinoless double-β decay of ^{76}Ge with* GERDA, GERDA-collaboration, M. Agostini *et al.*, Nature 544 (2017) 47.

[2] *Limits on uranium and thorium bulk content in* GERDA *Phase I detectors*, GERDA-collaboration, M. Agostini *et al.*, Astroparticle Physics 91 (2017) 15.

[3] *Resistor-less charge sensitive amplifier for semiconductor detectors*, K. Pelczar, K. Panas, and G. Zuzel, Nucl. Instr. Methods A 835 (2016) 142.

[4] *Flux modulations seen by the muon veto of the* GERDA *experiment*, GERDA-collaboration, M. Agostini *et al.*, Astroparticle Physics 84 (2016) 29.

[5] *Search of Neutrinoless Double Beta Decay with the* GERDA *Experiment*, GERDA-collaboration, M. Agostini *et al.*, Nucl. Part. Physics Procs. 273 – 275 (2016) 1876.

[6] *The performance of the Muon Veto of the* GERDA *experiment*, K. Freund, R. Falkenstein, P. Grabmayr, A. Hegai, J. Jochum, M. Knapp, B. Lubsandorzhiev, F. Ritter, C. Schmitt, A.-K. Schütz, I. Jitnikov, E. Shevchik, M. Shirchenko, D. Zinatulina, Eur. Physis J. C 76 (2016) 298.

[7] *Optimized digital filtering techniques for radiation detection with HPGe detectors*, Marco Salathe and Thomas Kihm, Nucl. Instr. Methods A 808 (2016) 150.

LUNA

M. Aliotta[a], D. Bemmerer[b], A. Best[c], A. Boeltzig[d], C. Broggini[e], C. Bruno[a], A. Caciolli[f], F. Cavanna[g], G. F. Ciani[d], P. Corvisiero[g], T. Davinson[a], R. Depalo[f], G. D'Erasmo[h], A. Di Leva[c], L. di Paolo[i], Z. Elekes[j], F. Ferraro[k], E. M. Fiore[h], A. Formicola[i], Zs. Fülöp[j], G. Gervino[l], A. Guglielmetti[m], C. Gustavino[n], Gy. Gyürky[j], G. Imbriani[c], M. Lugaro[o], P. Marigo[f], V. Mossa[h], M. Junker[i], I. Kochanek[i], R. Menegazzo[e], F. R. Pantaleo[h], V. Paticchio[h], R. Perrino[p], D. Piatti[f], P. Prati[k], L. Schiavulli[h], O. Straniero[q], T. Szücs[j], M. P. Takács[b], D. Trezzi[m], A. Valentini[h], S. Zavatarelli[g]
Spokesperson: P. Prati

[a]University of Edinburgh, Edinburgh, United Kingdom
[b]Helmholtz-Zentrum Dresden-Rossendorf, Dresden, Germany
[c]Università degli Studi di Napoli "Federico II", and INFN, Napoli, Italy
[d]Gran Sasso Science Institute (GSSI), L'Aquila, Italy
[e]INFN, Padova, Italy
[f]Università degli Studi di Padova and INFN, Padova, Italy
[g]INFN, Genova, Italy
[h]Università degli Studi di Bari and INFN, Bari, Italy
[i]INFN, Laboratori Nazionali del Gran Sasso (LNGS), Assergi (AQ), Italy
[j]Institute for Nuclear Research (MTA ATOMKI), Debrecen, Hungary
[k]Università degli Studi di Genova and INFN, Genova, Italy
[l]Università degli Studi di Torino and INFN, Torino, Italy
[m]Università degli Studi di Milano and INFN, Milano, Italy
[n]INFN, Roma, Italy
[o]Monarch University Budapest, Budapest, Hungary
[p]INFN, Lecce, Italy
[q]Osservatorio Astronomico di Collurania, Teramo, and INFN Napoli, Italy

Abstract

Aim of the LUNA experiment is the direct measurement of the cross section of nuclear reactions relevant for stellar and primordial nucleosynthesis. The year 2016 was dedicated to the measurement of the ^{22}Ne(p,γ)^{23}Na, ^{22}Ne(α,γ)^{26}Mg, ^{2}H(p,γ)^{3}He, ^{23}Na(p,γ)^{24}Mg and ^{18}O(p,γ)^{19}F reactions. Data analysis on ^{17}O(p,α)^{14}N and ^{18}O(p,α)^{15}N was completed as well. The ^{22}Ne(p,γ)^{23}Na, ^{22}Ne(α,γ)^{26}Mg and ^{2}H(p,γ)^{3}He reactions were studied by a windowless gas target suited to fit into a 4π segmented BGO crystal. A solid target setup, exploiting again a high efficiency BGO detector was used for the ^{23}Na(p,γ)^{24}Mg and ^{18}O(p,γ)^{19}F experiments. The LUNA MV project was pursued in parallel to the LUNA activities and new progresses were obtained.

1 The ^{17}O$(p,\alpha)^{14}$N reaction

The ^{17}O$(p,\alpha)^{14}$N reaction (Q_{val}=1.2 MeV) plays a key role in several astrophysical scenarios, and in AGB stars in particular. We employed a purpose-built setup [1] to measure the strength of the $E_p = 70$ keV resonance that dominates the reaction rates at temperatures of astrophysical interest ($T = 10 - 100$ MK). We determined [2] a strength of this $E_p = 70$ keV resonance that is twice as high as previously reported. Our result has dramatic effects in a number of astrophysical scenarios [3] and potentially solves a long-standing issue in the identification of some pre-solar grains [4] produced in massive AGB stars.

2 The ^{18}O$(p,\alpha)^{15}$N reaction

The ^{18}O$(p,\alpha)^{15}$N reaction (Q_{val}=3.98 MeV) plays a role in Giant Branch Stars where it influences the abundance of the rare ^{18}O isotope. Our investigation was carried out employing the same purpose-built setup commissioned for the ^{17}O$(p,\alpha)^{14}$N campaign [1]. We measured the excitation function of the ^{18}O$(p,\alpha)^{15}$N reaction from E_p=360 keV to E_p=60 keV, the lowest energy achieved to date corresponding to a cross-section of the order of the picobarn. We employed the powerful R-matrix formalism [5] to perform a single fit to our data and to data acquired at higher energies (i.e. not accessible at the LUNA-400kV machine), using a small set of physically meaningful parameters. Thanks to the improved constraints to the cross-section, we were able to greatly reduce the uncertainty in the rate of the ^{18}O$(p,\alpha)^{15}$N reaction. A paper [6] on our results is currently in preparation.

3 The ^{23}Na(p,γ)^{24}Mg and ^{18}O(p,γ)^{19}F reactions

The data analysis for ^{18}O(p,γ)^{19}F and ^{23}Na(p,γ)^{24}Mg is ongoing for the data collected during the two experimental phases that used a high-efficiency BGO detector and a high-resolution HPGe detector.

Measurements of ^{18}O(p,γ)^{19}F were taken from 400 keV down to proton energies of 140 keV and 90 keV, respectively during the HPGe and BGO phase. Signals from ^{18}O(p,γ)^{19}F were observed down to the lowest energies for both setups. These measurements extend the energy range with direct cross section data previously available [7]. In addition, information about minor resonances in ^{18}O(p,γ)^{19}F at higher energies, can be obtained from the HPGe data. The BGO runs mainly focused on a resonance at 95 keV proton energy, whose strength has been disputed [8, 9]. Our results exclude one of the two claims. Data analysis is ongoing, focusing on a more precise determination of the higher-energy resonance gamma-branchings and a determination of the direct capture cross section using the combined BGO and HPGe data.

For ^{23}Na(p,γ)^{24}Mg, the HPGe phase of the experiment focused on the two stronger, astrophysical relevant resonances at proton energies of 251 keV and 309 keV. In addition, measurements of minor resonances were obtained in this phase of the experiment. Moreover, we have detected for the first time direct capture signals at about 400 keV, which is the highest energy available at LUNA. The BGO phase focused on the search for a resonance at 140 keV, which is expected to be weak, but potentially relevant for astrophysics [10]. The uncertainty of the HPGe data analysis depends strongly on knowledge of the target composition. The analysis of the two major resonances relies on stoichiometry information of selected targets from Elastic Recoil Detection Analysis (ERDA) performed at the Helmholtz Center Dresden-Rossendorf (HZDR), and the minor resonances are analyzed relative to the stronger resonances to account for effects of the target stoichiometry. The current focus in the search for the 140 keV resonance is set on a more precise characterization and subtraction of beam-induced backgrounds (^{11}B(p, γ)^{12}C and ^{7}Li(p, γ)^{8}Be), in order to increase the sensitivity and reduce the systematic uncertainty of the result.

4 The ^{2}H(p,γ)^{3}He reaction

Big Bang Nucleosynthesis (BBN) describes the production of light nuclei in the first minutes of cosmic time. It started with deuterium formation through the p(n,γ)^{2}H reaction, when the Universe was cold enough to allow ^{2}H nuclei to survive to photo-disintegration. The main source of uncertainty on standard BBN prediction for the deuterium abundance is actually due to the radiative capture process ^{2}H(p,γ)^{3}He that destroys deuterium, because of the poor knowledge of its S-factor at BBN energies. Moreover, the paucity of ^{2}H(p,γ)^{3}He data represents the main obstacle to improve the accuracy on the determination of the baryon density and to constrain of the density of relativistic species existing at BBN epoch (only photons and 3 families of neutrinos are foreseen in the standard model). A measurement of this reaction cross section with a 3% accuracy in the BBN energy range (30 keV $\lesssim$ E$_{cm}$ $\lesssim$ 300 keV) is thus desirable [11].

The ^{2}H(p,γ)^{3}He experiment at LUNA consists of two main phases characterized by different setups. The former is a windowless gas target filled with deuterium surrounded by a 4π BGO detector. The high efficiency ($\sim$ 70%) of the BGO detector reduces the dependence of the reaction yield on the angular distribution of the emitted γ rays and thus allows to achieve a low systematic uncertainty. During last year, the detection efficiency has been determined by precise Monte Carlo simulations, as well as by measurements with radioactive sources (^{60}Co, ^{137}Cs, ^{88}Y) and ^{14}N(p,γ)^{15}O resonant reaction. The study of systematic uncertainties included also the determination of the beam heating effect obtained by varying the target pressure and beam intensity. The beam intensity value and uncertainty was determined by a proper calibration of the calorimeter. The ^{2}H(p,γ)^{3}He excitation function has been measured in the energy range 30 keV $\lesssim$ E$_{cm}$ $\lesssim$ 200 keV. A sample spectrum is shown in figure 1.

In the last months of 2016, the second phase focusing on the 70 keV $\lesssim$ E$_{cm}$ $\lesssim$ 260 keV energy range started. The set up consists of a 137% HPGe detector in close geometry and a new target chamber. With this setup the angular distribution can be inferred by exploiting the high energy resolution of the detector and the Doppler effect that changes along the beam line the energy of the detected γ rays. This study provides an important experimental ground for theoretical nuclear physics. The year 2017 will be devoted to the data taking.

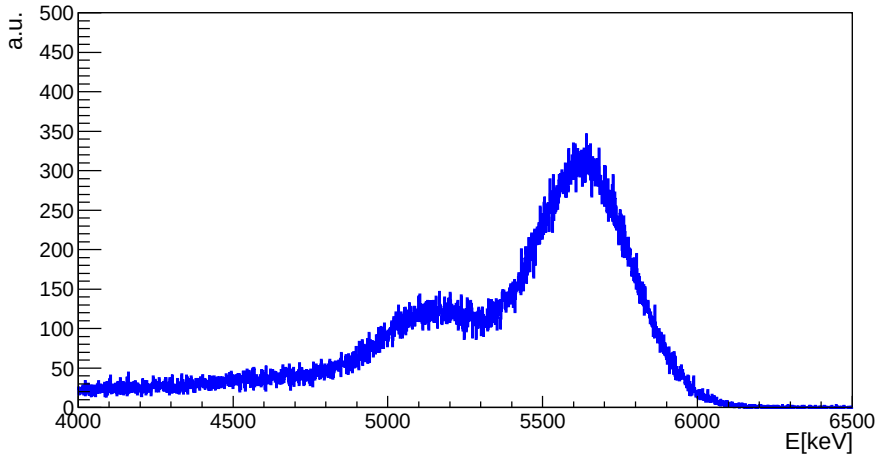

Figure 1: Zoom of a sample spectrum measured at $E_p = 100$ keV. The ^{2}H(p,γ)^{3}He peak is visible together with the first escape peak.

5 The ^{22}Ne(p,γ)^{23}Na reaction

The ^{22}Ne(p,γ)^{23}Na reaction is included in the hydrogen burning neon-sodium (NeNa) cycle. This cycle affects the nucleosynthesis of neon and sodium. It has repercussions on the surface composition of Red Giant Branch stars (Gamow peak 30-100 keV), on Asymptotic Giant Branch Star nucleosynthesis, on classical novae (Gamow peak 100-600 keV) [12], and possibly even on the simmering phase prior to the explosion of a type Ia supernova [13].

Before the LUNA study, the ^{22}Ne(p,γ)^{23}Na reaction rate was poorly known because of the contribution of a large number of resonances, many of which have never been observed directly [14, 15]. The literature data have recently been greatly improved by phase I of the LUNA ^{22}Ne(p,γ)^{23}Na experiment, using two heavily shielded HPGe detectors [20]. The resonance strengths of three resonances in ^{22}Ne(p,γ)^{23}Na were directly measured for the first time. The results of this experiment are reported in [21, 22] and their astrophysical impact in AGB stars is discussed in [23]. Very recently, an independent study by an American group working at the surface of the Earth has been published in 2017 [24], confirming the reaction rate reported by LUNA but showing some differences in details, presumably due to their much higher background.

After the successful conclusion of phase I, the contribution of two reported resonances at low energy, 71 and 105 keV, still dominates the reaction rate error at low temperatures $T_9 < 0.1$, even though already the phase I data significantly lowered the upper limits on the strengths of these resonances [22].

In phase II of the LUNA ^{22}Ne(p,γ)^{23}Na experiment, a high-efficiency setup, made of a 4π-BGO detector [26] surrounding the scattering chamber, is used to precisely study those two resonances and to study the direct capture contribution. The new setup reaches 60% detection efficiency for the γ-rays produced by the reaction. The data taking concluded in April 2016 and the data is currently under analysis. In Fig. 2 a typical spectrum acquired to study the direct capture component of the cross section.

The final results of this new experiment are expected for the end of 2017.

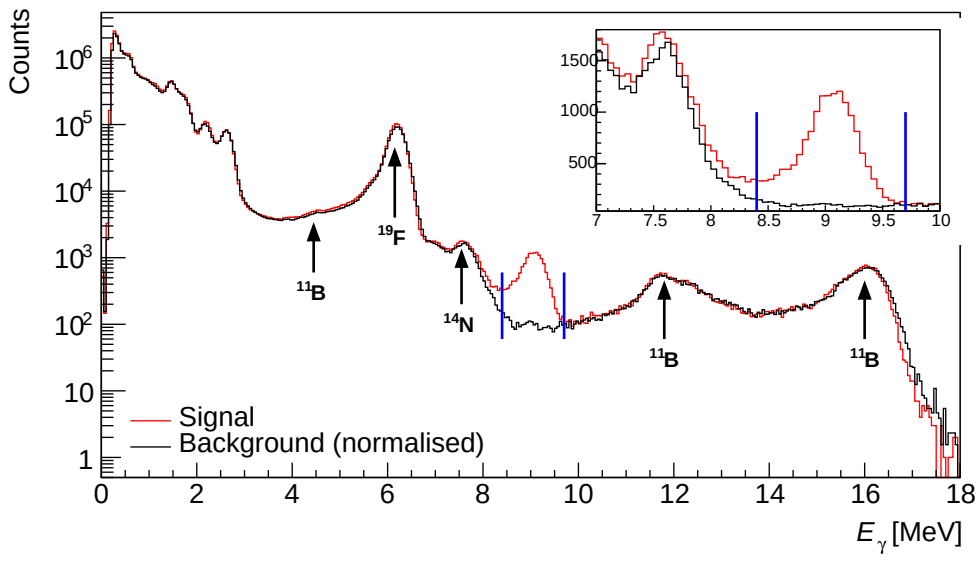

Figure 2: Experimental spectrum at $E_p = 250.0$ keV, to study the direct capture contribution in the ^{22}Ne(p,γ)^{23}Na reaction. The peak from the reaction under study is clearly apparent near 9.0 MeV, i.e. the Q-value plus the center-of-mass energy.

6 Study of the ^{22}Ne(α,γ)^{26}Mg reaction

The ^{22}Ne(α,γ)^{26}Mg reaction works as a competitor to the ^{22}Ne(α,n)^{25}Mg reaction, which is one of the two main neutron sources for the astrophysical s-process. Within the energy range of the LUNA 400kV accelerator, there is a possible resonance at $E_\alpha = 395$ keV. Existing upper limits are solely based on indirect data and range from $10^{-9} - 10^{-13}$ eV, reflecting great uncertainty [27, 14, 28, 29]. If the true strength is near the upper range of these limits, it would effectively shut down the ^{22}Ne(α,n)^{25}Mg reaction for a wide range of scenarios. If it is near the lower range of these limits, it would only negligibly affect the ^{22}Ne(α,n)^{25}Mg neutron source.

Using an enriched ^{22}Ne gas target and the experimental setup from the ^{22}Ne(p,γ)^{23}Na experiment with the 4π BGO detector, an attempt has been made to observe or disprove the existence of such a resonance. The data taking has been performed in summer 2016. 18 days of statistics has been acquired running the beam on neon gas and an equivalent time for offline background.

The preliminary analysis of this first beam time shows that the sensitivity of the present setup is in the range of 10^{-10} eV. Comparing the spectra obtained with neon-22 gas and the environmental background, a small but not significant excess has been observed in the data. This excess suggests further study, which is tentatively foreseen for 2018.

A new setup including borated polyethylene shielding to suppress ambient neutrons is under study, hoping to improve the sensitivity of the experimental setup.

7 LUNA MV

The LUNA MV accelerator will provide intense beams of H^+, $^4H^+$, $^{12}C^+$ e $^{12}C^{++}$ in the energy range: 350 keV - 3.5 MeV. The procedure related to the accelerator supply is under the responsibility of the RUP (Responsible of the Procedure), G. Imbriani (University and INFN Neaples) while the designer and DEC (Executive Work Director) is M. Junker (INFN-LNGS). Delivery

at LNGS is presently scheduled for July 2018. A six months commissioning phase is scheduled thereafter so that the first physics experiments are envisaged at beginning 2019. The provider, HVEE, has submitted on September 26th, 2016 the first set of technical drawings which is now under evaluation at the DEC office.

Since spring 2016, a working group composed by several member of the LNGS technical and administrative divisions started an intense and very productive work finalized to the design and construction of the new LUNA-MV laboratory inside Hall B. A group member, L. Di Paolo, has been hired at June 2016 specifically for this task and he's acting as coordinator of the several professionals involved in the projects. A synthetic view of the new LUNA-MV facility is given in Figure 3. The working plane foresees the clearance of the LUNA-MV area in Hall B in late spring/summer 2017, the beginning of the construction works in September 2017 and the delivering of the full equipped LUNA-MV laboratory (accelerator room and technical building) by march 2018. The main steps in the project development during 2016 are listed below

- The executive design of the new LUNA shielded building in Hall B has been received and approved: the tender for the underground works has been opened (technical and economical offers must arrive within end of March 2017) and the contract with the selected firm will be signed in June-July 2017.
- The tender for the executive design of all the plants to be installed in the shielded building and in the underground control room has been closed. The following tender for plants delivering and deployment should be opened within June 2017.
- The request of authorization to install and use the new LUNA-MV accelerator ("Nulla Osta") has been finalized by the Radioprotection Officer, F. Bartolucci, and sent to the Regional Authority ("Prefettura dellAquila"). The whole procedure is expected to be completed in six-twelve months from the submission.
- The tender for the construction of the LUNA-MV control room, the last item to complete the underground infrastructure, will be opened by July 2017.

In summary: the project schedule is presently respected.

A full proposal (available on the LUNA web site https://luna.lngs.infn.it/) for the first five years of activity at LUNA-MV has been approved by the LUNA Collaboration in July 2016 and submitted both to LNGS and to INFN-CSN3. In particular, we decided to start by measuring over a much wider energy region the cross section of a reaction we already studied with the 400 kV accelerator: ^{14}N(p,γ)^{15}O. This way we will perform the tuning of LUNA MV and we will more precisely extrapolate the reaction cross section within the Gamow peak of the Sun, i.e. the burning energy region. Then, we will focus the activity of one of the two beam lines on the study of ^{12}C+^{12}C: the understanding of its cross section at low energy will be the main goal of the first 5 years of LUNA MV. Alternating in time with ^{12}C+^{12}C, the study of ^{13}C(α,n)^{16}O will be performed on the other beam line (the accelerator can feed only one line at a time). Finally, ^{22}Ne(α,n)^{25}Mg will be the last reaction covered by this scientific plan. On the other hand, ^{12}C(α,γ)^{16}O will be the main goal of the second scientific plan at LUNA MV, starting in the year 2023.

The final version of a MoU to manage both LUNA-MV and LUNA400 has been approved by all the LUNA Institutions and is ready to be sent official signatures.

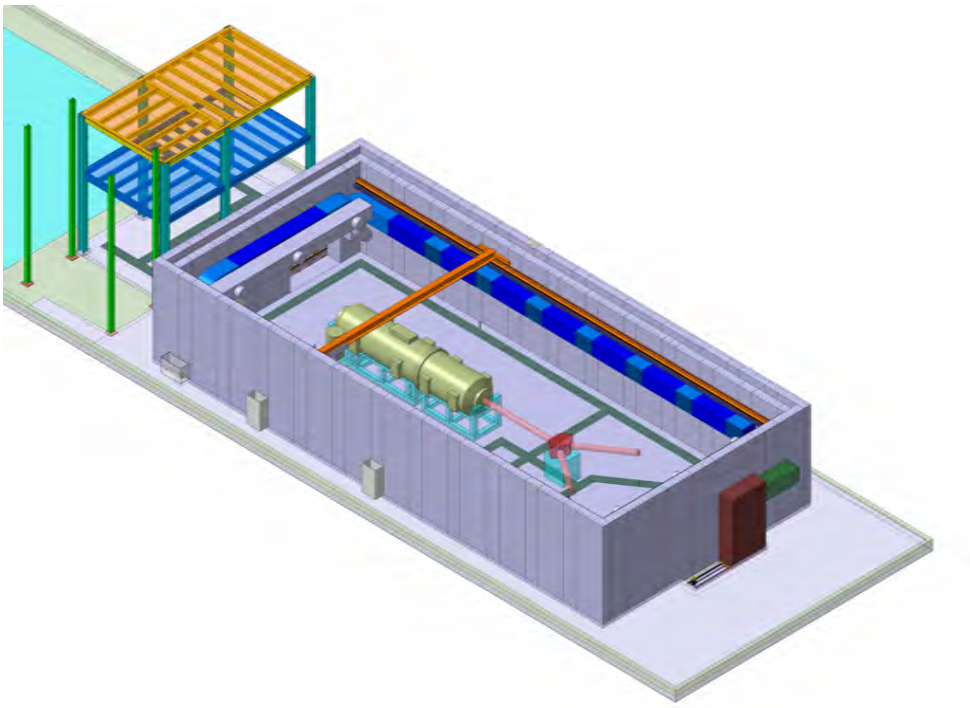

Figure 3: Rendering of the LUNA-MV experimental hall. The accelerator and the two beam lines are visible.

References

[1] C.G. Bruno *et al.*, Eur. Phys. J. A **51** (2015) 94

[2] C.G. Bruno *et al.*, Phys. Rev. Lett. **117** (2016) 142502

[3] O. Straniero *et al.*, A&A **598** (2017) A128

[4] M. Lugaro *et al.*, Nat. Astron. **1** (2017) 0027

[5] P. Descouvemont and D. Baye, Rep. Prog. Phys. **73** (2010) 036301

[6] C.G. Bruno *et al.*, *in preparation*

[7] C. Rolfs et al., Nucl. Phys. A349 (1980) 165-216

[8] M. Q. Buckner et al., Phys. Rev. C 86, 065804 (2012)

[9] H. T. Fortune et al., Phys. Rev. C 88, 015801 (2013)

[10] J. M. Cesaratto et al., Phys. Rev. C 88, 065806 (2013)

[11] E. Di Valentino *et al.*, Phys. Rev. D **90** (2014) 023543

[12] C. Iliadis, A. Champagne, J. José, S. Starrfield, and P. Tupper, Astrophys. J. Suppl. Ser. **142**, 105 (2002).

[13] D. A. Chamulak, E. F. Brown, F. X. Timmes, and K. Dupczak, Astrophys. J. **677**, 160 (2008), 0801.1643.

[14] C. Angulo *et al.*, Nucl. Phys. A **656**, 3 (1999).

[15] C. Iliadis, R. Longland, A. E. Champagne, and A. Coc, Nucl. Phys. A **841**, 251 (2010).

[16] R. B. Firestone, Nucl. Data Sheets **108**, 1 (2007).

[17] R. Longland *et al.*, Phys. Rev. C **81**, 055804 (2010).

[18] J. Görres, C. Rolfs, P. Schmalbrock, H. P. Trautvetter, and J. Keinonen, Nucl. Phys. A **385**, 57 (1982).

[19] J. Görres *et al.*, Nucl. Phys. A **408**, 372 (1983).

[20] F. Cavanna *et al.*, Eur. Phys. J. A **50**, 179 (2014), 1411.2888.

[21] F. Cavanna *et al.*, Phys. Rev. Lett. **115** (2015), 252501.

[22] R. Depalo *et al.*, Phys. Rev. C **94** (2016), 055804.

[23] A. Slemer *et al.*, MNRAS **465** (2017), 4817-4837.

[24] K. J. Kelly *et al.*, Phys. Rev. C **95** (2017), 015806.

[25] A. L. Sallaska *et al.* Astrophys. J. Supp. **207** (2013) 18.

[26] C. Casella *et al.*, Nucl. Inst. Meth. A **489**, 160 (2002).

[27] U. Giesen *et al.*, Nucl. Phys. A **561** (1993) 95.

[28] C. Iliadis *et al.*, Nucl. Phys. A **841** (2010) 251.

[29] R. Longland *et al.*, Phys. Rev. C **85**, 065809 (2012).

8 List of Publications

1. *Neon and Sodium ejecta from intermediate mass stars: The impact of the new LUNA rate for the $^{22}Ne(p,\gamma)^{23}Na$*
   A. Slemer, P. Marigo, D. Piatti, M. Aliotta, D. Bemmerer, A. Best, A. Boeltzig, A. Bressan, C. Broggini, C.G. Bruno, A. Caciolli, F. Cavanna, P. Corvisiero, T. Davinson, R. Depalo, A. Di Leva, Z. Elekes, F. Ferraro, A. Formicola, Zs. Flp, G. Gervino, A. Guglielmetti, C. Gustavino, Gy. Gyürky, G. Imbriani, M. Junker, R. Menegazzo, V. Mossa, F. R. Pantaleo, P. Prati, O. Straniero, T. Szücs, M. P. Takács, D. Trezzi (LUNA Collaboration)
   Monthly Notices of the Royal Astronomical Society 465 (2016) 4817

2. *Direct measurement of the low-energy $^{22}Ne(p,\gamma)^{23}Na$ resonances*
   R. Depalo, F. Cavanna, M. Aliotta, M. Anders, D. Bemmerer, A. Best, A. Boeltzig, C. Broggini, C.G. Bruno, A. Caciolli, G.F. Ciani, P. Corvisiero, T. Davinson, A. Di Leva, Z. Elekes, F. Ferraro, A. Formicola, Zs. Flp, G. Gervino, A. Guglielmetti, C. Gustavino, Gy. Gyürky, G. Imbriani, M. Junker, R. Menegazzo, V. Mossa, F. R. Pantaleo, D. Piatti, P. Prati, O. Straniero, F. Strieder, T. Szücs, M. P. Takács, D. Trezzi (LUNA Collaboration)
   Physical Review C 94 (2016) 055804

3. *Improved Direct Measurement of the 64.5 keV Resonance in the $^{17}O(p,\alpha)^{14}N$ Reaction at LUNA*
   C.G. Bruno, D.A. Scott, M. Aliotta, A. Formicola, D. Bemmerer, A. Best, A. Boeltzig, C. Broggini, A. Caciolli, F. Cavanna, G.F. Ciani, P. Corvisiero, T. Davinson, R. Depalo, A. Di Leva, Z. Elekes, F. Ferraro, Zs. Flp, G. Gervino, A. Guglielmetti, C. Gustavino, Gy. Gyürky, G. Imbriani, M. Junker, R. Menegazzo, V. Mossa, F. R. Pantaleo, D. Piatti, P. Prati, E. Somorjai, O. Straniero, F. Strieder, T. Szücs, M. P. Takács, D. Trezzi (LUNA Collaboration)
   Physical Review Letters 117 (2016) 142502

4. *Ultra-sensitive gamma-ray spectroscopy set-up for investigating primordial lithium problem*
   G. Gervino, C. Gustavino, D. Trezzi, M. Aliotta, M. Anders, A. Boeltzig, D. Bemmerer, A. Best, C. Broggini, C. Bruno, A. Caciolli, F. Cavanna, P. Corvisiero, T. Davinson, R. Depalo, A. Di Leva, Z. Elekes, F. Ferraro, A. Formicola, Zs. Fülöp, A. Guglielmetti, Gy. Gyürky, G. Imbriani, M. Junker, R. Menegazzo, P. Prati, D.A. Scott, O. Straniero, T. Szücs, (LUNA Collaboration)
   Nuclear Instruments and Methods in Physics Research Section A, 824 (2016) 617

5. *Underground nuclear astrophysics: Why and how*
   A. Best, A. Caciolli, Zs. Fülöp, Gy. Gyürky, M. Laubenstein, E. Napolitani, V. Rigato, V. Roca, and T. Szücs
   European Physical Journal - Topical Issue 52 (2016) 72

6. *The nuclear physics of the hydrogen burning in the Sun*
   A. Formicola, P. Corvisiero, and G. Gervino
   European Physical Journal - Topical Issue 52 (2016) 73

7. *Primordial nucleosynthesis*
   C. Gustavino, M. Anders, D. Bemmerer, Z. Elekes and D. Trezzi
   European Physical Journal - Topical Issue 52 (2016) 74

8. *Shell and explosive hydrogen burning - Nuclear reaction rates for hydrogen burning in RGB, AGB and Novae*
   A. Boeltzig, C.G. Bruno, F. Cavanna, S. Cristallo, T. Davinson, R. Depalo, R.J. de Boer, A. Di Leva, F. Ferraro, G. Imbriani, P. Marigo, F. Terrasi, and M. Wiescher
   European Physical Journal - Topical Issue 52 (2016) 75

9. *Helium burning and neutron sources in the stars*
   M. Aliotta, M. Junker, P. Prati, and F. Strieder
   European Physical Journal - Topical Issue 52 (2016) 76

10. *Topical issue on underground nuclear astrophysics and solar neutrinos: Impact on astrophysics, solar and neutrino physics*
    G Bellini, C Broggini and A Guglielmetti
    European Physical Journal -Topical Issue 52 (2016) 88

9 Conference Proceedings

1. F. Cavanna, R. Depalo, *Three New Low-Energy resonances in the $^{22}Ne(p,\gamma)^{23}Na$ reaction*, Nuclei in the Cosmos XIV, Toki Messe, Niigata, Japan

Proceedings of the 14th International Symposium on Nuclei in the Cosmos (2016)

2. R. Depalo, *Towards a study of $^{22}Ne(p,\gamma)^{23}Na$ at LUNA*, VI NPA Conference, Lisbon, Portugal
   Journal of Physics G: Conference Series 665 (2016) 012017

3. G. Gervino, *The underground nuclear astrophysics in the precision era of BBN: Present results and future perspectives*, VI NPA Conference, Lisbon, Portugal
   Journal of Physics G: Conference Series 665 (2016) 012004

4. C. Gustavino, *Study of Big Bang nucleosynthesis deep underground*, Rencontres de Moriond, Cosmology 2016, La Thuile, Italy
   Proceedings of the 51st RENCONTRES DE MORIOND pag. 347 (2016)

5. M. Junker, *Experiences and Prospects of Nuclear Astrophysics in Underground Laboratories*, VI NPA Conference, Lisbon, Portugal
   Journal of Physics G: Conference Series 665 (2016) 012029

10 Invited talks

1. M. Aliotta, Silver Moon International Workshop, Gran Sasso, 1-2 December 2016, Italy

2. D. Bemmerer, Silver Moon International Workshop, Gran Sasso, 1-2 December 2016, Italy

3. D. Bemmerer, 2nd Workshop on Nuclear Astrophysics at the Canfranc Underground Laboratory, Canfranc, 29 February - 1 March, 2016, Spain

4. D. Bemmerer, Spring Meeting of the German Physical Society, Darmstadt, 17 March 2016, Germany

5. A. Best, Brazilian Meeting on Nuclear Physics, 2016, Brazil

6. C. Broggini, Roma Int. Conf. on Astroparticle Physics, Frascati 21-24 June 2016, Italy

7. C. Broggini, Frontier Research in Astrophysics Workshop of Palermo 22-28 May 2016, Italy

8. C. Broggini, International School of Nuclear Physics, Erice 16-24 September, Italy

9. F. Cavanna, Magellan Workshop, DESY 17-18 March 2016, Germany

10. F. Cavanna, Terzo Incontro di Fisica Nucleare INFN 2016 Workshop, Frascati 14-16 November 2016, Italia

11. F. Cavanna, NAVI Physics Days, GSI, Darmstadt, 18-19 January 2016, Germany

12. A. Formicola, XIV Nuclei in the Cosmos Conference, 19-24 June 2016, Japan

13. A. Guglielmetti, Physics Colloquium at the Max-Planck-Institute for Physics, Munich 2 February 2016, Germany

14. A. Guglielmetti, LIA COLL-AGAIN Copigal Polita, LNS Catania 28 April 2016, Italy

15. C. Gustavino, 6th Roma International Conference on Astroparticle Physics, Roma 21-24 June 2016, Italy

16. C. Gustavino, Vulcano Workshop 2016 Frontier Objects in Astrophysics and Particle Physics, 22-28 May 2016 Vulcano, Italy

17. C. Gustavino, Roma Int. Conf. on Astroparticle Physics, Frascati 21-24 June 2016, Italy

18. M. Junker, Fission and Properties of Neutron-Rich Nuclei (ICFN6) 6-12 November 2016, US

19. M. Lugaro, Meteorical Society Meeting, Berlin 7-12 August 2016, Germany

20. M. Lugaro, International Nuclear Physics Conference, Adelaide 11-16 September 2016, Australia

21. M. Lugaro, The IAU Symposium 323 on Planetary Nebulae, 10-14 October 2016, Beijing, China

22. M. Lugaro, Nuclei in the Cosmos XIV international school, 13-17 June 2016, Nigata, Japan

23. R. Menegazzo, 2nd Workshop on Nuclear Astrophysics at the Canfranc Underground Laboratory, Canfranc, 29 February - 1 March, 2016, Spain

24. P. Prati, 8th Japan-Italian Symposium on Nuclear Physics, Tokyo 7-10 March 2016, Japan

25. T. Szücs, Carpathian Summer School of Physics, Sinaia 26 June - 9 July 2016, Romania

26. D. Trezzi, New Vistas in Low-Energy Precision Physics Conference, Mainz 4-7 April 2016, Germany

27. D. Trezzi, 2nd Workshop on Nuclear Astrophysics at the Canfranc Underground Laboratory, Canfranc, 29 February - 1 March, 2016, Spain

11 Contributed talk

1. F. Cavanna, 14th International Symposium on Nuclei in the Cosmos XIV Toki Messe, Niigata, 19 - 24 June 2016, Japan

2. R. Depalo, XII Torino Workshop, Budapest, 1 - 5 August 2016, Hungary

3. F. Ferraro, International Nuclear Physics Conference 2016 (INPC2016), Adelaide, 11 - 16 September 2016, Australia

4. F. Ferraro, 2nd Workshop on Nuclear Astrophysics at the Canfranc Underground Laboratory, Canfranc, 29 February - 1 March, 2016, Spain

5. F. Ferraro, Incontri di Fisica delle Alte Energie 2016, Genova, 30 marzo - 1 aprile 2016, Italy

6. G. Gervino, Frontier detector for frontier Physics - 13th Pisa Meeting, la Biodola, Isola d'Elba, 24 - 30 May 2015, Italy

7. C. Gustavino, International Nuclear Physics Conference 2016 (INPC2016), Adelaide, 11 - 16 September 2016, Australia

8. V. Mossa, Terzo Incontro Nazionale di Fisica Nucleare INFN2016, Frascati, 14-16 Novembre 2016, Italy

9. F. Pantaleo, 13th Russbach School on Nuclear Astrophysics, Russbach, 6-12 March 2016, Austria

10. D. Piatti, 13th Russbach School on Nuclear Astrophysics, Russbach, 6-12 March 2016, Austria

11. D. Piatti, 102 Congresso S.I.F., 26 - 30 Settembre, Padova, Italy

12. D. Piatti, INTERNATIONAL SCHOOL OF SUBNUCLEAR PHYSICS 54th Course: THE NEW PHYSICS FRONTIERS IN THE LHC-2 ERA, 14 - 23 June 2016, Italy

12 PhD Theses

Direct Measurements of the $^{23}Na(p,\gamma)^{24}Mg$ Cross Section at Stellar Energies
Axel Boeltzig, PhD thesis
GSSI and LNGS, December 2016
Supervisors: Matthias Junker, Michael Wiescher
Tutors: Andreas Best, Gianluca Imbriani

THEORY GROUP

The theory group consists of physicists belonging to three different institutions: the National Laboratories of Gran Sasso, the Gran Sasso Science Institute and the University of L'Aquila. The theory group is organized in five working subgroups, local nodes of the INFN research network: AAE, High-energy astrophysics; INDARK, Inflation, dark matter and the large-scale structure of the universe; NPQCD, Non-Perturbative quantum chromodynamics; NUMAT, Nuclear matter and compact stellar objects; TASP, Theoretical astroparticle physics. The local coordinators are indicated in bold face in the members list below. Note that starting from 2017 the names of the working subgroups have changed and the local node of NPQCD has been closed.

The scientific production of the theory group is of very high level with publications on most renowned international journals. The scientific achievements have been presented in a number of international conferences. Moreover, there is a long-standing and very fruitful tradition of collaboration between the theory group and several experimental groups, in particular with those of the National Laboratories of Gran Sasso. In this report, we briefly describe the activities of the theory group in 2016.

Members of the group: A. Addazi, R. Aloisio, Z. Berezhiani, V. Berezinsky, R. Biondi, P. Blasi, S. Carignano, M. D'Angelo, G. Di Carlo, A.T. Esmaili, C. Evoli, P. Giammaria, A. Mammarella, **M. Mannarelli**, S. Marcocci, G. Morlino, A. Palladino, G. Pagliaroli, L. Pilo, S. Ramazanov, S. Recchia, F. Tonelli, F.L. Villante, F. Vissani.

More information can be found at: `http://theory.lngs.infn.it/index.html`

NPQCD

Member: **G. Di Carlo**.

– Collaboration with: V. Azcoiti, E. Follana (Zaragoza University) and A. Vaquero (Zaragoza University and Cyprus Inst.).

Scientific work

The severe sign problem is a longstanding challenge for high energy and solid-state theorists, but only in this century some first attempts to overcome this problem have been proposed, making this field very active at present. In this framework in [1] we analyzed a two-dimensional antiferromagnetic Ising model within an imaginary magnetic field by means of analytical techniques, computing the first eight cumulants of the expansion of the effective Hamiltonian in powers of the inverse temperature, and calculating physical observables for a large number of degrees of freedom with the help of standard multi-precision algorithms. We obtained accurate results for the free energy density, internal energy, standard and staggered magnetization, and the position and nature of the critical line, which confirm the mean field qualitative picture, and which should

be quantitatively reliable, at least in the high temperature regime, including the entire critical line.

Switching to gauge models we concluded an extensive simulation of the Schwinger model with an imaginary θ-term, to study the (possible) disappearance of the (first order) phase transition, and with real values of θ, at $\theta = \pi$ for small enough value of the mass. We succeeded in reconstructing the behavior of the massive Schwinger model with θ-term, and our results support Coleman's conjecture on the phase diagram of this model. Preliminary results have been presented at Lattice2016. We have also started a study of the same issue (θ dependence) for quenched QCD.

AAE

Members: A. Addazi, **Z. Berezhiani** and R. Biondi.

– Collaboration with: A. D. Dolgov (Univ. Ferrara), A. Vainshtein (ITP, Minneapolis, USA), Yu. Kamyshkov (Univ. Tennessee, USA), J.W.F. Valle (IFIC Valencia), S. Capozziello (Univ. Naples) amd M. Bianchi (Univ. Roma II).

Scientific work

The research activity has been mainly focused on the following topics and the following results were obtained:

- **Baryon number violation and neutron oscillations.**
  We worked on different models of baryon number violation and neutron oscillations, with special attention to $\Delta B = 2$ processes leading to neutron-antineutron oscillation and $\Delta B = 1$ ones leading to neutron-mirror neutron oscillations. Extended report on the neutron oscillations is published in Physics Reports [2] which summarizes the theoretical motivations and the experimental efforts to search for baryon number violation, focussing on nucleon decay and neutron-antineutron oscillations. Present and future nucleon decay search experiments using large underground detectors, as well as planned experiments with free high intensity neutron beams at ESS were highlighted. The cases of spontaneous violation of baryon violation and its relations with the lepton number violation was studied, and the possibility that QCD may break the baryon number via fuzzy six-quark condensates was discussed [3]. The case of spontaneous breaking of local $B-L$ symmetry with very small gauge coupling constant was studied which could induce long-range fifth forces. It was shown that that the discovery of neutron–antineutron mixing would settle strong limits also on such fifth-force, up to four orders of magnitude stringer than the present torsion balance experiments for testing the weak equivalence principle [4]. Also, some exotic instanton effects were discussed as a source of neutron-antineutron oscillation [5, 6, 7].

- **Lepton number violation and neutrino masses.**
  String-inspired models for lepton number violation and neutrino Majorana masses were discussed that could be induced by exotic instant on effects, and the leptogenesis scenario was discussed in the context of such models [8, 9, 10]. Some related questions were also discussed in the context of supersymmetry [11, 12].

- **High energy astrophysical neutrinos and sterile neutrinos.**
  It was shown that active–sterile neutrino oscillations can have a strong implications for the flavor composition of the high energy neutrino events detected by the IceCube Collaboration. The case of sterile neutrinos corresponding to neutrino species of a hidden mirror sector was studied in details [13].

R. Biondi (XXVIII ciclo) presented Doctoral Thesis "Oscillation phenomena between ordinary and dark matter particles: the case of neutron and neutrinos" in March 2016 (supervisor Z. Berezhiani)

INDARK

Members: A. Mammarella, **L. Pilo**, S. Ramazanov, F.L. Villante.

– Collaboration with: G. Ballesteros (CERN and IPh CEA Saclay), M. Crisostomi (ICG-Portsmouth), D. Comelli (INFN-Ferrara), K. Koyama (ICG-Portsmouth), S. Matarrrese (Univ. Padova and GSSI), F. Nesti, (Boskovic Institue-Zagreb), M. Pinsonneault (Ohio State Univ.), G. Tasinato(Swansea Univ.)

Scientific work

The research activity has been focused on the following topics: modified gravity and cosmology, dark matter.

- **Low-energy dynamics of self-gravitating media (SGM).**
  The SGM can be described as a shift-symmetric effective theory of four scalar fields. These scalars describe the embedding in spacetime of the medium and play the role of Stuckelberg fields for spontaneously broken spatial and time translations. Perfect fluids are selected imposing a stronger symmetry group or reducing the field content to a single scalar. The relation between the field theory description of perfect fluids and thermodynamics is explored. By drawing the correspondence between the allowed operators at leading order in derivatives and the thermodynamic variables, it is found that a complete thermodynamic picture requires the four Stuckelberg fields. It can be shown that thermodynamic stability plus the null-energy condition imply dynamical stability. One can also argue that a consistent thermodynamic interpretation is not possible if any of the shift symmetries is explicitly broken.

- **Effective field theory for the low-energy physics of self-gravitating media.**
  The field content consists of four derivatively coupled scalar fields that can be identified with the internal comoving coordinates of the medium. Imposing SO(3) internal spatial invariance, the theory describes supersolids. Stronger symmetry requirements lead to superfluids, solids and perfect fluids, at lowest order in derivatives. In the unitary gauge, massive gravity emerges, being thus the result of a continuous medium propagating in spacetime. Our results can be used to explore systematically the effects and signatures

of modifying gravity consistently at large distances. The dark sector is then described as a self-gravitating medium with dynamical and thermodynamic properties dictated by internal symmetries. These results indicate that the divide between dark energy and modified gravity, at large distance scales, is simply a gauge choice.

- **Projectable Horava-Lifshitz model exhibiting ghost instabilities.**
  It turns out that, due to the Lorentz violating structure of the model and to the presence of a finite strong coupling scale, the vacuum decay rate into photons is tiny in a wide range of phenomenologically acceptable parameters. The strong coupling scale, understood as a cutoff on ghosts spatial momenta, can be raised up to 10 TeV. At lower momenta, the projectable Horava-Lifshitz gravity is equivalent to General Relativity supplemented by a fluid with a small positive sound speed squared ($10^{-42} \leq c_s^2 \leq 10^{-20}$), that could be a promising candidate for the Dark Matter. Despite these advantages, the unavoidable presence of the strong coupling obscures the implementation of the original Horava's proposal on quantum gravity. Apart from the Horava-Lifshitz model, conclusions of the present work hold also for the mimetic matter scenario, where the analogue of the projectability condition is achieved by a non-invertible conformal transformation of the metric.

- **Phenomenology of kev-sterile neutrinos as dark matter candidates.**
  Determination of the galaxy structure in scenarios with fermionic warm dark matter. Limit on the mass of kev-sterile neutrinos from dwarf spheroidal galaxies.

Theoretical Astroparticle Physics (TAsP)

Members: R. Aloisio, V. Berezinsky, P. Blasi, M. D'Angelo, C. Evoli, A.T. Esmaili, P. Giammaria, G. Morlino, A. Palladino, S. Recchia, **F.L. Villante**, F. Vissani.

– Collaboration with: A. Serenelli (IEEC-CSIC, Spagna), M.C. Gonzalez-Garcia (Departament de Fisica Quantica i Astrofisica and ICC-UB, Universitat de Barcelona, Spagna), S. Celli (GSSI), A. Gallo Rosso (GSSI), S. Basu (Department of Astronomy, Yale University, USA), C. Pena-Garay (Instituto de Fisica Corpuscular, CSIC Valencia, Spagna), F. Aharonian (Dublin Institute for Advanced Studies, Irlanda).

Scientific work

Research topics:

- **Neutrino physics and astronomy.**
  - Quantitative study of the solar composition problem and analysis of the role of future CNO neutrino measurements;
  - Analysis of the implications of recent solar wind measurements for solar models and composition;
  - Evaluation of the expected high energy diffuse galactic neutrino flux for different cosmic ray distributions;
  - Analysis of the IceCube High Energy neutrino data in the framework of models with galactic plus extragalactic contributions;

- Discussion of the possibility to use high energy neutrinos produced by Glashow resonance to determine the production mechanism of astrophysical neutrinos;
- Predictions for high energy neutrinos and gamma from the galactic center after HESS multi-TeV measurement.

- **Cosmic ray and gamma ray astronomy.**
  - Study of high energy cosmic ray propagation in the Galaxy;
  - Analysis of the diffuse gamma ray emissivity in the Galaxy and determination of the radial distribution of Galactic cosmic rays;
  - Analysis of the effects of a cosmic axion background on reionization and determination of limits for axion-photon conversion in extragalactic magnetic fields;
  - Production of secondary particles due to the propagation of ultra high energy extragalactic cosmic rays: comparison of the results obtained by different numerical simulations.
  - Analysis of the potential of dark matter indirect search in dwarf spheroidal galaxy with Cherenkov Telescopes (MAGIC, ASTRI and CTA).

NUMAT

Members: S. Carignano, M. Mannarelli, S. Marcocci, **G. Pagliaroli** and F. Vissani.

– Collaboration with: S. Alekhin, S. Adrian-Martinez, M. Buballa, S. Celli, S. Dell'Oro, N. Di Marco, W. Elkamhawy, A. Esmaili, C. Evoli, L. Lepori, A. Mammarella, S. Marcocci, D. Nowakowski, A. Palladino, M. Spurio. M. Viel and F.L. Villante.

Scientific work

The scientific achievements concern several aspects of ultra-dense matter and neutrino physics/astrophysics.

- **Properties of ultra-dense matter.**
  We re-examined the pion condensed phase using different approaches within the chiral perturbation theory framework. As a first step, we performed a low-density expansion of the chiral Lagrangian valid close to the onset of the Bose-Einstein condensation. We obtained an effective theory that can be mapped to a Gross-Pitaevskii Lagrangian in which, remarkably, all the coefficients depend on the isospin chemical potential. This new approach leads to a Lagrangian similar to the one used for describing quantum magnets [57]. We studied the thermodynamic properties of matter at vanishing temperature for non-extreme values of the isospin chemical potential and of the strange quark chemical potential. From the leading-order pressure obtained by maximizing the static chiral Lagrangian density, we derived a simple expression for the equation of state in the pion condensed phase and in the kaon condensed phase. We derived an analytical expression for the maximum of the ratio between the energy density and the Stefan-Boltzmann energy density as well as for the isospin chemical potential at the peak both in good agreement with lattice simulations of quantum chromodynamics. We also speculated on the location of the crossover from the

Bose-Einstein condensate state to the Bardeen-Cooper-Schrieffer state by a simple analysis of the thermodynamic properties of the system [58].

We revisited the renormalization prescription for the quark-meson model in an extended mean-field approximation, where vacuum quark fluctuations are included. We investigated the influence of the parameter-fixing scheme on the phase structure of the model at finite temperature and chemical potential. Despite large differences between the model parameters in the two schemes, we found that in homogeneous matter the effect on the phase diagram is relatively small. For inhomogeneous phases, on the other hand, the choice of the proper renormalization prescription is crucial. In particular, we pointed out that if renormalization effects on the pion decay constant are not considered, the model does not even present a well-defined renormalized limit when the cutoff is sent to infinity [59].

- **Compact stellar objects.**
  We discussed the effects of an inhomogeneous chiral condensate on the properties of compact stars. After introducing two commonly studied spatial modulations of the chiral condensate, the chiral density wave and the real kink crystal, we focused on their properties and their effect on the equation of state of quark matter. We also described how these crystalline phases are affected by the charge neutrality requirement, by the presence of magnetic fields, by vector interactions and the interplay with color superconductivity. Finally, we discussed possible signatures of inhomogeneous chiral symmetry breaking in the core of compact stars, considering the mass-radius relations and neutrino emissivity [60].

- **General properties of neutrinos.**
  We reviewed the main features of neutrinoless double beta decay ($0\nu\beta\beta$), underlining its key role both from the experimental and theoretical point of view. In particular, we contextualized the $0\nu\beta\beta$ in the panorama of lepton-number violating processes, also assessing some possible particle physics mechanisms mediating the process. Since the $0\nu\beta\beta$ existence is correlated with neutrino masses, we also reviewed the state-of-art of the theoretical understanding of neutrino masses [37]. We performed a statistical investigation of the neutrino invisible decay hypothesis in the $\nu_\mu \to \nu_\tau$ appearance channel. We pointed out that the neutrino decay provides an enhancement of the expected tau appearance signal with respect to the standard oscillation scenario for the long-baseline OPERA experiment. Despite data showing a very mild preference for invisible decays with respect to the oscillations only hypothesis, we provided the first upper limit for the neutrino decay lifetime in this channel[61].

- **Astrophysical neutrinos**.
  We studied the diffuse high energy neutrinos expected by the interaction of cosmic rays with the gas contained in our Galaxy. We provided expectations for this component by considering different assumptions for the cosmic ray distribution in the Galaxy which are intended to cover the large uncertainty in cosmic ray propagation models. We calculated the angular dependence of the diffuse galactic neutrino flux and the corresponding rate of High Energy Starting Events in IceCube by including the effect of detector angular resolution [23].

  We also considered two categories of events that can help to diagnose cosmic neutrinos: double pulse, which may allow us to clearly discriminate the cosmic component of ν_τ, and cascades with deposited energy above 2PeV, including events produced at the Glashow resonance, which can be used to investigate the neutrino production mechanisms. We

show that one half of the double pulse signal is due to the neutrinos spectral region already probed by IceCube [25]. We investigated the hypothesis of a PeVatron in the Galactic Center, emerged with the recent γ-ray measurements of H.E.S.S. as high energy neutrino source and its detectability. We derived precise upper limits on neutrino fluxes and the underlying hypotheses are discussed. The expected number of events for ANTARES, IceCube and KM3NeT, based on the H.E.S.S. measurements, are calculated [62].

We critically analyzed the hypothesis that high energy cosmic neutrinos are power law distributed. We proposed a model with two-components that explains better the observations. The extragalactic component of the high energy neutrino flux has a canonical E^{-2} spectrum while the galactic component has a $E^{-2.7}$ spectrum; both of them are significant. This model has several implications, that can be tested by IceCube and ANTARES in the next years [38]. We extended the previous work to investigate the IceCube spectral anomaly, that suggests that they observe a multicomponent spectrum. The stability of the expectations is studied by introducing free parameters, motivated by theoretical considerations and observational facts. The upgraded model here examined has 1) a Galactic component with different normalization and shape $E^{-2.4}$; 2) an extragalactic neutrino spectrum based on new data; 3) a non-zero prompt component of atmospheric neutrinos [27].

- **Multimessanger physics.**
  Within the large collaboration involving gravitational waves detectors, i.e. Ligo and Virgo, and neutrinos detectors, i.e. LVD, Borexino, Kamland (just joined to the MoU) and IceCube, we developed a Monte Carlo describing LVD, Borexino and Kamland detectors to increase the sensitivity for the detection of distant CCSNe. We also started to implement the coincidences search pipeline between Neutrinos and Gravitational Waves data.

Conferences and seminars

1. PSI 2016 "Physics of fundamental Symmetries and Interactions", 16–20 Oct. 2016, Villingen, Switzerland
   Invited talk by Z. Berezhiani
   https://indico.psi.ch/conferenceDisplay.py?confId=3914

2. NOW 2016 "Neutrino Oscillation Workshop", 4–11 Sept. 2016, Otranto, Lecce, Italy
   Invited talks by Z. Berezhiani and F.L. Villante
   http://www.ba.infn.it/~now/now2016

3. IV Summer School On High Energy Physics and Quantum Field Theory 20–23 Aug. 2016, Yerevan, Armenia
   Invited lectures by Z. Berezhiani
   http://theorphyslab.ysu.am/VW_ASW-2016/

4. Int. Workshop "Baryons over antibaryons: the nuclear physics of Sakharov", 25–29 July 2016, ECT*, Trento, Italy
   Invited talks by Z. Berezhiani
   http://www.ectstar.eu/node/1663

5. ICNFP 2016, 5th International Conference on "New Frontiers in Physics", 6–14 July 2016, OAC, Creta, Greece
   Invited talk by Z. Berezhiani
   https://indico.cern.ch/event/442094/page/7521-program

6. International school of subnuclear physics 2016, 54th course: new physics frontiers in the lhc-2 era, Erice, Italy, 14–23 June 2016
   Invited lecture by Z. Berezhiani
   http://www.ccsem.infn.it/issp2016/index.html

7. International school of subnuclear physics 2016, 54th Course: New Physics Frontiers In The Lhc-2 Era, Erice, Italy, 14–23 June 2016
   Participant talk by R. Biondi, premiated with Y. Nambu Prize
   http://www.ccsem.infn.it/issp2016/index.html

8. Int. Workshop "Probing Fundamental Symmetries and Interactions with Neutrons", 11–15 April 2016, Mainz, Germany
   Invited talk by Z. Berezhiani
   https://indico.mitp.uni-mainz.de/event/59

9. Theoretical Cosmology in the Era of Large Surveys, Galileo Galilei Institute (GGI). Florence 04-17 April 2016.
   Invited talk by L. Pilo
   http://www.ggi.fi.infn.it/index.php?page=workshops.inc&id=210

10. GR21, Columbia University New York (USA). July 2016
    Talk by L. Pilo
    http://www.gr21.org/

11. NuPhys2016: Prospects in Neutrino Physics, 12-12-2016, London, UK
    Talk by F.L. Villante
    https://indico.ph.qmul.ac.uk/indico/conferenceDisplay.py?confId=112

12. XXVII International Conference on Neutrino Physics and Astrophysics (Neutrino 2016), 04-07-2016, London, UK
    Talk by F.L. Villante
    http://neutrino2016.iopconfs.org/home

13. International Conference on UHECR 2016, Kyoto, Japan
    Invited talks by R. Aloisio and V. Berezinsky
    https://indico.cern.ch/event/504078/

14. FFLO-Phase in Quantum Liquids, Quantum Gases, and Nuclear Matter, June 2016, Germany
    Invited talk by M. Mannarelli
    https://www.mpipks-dresden.mpg.de/fflo16/

15. Bari Theory XMAS workshop, December 2016, Bari, Italy
    Talk by M. Mannarelli
    https://agenda.infn.it/conferenceDisplay.py?confId=12266

16. 8th Symposium on Large TPCs for Low Energy Rare Events, December 2016, Paris, France
Talk by G. Pagliaroli
https://indico.cern.ch/event/473362/

17. Compact Stars in the QCD phase diagram V, May 2016, L'Aquila, Italy
Talk by G. Pagliaroli
http://agenda.infn.it/event/compact-stars

18. Quarkyonic matter, from theory to experiment, 24-28 October 2016 , Wuhan, China
Invited talk by S. Carignano
https://indico.cern.ch/event/555970/

Activity in INFN and International organizations

- R. Aloisio is a member of the GSSI Scientific Board.
- V. Berezinsky is a member of Council "Cosmic Ray Research" (Russia), a member of Int. Advisory Board of JEM-EUSO, a member of Int. Scientific Advisory Committee of Gigaton Volume Detector of High Energy Neutrinos.
- Z. Berezhiani has been co-organizer of the Workshop "Hot Topics in Modern Cosmology"
http://www.cpt.univ-mrs.fr/%7Ecosmo/SW_2015/SW9.html
- M. Mannarelli has been co-chair of the workshop "Compact stars in the QCD phase diagram V".
http://agenda.infn.it/event/compact-stars
- M. Mannarelli and F. Vissani have been co-organizer of the LNGS seminars.
- M. Mannarelli has been cochair of the "Particle and Astroparticle Physics Autumn Program"
https://agenda.infn.it/conferenceDisplay.py?confId=12089.
- S. Carignano, G. Pagliaroli, A. Mammarella and F. Vissani were in the Organizing Committee of the workshop "Compact stars in the QCD phase diagram V".
http://agenda.infn.it/event/compact-stars
- Z. Berezhiani and L. Pilo are members of the Doctorate Collegium of the Physics Dept. and of the Doctorate Commission, University of L'Aquila.
- Z. Berezhiani obtained an Award for Research from the University of Sydney, Australia.
- F. Vissani is the physics area coordinator and Chair of the GSSI Astroparticle Physics PhD Committee, observer in Comm.II on behalf of Comm.IV, referee for the INFN National Permanent Committees II on non-accelerator physics; member of the scientific committee for the ICRANet-INFN agreement; associate editor of European Physical Journal C.
- F. Vissani has been organizing the Asimov Prize.
https://it.wikipedia.org/wiki/Premio_Asimov.

Publications in journals and proceedings

[1] Azcoiti V, Di Carlo G, Follana E and Royo-Amondarain E 2016 (*Preprint* 1612.08598)

[2] Phillips II D G *et al.* 2016 *Phys. Rept.* **612** 1–45 (*Preprint* 1410.1100)

[3] Berezhiani Z 2016 *Eur. Phys. J.* **C76** 705 (*Preprint* 1507.05478)

[4] Addazi A, Berezhiani Z and Kamyshkov Y 2016 (*Preprint* 1607.00348)

[5] Addazi A 2016 *Phys. Lett.* **B757** 462–467 (*Preprint* 1506.06351)

[6] Addazi A 2015 (*Preprint* 1504.06799)

[7] Addazi A 2016 *Int. J. Mod. Phys.* **A31** 1650084 (*Preprint* 1505.02080)

[8] Addazi A, Valle J W F and Vaquera-Araujo C A 2016 *Phys. Lett.* **B759** 471–478 (*Preprint* 1604.02117)

[9] Addazi A, Bianchi M and Ricciardi G 2016 *JHEP* **02** 035 (*Preprint* 1510.00243)

[10] Addazi A, Capozziello S and Odintsov S 2016 *Phys. Lett.* **B760** 611–616 (*Preprint* 1607.05706)

[11] Addazi A 2016 *Electron. J. Theor. Phys.* **13** 39–56 (*Preprint* 1505.00625)

[12] Addazi A and Khlopov M 2016 *Mod. Phys. Lett.* **A31** 1650111 (*Preprint* 1604.07622)

[13] Biondi R 2016 *Nuovo Cim.* **C39** 271

[14] Addazi A and Capozziello S 2016 *Mod. Phys. Lett.* **A31** 1650054 (*Preprint* 1602.00485)

[15] Addazi A 2016 *Mod. Phys. Lett.* **A32** 1750014 (*Preprint* 1607.01203)

[16] Addazi A 2016 *Int. J. Geom. Meth. Mod. Phys.* **14** 1750012 (*Preprint* 1607.02593)

[17] Addazi A 2016 (*Preprint* 1603.08719)

[18] Addazi A 2015 (*Preprint* 1505.07357)

[19] Addazi A 2016 *Europhys. Lett.* **116** 20003 (*Preprint* 1607.08107)

[20] Ramazanov S, Arroja F, Celoria M, Matarrese S and Pilo L 2016 *JHEP* **06** 020 (*Preprint* 1601.05405)

[21] Ballesteros G, Comelli D and Pilo L 2016 *Phys. Rev.* **D94** 124023 (*Preprint* 1603.02956)

[22] Ballesteros G, Comelli D and Pilo L 2016 *Phys. Rev.* **D94** 025034 (*Preprint* 1605.05304)

[23] Pagliaroli G, Evoli C and Villante F L 2016 *JCAP* **1611** 004 (*Preprint* 1606.04489)

[24] Serenelli A, Scott P, Villante F L, Vincent A C, Asplund M, Basu S, Grevesse N and Pena-Garay C 2016 *Mon. Not. Roy. Astron. Soc.* **463** 2–9 (*Preprint* 1604.05318)

[25] Palladino A, Pagliaroli G, Villante F L and Vissani F 2016 *Eur. Phys. J.* **C76** 52 (*Preprint* 1510.05921)

[26] Pagliaroli G, Palladino A, Villante F L and Vissani F 2016 *J. Phys. Conf. Ser.* **718** 062046

[27] Palladino A, Spurio M and Vissani F 2016 *JCAP* **1612** 045 (*Preprint* 1610.07015)

[28] Berezinsky V, Gazizov A and Kalashev O 2016 *Astropart. Phys.* **84** 52–61 (*Preprint* 1606.09293)

[29] Nava L, Gabici S, Marcowith A, Morlino G and Ptuskin V S 2016 *Mon. Not. Roy. Astron. Soc.* **461** 3552–3562 (*Preprint* 1606.06902)

[30] Recchia S, Blasi P and Morlino G 2016 *Mon. Not. Roy. Astron. Soc.* **462** L88–L92 (*Preprint* 1604.07682)

[31] Cardillo M, Amato E and Blasi P 2016 *Astron. Astrophys.* **595** A58 (*Preprint* 1604.02321)

[32] Marcowith A *et al.* 2016 *Rept. Prog. Phys.* **79** 046901 (*Preprint* 1604.00318)

[33] Recchia S, Blasi P and Morlino G 2016 *Mon. Not. Roy. Astron. Soc.* **462** 4227–4239 (*Preprint* 1603.06746)

[34] Berezinsky V and Kalashev O 2016 *Phys. Rev.* **D94** 023007 (*Preprint* 1603.03989)

[35] Evoli C, Leo M, Mirizzi A and Montanino D 2016 *JCAP* **1605** 006 (*Preprint* 1602.08433)

[36] Yang R, Aharonian F and Evoli C 2016 *Phys. Rev.* **D93** 123007 (*Preprint* 1602.04710)

[37] Dell'Oro S, Marcocci S, Viel M and Vissani F 2016 *Adv. High Energy Phys.* **2016** 2162659 (*Preprint* 1601.07512)

[38] Palladino A and Vissani F 2016 *Astrophys. J.* **826** 185 (*Preprint* 1601.06678)

[39] Ahnen M L *et al.* (Fermi-LAT, MAGIC) 2016 *JCAP* **1602** 039 (*Preprint* 1601.06590)

[40] D'Angelo M, Blasi P and Amato E 2016 *Phys. Rev.* **D94** 083003 (*Preprint* 1512.05000)

[41] Morlino G and Blasi P 2016 *Astron. Astrophys.* **589** A7 (*Preprint* 1511.05343)

[42] Alekhin S *et al.* 2016 *Rept. Prog. Phys.* **79** 124201 (*Preprint* 1504.04855)

[43] Giammaria P, Aleksić J, Lombardi S, Maggio C, Palacio J, Rico J, Vanzo G and Vazquez Acosta M (MAGIC) 2016 *J. Phys. Conf. Ser.* **718** 042024

[44] Giammaria P, Lombardi S, Antonelli L A, Brocato E, Bigongiari C, Pierro F D and Stamerra A (CTA Consortium) 2016 *J. Phys. Conf. Ser.* **718** 042068

[45] Esmaili A, Palladino A and Vissani F 2016 *EPJ Web Conf.* **116** 11002

[46] Aloisio R 2016 *Nucl. Part. Phys. Proc.* **279-281** 95–102 (*Preprint* 1603.05886)

[47] Aloisio R 2016 *J. Phys. Conf. Ser.* **718** 052001 (*Preprint* 1601.04867)

[48] D'Angelo M, Blasi P and Amato E 2016 *PoS* **ICRC2015** 534

[49] Krause J, Morlino G and Gabici S 2016 *PoS* **ICRC2015** 518

[50] Calore F, Cholis I, Evoli C, Hooper D, Linden T and Weniger C 2016 *PoS* **ICRC2015** 915

[51] Nava L, Gabici S, Marcowith A, Morlino G and Ptuskin V 2016 *PoS* **ICRC2015** 541 (*Preprint* 1509.02174)

[52] Recchia S, Blasi P and Morlino G 2016 *PoS* **ICRC2015** 522

[53] Boncioli D, di Matteo A, Salamida F, Aloisio R, Blasi P, Ghia P L, Grillo A, Petrera S and Pierog T 2016 *PoS* **ICRC2015** 521 (*Preprint* 1509.01046)

[54] Blasi P, Amato E and D'Angelo M 2016 *PoS* **ICRC2015** 505

[55] Morlino G, Gabici S and Krause J 2016 *PoS* **ICRC2015** 486 (*Preprint* 1509.05128)

[56] Cardillo M, Amato E and Blasi P 2016 *PoS* **ICRC2015** 531 (*Preprint* 1507.06086)

[57] Carignano S, Lepori L, Mammarella A, Mannarelli M and Pagliaroli G 2017 *Eur. Phys. J.* **A53** 35 (*Preprint* 1610.06097)

[58] Carignano S, Mammarella A and Mannarelli M 2016 *Phys. Rev.* **D93** 051503 (*Preprint* 1602.01317)

[59] Carignano S, Buballa M and Elkamhawy W 2016 *Phys. Rev.* **D94** 034023 (*Preprint* 1606.08859)

[60] Buballa M and Carignano S 2016 *Eur. Phys. J.* **A52** 57 (*Preprint* 1508.04361)

[61] Pagliaroli G, Di Marco N and Mannarelli M 2016 *Phys. Rev.* **D93** 113011 (*Preprint* 1603.08696)

[62] Celli S, Palladino A and Vissani F 2017 *Eur. Phys. J.* **C77** 66 (*Preprint* 1604.08791)

[63] Nowakowski D and Carignano S 2016 *PoS* **MPCS2015** 010 (*Preprint* 1602.04798)

[64] Adrian-Martinez S *et al.* (KM3Net) 2016 *J. Phys.* **G43** 084001 (*Preprint* 1601.07459)

[65] Carignano S, Ferrer E J and de la Incera V 2016 *Nucl. Part. Phys. Proc.* **273-275** 1559–1564 (*Preprint* 1411.1686)

XENON

E. Aprile[a]*, J. Aalbers[b], F. Agostini[c,d], M. Alfonsi[e], F. D. Amaro[f], M. Anthony[a], F. Arneodo[g], P. Barrow[h], L. Baudis[h], B. Bauermeister[i], M. L. Benabderrahmane[g], T. Berger[j], P. A. Breur[b], A. Brown[b], E. Brown[j], S. Bruenner[k], G. Bruno[c], R. Budnik[l], L. Butikofer[m], J. Calvén[i], J. M. R. Cardoso[f], M. Cervantes[n], D. Chicon[k], D. Coderre[m], A. P. Colijn[b], J. Conrad[i], †J. P. Cussonneau[o], M. P. Decowski[b], P. de Perio[a], P. Di Gangi[d], A. Di Giovanni[g], S. Diglio[o], E. Duchovni[l], G. Eurin[k], J. Fei[p], A. D. Ferella[i], A. Fieguth[q], D. Franco[h], W. Fulgione[c,r], A. Gallo Rosso[c], M. Galloway[h], F. Gao[a], M. Garbini[d], C. Geis[e], L. W. Goetzke[a], L. Grandi[s], Z. Greene[a], C. Grignon[e], C. Hasterock[k], E. Hogenbirk[b], R. Itay[l], B. Kaminsky[m], G. Kessler[h], A. Kish[h], H. Landsman[l], R. F. Lang[n], D. Lellouch[l], L. Levinston[l], M. Le Calloch[o], Q. Lin[a], S. Lindemann[k,m], M. Lindner[k], J. A. M. Lopes[f], ‡A. Manfredini[l], I. Maris[g], T. Marrodán Undagoitia[k], J. Masbou[o], F. V. Massoli[d], D. Masson[n], D. Mayani Paras[h], Y. Meng[t], M. Messina[a], K. Micheneau[o], B. Miguez[r], A. Molinario[c], M. Murra[q], J. Naganoma[u], K. Ni[p], U. Oberlack[e], S. E. A. Orrigo[f]§, P. Pakarha[h], B. Pelssers[i], R. Persiani[o], F. Piastra[h], J. Pienaar[n], M.-C. Piro[j], V. Pizzella[k], G. Plante[a], N. Priel[l], L. Rauch[k], S. Reichard[n], C. Reuter[n], A. Rizzo[a], S. Rosendahl[q], N. Rupp[k], R. Saldanha[s], J. M. F. dos Santos[f], G. Sartorelli[d], M. Scheibelhut[e], S. Shindler[e], J. Schreiner[k], M. Schumann[m], L. Scotto Lavina[v], M. Selvi[d], P. Shagin[u], E. Shockley[s], M. Silva[f], H. Simgen[k], M. von Sivers[m], A. Stein[t], D. Thers[o], A. Tiseni[b], G. Trinchero[r], C. Tunnell[b,s], N. Upole[s], H. Wang[t], Y. Wei[h], C. Weinheimer[q] J. Wulf[h], J. Ye[p], Y. Zhang[a].

(The XENON Collaboration)

*Spokesperson

†Wallenberg Academy Fellow

‡Also with Coimbra Engineering Institute, Coimbra, Portugal

§Present address: IFIC, CSIC-Universidad de Valencia, Valencia, Spain

[a] Physics Department, Columbia University, New York, NY, USA
[b] Nikhef and the University of Amsterdam, Science Park, Amsterdam, Netherlands
[c] INFN-Laboratori Nazionali del Gran Sasso and Gran Sasso Science Institute, L'Aquila, Italy
[d] Department of Physics and Astrophysics, University of Bologna and INFN-Bologna, Bologna, Italy
[e] Institut für Physik & Exzellenzcluster PRISMA, Johannes Gutenberg-Universität Mainz, Mainz, Germany
[f] Department of Physics, University of Coimbra, Coimbra, Portugal
[g] New York University in Abu Dhabi, Abu Dhabi, United Arab Emirates
[h] Physik-Institut, University of Zürich, Zürich, Switzerland
[i] Oskar Klein Centre, Department of Physics, Stockholm University, AlbaNova, Stockholm, Sweden
[j] Department of Physics, Applied Physics and Astronomy, Rensselaer Polytechnic Institute, Troy, NY, USA
[k] Max-Planck-Institut für Kernphysik, Heidelberg, Germany
[l] Department of Particle Physics and Astrophysics, Weizmann Institute of Science, Rehovot, Israel
[m] Physikalisches Institut, Universität Freiburg, 79104 Freiburg, Germany
[n] Department of Physics and Astronomy, Purdue University, West Lafayette, IN, USA
[o] SUBATECH, Ecole des Mines de Nantes, CNRS/In2p3, Université de Nantes, Nantes, France
[p] Department of Physics, University of California, San Diego, CA, USA
[q] Institut für Kernphysik, Wilhelms-Universität Münster, Münster, Germany
[r] INFN-Torino and Osservatorio Astrofisico di Torino, Torino, Italy
[s] Department of Physics & Kavli Institute of Cosmological Physics, University of Chicago, Chicago, IL, USA
[t] Physics & Astronomy Department, University of California, Los Angeles, CA, USA
[u] Department of Physics and Astronomy, Rice University, Houston, TX, USA
[v] LPNHE, Université Pierre et Marie Curie, Université Paris Diderot, CNRS/IN2P3, Paris 75252, France

Abstract

The year 2016 was a very important milestone for the XENON collaboration. While analyzing and publishing data from the running XENON100 experiment, performing novel ER calibrations, and testing new purifications tools, we completed the commissioning of all the subsystems of the XENON1T experiment. After testing the cryogenic, purification and recovery systems in the spring, we filled the water shield and started the operations in a low background environment in July. We performed the first ER and NR calibrations during summer and fall. At the same time, starting in October we continuously distilled krypton from xenon while running the experiment. At the end of November we started the first XENON1T science run, after reaching a record low background level below 10^{-3} $(\mathrm{kg} \cdot \mathrm{day} \cdot \mathrm{keV})^{-1}$.

1 Introduction

The XENON collaboration operates a series of direct detection experiments at LNGS to search for dark matter particles in our Milky Way. The experiments use dual-phase liquid xenon time-projection chambers (TPCs) which are particularly well-suited to search for one of the most compelling dark matter candidate particle, the Weakly Interacting Massive Particle (WIMP), over a broad range of parameters. Starting with the XENON10 experiment more than a decade ago, the collaboration has successively built larger and more sensitive detectors. The XENON100 experiment was the world's most sensitive direct detection dark matter experiment for a number of years, until late 2013. In 2016 we published the results of the combination of the main three XENON100 science runs, and we started the search of annual modulations over the whole data sample. We also used XENON100 as a very useful tool to test new calibration sources and purification techniques.

After about three years of construction, the collaboration commissioned the new phase of the project, XENON1T, which itself will be two orders of magnitude more sensitive than XENON100. The XENON1T sensitivity goal is $2 \times 10^{-47}\,\mathrm{cm}^2$ after 2 t $\times$ y of exposure. At the end of November 2016, we successfully started its first science run. Most of the infrastructure and detector design of XENON1T are such that they can be reused for an even larger upgrade in the future, called XENONnT, with $\sim$ 8 t of liquid xenon inside, to gain another order of magnitude in sensitivity.

2 XENON100

2.1 Operation status, calibrations and purification techniques

2.1.1 Operation status

Following the degraded cooling system performance over more than two years of continuous operation, the XENON100 detector was stopped in August 2016 with liquid xenon recovered. The detector was then operated in low pressure mode and several systems, including the cryogenic cooling tower, the slow control and gas circulation systems, will be serviced to improve the performance and reliability. Several ideas to use the detector as a test facility for calibration and novel liquid xenon detector components are being discussed in the collaboration. The detector is well suited for a measurement of low energy calibration source ^{37}Ar with 2.82 keV (K-shell EC) and 270 eV (L-shell EC) lines. A ^{37}Ar source is being prepared and a calibration measurement is foreseen following the maintenance of the detector. The detector will be used further to test novel ideas for upgrading the XENON1T detector to XENONnT. These include testing new electrodes to reduce the single electron emission rate, reduction of radon emanation by plating on the detector surface, and fast purification combining the gas and liquid circulations. The schedule for completing the maintenance of various systems and for operating XENON100 with new calibration sources and further tests will be affected by the XENON1T schedule.

2.1.2 Calibrations

The XENON100 detector was used to test several new calibration sources for low energy nuclear recoils (^{88}YBe), and electronic recoils ($^{83\mathrm{m}}$Kr, ^{220}Rn, and CH_3T) for next-generation detectors. The calibration campaign has yielded important information not only on the low energy response of liquid xenon, but also on the detector behavior that is relevant for the operation of XENON1T. Several papers on the operation and calibration results with these sources are being prepared.

We presented a novel calibration method for liquid noble element detectors using a source of dissolved ^{220}Rn [1]. The ^{220}Rn decay chain provides several isotopes that allow for a variety of different calibrations, including the response to low-energy beta decays, high-energy alpha lines, and the important ^{222}Rn background. The isotope enters the active volume as soon as the source is opened to the gas purification system. No contamination is observed from long-lived isotopes, and the introduced activity naturally decays within a week after the source is closed. Since this dissipation time is independent of the size of the detector, calibration with ^{220}Rn is particularly appealing for future large-scale detectors.

The primary utility of the source is the beta decay of ^{212}Pb, which can be employed to calibrate a detector's response to low-energy electronic recoil backgrounds in the search for dark matter. The ^{212}Pb atoms permeate the entire active region, including the center, which is beyond the reach of traditional calibration methods with external Compton sources.

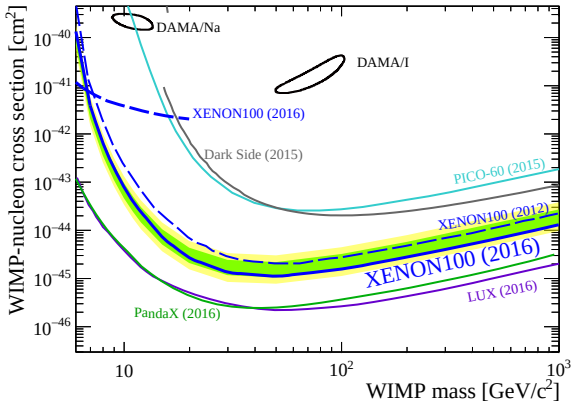

Figure 1: Spin-independent cross section limit (blue line) and 1σ (green band) and 2σ (yellow band) expected sensitivity regions at 90% C.L. from the combined analysis of the three XENON100 science runs. For comparison, a subset of other experimental limits (90 %C.L.) and detection claims (2σ) are also shown [2, 3, 4, 5, 6, 7, 8].

Furthermore, the high-energy alpha decays of ^{220}Rn and ^{216}Po provide a way to map atomic motion. We observed a single convection cell in XENON100 at speeds up to $\sim 7\,$mm/s as well as subdominant ion drift in the electric field of the TPC. Such an improved understanding of fluid dynamics within a detector promises to motivate novel analytic techniques for background mitigation.

Beyond the development of calibration techniques, we have used the beta decay of ^{212}Bi and the alpha decay of ^{212}Po to make a high-purity, high-statistics measurement of the half-life of ^{212}Po yielding a competitive measurement of $t_{1/2} = (293.9 \pm (1.0)_{\rm stat} \pm (0.6)_{\rm sys})\,$ns.

2.2 Physics Analyses and New Results

As the pioneering liquid xenon dark matter experiment, XENON100 has accumulated in total 477 live-days since it started science operations in 2009. These data allowed us to search for a variety of dark matter candidates and other rare events, leading to several new papers released this year.

First, the collaboration reported a low-mass dark matter search using only the ionization signal (S2) to determine the interaction energy [9]. A nuclear recoil energy threshold of 0.7 keV was achieved. A spin-independent WIMP-nucleon cross section of 1.2×10^{-41} cm^2 is obtained at a WIMP mass of 6 GeV/c^2.

Second, a search for two-neutrino double electron capture from the K-shell of ^{124}Xe was carried out using 7636 kg $\times$ d of data, leading to a 90% C.L. limit of $T_{1/2} > 6.5 \times 10^{20}$ yr [10].

Third, we perfomed a combined analysis of the main three XENON100 science runs. Data from the first two runs had been already published. A blind analysis was applied to the last run recorded between April 2013 and January 2014 prior to combining the results. The ultralow electromagnetic background of the experiment, $\sim 5\times10^{-3}$ events/(keV$_{\rm ee}\times$kg$\times$day) before electronic recoil rejection, together with the increased exposure of 48 kg $\times$ yr improved the sensitivity. A profile likelihood analysis using an energy range of $(6.6 - 43.3)$ keV$_{\rm nr}$ set a limit on the elastic, spin-independent WIMP-nucleon scattering cross section for WIMP masses above 8 GeV/c^2, with a minimum of 1.1×10^{-45} cm^2 at 50 GeV/c^2 and 90% confidence level, as shown in figure

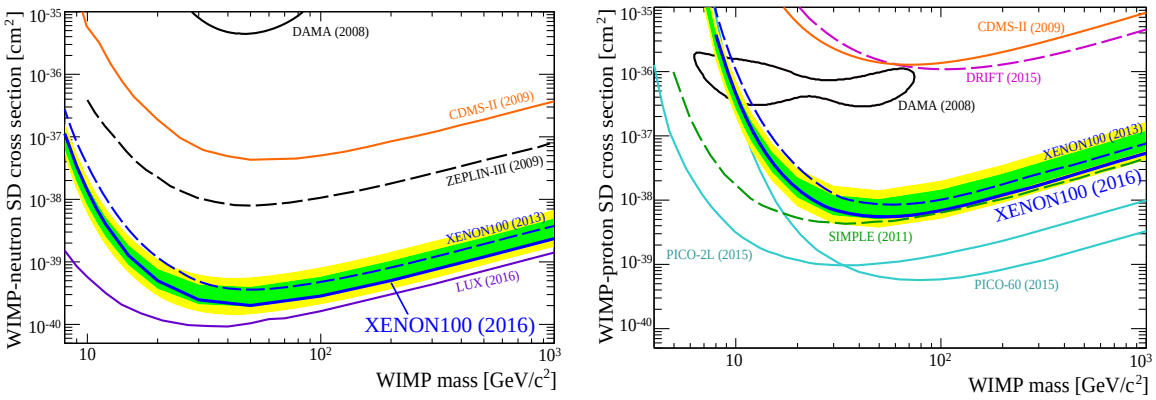

Figure 2: Spin-dependent cross section limit (blue line) and 1σ (green band) and 2σ (yellow band) expected sensitivity regions at 90% C.L. from the combined analysis of the three XENON100 science runs. The top (bottom) panel shows the individual neutron (proton) only cross sections. For comparison, other experimental limits (90 %C.L.) and detection claims (2σ) are also shown [12, 4, 13, 14, 15, 16, 17, 18, 19].

1. We also reported an updated constraints on the elastic, spin-dependent WIMP-nucleon cross sections obtained with the same data. We set upper limits on the WIMP-neutron (proton) cross section with a minimum of 2.0×10^{-40} cm^2 (52×10^{-40} cm^2) at a WIMP mass of 50 GeV/c^2, at 90% confidence level, shown in figure 2.

The combined dark matter data, spanning over three entire years, allow us to search for potential annual modulation signals with a better sensitivity compared to the previous published modulation search results. The combined modulation search analysis was completed and the manuscript submitted in early 2017.

3 XENON1T

XENON1T is the successor to the XENON100 experiment. With a design sensitivity two orders of magnitude better than XENON100, over a broad range of WIMP masses and interaction types, this first LXe TPC experiment at the tonne-scale will have significant discovery potential. In designing the experiment, we have built-in the possibility for a rapid sensitivity scale-up by another order of magnitude, by enabling a factor two to three larger LXe detector, named XENONnT, to fit into the same cryostat while re-using most of the other systems developed for XENON1T.

The year 2016 was a crucial one for XENON1T: we completed the commissioning of the experiment in all its various subsystems. After testing the cryogenic, purification and recovery systems in the spring, we filled the water shield and start the operations in a low background environment in July. During summer and fall, we performed the first ER and NR calibrations. At the same time, starting in October, we successfully distilled the krypton from xenon while running the experiment. At the end of November we started the first XENON1T science run, after reaching a record low background level below 10^{-3} $(\mathrm{kg}\cdot\mathrm{day}\cdot\mathrm{keV})^{-1}$.

In the following we detail the main progress in the various subsystems, achieved in 2016.

Figure 3: View of the XENON1T experiment in Hall B of the LNGS. The cryostat housing the dual-phase xenon TPC is hanging in the middle of the water tank. The service building with all equipment to support running the experiment, has three, fully packed, floors.

General Commissioning

The commissioning was completed in the second half of 2016. TPC and DAQ were fully commissioned after water tank filling, allowing calibration and characterization of the TPC for science data.

Muon Veto

In July 2016, the floor of the water tank was cladded with reflective foil and 24 of the remaining PMTs were installed on the floor of the water tank. This last step of the Muon Veto (MV) installation was followed by a commissioning of the Cherenkov detector in its final state: an average dark rate of 2 kHz at a threshold of 1 pe was observed, once the water tank was filled completely with water. The same DAQ and processing software as used for the TPC were adapted and validated for the MV system. To have the TPC and the MV working concurrently, the MV trigger output is sent to the TPC DAQ whether or not the MV DAQ is in a busy state; final tests of the GPS timing module are ongoing. To give more control of the calibration system during the commissioning phase, the slow control system for the LED pulser was improved to include an expert mode that allows to send specific commands to the pulse generator and to also generate scripts through the dedicated slow control SQL database. Finally, a study of the electronic noise reduction using a CRC (capacitance-resistance-capacitance) filter is being completed.

In the initial phases of the commissioning, the Water Tank (WT) was filled with water up to the nominal level while the cryostat was under vacuum, testing the system under extreme buoyancy conditions (never realized under routine operations). No worsening of the insulation

vacuum or any other failures of the cryostat were observed. However a small water leak (flow rate of less than 10 liters/day) was detected near the floor of Hall B. This prompted emptying of the WT. The company that built the WT subsequently performed a leak search using penetrating dye-liquid but no crack was found even after several repetitions. The anchoring points of the chains of the anti-buoyancy system, situated at the base of the support structure were sealed with stainless-steel boxes and were connected to a reinforcement stainless steel disk installed at the center of the WT on the floor. No leak was detected after this intervention.

Cryostat, Cryogenics, ReStoX

The commissioning tests of the integrated cryostat, cryogenics, purification, and ReStoX (storage) systems, the core xenon handling systems, were completed prior to the installation of the TPC. In February 2016, the collaboration completed an additional internal operative safety review to identify potential improvements and possibly recommend modifications to the core xenon handling systems and automated procedures to minimize detector downtime and risk of xenon loss. The recommendations were successfully implemented and thoroughly tested in March and April 2016, prior to the start of regular operations with the detector. The detector was filled with 3.3 tons of liquid xenon from ReStoX in mid-April 2016. The operation lasted about two weeks, reaching a filling speed of 650 kg/d after the initial cooldown period. The core xenon handling systems performance met or exceeded the design specifications and the filling operation was completed in the expected duration. The cryostat liquid nitrogen backup cooling system was commissioned shortly thereafter. With the cryostat filled, the cryogenic system has been in continuous operation for the following months, maintaining the liquid xenon at constant temperature and pressure (temperature RMS < 0.04 ° C, pressure RMS 1 mbar).

Slow Control

The Slow Control System has made significant progress on its interfaces to the experiments collaborators and its infrastructure. Throughout the ongoing commissioning, the system has controlled the experiments equipment, reported alarms and provided graphic tools for visualizing the data collected. In the second half of 2016 we have seen a significant consolidation of all parts of the system, adding features and increasing reliability. The web viewer that displays the current values and recent trends of most significant variables for collaborators anywhere is now more interactive. The Historian Analysis program allows plotting historical variables and correlations. User, shifter and expert roles have been defined with appropriate rights and the login system has been set up to apply them. Experts can securely control the system remotely. Major work is in progress to clarify all alarm messages and to append explanatory text from a manual to the alarm messages sent by email and cellular text messages. A second collaboration site is now monitoring the heartbeat from the alarm notification service and will signal the collaboration if the Slow Control system is unable to send alarms from LNGS. In addition to enhancing the Cryogenic, Purification, ReStoX, Kr Distillation, TPC and Muon Veto PMT High Voltage and water circulation systems that have been operating for some time, more equipment has been included: the TPC HV supply, TPC LXe level meters, and the LED pulsers for PMT calibration. The control of the motors for positioning the radioactive calibration sources is fully operational. The control and monitoring of two additional QDrive pumps is now being added (see also next section). Variables critical to the safety of the experiment are now being exchanged with the LNGS Safety System. Key variables are now exchanged with the Data Acquisition system. Upcoming plans include installing a control room above ground at LNGS, continuing the development of the high-level control software to orchestrate the transitions between various

operating modes, and deploying the machinery for exporting data for use in the science data analysis.

Purification, Distillation Column

The purification system has been in continuous use since the detector was filled in April 2016. A combination of liquid and gaseous xenon were extracted from the detector for electronegative purification at a flow rate of around 50 SLPM, reaching an electron drift lifetime on the order of a hundred microseconds. An upgrade of the recirculation pumps has been performed to reach the targeted electron lifetime (> 1 ms) on a shorter timescale. In particular, additional QDrive pumps were added to the purification system so that two pumps can work in series on each of the two purification circuits, allowing an increased flow with lower demands on each pump. This is expected to improve the electron drift lifetime as well as the stability of the pumps. The pump upgrade also includes the addition of new temperature and pressure sensors, which will provide more information about the performance of individual parts of the purification system and should prevent potential pump failures.

Removal of Kr and other light noble gases out of Xe with the dedicated cryogenic distillation column is on-going without any problems and with great success. The offline RGMS investigation of the sample taken at a He-removal campaign in spring resulted in a krypton-in-xenon concentration of (12 ± 24) ppq (1 ppq $= 10^{-15}$) or upper limits of < 48 ppq (< 56 ppq) at 90% CL (95% CL) respectively [20]. This demonstrates that the cryogenic distillation column is clearly surpassing the purity requirements even for XENONnT not only at test experiments in the laboratory but also with the full phase-2 column at XENON1T at LNGS. The purity of the xenon in the XENON1T detector was at the ppb level in summer because the majority of it was not distilled yet. A full distillation campaign of the whole XENON1T inventory would take about 2 months. Therefore to not lose time in improving the detector performance and effective electron lifetime an interrupted online-distillation is being performed since summer: a fraction of the xenon sent to the purification system to remove electronegative impurities is passed through the cryogenic distillation column. The online monitoring of the krypton-in-xenon concentration by an RGA-system at the distillation column and the ^{85}Kr determination by the XENON1T detector itself showed a krypton removal time constants below 10 days in this online mode, which was fast enough to favor online distillation against a full distillation of the XENON1T inventory into ReSToX and back into XENON1T. Some additional valves and pipes were installed to allow a free adjustment of the xenon fluxes from the LXe and the GXe reservoirs of the XENON1T detector, which are cycled through the cryogenic distillation column, in future. These new connections allow also to run the cryogenic distillation column in radon-removing online-mode as having been tested at XENON100 nearly two years ago.

At the end of November the Kr concentration reached the few ppt level, such that the ER background from Kr was smaller than the one from ^{214}Pb in the ^{222}Rn chain. This set the start of the first XENON1T science run on November 22$^{\text{nd}}$.

Time Projection Chamber and Photomultipliers

XENON1T is fully filled with liquid xenon since April 2016 and soon after, the electric fields of the TPC have been established. In order to benefit from low field quenching and therefore more scintillation light and thus better electron recoil rejection, we are currently operating at the same drift field as LUX (0.12 kV/cm). The extraction field is around 10 kV/cm which ensures 100% electron extraction efficiency. High voltage operation is stable and only occasionally affected by sudden changes in the detectors thermodynamic conditions (usually occurring during

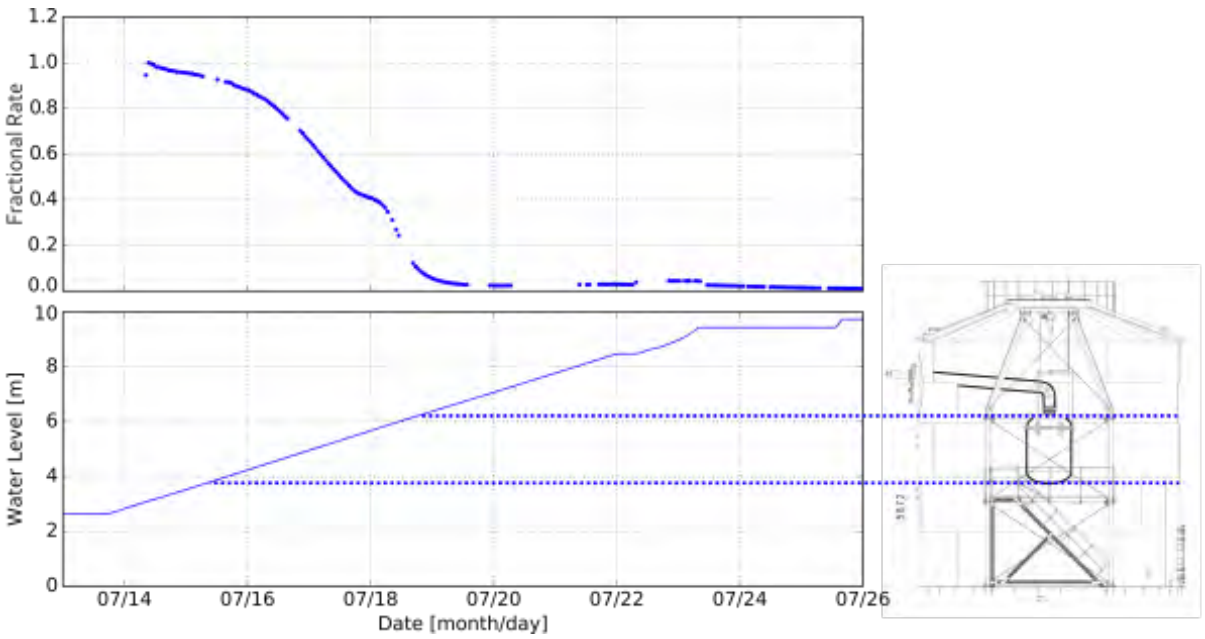

Figure 4: The relative rate observed in the detector and the water level in the water tank as a function of time.

commissioning actions). The diving bell system allows us to keep the liquid xenon level constant for several months. Initially, the TPC has been levelled using the feedback from its four precision level sensors. The charge signal response thus does not show any significant azimuthal variation.

In April 2016, the detector was cooled with xenon gas down to 175 K at the rate of 0.36 K/hour, and filled with liquid xenon over a two weeks period; the 248 PMTs are in operation since then. An equalization of the PMT gains to 2.5×10^6 was performed at the beginning of September 2016, and are calibrated regularly (twice a week). Three independent calibration methods have been developed, based both on external LED light sources and low-intensity (single photon) scintillation pulses, and yield consistent results.

Calibration

The calibration systems are up and running, not least thanks to the good cooperation with LNGS safety personnel. Using ^{83m}Kr, calibration has been performed routinely on XENON1T. Regarding ^{220}Rn, the calibration was successfully performed on XENON100 [1], and extensively used in fall 2016 to characterize the ER band of XENON1T. The NR band calibration has been performed by means of neutrons from an AmBe source, since mid October, for a few weeks. Finally, the neutron generator has been characterized in detail and has been delivered to LNGS to be used for nuclear recoil calibrations. Our thanks go to LNGS safety staff for their help in making these sources available to the XENON1T experiment.

Data acquisition and Electronics, Data Processing, Computing and Analysis

The XENON1T data acquisition system has been installed and is operational since the end of 2015. The DAQ system has allowed us to characterize the performance of the TPC. We recorded first signals when the TPC was initially filled with xenon gas and recorded first S1/S2 coincidences in April, after it was filled with liquid xenon, even before there was water in the

active muon veto system. After the LXe filling, we saw a high rate of relatively small pulses from the TPC which stressed the DAQ system up to our highest anticipated calibration rates. In the second half of 2016, we have focused on enhancing various parts of the DAQ to handle extreme rates and removing bottlenecks. This included additional hardware purchases (e.g., two more machines to read out the ADC system, swapping traditional disks for solid-state disks), redistribution of software over different computers, and optimizing the data acquisition and triggering software. The DAQ software has now been benchmarked at sustained data rates at up to 500 MB/s. While the DAQ is capable of handling these high rates, they are not expected during regular dark matter data-taking due to the extremely low external backgrounds. This is illustrated in figure 4, where we show the relative DAQ trigger rate dropping by almost three orders of magnitude as the water level increases in the muon veto. The high-energy veto, which will also substantially reduce the acquisition rates during detector calibration, has been commissioned.

Finally, with the filling of the water tank, we were able to also include the commissioning of the muon veto data acquisition system. While the muon veto and the TPC are operated by two independent hardware systems, they share the same underlying DAQ and are controlled by the same run control system.

At the end of April 2016 a new host and a Fiber Channel Storage Array were installed at the computing center of LNGS which should serve as data management (data transfer, offline monitoring, RAID6 management) and database server. A virtualization system called PROXMOX was installed in the host in order to create and manage different Virtual Machines to handle the different tasks. The XENON1T data which come from DAQ, are stored in a buffer, configured as RAID6, and then transferred to other XENON1T farms located outside LNGS, like OSG/Midway (Chicago), and PDC (Stockholm) ready to be processed. Tools for synchronization and book-keeping of the datastream were developed and test, and a tape storage backup has been commissioned at PDC. In addition to the external XENON farms, the data will also be transferred to EMI GRID storage elements for reprocessing purposes. At the end of July 2016 another host was installed at the LNGS computing center which should serve as container services (such as home user, wiki or SVN) for XENON1T users. PROXMOX was also installed in the host, which will guarantee, together with the hardware configuration, a complete redundancy in case of software/hardware failure.

While all systems were undergoing commissioning, we continued data taking and analysis for TPC commissioning/characterization, initial calibration and background assessment. In particular, we have observed both S1 and S2 signals. The light yield for S1 is studied by analysis of ^{83m}Kr and ^{137}Cs calibration data and alpha tagging. S2 signals could be detected in the entire active region of the detector. This is true also for the bottom of the detector, see further figure 5. Turning to the backgrounds, we measured the level of radon. The design sensitivity of XENON1T [21] was calculated assuming a ^{222}Rn concentration of 10 Bq/kg of LXe. The analysis based on counting the α-events following the Rn decay indicates that this concentration was achieved, even without employing on-line reduction techniques. With ^{85}Kr reduced to the ppt level, the resulting overall ER background rate at the beginning of the science run was already below 10^{-3} $(\mathrm{kg} \cdot \mathrm{day} \cdot \mathrm{keV})^{-1}$.

Monte Carlo Simulations

After the publication of the analysis of the XENON1T background and sensitivity in April 2016 [21], the focus of the MC working group has been dedicated mainly to the validation of the optical model against the first data coming from the detector, in particular the calibration with

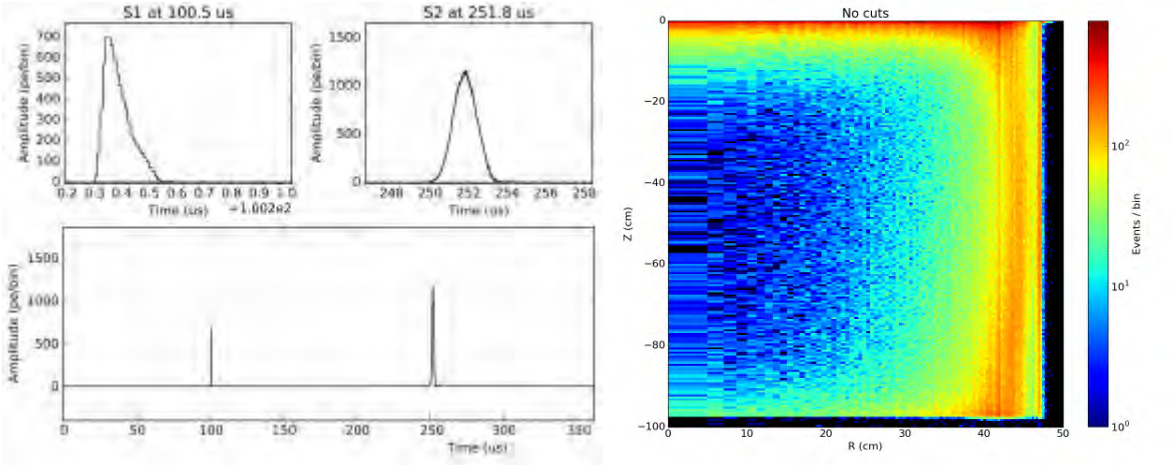

Figure 5: Left: Observed S1 and S2 signals from an interaction inside the middle of the TPC. Unidentified peaks have been suppressed for clarity. Right: Event distribution inside the TPC, radial versus depth coordinate. No cuts have been applied, but an identified S1/S2 pair was required for each event.

.

^{83m}Kr inside the TPC. The results are in agreement with the prediction of the Monte Carlo simulation, with a light yield in XENON1T which is twice the one obtained in XENON100. The MC group has also been involved in the refinement of the waveform generator, in order to produce MC data sets with the same characteristics of the data obtained from the experiment. In this way the MC data will be processed with the same analysis chain of the real data to correctly estimate all the efficiencies and acceptances of the various selection cuts.

4 Conclusions

During 2016 we completed several XENON100 analysis on the combination of the three main runs, for a total live-time of 17600 kg $\times$ d, and performed a successful test with a novel ^{220}Rn ER calibration. Meanwhile, we completed the commissioning of the XENON1T experiment in all its various subsystems. After testing the cryogenic, purification and recovery system in spring, in July we could fill the water shield and start the operations in a low background environment. During summer and fall, we performed the first ER and NR calibrations using with ^{220}Rn and AmBe, respectively. At the same time, starting in October we successfully continuously distilled the xenon from Kr while running the experiment, and at the end of November we could start the first XENON1T science run, after reaching a record low background level below 10^{-3} $(\mathrm{kg} \cdot \mathrm{day} \cdot \mathrm{keV})^{-1}$.

5 List of Publications

The XENON Collaboration published the following papers during 2016:

- "Physics reach of the XENON1T dark matter experiment ", E. Aprile *et al.* [XENON Collaboration], JCAP 1604 (2016) no.04, 027; arXiv:1512.07501 [physics.ins-det]

- "Low-mass dark matter search using ionization signals in XENON100 ", E. Aprile *et al.* [XENON Collaboration], Phys.Rev. D94 (2016) no.9, 092001, Erratum: Phys.Rev. D95 (2017) no.5, 059901; arXiv:1605.06262 [astro-ph.CO]
- "Search for two-neutrino double electron capture of ^{124}Xe with XENON100", E. Aprile *et al.* [XENON Collaboration], Phys.Rev. C95 (2017) no.2, 024605; arXiv:1609.03354 [nucl-ex]
- "XENON100 Dark Matter Results from a Combination of 477 Live Days", E. Aprile *et al.* [XENON Collaboration], Phys.Rev. D94 (2016) no.12, 122001; arXiv:1609.06154 [astro-ph.CO]
- "Results from a Calibration of XENON100 Using a Source of Dissolved Radon-220", E. Aprile *et al.* [XENON Collaboration], Phys.Rev. D95 (2017) no.7, 072008; arXiv:1611.03585 [physics.ins-det]
- "Removing krypton from xenon by cryogenic distillation to the ppq level", E. Aprile *et al.* [XENON Collaboration], Eur.Phys.J. C77 (2017) no.5, 275; arXiv:1612.04284 [physics.ins-det]

References

[1] **XENON** Collaboration, E. Aprile *et al.* "Results from a Calibration of XENON100 Using a Source of Dissolved Radon-220", Phys.Rev. D95 (2017) no.7, 072008; arXiv:1611.03585 [physics.ins-det]

[2] **DAMA** Collaboration, R. Bernabei *et al.*, "First results from DAMA/LIBRA and the combined results with DAMA/NaI," *Eur. Phys. J.* **C56** (2008) 333, `arXiv:0804.2741`.

[3] **XENON** Collaboration, E. Aprile *et al.* "Dark Matter Results from 225 Live Days of XENON100 Data," Phys. Rev. Lett. **109**, 181301 (2012) [arXiv:1207.5988 [astro-ph.CO]].

[4] **PICO** Collaboration, C. Amole *et al.*, "Dark matter search results from the PICO-60 CF_3I bubble chamber," *Phys. Rev.* **D93** no. 5, (2016) 052014, `arXiv:1510.07754`.

[5] **XENON** Collaboration, E. Aprile *et al.*, "A low-mass dark matter search using ionization signals in XENON100," `arXiv:1605.06262`.

[6] **PandaX-II** Collaboration, A. Tan *et al.*, "Dark Matter Results from First 98.7-day Data of PandaX-II Experiment," `arXiv:1607.07400`.

[7] **LUX** Collaboration, D. S. Akerib *et al.*, "Results from a search for dark matter in LUX with 332 live days of exposure," `arXiv:1608.07648`.

[8] **DarkSide** Collaboration, P. Agnes *et al.*, "Results from the first use of low radioactivity argon in a dark matter search," *Phys. Rev.* **D93** no. 8, (2016) 081101, `arXiv:1510.00702`.

[9] **XENON** Collaboration, E. Aprile *et al.*, "Low-mass dark matter search using ionization signals in XENON100 ", Phys.Rev. D94 (2016) no.9, 092001, Erratum: Phys.Rev. D95 (2017) no.5, 059901; arXiv:1605.06262 [astro-ph.CO]

[10] **XENON** Collaboration, E. Aprile *et al.*, "Search for two-neutrino double electron capture of ^{124}Xe with XENON100", Phys.Rev. C95 (2017) no.2, 024605; arXiv:1609.03354 [nucl-ex]

[11] **XENON** Collaboration, E. Aprile *et al.*, "XENON100 Dark Matter Results from a Combination of 477 Live Days", Phys.Rev. D94 (2016) no.12, 122001; arXiv:1609.06154 [astro-ph.CO]

[12] **LUX** Collaboration, D. S. Akerib *et al.*, "First spin-dependent WIMP-nucleon cross section limits from the LUX experiment," `arXiv:1602.03489`.

[13] **PICO** Collaboration, C. Amole *et al.*, "Improved dark matter search results from PICO-2L Run 2," *Phys. Rev.* **D93** no. 6, (2016) 061101, `arXiv:1601.03729`.

[14] **DRIFT** Collaboration, J. B. R. Battat *et al.*, "First background-free limit from a directional dark matter experiment: results from a fully fiducialised DRIFT detector," *Phys. Dark Univ.* **9** (2014) 1, `arXiv:1410.7821`.

[15] **XENON** Collaboration, E. Aprile *et al.*, "Limits on spin-dependent WIMP-nucleon cross sections from 225 live days of XENON100 data," *Phys. Rev. Lett.* **111** (2013) 021301, `arXiv:1301.6620`.

[16] **DAMA** Collaboration, R. Bernabei *et al.*, "Investigating the DAMA annual modulation data in a mixed coupling framework," *Phys. Lett.* **B509** (2001) 197.

[17] **ZEPLIN-III** Collaboration, V. N. Lebedenko *et al.*, "Limits on the spin-dependent WIMP-nucleon cross-sections from the first science run of the ZEPLIN-III experiment," *Phys. Rev. Lett.* **103** (2009) 151302, `arXiv:0901.4348`.

[18] **CDMS** Collaboration, Z. Ahmed *et al.*, "Search for Weakly Interacting Massive Particles with the First Five-Tower Data from the Cryogenic Dark Matter Search at the Soudan Underground Laboratory," *Phys. Rev. Lett.* **102** (2009) 011301, `arXiv:0802.3530`.

[19] **SIMPLE** Collaboration, M. Felizardo, T. Girard, T. Morlat, A. Fernandes, A. Ramos, *et al.*, "Final Analysis and Results of the Phase II SIMPLE Dark Matter Search," *Phys. Rev. Lett.* **108** (2012) 201302, `arXiv:1106.3014`.

[20] **XENON** Collaboration, E. Aprile *et al.*, "Removing krypton from xenon by cryogenic distillation to the ppq level", Eur.Phys.J. C77 (2017) no.5, 275; arXiv:1612.04284 [physics.ins-det]

[21] **XENON** Collaboration, E. Aprile *et al.*, "Physics reach of the XENON1T dark matter experiment," *JCAP* **1604** (2016) 027, `arXiv:1512.07501`.

Cosmic Silence

L. Satta[a], E. Bortolin[b], C. De Angelis[b], G. Esposito[b], P. Fattibene[b], C. Nuccetelli[b], M. A. Tabocchini[a,b,*], E. Alesse[c], R. Iorio[c], M. Balata[d], L. Ioannuci[d], A. Esposito[e], O. Frasciello[e], M. Chiti[e], G. Cenci[a,f], F. Cipressa[a,f] PF. Morciano[f]

[a]Museo Storico della Fisica e Centro Studi e Ricerche Enrico Fermi
[b]Istituto Superiore di Sanitá, Technology and Health Department, and INFN-Roma1 Gr. coll. Sanitá, 00161 Roma, Italy
[c]LAquila University, Department of Biotechnological and Applied Clinical Sciences
[d]INFN - Gran Sasso National Laboratory
[e]INFN - Frascati National Laboratory
[f]La Sapienza University of Rome, "C. Darwin"Department of Biology and Biotechnologies
(*) Spokepersons

Abstract

A relevant role during the evolution of living organisms was played by natural background radiation of Earth and cosmic rays. However, it is not yet clear how chronic low doses of radiation can affect biological processes. A contribution in this field can be given by the Silence Cosmic project, funded by the Istituto Nazionale di Fisica Nucleare (INFN) and Centro Fermi (Italy). In this project the influence of the environmental radiation on the metabolism and the genotoxic stress response capability of in vitro and in vivo biological systems is studied. Parallel experiments are performed in different environmental conditions, i.e. at the underground Gran Sasso National Laboratory (LNGS), where a sharp reduction of environmental radiation, in particular for the directly ionizing cosmic rays and neutron components, is achieved and in reference laboratories located at the ISS/Sapienza University of Rome and at the LAquila University. Here we report the current status and the future developments of the in vivo experiments carried out using the fruit fly *Drosophila melanogaster* as model system. In order to allow a comprehensive interpretation of the obtained results in terms of biophysical mechanisms, a characterization of radiation field and of other environmental parameters, namely temperature, pressure and relative humidity in the experimental sites is ongoing.

1 Introduction

Natural variations of background radiation likely represented a critical role during the evolution and contributed to the development of still poorly characterized defense mechanisms to minimize genotoxic damage. The experiments carried out at the underground Gran Sasso National Laboratory (LNGS) of the Italian Institute of Nuclear Physics (INFN) on cultured mammalian

cells of rodent and human origin represent the largest evidence on the effects of reduced environmental radiation on eukaryotic cellular systems [1-6]. The unique characteristics of LNGS, where the presence of radiation is strongly reduced, made this laboratory the ideal place to host not only physic experiments and study rare events such as solar neutrino detection and proton decay, but also to explore the effects of low radiation on biological systems.
So far the overall scenario coming from long and short term in vitro experiments is that cells cultured underground LNGS in reduced environmental radiation conditions (Low Radiation Environment, LRE) are less tolerant to DNA damage and less efficient in scavenging reactive oxygen species than cells cultured in an external reference laboratory (Reference Radiation Environment, RRE), e.g. at the Istituto Superiore di Sanit (ISS, Rome) or at the external LNGS cell culture laboratory.
Recently, we started employing *Drosophila melanogaster*, the common fruit fly, as a multicellular model system to investigate whether the reduced background radiation at the LNGS affects development and growth of a complex multicellular organism. *Drosophila* is emerging as one of the most effective tools for analyzing the function of human disease genes, including those responsible for developmental and neurological disorders, cancer, cardiovascular disease, metabolic and storage diseases, and genes required for the function of the visual, auditory and immune systems [7-12]. Flies have several experimental advantages, including their rapid life cycle and the large numbers of individuals that can be generated, which make them ideal for sophisticated genetic screens, and in future should aid the analysis of complex multi-genic disorders. *Drosophila* has also been already used as an in vivo model to study radiation induced oxidative stress and radioprotective agents. More recently, many of the important neurotoxic side effects resulting from radiation therapy during development in humans have been mimicked in *Drosophila* suggesting that fruit flies can serve as a useful experimental model for studying the neurotoxic consequence of radiation exposure, and ultimately for identifying specific genes and proteins involved in the molecular mechanism of radiation-induced damage [13]. Although humans and fruit flies may not look very similar, it is widely accepted that most of the fundamental biological mechanisms and pathways that control development and survival are conserved across evolution between these species.

2 The Cosmic Silence facility for in vivo studies at the LNGS

The Cosmic Silence facility, located in the bypass of the LNGS, next to the PULEX cell culture laboratory, has been set up to perform in vivo experiments on living organisms of different complexity in the phylogenetic tree. In particular, the facility has been designed to host small animals (e.g. insects, worms, fishes) and also a 60 cages mice rack (Fig. 1). It is provided with temperature, humidity and light control systems as well as with an independent ventilation system.

Among the parameters routinely monitored, one of the most relevant, because related to the radiation environment, is the presence of radon. The monitoring carried out before starting the in vivo experiments indicated the need to increase the ventilation inside the laboratory being the values higher than expected. In the past, the measurements inside the underground facility were lower than those monitored in the external environment and only during a temporary failure of the ventilation system the radon level reached values around $100Bq/m3$.
Aware of this, we decided to start anyway the experiments with *Drosophila melanogaster*, with the precaution of keeping continuously monitored the radon levels.

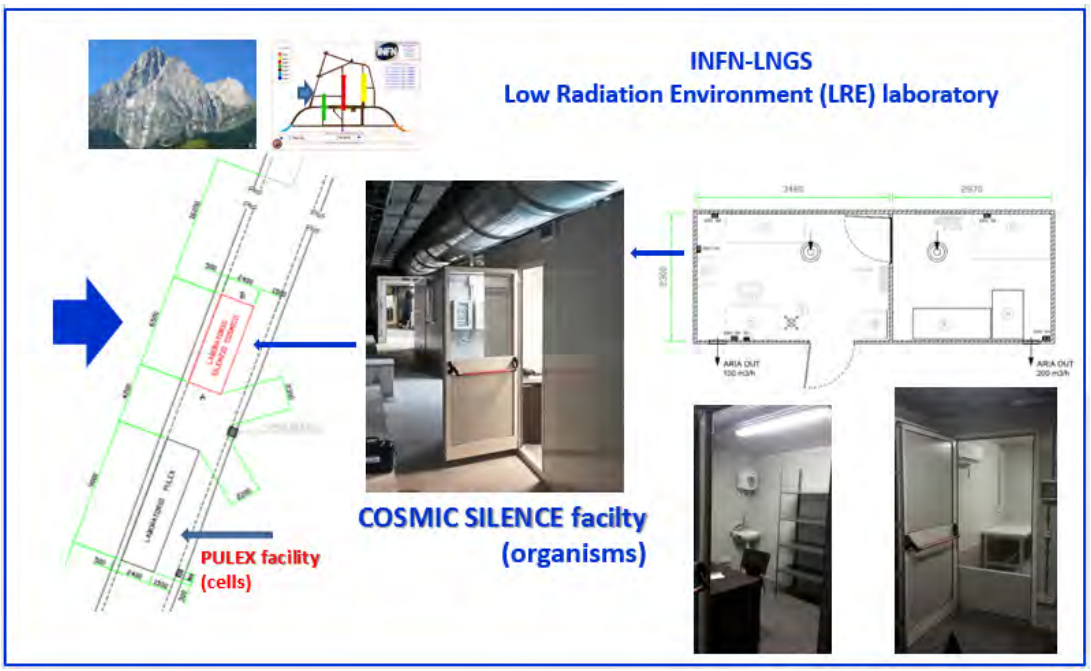

Figure 1: The Cosmic Silence facility for in vivo experiments on living organisms of different complexity.

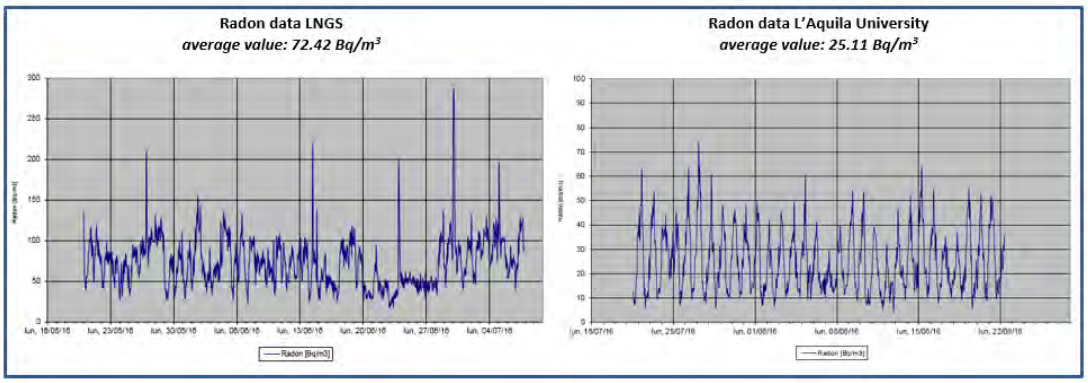

Figure 2: Radon monitoring inside the PULEX-COSMIC SILENCE facility and in the reference external laboratory (LAquila University).

Presently, the radon levels inside the facility are still higher than those in the reference laboratory (see Fig.2) and we are waiting for a solution to this problem.

3 Characterization of the radiation field and other environmental parameters in the different experimental sites

During the experiments, as reported above, we carried out radon monitoring in both underground and external reference laboratories using the Alfaguard equipment. As mentioned above, the

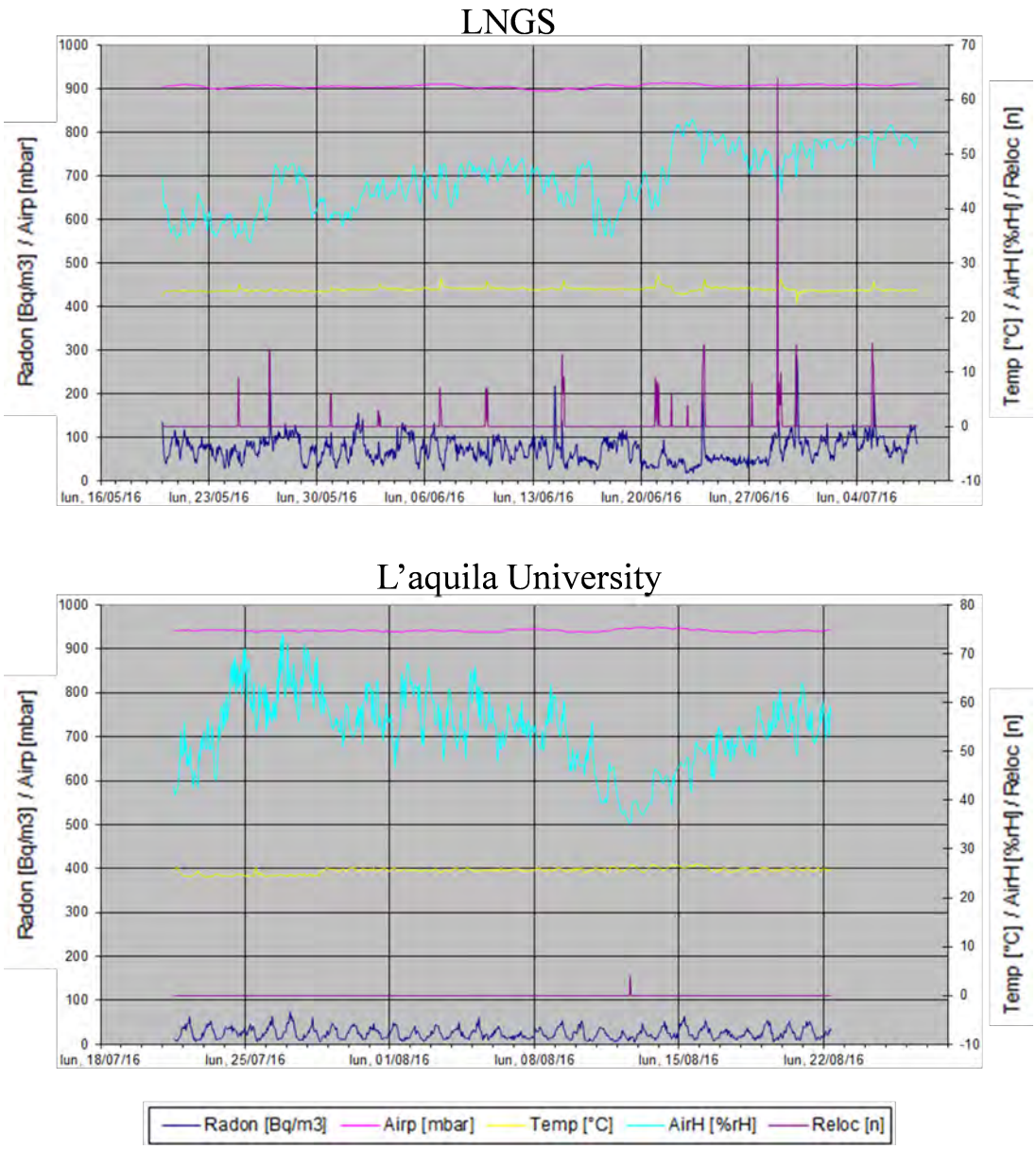

Figure 3: Output of the Alfaguard equipment showing, besides radon, the temperature, pressure and humidity in the different laboratories.

radon values in the underground facility are still higher than those at the reference laboratory. This aspect needs to be solved.
Besides radon, other environmental parameters, namely temperature, pressure and relative humidity have also been recorded by the Alfaguard equipment (see an example in Fig.3).

While the temperature was constant in the two experimental sites ($25.60.6C vs 25.20.4C$), we registered in the external laboratory a slight increase in the average values of pressure ($941.92.7mbar vs 906.74.0mbar$) and relative humidity ($54.17.6\% vs 45.55.6\%$). On the basis of the literature evidence, these mild differences can be considered negligible for the biology of *Drosophila*.

The dosimetric characterization of the different experimental sites where the biological experiments are performed is crucial for the interpretation of results. We have been carried out measurements of the gamma component in the PULEX facility and in two reference Laboratory, at the ISS and at the University of LAquila, using thermoluminescence dosimeters, specifically TLD-700H. We found that the dose rate due to gamma components of the radiation background in the underground (incubator shielded with 5 cm thick iron) laboratory is about 50-fold lower compared to the external laboratory at ISS and about 16-fold lower with respect to the one at LAquila University. The incubator structure induces a shielding effect corresponding to a dose reduction inside of about 20%. The iron shield reduces the dose rate inside the incubator of about 70 %. A new campaign of dose rate measurements is scheduled in the new COSMIC SILENCE facility where, due to the absence of incubators, some, although small, variations in the radiation environment are expected with respect to the PULEX facility. The dose rate monitoring of the other sites will continue in parallel. As for the planned simulations, they should be carried out by students of the Milano-Bicocca University, supervised by the Prof. Maura Pavan. They will help to better understand the distribution, spectrum and composition of the background radiation inside the facilities and, by installing some radiation monitors, to verify or calibrate the predictions.

4 Influence of radiation environment on the life span, fertility and DNA repair genes of *Drosophila melanogaster*

We used *Drosophila melanogaster* as a multicellular model system to investigate whether the reduced background radiation at the LNGS affects development and growth of a complex multicellular organism. We sought to compare different developmental parameters, such as life span, fertility and motility activity, between flies maintained for different generations at the LNGS (Low Radiation Environment, LRE) and at the reference Laboratory at LAquila University (Reference Radiation Environment, RRE).

Life span test

For the life span test, we have checked the survival of a standard wild-type line (Oregon-R). Flies were collected up to a $2-3$ days and sorted males transferred to fresh vials (10 males per vial) containing standard medium and aged at $25C$ in both LRE and RRE laboratories. Flies were transferred to fresh food every 3 days, at which time the number of surviving males was recorded. Each experiment was carried out on at least 30 flies for generation. Starting from April 2016, single populations (referred to as A and B) were consecutively raised at LRE with A indicating the population brought to LRE the first month and B the population brought the next month and so on. For sake of clarity, each generation was indicated as the exponent of each population so that, for instance, B4 indicates the $4th$ generation from population B. We have also maintained the same fly lines in the RRE, which is very close to LNGS ($5km$). These flies were referred to as R. We found that the median life span in A6, A8 and B1 generations was significantly increased by 20%, 7% and 15%, respectively, relative to that of R wild-type flies indicating that reduction of natural background radiation alters the survival ratio (Fig. 4).

Motility test

To assess whether LNGS background radiation influenced locomotion, we examined climbing activity of wild-type adults from A^9, A^12, B^1 and B^7 and from R flies. Climbing activity tests were then repeated on the same individuals that were aged for additional 30 days. These analyses revealed that the locomotive behavior of LRE flies was not different from that exhibited by R

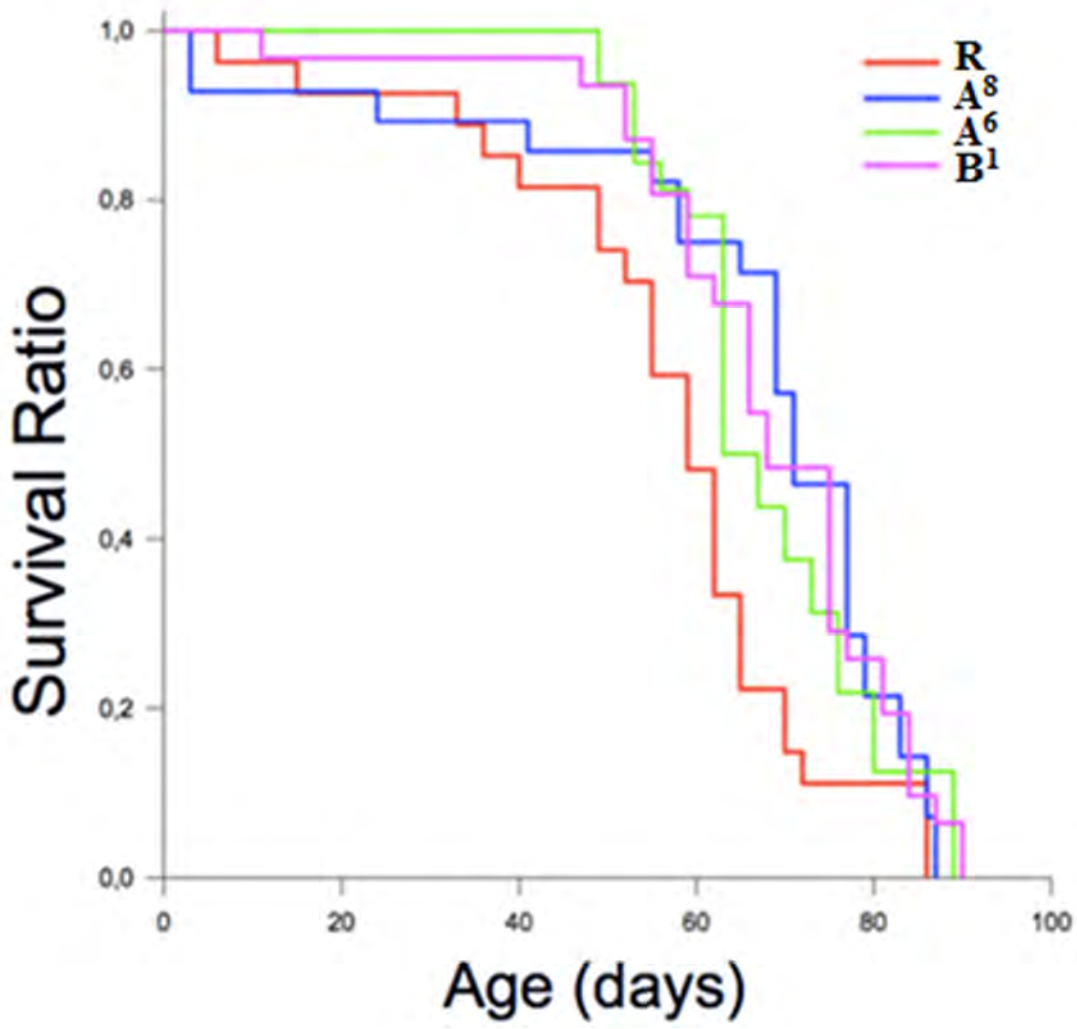

Figure 4: Reduced background radiation extends the lifespan of males flies. Kaplan-Meier survival curves are shown for the reference (R) and LNGS Oregon flies from generation A^8, A^6, and B^1 with p values calculated using the log-rank test. Pairwise multiple comparison by the Holm-Sidak method demonstrated a significant extension in median life span in A^8 (median survival = 71 ± 2.6 days; log-rank = $6,339$; p = $0,0118$), A^6 (median survival 63 ± 2.0 days; log-rank = $6,590$; p = $0,0103$), and B^1 (median survival 68 ± 3.0 days; log-rank = $6,283$; p = $0,0122$) flies compared with line R (median survival = 59.0 ± 2.6). Survival was assessed from 30 males flies.

flies even after aging (data not shown).

Fertility tests

Fertility tests that were performed on both wild-type Oregon male and female adults from the same generation time have shown that LNGS background radiation reduces by 30% the fertility of both male and female adults (Fig. 5). Interestingly, fertility reduction is an early effect and remained unchanged along different generation time.

To verify a possible influence of low radiation background on the response on genotoxic stress, we analyzed the effect of LRE environment on the growth of 3 different *Drosophila* mutants

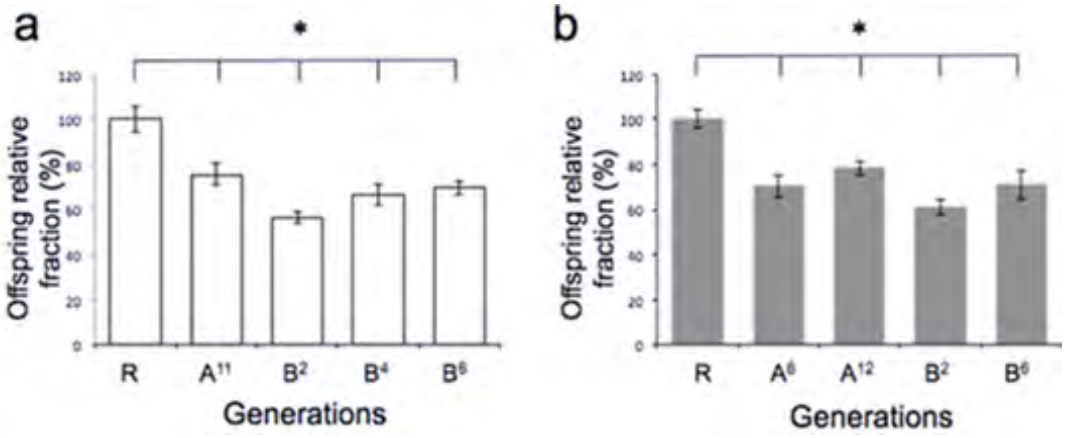

Figure 5: Fertility tests of Oregon females (a) and males (b) that were isolated from two independent lines (A and B) after different generations (exponents) kept at LNGS. Columns indicate the fraction of progeny relative to the progeny observed in the reference laboratory (R) from 4 independent crosses of either one LRE female or male with 2 R males or females, respectively. For all generations tested, the progeny/adult ratio from each fertility test at LRE is significantly reduced ($p < 0.01$) compared to that observed at RRE (R). (*) $p < 0.01$ (ANOVA test followed by Holm-Sidak test). Bar indicates SEM.

with defective DNA repair and which, as a consequence, are sensitive to genotoxic stress. As expected, these mutants are semi-lethal (that is only rare adults are found) if raised on RRE. Surprisingly, only for one of these (the tefu mutant line, bearing a mutation in the ATM encoding gene), we found that the number of adults was much higher (20% vs 1.3%) than that observed at RRE, indicating that LRE conditions positively select the survival of flies with little ATM protein (adults from the remaining mutants were as rare as in RRE) (Fig.6). To rule out that this outcome was due to a spurious effect in the genome of this mutant line, we have replaced all chromosomes, but the one with the mutation, with different chromosomes (nb lines) and found the same results (Fig. 7). This indicated that the positive selection at LRE was specific to the mutation. Moreover, we observed that this effect is also maintained if LRE mutant lines are moved and kept to RRE for 2 more generations indicating that it is retained in a trans-generational manner. Why this takes place only for mutations in ATM encoding gene seeks further investigation.

All of these results have been extensively discussed in our published paper [14].

5 Acknowledgements

We are indebted with M. Belli the interesting discussions and suggestions

6 References

1. L. Satta, G. Augusti-Tocco, R. Ceccarelli, A. Esposito, M. Fiore, P. Paggi, I. Poggesi, R. Ricordy, G. Scarsella, E. Cundari. *Low environmental radiation background impairs biological defence of the yeast Saccharomyces cerevisiae to chemical radiomimetic agents.* Mutat. Res. 347(3-4):129-33, 1995

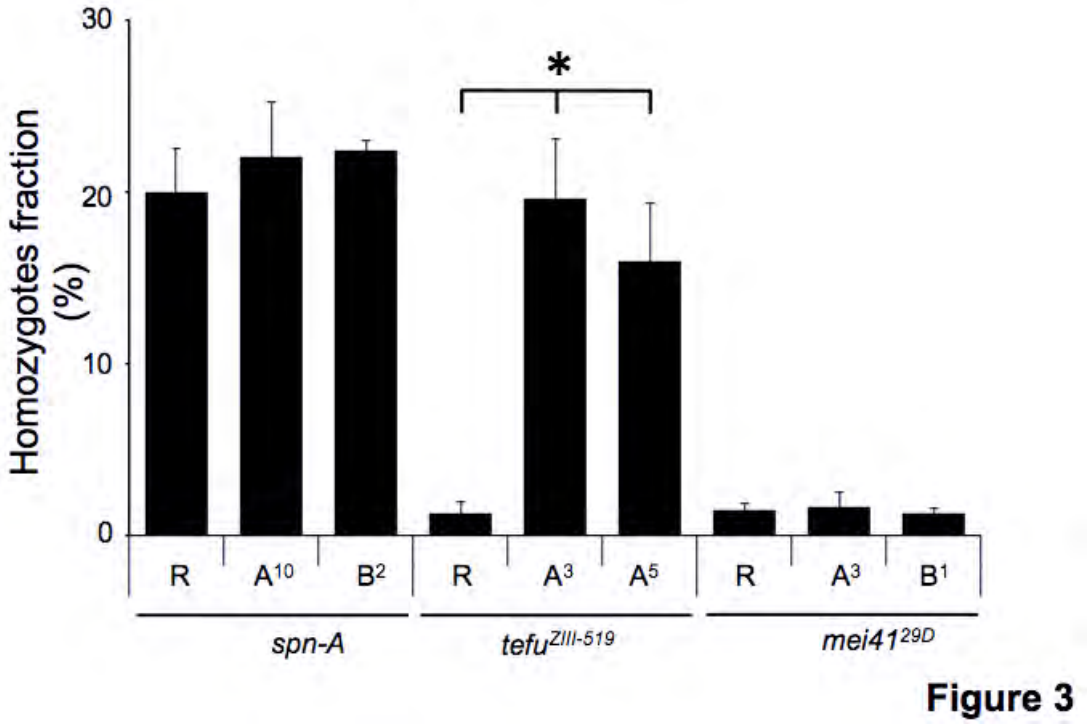

Figure 6: Effects of reduced background radiations on DNA-repair gene mutants. Columns show the percentage of homozygotes/total progeny from independent spn-A, tefu and mei41 lines maintained either at LRE (A, B) or at RRE (R). Homozygotes were scored at different generation times (exponents). (*) $p < 0.01$ (ANOVA test followed by Holm-Sidak test). Bar indicates SEM.

2. L. Satta, F. Antonelli, M. Belli, O. Sapora, G. Simone, E. Sorrentino, M.A. Tabocchini, F. Amicarelli, C. Ara, M.P. Cer, S. Colafarina, L. Conti Devirgiliis, A. De Marco, M. Balata, A. Falgiani, S. Nisi. *Influence of a low background radiation environment on biochemical and biological responses in V79 cells.* Radiat. Environ. Biophys. 41 (3):217-24, 2002

3. M.C. Carbone, M. Pinto, F. Antonelli, F. Amicarelli, M. Balata, M. Belli, L. Conti Devirgiliis, L. Ioannucci, S. Nisi, O. Sapora, et al. *The Cosmic Silence Experiment: on the putative adaptive role of environmental ionizing radiation.* Radiat. Environ. Biophys. 48:189-196, 2009

4. M.C. Carbone, M. Pinto, F. Antonelli, F. Amicarelli, M. Balata, M. Belli, L. Conti Devirgiliis, O. Sapora, G. Simone, E. Sorrentino, M.A. Tabocchini, L. Satta. *Effects of deprivation of background environmental radiation on cultured human cells.* Il Nuovo Cimento 4:469-477, 2010

5. E. Fratini, C. Carbone, D. Capece, G. Esposito, G. Simone, M.A. Tabocchini, M. Tomasi, M. Belli, L. Satta. *Low-radiation environment affects the development of protection mechanisms in V79 cells.* Radiat. Environ. Biophys. 54(2):183-94, 2015

6. E. Fratini, M.F. Fischietti, G. Simone, E. Bortolin, C. De Angelis, G. Esposito, P. Fattibene, C. Nuccetelli, C. Quattrini, M. A. Tabocchini, E. Alesse, A. Tessitore, F. Zazzeroni,

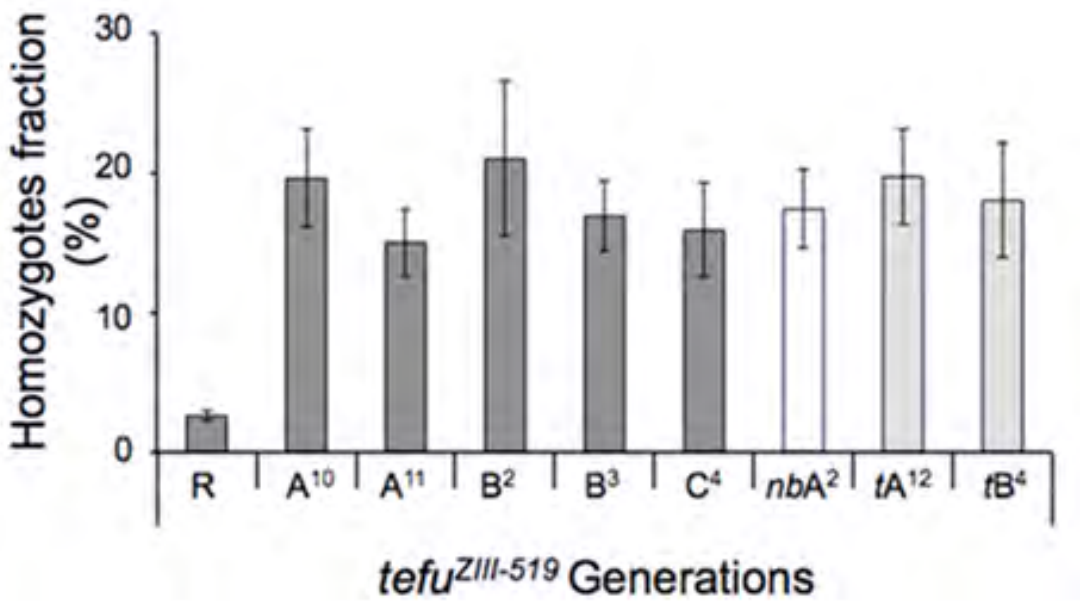

Figure 7: LRE is beneficial to tefu mutants. Columns indicate the proportion (%) of tefu homozygotes obtained from mating ten 3-day old tefu heterozygous females to ten 3-day old tefu heterozygous males. Each column represents results from at least 4 independent crosses. Capital letters refer to tefu mutant lines brought to LRE at different times, while exponents indicate the number of generations from each progenitor line. nb (new balanced) A^2 refers to a tefu mutant line in which the original chromosomes and balancers have been replaced by other multi inverted chromosomes, while t (transgenerational)A^12 and tB^4 columns refer to the A^12 and B^4 LRE lines moved to RRE and maintained for 2 more generations. R= RRE lines. Bar indicates SEM.

M. Balata, L. Ioannuci, A. Esposito, M. Chiti, O. Frasciello, L. Satta, M. Pavan, G. Cenci. Cosmic Silence. *LNGS Annual Report* 202-212, 2015

7. E. Bier. *Drosophila, the Golden Bug, Emerges as a Tool for Human Genetics.* Nat. Rev. Genetic 6(1):9-23, 2005

8. J. Bilen, N.M. Bonini. 2005. *Drosophila as a model for human neurodegenerative disease.* Annu Rev Genet 39:153-171.

9. K. Ocorr, T. Akasaka, R. Bodmer. 2007. *Age-related cardiac disease model of Drosophila.* Mech Ageing Dev 128(1):112-116.

10. W.O. Miles, N.J. Dyson, J.A. Walker. 2011. *Modeling tumor invasion and metastasis in Drosophila.* Dis Model Mech 4(6):753-761.

11. I. Kounatidis, P. Ligoxygakis. 2012. Drosophila *as a model system to unravel the layers of innate immunity to infection.* Open Biol 2(5):120075.

12. M.J. Moulton, A. Letsou. 2016. *Modeling congenital disease and inborn errors of development in* Drosophila *melanogaster.* Dis Model Mech 9(3):253-269.

13. N. Nakamura, A. Suyama, A. Noda, Y. Kodama. 2013. *Radiation effects on human heredity.* Annu Rev Genet 47:33-50.

14. P. Morciano, R. Iorio, D. Iovino, F. Cipressa, G. Esposito, A. Porrazzo, L. Satta, E. Alesse, M.A. Tabocchini and G. Cenci. 2017. *Effects of reduced natural background radiation on* Drosophila *melanogaster growth and development as revealed by the FLYINGLOW program.* Journal of Cellular Physiology (doi: 10.1002/jcp.25889. [Epub ahead of print].

7 List of publications and international meetings presentations

- G. Esposito, P. Anello, I. Pecchia, M.A. Tabocchini, A. Campa (2016). Facility for gamma irradiations of cultured cells at low dose rates: design, physical characteristics and functioning. *Appl. Radiat. Isot.* 115: 227-234

- F. Cipressa, P. Morciano, S. Bosso, L. Mannini, A. Galati, G.D. Raffa, S. Cacchione, A. Musio A, G. Cenci. (2016). A role for Separase in telomere protection. *Nat Comm*, 7:10405 doi: 10.1038/ncomms10405.

- A. Cicconi, E. Micheli, F. Vern, A. Jackson , A. Gradilla, F. Cipressa, D. Raimondo, G. Bosso, J. Wakefield, L. Ciapponi, G. Cenci, M. Gatti, S. Cacchione, G. Raffa. (2016). The *Drosophila* telomere-capping protein Verrocchio binds single-stranded DNA and protects telomeres from DNA damage response. *Nucleic Acid Research* Dec 9. pii: gkw1244. [Epub ahead of print].

- De Angelis, E. Bortolin, P. Fattibene, M.C. Quattrini, M.A. Tabocchini. *Use of TLD-700H for environmental measurements.* 18th International Conference on Solid State Dosimetry, Munich, 3-8 July 2016.

- F. Cipressa, P. Morciano, G. Esposito, R. Iorio, L. Satta, M.A. Tabocchini, and G. Cenci. *FLYINGLOW: biological effects of protracted low radiation doses in Drosophila melanogaster.* Italian *Drosophila* Research Conference (IDRC) 2016 Bologna 14-16 settembre 2016.

- M.A. Tabocchini. *Challenging the LNT model: lines of evidence for sublinear cancer risk extrapolation.* Radiation Protection Week 2016 (RPW2016), Oxford, UK, 19 - 23 September 2016.

- F. Cipressa, P. Morciano, G. Esposito, R. Iorio, L. Satta, M.A. Tabocchini, and G. Cenci. *FLYINGLOW: biological effects of protracted low radiation doses in Drosophila melanogaster.* Radiation Protection Week 2016 (RPW2016), Oxford, UK, 19 - 23 September 2016.

- F. Cipressa, P. Morciano, G. Esposito, R. Iorio, A. Tabocchini and G. Cenci. *FLYINGLOW: effects of protracted low radiation doses on Drosophila metabolism.* 102 Congresso della Societ Italiana di Fisica (SIF), Padova 26-30 settembre 2016.

ERMES
^{137}Cs and ^{134}Cs in Spain after the Fukushima Dai-Ichi NPP accident

Arturo Vargas[a], Antonia Camacho[a],
Matthias Laubenstein[b], Wolfango Plastino[c,d]

[a] Universitat Politècnica de Catalunya, Institut de Tècniques Energètiques, Spain
[b] National Institute of Nuclear Physics (INFN), Gran Sasso National Laboratory, Italy
[c] Roma Tre University, Department of Mathematics and Physics, Italy
[d] National Institute of Nuclear Physics (INFN), Section of Roma Tre, Italy

Abstract

Samples were collected in Barcelona with a high-volume airborne particulate sampling system, and with a dry and wet deposition collection system for subsequent analysis. Within the framework of the Environmental Radioactivity Monitoring for Earth Sciences (ERMES) research project the filters were measured at the Gran Sasso National Laboratory. This has enabled the characterization of dry velocity deposition for ^{134}Cs and ^{137}Cs. Results show a dry velocity deposition of 0.07 cm s^{-1}.

1 Introduction

Weekly airborne particulate samples have been routinely collected at the Campus-Sud surveillance radiological station at the Institut de Tècniques Energètiques (INTE) of the Technical University of Catalonia (UPC) in Barcelona (Spain), and measured using a high-volume air sampling system since March 2000. There was no evidence of detection of ^{131}I and ^{134}Cs in air in Barcelona, before March 23^{rd} 2011, although small amounts of ^{137}Cs were detected in about 10 % of filters of high-volume air sampling [1]. In Barcelona, radioisotopes released from Fukushima Dai-ichi NPP were detected at first by the high-volume air sampling filter during the period of 23^{rd}-28^{th} March 2011 and were detectable until $11t^{th}$ May 2011. The maximum values of ^{137}Cs and ^{134}Cs were observed in the filter collected from 1^{st} to 4^{th} of April 2011. Meteorological conditions in the Iberian Peninsula during the sampling period were characterized mainly by a low pressure gradient leading to low synoptic forcing which did not favor transport across the Iberian Peninsula. Then, the characterization of ^{134}Cs and ^{137}Cs dry velocity deposition is an important parameter that is needed to improve atmospheric transport models. As the activity of the dry deposition collected falls below MDA measurable at surface laboratories, within the ERMES research project the collected filters were measured at the Gran Sasso National Laboratory of the Istituto Nazionale di Fisica Nucleare (INFN-LNGS) [2].

2 Results and discussion

The measured deposition fluxes were 0.024 μBq s^{-1} m^{-2}, 0.039 μBq s^{-1} m^{-2}, for ^{134}Cs and ^{137}Cs, respectively. The deposited flux of ^{137}Cs is larger than ^{134}Cs because of the larger radioactivity of ^{137}Cs measured in the dry deposition filter, 1.3 $\pm$ 0.5 mBq and 2.1$\pm$ 0.7 mBq, for ^{134}Cs and ^{137}Cs, respectively. The reason for this difference may be explained by the contribution of the re-suspended ^{137}Cs particles that were deposited on the ground from the Chernobyl NPP accident and nuclear weapons tests [2]. The ^{137}Cs volumetric activity in the air over Barcelona due to re-suspension, according to the average and the standard deviation of the mean for the 28 filters in which ^{137}Cs was detected in the period 2006-2010, was 0.53 $\pm$ 0.10 μBq m^3 [3]. Therefore, if we consider that the dry deposition velocity is 2.4 cm s^{-1}, an activity contribution in the deposited filter from re-suspension can be estimated to be 0.7 $\pm$ 0.4 mBq. Subtracting this 0.7 mBq from the measured 2.1 mBq, indicates that the ^{137}Cs deposited activity from the Fukushima Dai-ichi NPP is about 1.4 $\pm$ 0.7 mBq. Therefore the value attributable to the flux of ^{137}Cs of Fukushima origin is 0.026 $\pm$ 0.014 μBq s^{-1} m^{-2} [2]. Finally, it should be pointed out that the deposition velocities measured in a city show significant differences due to the substrate characteristics and, therefore, standardization in terms of sampling site characteristics and sampling method is desirable for comparability of results [4].

3 Conclusion

The dry deposition velocity measured for both ^{137}Cs and ^{134}Cs from Fukushima Dai-ichi NPP in Barcelona was approximately 0.07 cm s^{-1}, taking into account the contribution from re-suspended ^{137}Cs, which is subtracted from the total activity measured in the dry deposition filter. This contribution has been evaluated to be approximately 30 % of the total deposited ^{137}Cs. The results obtained in this study could be used as input parameters foratmospheric transport models [2].

References

[1] Valls I, Camacho A, Ortega X, Serrano I, Blzquez S, Prez S, 2009. Natural and anthropogenic radionuclides in airborne particulate samples collected in Barcelona (Spain). J.Environ.Radioact.100, 102-107.

[2] Vargas A, Camacho A, Laubenstein M, Plastino W, 2016. Dry deposition velocity of ^{137}Cs and ^{134}Cs in Spain after the Fukushima Dai-Ichi Nuclear Power Plant Accident. Appl. Rad. Isot., 109, 441-443.

[3] Camacho A, Laubenstein M, Vargas A, Serrano I, Valls I, Plastino W, Duch MA, 2014. Validation of aerosol low-level activities by comparison with a deep underground laboratory. Appl. Radiat. Isot. 87, 66-69.

[4] Roed J, 1987. Dry deposition in rural and in urban areas in Denmark. Radiat. Prot. Dosim. 21, 33-36.

GINGER

G-GranSasso Collaboration

The experiment G-GranSasso is aiming at developing an array of ring-lasers in order to measure on earth the LenseThirring effect with 1% precision. This project is commonly called GINGER (Gyroscopes IN GEneral Relativity). In the last year three main activities have been carried on: data taking and analysis of GINGERino, the control of the geometry with the GP2 apparatus in Pisa and the revision of the General Relativity test. In the following the activity around these three points will be summarised.

1 GINGERino

GINGERino has been operational for several weeks, in Fig. 1 the raw data are reported, the periods, amounting to less than 10% of the total time, in which the laser was in 'split mode', have been removed, the duty cycle of the gyroscope is above 90%. In November the experiment has been restarted, unfortunately because a failure of the DAQ system the acquisition stopped abruptly just before Christmas. In February 2017 we have been able to access the experimental area, GINGERino was perfectly operational, but we have not been able to restart the DAQ system. On February 2017, a simple DAQ based on the computer available in the GINGERino area has been installed, unfortunately also this system at a certain point has stopped. We have accessed again the area on February 28, GINGERino was perfectly operational, but we regret to say that the failure in the computer was not repairable. In summary since November GINGERino is operational, the only problem is the DAQ system. It is based on Labview and PXI, it has been developed in 2010 at the time of the first installation inside the Virgo central area, using the controlled coming from an older apparatus. The PXI is now in Pisa, it has been re-inetializated, the software has been upgraded and a new hard disk installed, at the same time we are preparing a new computer in order to have redundancy in the DAQ, this new computer will be of 'industrial standard', since there is evidence that the high level of relative humidity is originating the troubles.

It has been possible to record a portion of the 2016 earthquake swarm, the Phd Andreino Simonelli (joint Phd University of Pisa and LMU of Mu-

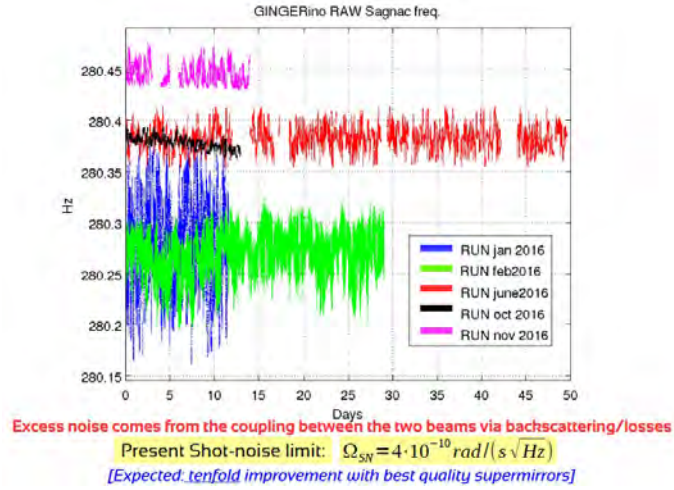

Figure 1: The good portions of data acquired by the DAQ system of GINGERino in 2016. The November run has interrupted just before Christmas for a failure of the DAQ system.

nich) is carrying on the analysis under the supervision of Heiner Igel, we hope to see the paper late spring 2017 and the poster will be presented in April at the conference EGU2017. We have not been able to make improvement in GINGERino, in particular the perimeter control, since we have at present a very serious problem of manpower.

The ring-laser GINGERino is an R&D apparatus; it has been developed using an old mechanical structure, the perimeter stabilisation can be implemented, but the full control of the geometry (following the scheme under test with the prototype GP2) cannot be implemented. It has been so successful thanks to the very quiet environment of LNGS, and to the monument in granite which provides several advantages. It is possible to say that as far as the LenseThirring test is concerning, GINGERino has completed its duty, since it has shown that the LNGS provides a very high thermal stability, the seismometer data are close to the LNM, and the local subsidences are smaller than 10^{-6}rad, see Fig. 3, important point for the installation of a ring-laser at the maximum signal, which is the most simple apparatus to measure the fast variations of the LOD. The only concern is the pressure which exhibits a rather high variability, see Fig. 4, this problem can be cured with pressure-tight doors.

It is clear that GINGERino is in practice an observatory for seismology, INGV is interested in long term measurements, at the moment it is under discussion if GINGERino will become an observatory at least until GINGER will be ready. It is important to say that the data relative to the earthquake have been sent to INGV people, and it has been tested the pipeline to

transfer the data to the INGV database. Several software routines have been developed for the analysis and in particular for the backscattering subtraction. Most of its automatisation has been done.

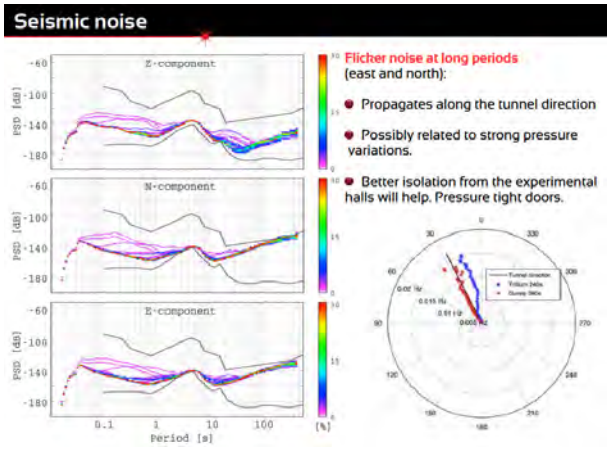

Figure 2: Response of the 3 channels of the seismometer installed on top of the monument of GINGERino. The left side diagram shows that the perturbation with longer periods is traveling along the tunnel, so consistent with the hypothesys that it is induced by the air flow inside the tunnel.

In the last year we have investigated several points which could contribute to improve the response of the gyroscope. For instance a model has been developed to describe the effect of the capillary and its misalignment. In practice the discharge tube causes losses whose amount changes as the discharge tube changes its position with respect to the light beams; as a consequence it could be advantageous to have a larger aperture of the capillary and use a spacial filter to select the mode of the light. Several upgradings are in principle feasible with the aim of increasing the long term stability and the sensitivity. The sensitivity will improve installing better mirrors. A different scheme could be installed recombining the beams with specially designed prisms; in this way the readout will not be affected by small variation on the relative phase between the two interfering beams. The DAQ needs to be replaced. Not all the data sets have been analysed, in principle it would be good to complete and refine the analysis of the data taken so far, for example selecting the data taken during the night and with careful analysis it is possible to integrate the Allan for more than 1 hour, see Fig. 5.

However it must be well understood that GINGERino is not capable to evidenziate the LenseThirring effect, it is not big enough. Unfortunately we cannot at present make any program because we are facing a very severe manpower shortage.

We are please to say that the paper about the GINGERino results has been

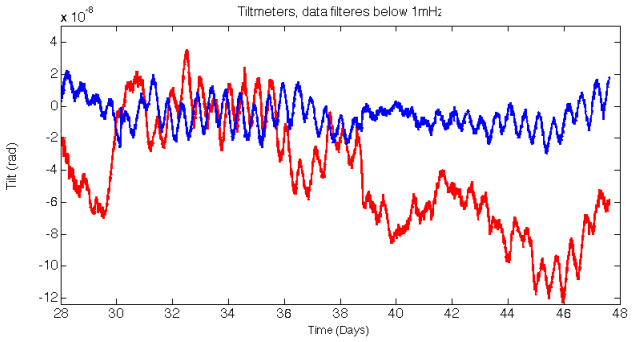

Figure 3: Long term stability of the monument of GINGERino as measured with the two channels of the tilt-meter installed on top of the granite monument. The effect of thermal drift of the room has been subtracted with a fit.

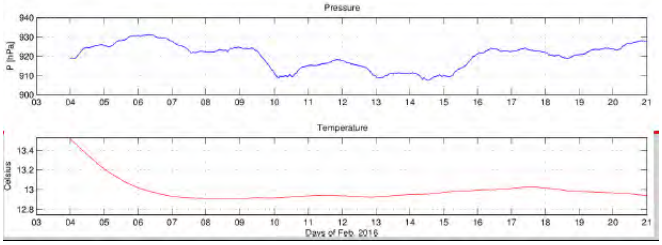

Figure 4: Temperature and Pressure behaviour inside the GINGERino experimental box.

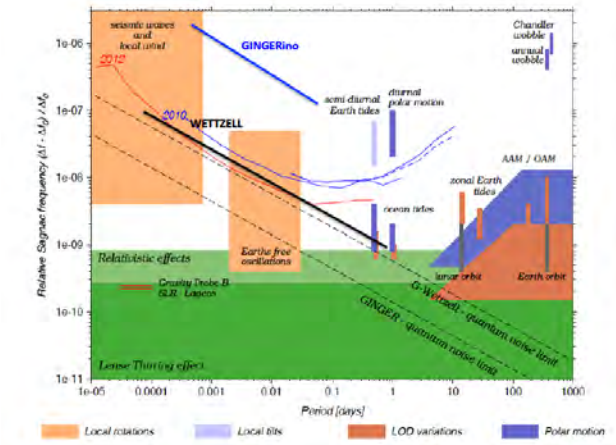

Figure 5: Comparison of GINGERino and G allan deviation, October 2016

accepted and published by Rev. of Scientific Instruments on March 14^{th} [1], this paper has been highly appreciated and it has been high-lighted by AIP and the media, in US and Italy (ANSA, Repubblica etc.).

2 The work in Pisa: GP2 and the facility to test the super mirrors one by one

GP2 is the ring-laser installed inside the INFN section, it is based on a square ring 1.6m in side oriented at the maximum Sagnac frequency with an error of 1^{o}. It has been developed to test the geometry control based on the control of the two diagonals of the square cavity. In the past years we have developed an interrogation apparatus based on a diode laser injection locked to a stabilised iodine reference laser. In the autumn 2016 the geometry of GP2 has been controlled keeping constant the length of the two diagonals, in this way several data have been collected and GP2 has been running continuously for more than one week (usually in a uncontrolled environment GP2 runs continuously for less that one hour). We are analysing the data and a paper is in preparation. The mirrors are one of the major concern, and we are not perfectly satisfied by the mirrors we have purchased so far. In particular we feel frustrated by the inconsistency of the measurement done by the factory with what we observe when the mirrors are installed inside the ring cavity. The factory declares total losses of the order of a few ppm, while the ring down time of the cavity is consistent with dozens times larger losses. It is possible to measure the losses of each sigle mirrors with little equipment, the major point here is the source, which should have a very narrow line. Enrico Maccioni has set up a technique based on 3 mirrors optical resonator, based on a simple diode laser whose line-width is narrowed by the radiation retro reflected from the optical cavity. It is important to handle those mirrors in a clean area, for this reason a clean cabinet has been installed inside the clean room of Pisa. This apparatus has been recently completed. This will give the possibility to test individually each mirror, to investigate a large portion of the surface, to detect bad mirrors before the installation and make tests avoiding the installation inside the ring cavity.

3 Revision of the GINGER project

Our original proposal was based on an octahedron, at least 3 ring-laser arranged following an octahedron, this has been published in 2011. We have pursued the revision of the experimental apparatus proposed for GINGER, following several criticisms, mainly more clearly clarifying the quantities to be measured, reducing as much as possible the cost of the whole apparatus and sketching a viable sequence for the installation. The revision work of the project has been carried on with 2 papers. The first one provides the detailed

description of the signal coming out of the ring-laser [2] and providing a very large list of useful relations between different signals. The second one is focused on the experimental part,[3] and gives the layout of the most simple apparatus providing the main experimental requirements. This two papers have been both submitted and accepted to EPJP, the second one [3] has been highlighted by EPJ on April 21 2017. Regarding the theoretical aspects we have started a collaboration with Salvatore Capozziello, University of Napoli and GSSI.

References

[1] J. Belfi, N. Beverini, Filippo Bosi et al., Review of Scientific Instruments 88, 034502 (2017); (highlighted paper, AIP 14 March 2017)

[2] A. Tartaglia, A. Di Virgilio, J. Belfi, N. Beverini and M.L. Ruggiero; Eur. Phys. J. Plus (2017) 132: 73 DOI 10.1140;

[3] A. Di Virgilio et al, 'GINGER: a feasibility study', Eur. Phys. J. Plus, al Eur. Phys. J. Plus (2017) 132: 157; (highlighted paper, EPJ 21 April 2017)

VIP

C.Curceanu (spokesperson) [a], S. Bartalucci[a], M. Bazzi[a], S. Bertolucci[b], C. Berucci[a,c], A.M. Bragadireanu[a,d], M. Cargnelli[a,c], A. Clozza[a], L. De Paolis[a], S.Di Matteo[e], J-P Egger[f], C. Guaraldo[a], M. Iliescu[a], M Laubenstein[g], J. Marton[e], E. Milotti[h], A. Pichler[a,c], K. Piscicchia[a,i], D. Pietreanu[a,d], A. Scordo[a],H. Shi[a], D. Sirghi[a,d], F. Sirghi[a,d], L. Sperandio[a], O. Vazquez Doce[j], E. Widmann[c], J. Zmeskal[a,c]

November 22, 2017

[a] INFN, Laboratori Nazionali di Frascati, CP 13, Via E. Fermi 40, I-00044, Frascati (Roma), Italy
[b] University and INFN Bologna, Via Irnerio 46, I-40126, Bologna, Italy
[c] The Stefan Meyer Institute for Subatomic Physics, Boltzmanngasse 3, A-1090 Vienna, Austria
[d] "Horia Hulubei"National Institute of Physics and Nuclear Engineering, Str. Atomistilor no. 407,P.O. Box MG-6, Bucharest - Magurele, Romania
[e] Institut de Physique UMR CNRS-UR1 6251, Université de Rennes1, F-35042 Rennes, France
[f] Institut de Physique, Université de Neuchâtel, 1 rue A.-L. Breguet, CH-2000 Neuchâtel, Switzerland
[g] INFN, Laboratori Nazionali del Gran Sasso, S.S. 17/bis, I-67010 Assergi (AQ), Italy
[h] Dipartimento di Fisica, Università di Trieste and INFN, Sezione di Trieste, Via Valerio, 2, I-34127 Trieste, Italy
[i] Museo Storico della Fisica e Centro Studi e Ricerche "Enrico Fermi", Roma, Italy
[j] Excellence Cluster Universe, Technische Universität München, Garching, Germany

Abstract

By performing X-rays measurements in the "cosmic silence" of the underground laboratory of Gran Sasso, LNGS-INFN, we test a basic principle of quantum mechanics: the Pauli Exclusion Principle (PEP) for electrons by searching for atomic transitions in copper prohibited by PEP. With the ongoing VIP2 experiment we aim to gain two orders of magnitude improvement with respect to the previous VIP experiment. VIP2 uses Silicon Drift Detectors (SDDs) to measure the X rays emitted in the copper target and a veto system (scintillators read by SiPM) to reduce the background.

1 The VIP scientific case and the experimental method

Within VIP and VIP2 an experimental test on the Pauli Exclusion Principle is being performed for electrons.

The Pauli Exclusion Principle (PEP), a consequence of the spin-statistics connection, plays a fundamental role in our understanding of many physical and chemical phenomena, from the periodic table of elements, to the electric conductivity in metals and to the degeneracy pressure which makes white dwarfs and neutron stars stable. Although the principle has been spectacularly confirmed by the huge number and accuracy of its predictions, its foundation lies deep in the structure of quantum field theory and has defied all attempts to produce a simple proof. Given its basic standing in quantum theory, it is appropriate to carry out high precision tests of the PEP validity and, indeed, mainly in the last 20 years, several experiments have been performed to search for possible small violations. Many of these experiments are using methods which are not obeying the so-called Messiah-Greenberg superselection rule. Moreover, the indistinguishability and the symmetrization (or antisymmetrization) of the wave-function should be checked independently for each type of particles, and accurate tests were and are being done.

The VIP (VIolation of the Pauli Exclusion Principle) experiment, performed by an international Collaboration among 10 Institutions of 6 countries, has the goal to either dramatically improve the previous limit on the probability of the violation of the PEP for electrons, ($P < 1.7 \times 10^{-26}$ established by Ramberg and Snow: *Experimental limit on a small violation of the Pauli principle*, Phys. Lett. **B 238** (1990) 438) or to find signals from PEP violation.

The experimental method consists in the introduction of "new" electrons into a copper strip, by circulating a current, and in the search for X-rays resulting from the forbidden radiative transition that occurs if some of the new electrons are captured by copper atoms and cascade down to the 1s state already filled by two electrons with opposite spins (Fig. 1.)

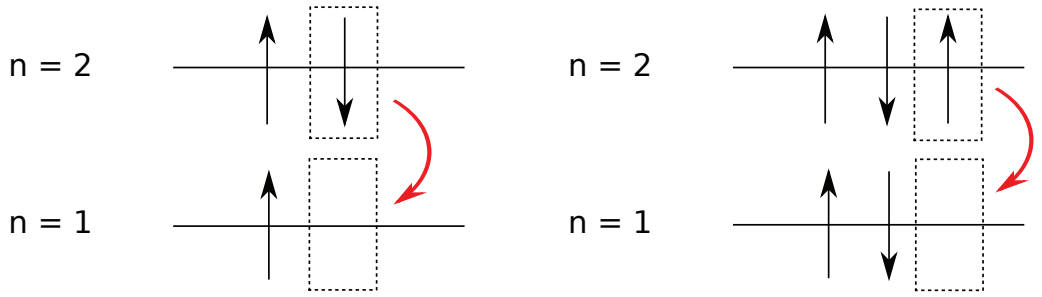

Figure 1: *Normal 2p to 1s transition with an energy around 8 keV for Copper (left) and Pauli-violating 2p to 1s transition with a transition energy around 7,7 keV in Copper (right).*

The energy of $2p \rightarrow 1s$ transition would differ from the normal K_α transition by about 300 eV (7.729 keV instead of 8.040 keV) providing an unambiguous signal of the PEP violation. The measurement alternates to the data taking with circulating current periods without current in the copper strip, in order to evaluate the X-ray background in conditions where no PEP violating transitions are expected to occur. The rather straightforward analysis consists in the evaluation of the statistical significance of the normalized subtraction of the two spectra in the region of interest (if no signal is seen). A more complex statistical analysis (Bayesian) is also being implemented.

The experiment is being performed at the LNGS underground Laboratories, where the X-ray background, generated by cosmic rays, is considerably reduced.

The VIP group is considering also the extension of its scientific program to the study of other items of the fundamental physics, such as collpase models studies.

2 The VIP and VIP2 apparata

The first VIP setup was realized in 2005, starting from the DEAR setup, reutilizing the CCD (Charge Coupled Devices) as X-ray detectors, and consisted of a copper cylinder, were current was circulated, 4.5 cm in radius, 50 μm thick, 8.8 cm high, surrounded by 16 equally spaced CCDs of type 55.

The CCDs were placed at a distance of 2.3 cm from the copper cylinder, grouped in units of two chips vertically positioned. The setup was enclosed in a vacuum chamber, and the CCDs cooled to 165 K by the use of a cryogenic system. The VIP setup was surrounded by layers of copper and lead to shield it against the residual background present inside the LNGS laboratory, see Fig. 2.

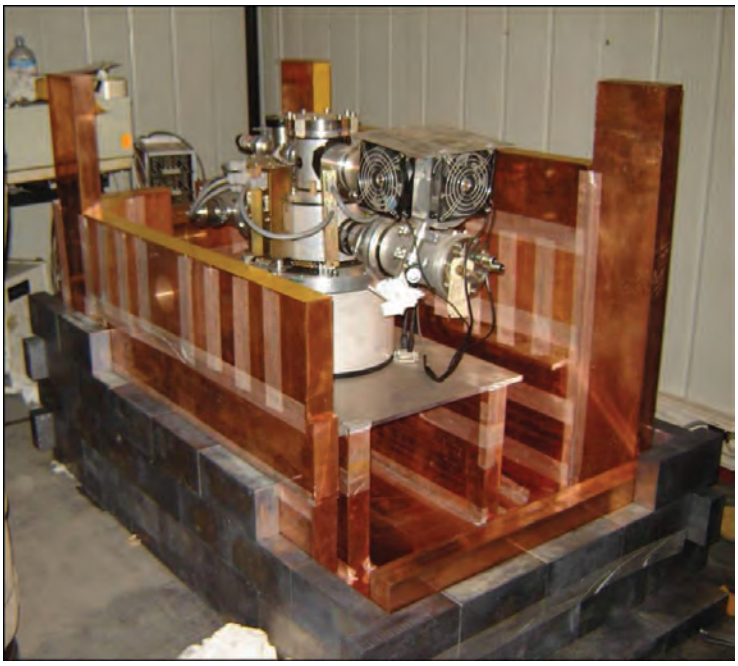

Figure 2: The VIP setup at the LNGS laboratory during installation.

The DAQ alternated periods in which a 40 A current was circulated inside the copper target with periods without current, representing the background.

VIP was installed at the LNGS Laboratory in Spring 2006 and was taking data until Summer 2010. The probability for PEP Violation was found to be: $\beta^2/2 < 4.6 \times 10^{-29}$.

In 2011 we started to prepare a new version of the setup, VIP2, which was finalized and installed at the LNGS-INFN in November 2015 and with which we will gain a factor about 100 in the probability of PEP violation in the coming years (see Table 1).

Table 1: List of expected gain factors of VIP2 in comparison to VIP (given in brackets).

Changes in VIP2	value VIP2(VIP)	expected gain
acceptance	12%	12
increase current	100A (50A)	2
reduced length	3 cm (8.8 cm)	1/3
total linear factor		8
energy resolution	170 eV(340 eV)	4
reduced active area	6 cm^2(114 cm^2)	20
better shielding and veto		5-10
higher SDD efficiency		1/2
background reduction		200-400
overall gain		**$\sim$120**

3 Activities in 2016

3.1 VIP2 - a new high sensitivity experiment

In order to achieve a signal/background increase which will allow a gain of two orders of magnitude for the probability of PEP violation for electrons, we built a new setup with a new target, a new cryogenic system and we use new detectors with timing capability and an active veto system. As X-ray detectors we use spectroscopic Silicon Drift Detectors (SDDs) which have an even better energy resolution than CCDs and provide timing capability which allow to use anti-coincidence provided by an active shielding.
The VIP2 system is providing:

1. signal increase with a more compact system with higher acceptance and higher current flow in the new copper strip target;

2. background reduction by decreasing the X-ray detector surface, more compact shielding (active veto system and passive), nitrogen filled box for radon radiation reduction.

In the Table 1 the numerical values for the improvements in VIP2 are given which will lead to an expected overall improvement of a factor about 100.

3.2 Status of VIP2 in 2016

In the VIP2 apparatus six SDDs units, with a total active area of 6 cm^2 each are mounted close to the Cu target. An active shielding system (veto) was implemented, to reduce the background in the energy region of the forbidden transition. This system will play an important role to improve the limit for the violation of the PEP by two orders of magnitude with the new data which are presently obtained by running the VIP2 experiment at LNGS.

In November 2015, the VIP2 setup was installed at Gran Sasso. In the year 2016, data with the VIP2 detector system at the LNGS without shielding were taken. In Figure 3 the VIP2 setup, as installed at LNGS, is shown.

Data with 100 Ampere DC current applied to the copper strip was collected together with the data collected without current. A preliminary analysis of the two spectra to determine a

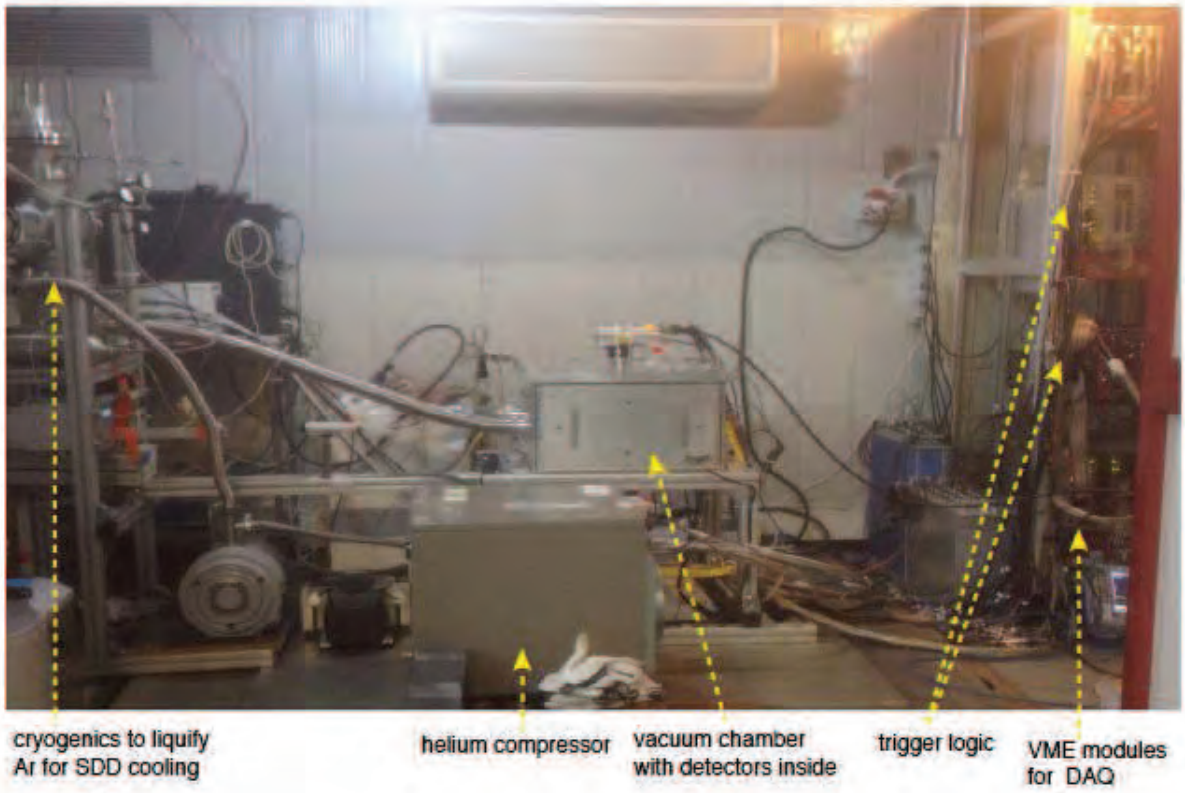

Figure 3: *A picture of the VIP-2 setup installed at LNGS .*

new value of the upper limit for PEP violation is on going. Figure 4 shows the summation of the data from 2016 of all the SDDs for 34 days of data taking with current and for 28 days without current. The preliminary analysis shows the energy resolution of the summed spectra at 8 keV is less than 190 eV FWHM.

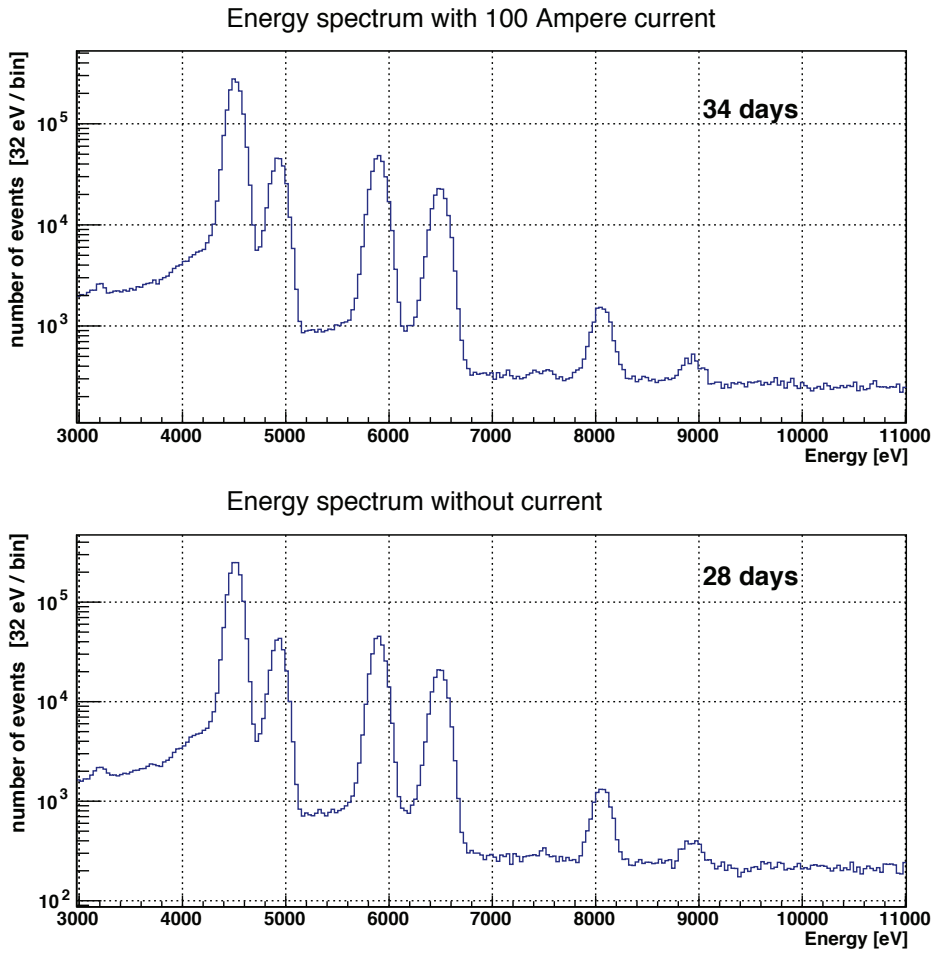

Figure 4: *Upper figure: the energy spectrum obtained by VIP2 in 34 days with current (I=100 A); Lower figure: the energy spectrum obtained by VIP2 in 28 days without current.*

4 Workshops organized in 2016

In 2016 the following events related to the physics of VIP, and, more generally, to quantum mechanics, were organized:

1. Training school for graduating students, PhD students and young researchers, "Are spin-statistics and quantum theory exact?", LNF-INFN, December 19-21, 2016.

2. Testing the limit of quantum superposition principle in nuclear, atomic and optomechanical systems, ECT*, Trento, 11-16 September 2016.

Also, VIP was included in about 20 lectures given by Catalina Curceanu in Australia, as Women in Physics Lectures award for 2016, awarded by the Australian Institute of Physics.

5 Future plans

In 2017 we will be in data taking with VIP2 at LNGS-INFN in the actual configuration until summer 2017. The preliminary data analysis will be finalized and published.

In summer 2017, we will implement new SDDs (higher active/total array ration) in the setup and build the shielding, so to start a new data taking campaign by the end of 2017.

Acknowledgements

The VIP2 Collaboration wishes to thank all the LNGS laboratory staff for the precious help and assistance during all phases of preparation, installation and data taking.

The support from the EU COST Action CA 15220 is gratefully acknowledged.

Furthermore, we acknowledge the support from the Foundational Questions Institute, FOXi ("Events" as we see them: experimental test of the collapse models as a solution of the measurement problem) and from the John Templeton Foundation (ID 581589).

6 Publications in 2016

1. M. Pawlik-Niedwiecka *et al*, J-PET detector system for studies of the electron-positron annihilations, EPJ Web Conf. **130** (2016) 07020.

2. P. Moskal *et al*, Studies of discrete symmetries in a purely leptonic system using the Jagiellonian Positron Emission Tomograph, EPJ Web Conf. **130** (2016) 07015.

3. D. Daminska *et al*, A feasibility study of ortho-positronium decays measurement with the J-PET scanner based on plastic scintillators, Eur. Phys. J. C **76** (2016) no.8, 445.

4. P. Moskal *et al*, Potential of the J-PET detector for studies of discrete symmetries in decays of positronium atom - a purely leptonic system, Acta Phys. Polon. B **47** (2016) 509 .

5. A. Pichler *et al*, Application of photon detectors in the VIP2 experiment to test the Pauli Exclusion Principle, J. Phys. Conf. Ser. **718** (2016) no.5, 052030.

6. C. Curceanu *et al*, Spontaneously emitted X-rays: an experimental signature of the dynamical reduction models, Found. Phys. **46** (2016) 263.

7. H. Shi *et al*, Searches for the Violation of Pauli Exclusion Principle at LNGS in VIP(-2) experiment, J. Phys. Conf. Ser. **718** (2016) no.4, 042055 .

THE PIERRE AUGER OBSERVATORY

D. Boncioli[a,⋆], A. di Matteo[b,*], A.F. Grillo[a], S. Petrera[b,c],
V. Rizi[b,a], F. Salamida[b,a]
for the Pierre Auger Collaboration

[a] INFN Laboratori Nazionali del Gran Sasso, Assergi (AQ), Italy
[b] INFN and Department of Physical and Chemical Sciences,
University of L'Aquila, L'Aquila, Italy
[c] GSSI, Gran Sasso Science Institute, L'Aquila, Italy
⋆ now at Deutsches Elektronen-Synchrotron (DESY), Zeuthen, Germany
* now at Service de Physique Théorique, Université Libre de Bruxelles, Brussels, Belgium

Abstract

The Pierre Auger Project is an international Collaboration involving about 450 scientists from 16 countries, with the objective of studying the highest energy cosmic rays. Recent results from the Collaboration as well as further developments in the detector are presented in this report.

1 Introduction

Ultra-high energy cosmic rays are of intrinsic interest as their origin and nature are unknown. It is quite unclear where and how particles as energetic as $\approx 10^{20}$ eV are accelerated. Over 40 years ago it was pointed out that if the highest energy particles are protons then a fall in the flux above an energy of about 4×10^{19} eV is expected because of energy losses by the protons as they propagate from distant sources through the photon background radiation. At the highest energies the key process is photo-pion production in which the proton loses part of its energy in each creation of a Δ resonance. This is the Greisen–Zatsepin–Kuzmin (GZK) effect. It follows that at 10^{20} eV any proton observed must have come from within about 50 Mpc and on this distance scale the deflections by intervening magnetic fields in the galaxy and intergalactic space are expected to be so small that point sources should be observed. If nuclei are propagated from sources their photo-disintegration in the photon background field plays a role similar to the GZK effect in the depletion of the flux above 10^{20} eV and the limitation of the CR horizon, but the angular correlation with the sources is expected weaker because of the higher charges.

The Observatory comprises about 1600 10 $m^2 \times 1.2$ m water-Cherenkov detectors deployed over 3000 km^2 on a 1500 m hexagonal grid, plus a sub array, the Infill, with 71 water Cherenkov detectors on a denser grid of 750 m covering nearly 30 km^2. This part of the Observatory (the surface detector, SD) is over-looked by 24 fluorescence telescopes in 4 clusters located on four hills around the SD area which is extremely flat. The surface detectors contain 12 tonnes of clear water viewed by $3 \times 9''$ hemispherical photomultipliers. The fluorescence detectors (FD) are designed to record the faint ultra-violet light emitted as the shower traverses the atmosphere. Each telescope images a portion of the sky of 30° in azimuth and 1°–30° in elevation using a spherical mirror of 3 m^2 effective area to focus light on to a camera of 440×18 cm^2 hexagonal pixels, made of photomultipliers complemented with light collectors, each with a field of view of 1.5° diameter. 3 High Elevation Auger Telescopes (HEAT) located at one of the fluorescence sites are dedicated to the fluorescence observation of lower energy showers. The Observatory also comprises a sub array of 124 radio sensors (AERA, Auger Engineering Radio Array) working in the MHz range and covering 6 km^2, a sub Array of 61 radio sensors (EASIER, Extensive Air Shower Identification with Electron Radiometer) working in the GHz range and covering 100 km^2, and two GHz imaging radio telescopes AMBER and MIDAS.

A review of main results from the Pierre Auger Observatory is presented with a particular focus on the energy spectrum measurements, the mass composition studies, the arrival directions analyses and the search for neutral cosmic messengers. Despite the results reached by Auger, the understanding of the nature of UHECRs and of their origin remains an open science case that the Auger collaboration is planning to address with the AugerPrime project to upgrade the Observatory.

2 Recent results from the Pierre Auger Observatory

2.1 Cosmic Ray Spectrum measurements

The measurement of the energy spectrum of UHECRs, the inference on their mass composition and the analysis of their arrival directions bring different information, complementary and supplementary one to the other, with respect to their origin.

The measurement of the flux of UHECRs has been one of the first outcomes of Auger data [1]. Two spectral features have been established beyond doubt [2, 3] : the hardening in the spectrum at about 5×10^{18} eV (the so-called ankle), and a strong suppression of the

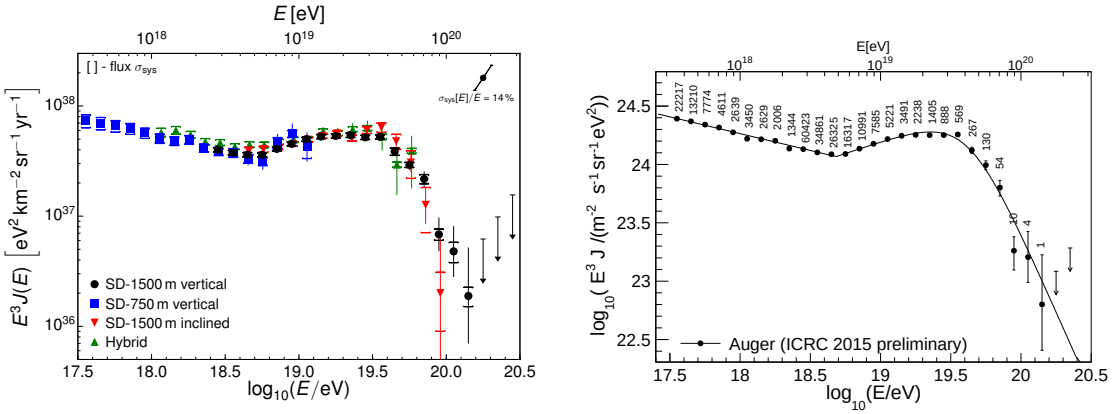

Figure 1: Left: The four energy spectra derived from SD and hybrid data. Right: The combined energy spectrum, fitted with a flux model (see text). As in the left panel, only statistical uncertainties are shown and the upper limits correspond to the 84% C.L.

flux at the highest energies, starting at about 4×10^{19} eV. The all-particle flux of cosmic rays presented at ICRC 2015 [4] is an update of such measurement, being based on an exposure now larger than 50000 km^2 sr yr and on 190000 events. Combining four independent spectra (see Figure 1, left) from the two different SDs (and two data sets from the SD-1500 m, vertical and horizontal events) and from hybrid events, the measurement is emblematic of the power of using multiple detectors. Data from the SD-750 m allow for the determination of the energy spectrum down to 10^{17} eV. The SD-1500 m vertical data are crucial above the energy of full trigger efficiency of 3×10^{18} eV up to the highest energies, with horizontal events contributing above 4×10^{18} eV and providing an independent measurement in this energy range. Hybrid data bridge those from the two SDs, between 10^{18} eV and $10^{19.6}$ eV. The four spectra, in agreement within uncertainties, are combined into a unique one shown in Fig. 1, right panel, taking into account the systematics of the individual measurements. The evident features are quantified by fitting a model that describes the spectrum with two power-laws around the ankle, the second of which includes a smooth suppression at the highest energies. The ankle is found to be at $E_{\rm ankle} = (4.8 \pm 0.1 \pm 0.8) \times 10^{18}$ eV. The spectral slope below the ankle is $\gamma_1 = 3.29 \pm 0.02 \pm 0.05$, and above the ankle is $\gamma_2 = 2.60 \pm 0.02 \pm 0.10$. The energy at which the differential flux falls to one-half of the value of the power-law extrapolation is $E_{\rm s} = (42.1 \pm 1.7 \pm 7.6) \times 10^{18}$ eV.

2.2 Mass composition studies

The origin of the very precisely determined features in the all-particle spectrum has been in parallel addressed by the Collaboration, likewise since many years [5], through the measurement of the depth of the shower maximum, $X_{\rm max}$, one of the most robust mass-sensitive EAS observables. The measurement, relying on hybrid data, has been recently updated in [6]. More than 18000 events collected by the standard FD telescopes (FD data) above $10^{17.8}$ eV, have been supplemented by about 5500 data collected with HEAT in coincidence with the closest FD, Coihueco (so-called HeCo data) [7]. The resulting $\langle X_{\rm max} \rangle$ and $\sigma(X_{\rm max})$ is shown in Fig. 2, left and right, respectively, as a function of energy. Data are confronted to simulations, for proton and iron primaries, performed using three hadronic interaction models that were found to agree with recent LHC data. Between 10^{17} and $10^{18.3}$ eV, $\langle X_{\rm max} \rangle$ increases by around 85 g cm^{-2} per decade of energy; around $10^{18.3}$ eV, the rate of change of $\langle X_{\rm max} \rangle$ becomes significantly smaller

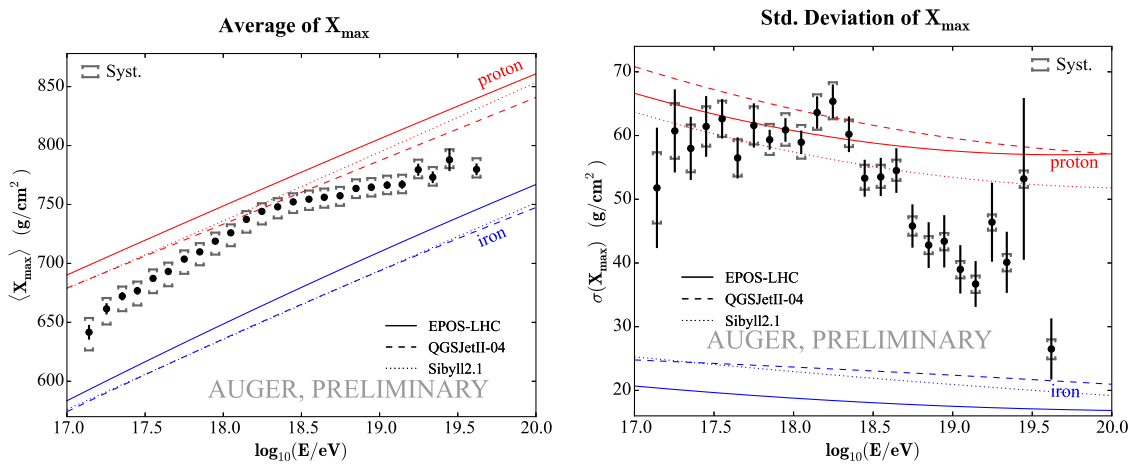

Figure 2: The mean (left) and the standard deviation (right) of the measured $X_{\rm max}$ distributions as a function of energy compared to air-shower simulations for proton and iron primaries.

($\sim$ 26 g cm^{-2}/decade). These two values, consistent with those found with FD data alone [6], allow to extend the inferences on the evolution of the average mass composition down to 10^{17} eV. As the first value is larger than the one expected for a constant mass composition ($\sim$ 60 g cm^{-2}/decade), it indicates that the mean primary mass is getting lighter all the way from 10^{17} to $10^{18.3}$ eV. Above this energy, the trend inverts and the composition becomes heavier. The fluctuations of $X_{\rm max}$ start to decrease above the same energy $\sim 10^{18.3}$ eV, being rather constant below.

2.3 Neutral cosmic messengers

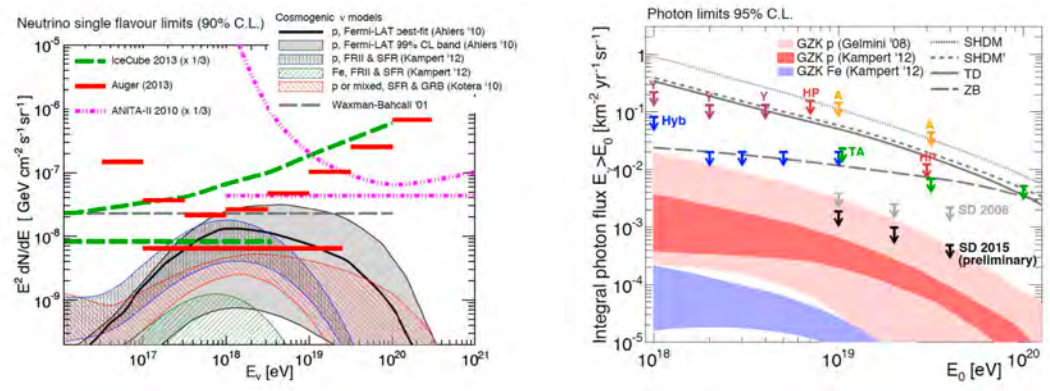

Figure 3: Left: neutrino flux upper limits (at 90% C.L.), in integrated (horizontal lines) and differential forms (see [9] for details). - Right : photon flux upper limits (95% C.L.) (see [8] for details).

Both neutrinos and photons are sought for in the flux of UHECRs detected by Auger. The neutrino search is performed by studying very inclined showers and earth-skimming ones [9]. The criteria are based on the characteristics expected for "young" showers initiated by neutrinos,

developing deep in the atmosphere, compared to "old" ones from inclined hadronic showers, having their electromagnetic component fully absorbed before reaching the detectors. Photon showers, due to their slower development and the dominance of the electromagnetic component can be distinguished from hadronic showers [8]. SD events on the one hand, and hybrid events on the other hand have been analyzed, to cover the energy range above 1 EeV. Assuming a differential flux $dN(E) = kE^2$ for both neutrinos and photons, stringent upper limits to their flux are derived. The Auger limits on neutrinos (Fig.3 left panel) outperform those from IceCube and ANITA, and also the Waxman-Bahcall limit; in the range 10^{17} - 10^{19} eV they are challenging the contribution from cosmogenic-neutrino models. The limits to the integral photon flux are shown in Fig.3 right panel. The obtained limits are the most stringent for E > 10 EeV and start to constrain the most optimistic predictions of cosmogenic photon fluxes under the assumption of a pure proton composition.

2.4 Anisotropy searches

The last piece of study regarding UHECRs included in this report is that of the distribution of arrival directions on large scales [10]. This integrates other anisotropy searches, not only in terms of angular scale, but also of inferences, as large-scale anisotropies can be reflective either of a collective motion of cosmic rays (e.g., of their propagation), or of the global distribution of their sources, or of both. As such studies are relevant at all energies, being complementary to spectrum and mass measurements, the large-scale analysis has been performed down to the lowest ones accessible by the Observatory, $\sim 10^{16}$ eV. The technique used is that of the harmonic analysis of the counting rate. The amplitudes of the first harmonic are obtained as upper limits to the equatorial component of the dipole as a function of energy, apart two energy bins where (between 1 and 2 EeV, and for the integral bin above 8 EeV, mean energy 14.5 EeV, respectively) amplitudes are determined. Both upper limits and measurements are at percent level. The evolution of the phases with energy shows a smooth transition of the first harmonic modulation in right ascension distribution from 270° to 100° around 1 EeV. Interestingly, the phase above 8 EeV is roughly the opposite than the one at energies below 1 EeV, which is in the general direction of the Galactic Centre. The percent limits to the amplitude of the anisotropy exclude the presence of a large fraction of Galactic protons at EeV energies [11]. Accounting for the inference from $X_{\rm max}$ data, that protons are in fact abundant at those energies, this might indicate that this component is extra-Galactic, gradually taking over a Galactic one. The low level of anisotropy would then be the sum of two vectors with opposite directions, naturally reducing the amplitudes. An intruiguing possibility, to be explored with additional data.

Similarly intruiguing is the indication of the departure from isotropy above 8 EeV, where the total amplitude of the dipole results to be 0.073±0.015 pointing to $(\alpha, \delta) = (95^\circ \pm 13^\circ, -39^\circ \pm 13^\circ)$. This finding is robust both assuming that the flux of cosmic rays is purely dipolar or purely dipolar and quadripolar [12]. Assumptions on the shape of the angular distribution can be avoided by analyzing it over the full sky. This has been done through a spherical harmonic analysis of Auger and Telescope Array data [13, 14]. No deviation from isotropy at discovery level is found at any multipoles. The largest deviation from isotropy, with a p-value of 5×10^{-3}, occurs for the dipolar moment. The amplitude, 0.065 ± 0.019, and the direction, $(\alpha, \delta) = 93^\circ \pm 24^\circ, 46^\circ \pm 18^\circ)$ are in agreement with that found with Auger-only data. The sky maps of the fluxes, in equatorial coordinates, in Fig. 4, offer a visualization of the dipolar patterns resulting from the two analyses.

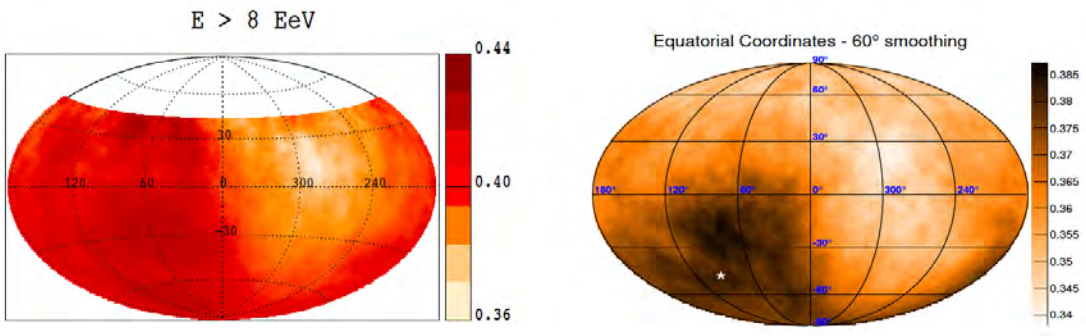

Figure 4: Sky maps in equatorial coordinates of flux, in km^{-2} yr^{-1} sr^{-1} units, smoothed in angular windows of 45° (60°) radius, for Auger (Auger and Telescope Array) events with E > 8 EeV (10 EeV), left (right) panel.

3 Activity of the L'Aquila–Gran Sasso Group

The activity of the group has followed two main lines:

- Development of a Monte Carlo code (*SimProp*) for the propagation of UHECR nuclei in extragalactic space, and its use for the study of physical observables
- Development and operation of the Raman Lidar system for an enhanced atmospheric test beam within the Observatory.
- Participation to the Auger-Telescope Array joint Spectrum and Anisotropies working groups
- Coordination responsibility of the paper [15]
- Study of Lorentz from the point of view of the effects on UHECR propagation and interactions of particles in atmosphere [19].

3.1 Talks

- A. di Matteo for the Pierre Auger Collaboration, "Astrophysical interpretation of Pierre Auger Observatory measurements of the UHECR energy spectrum and mass composition", RICAP, 2124 June 2016, Frascati
- A. Di Matteo, "Cosmogenic neutrinos and gamma-rays and the redshift evolution of UHECR sources" Neutrino Oscillation Workshop, 411 September 2016, Otranto
- A. di Matteo, "Computing cosmogenic gamma-ray fluxes with SimProp v2r4", SIF, 2630 September 2016, Padova
- D. Boncioli, "UHECR propagation in the extragalactic space", Arbeitstreffen Kernphysik, Schleching, February 18th 25th, 2016
- D. Boncioli, "Interactions of Cosmic Rays around the Universe: Models for UHECR data interpretation", 46th International Symposium on Multiparticle Dynamics South Korea, August 29th September 2nd, 2016

References

[1] J. Abraham *et al.* [Pierre Auger Collaboration], Phys. Rev. Lett. **101**, 061101 (2008) doi:10.1103/PhysRevLett.101.061101 [arXiv:0806.4302 [astro-ph]].

[2] J. Abraham *et al.* [Pierre Auger Collaboration], Phys. Lett. B **685**, 239 (2010) doi:10.1016/j.physletb.2010.02.013 [arXiv:1002.1975 [astro-ph.HE]].

[3] A. Aab *et al.* [Pierre Auger Collaboration], JCAP **1508**, 049 (2015) doi:10.1088/1475-7516/2015/08/049 [arXiv:1503.07786 [astro-ph.HE]].

[4] I. Valiño, for the Pierre Auger Collaboration, "The flux of ultra-high energy cosmic rays after ten years of operation of the Pierre Auger Observatory", ICRC 2015, [arXiv:1509.03732[astro-ph.HE]].

[5] J. Abraham *et al.* [Pierre Auger Collaboration], Phys. Rev. Lett. **104**, 091101 (2010) doi:10.1103/PhysRevLett.104.091101 [arXiv:1002.0699 [astro-ph.HE]].

[6] A. Aab *et al.* [Pierre Auger Collaboration], Phys. Rev. D **90**, no. 12, 122005 (2014) doi:10.1103/PhysRevD.90.122005 [arXiv:1409.4809 [astro-ph.HE]].

[7] A. Porcelli, for the Pierre Auger Collaboration, "Measurements of $X_{\rm max}$ above 10^{17} eV with the fluorescence detector of the Pierre Auger Observatory", ICRC 2015, [arXiv:1509.03732[astro-ph.HE]].

[8] C. Bleve, for the Pierre Auger Collaboration, "Updates on the neutrino and photon limits from the Pierre Auger Observatory", ICRC 2015, [arXiv:1509.03732[astro-ph.HE]].

[9] A. Aab *et al.* [Pierre Auger Collaboration], "Improved limit to the diffuse flux of ultrahigh energy neutrinos from the Pierre Auger Observatory," Phys. Rev. D **91**, no. 9, 092008 (2015) doi:10.1103/PhysRevD.91.092008 [arXiv:1504.05397 [astro-ph.HE]].

[10] I. Al Samarai for the Pierre Auger Collaboration, "Indications of anisotropy at large angular scales in the arrival directions of cosmic rays detected at the Pierre Auger Observatory", ICRC 2015, [arXiv:1509.03732[astro-ph.HE]].

[11] P. Abreu *et al.* [Pierre Auger Collaboration], Astrophys. J. Suppl. **203**, 34 (2012) doi:10.1088/0067-0049/203/2/34 [arXiv:1210.3736 [astro-ph.HE]].

[12] A. Aab *et al.* [Pierre Auger Collaboration], Astrophys. J. **802**, no. 2, 111 (2015) doi:10.1088/0004-637X/802/2/111 [arXiv:1411.6953 [astro-ph.HE]].

[13] A. Aab *et al.* [Telescope Array and Pierre Auger Collaborations], Astrophys. J. **794**, no. 2, 172 (2014) doi:10.1088/0004-637X/794/2/172 [arXiv:1409.3128 [astro-ph.HE]].

[14] O. Deligny for the Telescope Array and Pierre Auger Collaborations, "Large-Scale Distribution of Arrival Directions of Cosmic Rays Detected at the Pierre Auger Observatory and the Telescope Array above 10^{19} eV", ICRC 2015, [arXiv:1511.02103[astro-ph.HE]].

[15] A. Aab *et al.* [Pierre Auger Collaboration], JCAP**04** (2017)038

[16] J. Heinze, D. Boncioli, M. Bustamante and W. Winter, arXiv:1512.05988 [astro-ph.HE].

[17] R. Aloisio, D. Boncioli, A. di Matteo, A. F. Grillo, S. Petrera and F. Salamida, JCAP **1510**, no. 10, 006 (2015) doi:10.1088/1475-7516/2015/10/006 [arXiv:1505.04020 [astro-ph.HE]].

[18] R. Aloisio, D. Boncioli, A. di Matteo, A. F. Grillo, S. Petrera and F. Salamida, Nucl. Part. Phys. Proc. **265-266**, 251 (2015) doi:10.1016/j.nuclphysbps.2015.06.065 [arXiv:1505.04742 [astro-ph.HE]].

[19] D. Boncioli *et al.*, arXiv:1509.01046 [astro-ph.HE].

[20] C. Medina-Hernandez, for the Pierre Auger Collaboration, ICRC 2015, [arXiv:1509.03732[astro-ph.HE]].

4 List of Publications

1. A. Aab *et al.* [Pierre Auger Collaboration], JCAP **04** (2017)009
2. A. Aab *et al.* [Pierre Auger Collaboration], The Astrophysical Journal Letters, **837**:L25 (7pp), 2017 March 10
3. A. Aab *et al.* [Pierre Auger Collaboration], JINST **12** (2017) P03002
4. A. Aab *et al.* [Pierre Auger Collaboration], JINST **12** P02006 (2017)
5. A. Aab *et al.* [Pierre Auger Collaboration], JCAP **04** (2017) 038
6. A. Aab *et al.* [Pierre Auger Collaboration], Phys. Rev. D **94**, 122007 (2016)
7. A. Aab *et al.* [Pierre Auger Collaboration], PRL **117**, 192001 (2016)
8. A. Aab *et al.* [Pierre Auger Collaboration], Phys. Rev. D **94**, 082002 (2016)
9. A. Aab *et al.* [Pierre Auger Collaboration], Phys.Lett. **B762** (2016) 288-295
10. A. Aab *et al.* [Pierre Auger Collaboration], Phys. Rev. D **93**, 122005 (2016)
11. A. Aab *et al.* [Pierre Auger Collaboration], PRL **116**, 241101 (2016)
12. A. Aab *et al.* [Pierre Auger Collaboration], Phys. Rev. D **93**, 072006 (2016)
13. J. Heinze, D. Boncioli, M. Bustamante and W. Winter, arXiv:1512.05988 [astro-ph.HE].
14. A. Aab *et al.* [Pierre Auger Collaboration], JINST **11**, no. 01, P01018 (2016)
15. D. Boncioli *et al.* [Pierre Auger Collaboration], arXiv:1512.02314 [astro-ph.HE].
16. M. G. Aartsen *et al.* [IceCube and Pierre Auger and Telescope Array Collaborations], JCAP **1601**, no. 01, 037 (2016)

The Pierre Auger Collaboration

A. Aab[77], P. Abreu[68], M. Aglietta[49,48], I. Al Samarai[31], I.F.M. Albuquerque[18], I. Allekotte[1], A. Almela[8,11], J. Alvarez Castillo[64], J. Alvarez-Muñiz[76], G.A. Anastasi[40,42], L. Anchordoqui[83], B. Andrada[8], S. Andringa[68], C. Aramo[46], F. Arqueros[74], N. Arsene[70], H. Asorey[1,26], P. Assis[68], J. Aublin[31], G. Avila[9,10], A.M. Badescu[71], A. Balaceanu[69], F. Barbato[56], R.J. Barreira Luz[68],

J.J. Beatty[88], K.H. Becker[33], J.A. Bellido[12], C. Berat[32], M.E. Bertaina[58,48], X. Bertou[1], P.L. Biermann[b], P. Billoir[31], J. Biteau[30], S.G. Blaess[12], A. Blanco[68], J. Blazek[28], C. Bleve[52,44], M. Boháčová[28], D. Boncioli[42,d], C. Bonifazi[24], N. Borodai[65], A.M. Botti[8,35], J. Brack[h], I. Brancus[69], T. Bretz[37], A. Bridgeman[35], F.L. Briechle[37], P. Buchholz[39], A. Bueno[75], S. Buitink[77], M. Buscemi[54,43], K.S. Caballero-Mora[62], L. Caccianiga[55], A. Cancio[11,8], F. Canfora[77], L. Caramete[70], R. Caruso[54,43], A. Castellina[49,48], F. Catalani[18], G. Cataldi[44], L. Cazon[68], A.G. Chavez[63], J.A. Chinellato[19], J. Chudoba[28], R.W. Clay[12], A. Cobos[8], R. Colalillo[56,46], A. Coleman[89], L. Collica[48], M.R. Coluccia[52,44], R. Conceição[68], G. Consolati[55,50], F. Contreras[9,10], M.J. Cooper[12], S. Coutu[89], C.E. Covault[81], J. Cronin[90], S. D'Amico[51,44], B. Daniel[19], S. Dasso[5,3], K. Daumiller[35], B.R. Dawson[12], R.M. de Almeida[25], S.J. de Jong[77,79], G. De Mauro[77], J.R.T. de Mello Neto[24], I. De Mitri[52,44], J. de Oliveira[25], V. de Souza[17], J. Debatin[35], O. Deligny[30], C. Di Giulio[57,47], A. Di Matteo[53,k,42], M.L. Díaz Castro[19], F. Diogo[68], C. Dobrigkeit[19], J.C. D'Olivo[64], Q. Dorosti[39], R.C. dos Anjos[23], M.T. Dova[4], A. Dundovic[38], J. Ebr[28], R. Engel[35], M. Erdmann[37], M. Erfani[39], C.O. Escobar[f], J. Espadanal[68], A. Etchegoyen[8,11], H. Falcke[77,80,79], J. Farmer[90], G. Farrar[86], A.C. Fauth[19], N. Fazzini[f], F. Fenu[58], B. Fick[85], J.M. Figueira[8], A. Filipčič[72,73], O. Fratu[71], M.M. Freire[6], T. Fujii[90], A. Fuster[8,11], R. Gaior[31], B. García[7], D. Garcia-Pinto[74], F. Gaté[e], H. Gemmeke[36], A. Gherghel-Lascu[69], P.L. Ghia[30], U. Giaccari[24], M. Giammarchi[45], M. Giller[66], D. Głas[67], C. Glaser[37], G. Golup[1], M. Gómez Berisso[1], P.F. Gómez Vitale[9,10], N. González[8,35], A. Gorgi[49,48], P. Gorham[i], A.F. Grillo[42], T.D. Grubb[12], F. Guarino[56,46], G.P. Guedes[20], M.R. Hampel[8], P. Hansen[4], D. Harari[1], T.A. Harrison[12], J.L. Harton[h], A. Haungs[35], T. Hebbeker[37], D. Heck[35], P. Heimann[39], A.E. Herve[34], G.C. Hill[12], C. Hojvat[f], E. Holt[35,8], P. Homola[65], J.R. Hörandel[77,79], P. Horvath[29], M. Hrabovský[29], T. Huege[35], J. Hulsman[8,35], A. Insolia[54,43], P.G. Isar[70], I. Jandt[33], J.A. Johnsen[82], M. Josebachuili[8], J. Jurysek[28], A. Kääpä[33], O. Kambeitz[34], K.H. Kampert[33], I. Katkov[34], B. Keilhauer[35], N. Kemmerich[18], E. Kemp[19], J. Kemp[37], R.M. Kieckhafer[85], H.O. Klages[35], M. Kleifges[36], J. Kleinfeller[9], R. Krause[37], N. Krohm[33], D. Kuempel[37], G. Kukec Mezek[73], N. Kunka[36], A. Kuotb Awad[35], B.L. Lago[15], D. LaHurd[81], R.G. Lang[17], M. Lauscher[37], R. Legumina[66], M.A. Leigui de Oliveira[22], A. Letessier-Selvon[31], I. Lhenry-Yvon[30], K. Link[34], D. Lo Presti[54], L. Lopes[68], R. López[59], A. López Casado[76], Q. Luce[30], A. Lucero[8,11], M. Malacari[90], M. Mallamaci[55,45], D. Mandat[28], P. Mantsch[f], A.G. Mariazzi[4], I.C. Mariş[13], G. Marsella[52,44], D. Martello[52,44], H. Martinez[60], O. Martínez Bravo[59], J.J. Masías Meza[3], H.J. Mathes[35], S. Mathys[33], J. Matthews[84], J.A.J. Matthews[j], G. Matthiae[57,47], E. Mayotte[33], P.O. Mazur[f], C. Medina[82], G. Medina-Tanco[64], D. Melo[8], A. Menshikov[36], K.-D. Merenda[82], S. Michal[29], M.I. Micheletti[6], L. Middendorf[37], L. Miramonti[55,45], B. Mitrica[69], D. Mockler[34], S. Mollerach[1], F. Montanet[32], C. Morello[49,48], M. Mostafá[89], A.L. Müller[8,35], G. Müller[37], M.A. Muller[19,21], S. Müller[35,8], R. Mussa[48], I. Naranjo[1], L. Nellen[64], P.H. Nguyen[12], M. Niculescu-Oglinzanu[69], M. Niechciol[39], L. Niemietz[33], T. Niggemann[37], D. Nitz[85], D. Nosek[27], V. Novotny[27], L. Nožka[29], L.A. Núñez[26], L. Ochilo[39], F. Oikonomou[89], A. Olinto[90], M. Palatka[28], J. Pallotta[2], P. Papenbreer[33], G. Parente[76], A. Parra[59], T. Paul[87,83], M. Pech[28], F. Pedreira[76], J. Pękala[65], R. Pelayo[61], J. Peña-Rodriguez[26], L. A. S. Pereira[19], M. Perlín[8], L. Perrone[52,44], C. Peters[37], S. Petrera[40,42], J. Phuntsok[89], R. Piegaia[3], T. Pierog[35], P. Pieroni[3], M. Pimenta[68], V. Pirronello[54,43], M. Platino[8], M. Plum[37], C. Porowski[65], R.R. Prado[17], P. Privitera[90], M. Prouza[28], E.J. Quel[2], S. Querchfeld[33], S. Quinn[81], R. Ramos-Pollan[26], J. Rautenberg[33], D. Ravignani[8], B. Revenu[e], J. Ridky[28], F. Riehn[68], M. Risse[39], P. Ristori[2], V. Rizi[53,42], W. Rodrigues de Carvalho[18], G. Rodriguez Fernandez[57,47], J. Rodriguez Rojo[9], D. Rogozin[35], M.J. Roncoroni[8], M. Roth[35], E. Roulet[1], A.C. Rovero[5], P. Ruehl[39], S.J. Saffi[12], A. Saftoiu[69], F. Salamida[53], H. Salazar[59], A. Saleh[73], F. Salesa Greus[89], G. Salina[47], F. Sánchez[8], P. Sanchez-Lucas[75], E.M. Santos[18], E. Santos[8], F. Sarazin[82], R. Sarmento[68], C.A. Sarmiento[8], R. Sato[9], M. Schauer[33], V. Scherini[44], H. Schieler[35], M. Schimp[33], D. Schmidt[35,8], O. Scholten[78,c], P. Schovánek[28], F.G. Schröder[35], S. Schröder[33], A. Schulz[34], J. Schumacher[37],

S.J. Sciutto[4], A. Segreto[41,43], M. Settimo[31], A. Shadkam[84], R.C. Shellard[14], G. Sigl[38], G. Silli[8,35], O. Sima[g], A. Śmiałkowski[66], R. Šmída[35], G.R. Snow[91], P. Sommers[89], S. Sonntag[39], R. Squartini[9], D. Stanca[69], S. Stanič[73], J. Stasielak[65], P. Stassi[32], F. Strafella[52,44], A. Streich[34], F. Suarez[8,11], M. Suarez Durán[26], T. Sudholz[12], T. Suomijärvi[30], A.D. Supanitsky[5], J. Šupík[29], J. Swain[87], Z. Szadkowski[67], A. Taboada[34], O.A. Taborda[1], V.M. Theodoro[19], C. Timmermans[79,77], C.J. Todero Peixoto[16], L. Tomankova[35], B. Tomé[68], G. Torralba Elipe[76], P. Travnicek[28], M. Trini[73], R. Ulrich[35], M. Unger[35], M. Urban[37], J.F. Valdés Galicia[64], I. Valiño[76], L. Valore[56,46], G. van Aar[77], P. van Bodegom[12], A.M. van den Berg[78], A. van Vliet[77], E. Varela[59], B. Vargas Cárdenas[64], G. Varner[i], R.A. Vázquez[76], D. Veberič[35], C. Ventura[24], I.D. Vergara Quispe[4], V. Verzi[47], J. Vicha[28], L. Villaseñor[63], S. Vorobiov[73], H. Wahlberg[4], O. Wainberg[8,11], D. Walz[37], A.A. Watson[a], M. Weber[36], A. Weindl[35], L. Wiencke[82], H. Wilczyński[65], M. Wirtz[37], D. Wittkowski[33], B. Wundheiler[8], L. Yang[73], A. Yushkov[8], E. Zas[76], D. Zavrtanik[73,72], M. Zavrtanik[72,73], A. Zepeda[60], B. Zimmermann[36], M. Ziolkowski[39], Z. Zong[30], F. Zuccarello[54,43]

[1] Centro Atómico Bariloche and Instituto Balseiro (CNEA-UNCuyo-CONICET), San Carlos de Bariloche, Argentina

[2] Centro de Investigaciones en Láseres y Aplicaciones, CITEDEF and CONICET, Villa Martelli, Argentina

[3] Departamento de Física and Departamento de Ciencias de la Atmósfera y los Océanos, FCEyN, Universidad de Buenos Aires and CONICET, Buenos Aires, Argentina

[4] IFLP, Universidad Nacional de La Plata and CONICET, La Plata, Argentina

[5] Instituto de Astronomía y Física del Espacio (IAFE, CONICET-UBA), Buenos Aires, Argentina

[6] Instituto de Física de Rosario (IFIR) – CONICET/U.N.R. and Facultad de Ciencias Bioquímicas y Farmacéuticas U.N.R., Rosario, Argentina

[7] Instituto de Tecnologías en Detección y Astropartículas (CNEA, CONICET, UNSAM), and Universidad Tecnológica Nacional – Facultad Regional Mendoza (CONICET/CNEA), Mendoza, Argentina

[8] Instituto de Tecnologías en Detección y Astropartículas (CNEA, CONICET, UNSAM), Buenos Aires, Argentina

[9] Observatorio Pierre Auger, Malargüe, Argentina

[10] Observatorio Pierre Auger and Comisión Nacional de Energía Atómica, Malargüe, Argentina

[11] Universidad Tecnológica Nacional – Facultad Regional Buenos Aires, Buenos Aires, Argentina

[12] University of Adelaide, Adelaide, S.A., Australia

[13] Université Libre de Bruxelles (ULB), Brussels, Belgium

[14] Centro Brasileiro de Pesquisas Fisicas, Rio de Janeiro, RJ, Brazil

[15] Centro Federal de Educação Tecnológica Celso Suckow da Fonseca, Nova Friburgo, Brazil

[16] Universidade de São Paulo, Escola de Engenharia de Lorena, Lorena, SP, Brazil

[17] Universidade de São Paulo, Instituto de Física de São Carlos, São Carlos, SP, Brazil

[18] Universidade de São Paulo, Instituto de Física, São Paulo, SP, Brazil

[19] Universidade Estadual de Campinas, IFGW, Campinas, SP, Brazil

[20] Universidade Estadual de Feira de Santana, Feira de Santana, Brazil

[21] Universidade Federal de Pelotas, Pelotas, RS, Brazil

[22] Universidade Federal do ABC, Santo André, SP, Brazil

[23] Universidade Federal do Paraná, Setor Palotina, Palotina, Brazil

[24] Universidade Federal do Rio de Janeiro, Instituto de Física, Rio de Janeiro, RJ, Brazil

[25] Universidade Federal Fluminense, EEIMVR, Volta Redonda, RJ, Brazil

[26] Universidad Industrial de Santander, Bucaramanga, Colombia

[27] Charles University, Faculty of Mathematics and Physics, Institute of Particle and Nuclear Physics, Prague, Czech Republic

[28] Institute of Physics of the Czech Academy of Sciences, Prague, Czech Republic

[29] Palacky University, RCPTM, Olomouc, Czech Republic

[30] Institut de Physique Nucléaire d'Orsay (IPNO), Université Paris-Sud, Univ. Paris/Saclay, CNRS-IN2P3, Orsay, France

[31] Laboratoire de Physique Nucléaire et de Hautes Energies (LPNHE), Universités Paris 6 et Paris 7, CNRS-IN2P3, Paris, France

[32] Laboratoire de Physique Subatomique et de Cosmologie (LPSC), Université Grenoble-Alpes, CNRS/IN2P3, Grenoble, France

[33] Bergische Universität Wuppertal, Department of Physics, Wuppertal, Germany

[34] Karlsruhe Institute of Technology, Institut für Experimentelle Kernphysik (IEKP), Karlsruhe, Germany

[35] Karlsruhe Institute of Technology, Institut für Kernphysik, Karlsruhe, Germany

[36] Karlsruhe Institute of Technology, Institut für Prozessdatenverarbeitung und Elektronik, Karlsruhe, Germany

[37] RWTH Aachen University, III. Physikalisches Institut A, Aachen, Germany

[38] Universität Hamburg, II. Institut für Theoretische Physik, Hamburg, Germany

[39] Universität Siegen, Fachbereich 7 Physik – Experimentelle Teilchenphysik, Siegen, Germany

[40] Gran Sasso Science Institute (INFN), L'Aquila, Italy

[41] INAF – Istituto di Astrofisica Spaziale e Fisica Cosmica di Palermo, Palermo, Italy

[42] INFN Laboratori Nazionali del Gran Sasso, Assergi (L'Aquila), Italy

[43] INFN, Sezione di Catania, Catania, Italy

[44] INFN, Sezione di Lecce, Lecce, Italy

[45] INFN, Sezione di Milano, Milano, Italy

[46] INFN, Sezione di Napoli, Napoli, Italy

[47] INFN, Sezione di Roma "Tor Vergata", Roma, Italy

[48] INFN, Sezione di Torino, Torino, Italy

[49] Osservatorio Astrofisico di Torino (INAF), Torino, Italy

[50] Politecnico di Milano, Dipartimento di Scienze e Tecnologie Aerospaziali , Milano, Italy

[51] Università del Salento, Dipartimento di Ingegneria, Lecce, Italy

[52] Università del Salento, Dipartimento di Matematica e Fisica "E. De Giorgi", Lecce, Italy

[53] Università dell'Aquila, Dipartimento di Scienze Fisiche e Chimiche, L'Aquila, Italy

[54] Università di Catania, Dipartimento di Fisica e Astronomia, Catania, Italy

[55] Università di Milano, Dipartimento di Fisica, Milano, Italy

[56] Università di Napoli "Federico II", Dipartimento di Fisica "Ettore Pancini", Napoli, Italy

[57] Università di Roma "Tor Vergata", Dipartimento di Fisica, Roma, Italy

[58] Università Torino, Dipartimento di Fisica, Torino, Italy

[59] Benemérita Universidad Autónoma de Puebla, Puebla, México

[60] Centro de Investigación y de Estudios Avanzados del IPN (CINVESTAV), México, D.F., México

[61] Unidad Profesional Interdisciplinaria en Ingeniería y Tecnologías Avanzadas del Instituto Politécnico Nacional (UPIITA-IPN), México, D.F., México

[62] Universidad Autónoma de Chiapas, Tuxtla Gutiérrez, Chiapas, México

[63] Universidad Michoacana de San Nicolás de Hidalgo, Morelia, Michoacán, México

[64] Universidad Nacional Autónoma de México, México, D.F., México

[65] Institute of Nuclear Physics PAN, Krakow, Poland

[66] University of Łódź, Faculty of Astrophysics, Łódź, Poland

[67] University of Łódź, Faculty of High-Energy Astrophysics,Łódź, Poland

[68] Laboratório de Instrumentação e Física Experimental de Partículas – LIP and Instituto Superior Técnico – IST, Universidade de Lisboa – UL, Lisboa, Portugal

[69] "Horia Hulubei" National Institute for Physics and Nuclear Engineering, Bucharest-Magurele, Romania

[70] Institute of Space Science, Bucharest-Magurele, Romania

[71] University Politehnica of Bucharest, Bucharest, Romania

[72] Experimental Particle Physics Department, J. Stefan Institute, Ljubljana, Slovenia

[73] Laboratory for Astroparticle Physics, University of Nova Gorica, Nova Gorica, Slovenia

[74] Universidad Complutense de Madrid, Madrid, Spain

[75] Universidad de Granada and C.A.F.P.E., Granada, Spain

[76] Universidad de Santiago de Compostela, Santiago de Compostela, Spain

[77] IMAPP, Radboud University Nijmegen, Nijmegen, The Netherlands

[78] KVI – Center for Advanced Radiation Technology, University of Groningen, Groningen, The Netherlands

[79] Nationaal Instituut voor Kernfysica en Hoge Energie Fysica (NIKHEF), Science Park, Amsterdam, The Netherlands

[80] Stichting Astronomisch Onderzoek in Nederland (ASTRON), Dwingeloo, The Netherlands

[81] Case Western Reserve University, Cleveland, OH, USA

[82] Colorado School of Mines, Golden, CO, USA

[83] Department of Physics and Astronomy, Lehman College, City University of New York, Bronx, NY, USA

[84] Louisiana State University, Baton Rouge, LA, USA

[85] Michigan Technological University, Houghton, MI, USA

[86] New York University, New York, NY, USA

[87] Northeastern University, Boston, MA, USA

[88] Ohio State University, Columbus, OH, USA

[89] Pennsylvania State University, University Park, PA, USA

[90] University of Chicago, Enrico Fermi Institute, Chicago, IL, USA

[91] University of Nebraska, Lincoln, NE, USA

—

[a] School of Physics and Astronomy, University of Leeds, Leeds, United Kingdom

[b] Max-Planck-Institut für Radioastronomie, Bonn, Germany

[c] also at Vrije Universiteit Brussels, Brussels, Belgium

[d] now at Deutsches Elektronen-Synchrotron (DESY), Zeuthen, Germany

[e] SUBATECH, École des Mines de Nantes, CNRS-IN2P3, Université de Nantes, France

[f] Fermi National Accelerator Laboratory, USA

[g] University of Bucharest, Physics Department, Bucharest, Romania

[h] Colorado State University, Fort Collins, CO

[i] University of Hawaii, Honolulu, HI, USA

[j] University of New Mexico, Albuquerque, NM, USA

[k] now at Université Libre de Bruxelles (ULB), Brussels, Belgium